Università degli studi di Cagliari

PhD DEGREE

INGEGNERIA CIVILE E ARCHITETTURA
Cycle XXXI

Impact of Roof and Building Geometry on Urban Flows: from an idealised canopy to a real study

Scientific Disciplinary Sector
ICAR 01

PhD Student:	Michela Garau
Coordinator of the PhD Programme:	Roberto Deidda
Supervisor:	Giorgio Querzoli
	M.Grazia Badas

Final exam. Academic Year. 2017-2018
Thesis defence: January-February 2019 Session

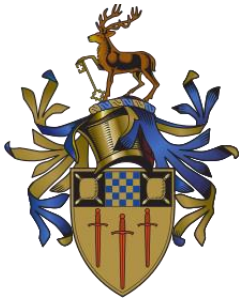

The work here presented was performed within the Hydraulic section of the Civil, Environmental Engineering and Architecture Department (DICAAR), at the University of Cagliari (Italy). The research has been realizable also thanks to the fruitful collaboration to the CRS4 (Centre for advanced studies, research and development in Sardinia), located within Science and Technology Park at Pula (Cagliari-Italy), which made its clusters available for the numerical computation. Finally a great part of the work was performed within the Department of Mechanical Engineering Sciences at the University of Surrey (Guildford-UK), as part of a Erasmus+ Traineeship programme.

Coordinator: Prof. Roberto Deidda
(University of Cagliari)

Supervisor: Prof. Giorgio Querzoli - Prof. M.Grazia Badas
(University of Cagliari)

Supervisor: Prof. Alan Robins - Prof. Matteo Carpentieri
(University of Surrey)

Acknowledgments

It would be reductive calling the PhD just a research project: it was indeed a piece of my life spent to know new persons, enrich my knowledge, make new experience, find motivations, discover limits, and much more. It is impossible to describe entirely what the PhD experience has been for me, so I limit myself to these few lines, as a little sample of how it was.

First of all, I would like to thank my supervisors Prof. Giorgio Querzoli and Prof. M.Grazia Badas, for guiding me, not only in a professional way, but also with passion and respect for me. I thank also Simone Ferrari, Alessandro Seoni with whom I had precious scientific collaboration, and Antonio Mascia, always helpful with his experience and professionalism as well as for a laugh and a coffee.

Moreover, I would like to stress how the friendship and interactions with the other young researchers and PhD students were precious for me. In particular, thanks to Laura, Enrica, Xeni, Luca and Jacopo.

Regarding scientific collaborations I need to thank Riccardo Rossi and the CRS4, which has made available the clusters needed for a large part of the present work. Especially thanks to Carlo Podda.

During these three years I have had many possibilities to travel participating to conferences both in Italy and abroad, and other activities and projects. Among these, the most important was the Erasmus+ treineeship, thanks to which I was able to spend seven months at the University of Surrey, taking part in the MAGIC-air-UK. It ended up being much more than a research project for me, providing me new inspirations and motivations for my life and work.

I would like to thank my UK supervisor Prof. Alan Robins, who has given me the opportunity to collaborate with the EnFlo and MAGIC research groups, enlarging my knowledge and connections. His guidance has been excellent and fruitful. I am also grateful to all the members of the MAGIC group who welcomed me as part of their teams, and to every person involved in the work at Surrey: William Lin, Paul Hyden, Matteo Carpentieri, Alan Wells, Zoe Ansell and Paul Nathan, whose help and presence were precious and pleasant.

Finally, I need to thank Davide, special help every day.

Ringraziamenti

Sarebbe riduttivo definire questo tempo solamente come un lavoro di ricerca: esso rappresenta tre anni di nuove conoscenze, esperienze maturate, persone e stimoli fondamentali, fatiche affrontate, limiti scoperti. Il testo che segue non deve e non riuscirebbe ad esprimere tutto quello che l'esperienza di dottorato ha significato per me, per cui lascio a queste poche righe un assaggio, grato, di ciò che è stato.

Vorrei prima di tutto esprimere gratitudine per i miei tutor accademici Prof. Giorgio Querzoli e Prof. M.Grazia Badas, con i quali ho avuto modo di lavorare giorno dopo giorno. Li ringrazio per avermi accompagnato non solo con professionalità, ma anche con tanta passione e stima in questo percorso, incoraggiandomi ed indirizzandomi verso una crescita anche professionale. Ringrazio inoltre Simone Ferrari e Alessandro Seoni con i quali ho collaborato a vario titolo, e Antonio Mascia, sempre disponibile con le sua esperienza e professionalità oltre che per una risata ed un caffè.

Ringrazio tutti i compagni di viaggio, dottorandi del mio ciclo e giovani ricercatori, con i quali il confronto e l'amicizia stretta sono stati supporto prezioso. In particolare Laura, Enrica, Xeni, Luca, Jacopo ed altri che per brevità non cito.

Tra le collaborazioni scientifiche, ringrazio Riccardo Rossi ed il CRS4 di Pula, in particolar modo nella persona di Carlo Podda, che ha messo a disposizione i cluster ai fini della ricerca, per mezzo dei quali è stato possibile svolgere buona parte del lavoro.

Durante i tre anni, ho avuto modo di compiere diverse esperienze sia in Italia che all'estero, per corsi di formazione e conferenze, a mio avviso esperienze fondamentali che aprono gli orizzonti e mettono in rete le idee, stimolano nuove collaborazioni e spronano la ricerca. Tra queste in particolare devo menzionare l'esperienza Erasmus+ treineeship, che mi ha permesso di svolgere sette mesi del mio dottorato presso l'Università del Surrey, in Inghilterra, dove ho preso parte al progetto MAGIC-air-UK. E' stata non solo una bella esperienza, ma fonte d'ispirazione nella vita e nel lavoro.

Desidero ringraziare il mio tutor Prof. Alan Robins, che mi ha accolto e dato la possibilità di lavorare insieme ai gruppi di ricerca del laboratorio EnFlo, Surrey, e del MAGIC, ampliando competenze e rete di conoscenze. Devo quindi ringraziare ogni componente del gruppo MAGIC, così come ogni persona del Surrey coinvolta nel lavoro: William Lin, Paul Hyden, Matteo Carpentieri, Alan Wells, Zoe Ansell and Paul Nathan.

Infine, ringrazio Davide, aiuto e presenza speciale ogni giorno.

Summary

Impact of Roof and Building Geometry on Urban Flows: from an idealised canopy to a real study

Nowadays, cities occupy 2% of the world soil, collecting 50% of global population. In a urban environment so complex and fragile, 75% of pollutant and 80% of CO_2 are emitted. As a consequence, finding healthy way to live cities is pressing, especially in relation to the continuous urbanisation process. The ventilation inside the urban pattern plays a key role in dispersion and comfort, so that many research dealt with it by facing several specific subjects and by employing different models, scales and techniques.

This thesis investigated the influence of two specific geometrical parameters: the building aspect ratio (i.e. the building width to height ratio) and the gable roof slope variability instead of the more common flat roofs. This was made at first considering some series of 2D street canyons and then by modelling a district of a real city. More specifically, numerical (LES) simulations were carried out performing street canyons with two different canyon aspect ratios (AR_C = 0.5, 1.0) and varying the building aspect ratio (AR_B = 0.1, 0.2, 0.3, 0.4, 0.5, 1.0, 1.5 and 2.0), in order to study wind flow and ventilation mechanism in narrow canyons, that are typical of the Mediterranean cities. Then by fixing the canyon width as 1.0, 2.0, and by changing the roof slope from 0° to 45° (0°, 10°, 20°, 30°, 45°), the variability of gable roof inclination was investigated. In addition to this, the influence of gable roofs 45° sloped was experimentally investigated (water channel), exploring the entire range of flow regimes (Oke, 1988), by means of the canyon width from 1 to 6.

Finally, a quasi-real 1:200 scaled model was employed, by means of the EnFlo wind tunnel and the study site on the South Bank of the Thames River in London, as part of the MAGIC-air-UK project. Here the influence of roofs with different shapes was evaluated in terms of ventilation mechanism and pollutant dispersion.

All the outcomes demonstrate the positive influence of roofs on ventilation and air exchange mechanism. Roofs increase turbulence, particularly in the upper part of the canyon, even if the behaviour at pedestrian level is not obvious. Roof employment appears to considerably affect the flow dynamics also in more complex models, suggesting that not employing roofs entails significant errors in results.

Sintesi

Impact of Roof and Building Geometry on Urban Flows: from an idealised canopy to a real study

Il tema dell'urbanizzazione è di primaria importanza sotto diversi punti di vista, tra questi quello ambientale, e della salute pubblica. Si stima che le città, occupino il 2% del suolo mondiale, accogliendo il 50% della popolazione. Si dimostra inoltre che esse siano sorgente di contaminanti nella misura del 75% dei contaminanti totali e che l'80% delle emissioni di CO_2 avvenga proprio in esse. Ne consegue che, trovare soluzioni per una vita più salubre in città sia un tema stringente, specie in considerazione del continuo sviluppo dei centri urbani anche nei Paesi in via di sviluppo. La ventilazione è un elemento chiave per la promozione della dispersione degli agenti inquinanti e del confort in generale, ragion per cui molte energie nel campo scientifico sono spese a suo favore, mediante l'utilizzo di diversi modelli, scale, obiettivi e tecniche di calcolo e stima degli scenari probabili.

Il presente lavoro di tesi fissa l'attenzione sull' influenza di due specifici parametri geometrici: il rapporto di forma degli edifici (AR_B, ovvero il rapporto tra la larghezza e l'altezza del palazzo) e la forma dei tetti, con particolare attenzione all'angolo d'inclinazione dei tetti a doppia falda, impiegati al posto dei più comuni edifici a tetto piano, considerati nella maggioranza dei lavori di letteratura. Ciò è stato realizzato in primo luogo considerando la configurazione dello *street canyon* bidimensionale ed in seguito modellando un quartiere di una città reale. Più specificatamente, simulazione numeriche di tipo LES (Large Eddy Simulations) sono state realizzate per lo studio di due serie di *street canyon* con rapporto di forma variabile (AR_C = 0.5, 1.0, inteso come rapporto tra la larghezza della strada e l'altezza degli edifici) e variando la larghezza degli edifici (AR_B = 0.1, 0.2, 0.3, 0.4, 0.5, 1.0, 1.5 and 2.0), con l'obiettivo di individuare la dinamica dei flussi in *street canyon* stretti, configurazioni tipiche delle città Mediterranee. In seguito, fissando la larghezza del canyon come 1.0, 2.0, e variando l'inclinazione del tetto da 0° a 45° (0°, 10°, 20°, 30°, 45°), è stata analizzata l'influenza della variabilità dei tetti a doppia falda. Per questo aspetto ulteriori analisi sono state svolte mediante simulazioni di laboratorio (canaletta), con l'intento di estendere il range a tutti e tre i regime di flusso individuati da Oke, (1988), ovvero variando la larghezza del canyon da 1 a 6.

Per concludere, alcune serie di analisi in galleria del vento (EnFlo wind tunnel) sono state svolte su un modello in scala 1:200 del quartiere South Bank of the Thames River di Londra, come parte del progetto MAGIC-air-UK. In questo contesto le analisi sono state svolte analizzando diverse forme delle coperture e stimando sia il meccanismo di ventilazione che la dispersione di contaminanti.

I risultati dimostrano che la presenza di tetti non piani, influenza la ventilazione ed i meccanismi di scambio. I tetti provocano un generale aumento della turbolenza, in particolare nelle zone alte del canyon, con comportamento non banale a livello pedonale. L'impiego dei tetti dunque, sembra influenzare grandemente la dinamica dei flussi anche nei modelli più complessi, suggerendo che il non utilizzo nella modellazione può comportare errori significativi nelle misure.

Table of Contents

Impact of Roof and Building Geometry on Urban Flows: from an idealised canopy to a real study

Michela Garau

University of Cagliari

Chapter 1

Introduction

1.1 Background

Air quality is a key environmental and social issue since pollution has got significant impacts on health, especially in urban areas, which continue to expand, becoming very densely populated. Pollution is a considerable economic problem since it reduces life expectation and increases medical assistance costs. Indeed, many cities in the world still exceed the pollutant concentration limits suggested by the World Health Organisation (WHO, 2006) Air Quality Guidelines (AQGs, 2016) or, in Europe, the Air Quality Directive (EU, 2004, 2008). The most dangerous pollutants for human health are PM, NO_2 and ground level O_3 (EEA Report, 2017; Thunis et al., 2017). These are categorised as secondary pollutants because they are formed in the atmosphere by the primary ones, directly released in the atmosphere, such as CO, NH_3, CH_4, C_6H_6, SO_x and others. Primary pollutants can have both natural and anthropogenic origins, being related to combustion processes (either industrial, domestic or from vehicular transport), human activities (like agriculture, by means of emissions from livestock, fertiliser use, etc.) or natural causes (like desert dust or sea salt).

As a consequence, to ensure good air quality is a complex problem that poses multiple challenges in terms of management and mitigation of harmful pollutants. Due to the complexity and the multidisciplinary of the problem, solutions, rules, research arguments and methods to face the problem involve different subjects, ranging from mathematic or chemical science to legal and social matters.

With the aim to study and find solutions to such a considerable issue, preventive or regulatory measures can be studied and activated. This involves technological development, structural and behavioural changes, for which rigorous study, monitoring, legislative decrees, international policy and agreement are needed. Some of these aspects will be introduced in the next paragraphs.

1.1.1 Policy and Legislation

Emissions are addressed under different policy packages. There are several major organs which shall monitor the global health and environmental welfare and which propose actions against its worsening. European Union (EU), Unite State (UN) with appropriate responsible bodies, the Intergovernmental Panel on Climate Change (IPCC) and the World Health Organisation (WHO) are the active bodies that attach particular importance to environmental aspects. They promote information, prevention and they regulate international conventions on climate and the environmental. In 1979 the United Nations Economic Commission for Europe (UNECE) enacted the Convention on Long-Range Transboundary Air Pollution (CLRTAP, 1979), which come into force in 1983. The aim of (CLRTAP, 1979) is to protect human health and the environment against air pollution risks, by reducing and preventing pollutant production and diffusion. This was possible through policy negotiation, scientific

collaboration and a series of eight protocols that defined specific actions to reduce pollutant emissions. The first edited programme was the European Monitoring and Evaluation Programme (EMEP), followed by several protocols, namely Helsinki, (1985), Sofia, (1988), about nitrogen oxide emissions, Geneva, (1991), about Volatile Organic Compounds, Oslo, (1994), Aarhus, (1998) about heavy metals and on POPs Aarhus, (1998), Gothenburg, (1999).

In the framework of the United Nations Climate Change actions, the Kyoto Protocol marked an important step. It is an international agreement binding the Member States to emission reductions, it was adopted in Kyoto in 1997 and entered in force in 2005 (UNFCC).

About Europe, the EEA Report, (2017) considering the large amount of data acquired from 2000 to 2015, describes the good achievements and the remaining goals. In this period, for example, 8% reduction in NH_3 and 72% reduction in sulphur dioxide was registered. For the sake of clarity, the EU demands to the single States, Regions and local Institutions the adoption of necessary measures. Nevertheless, all their actions must correspond to the EU standards and objectives inside a community vision about air, environment and goods. From this perspective, the EU commission with its laws, suggests, claims and coordinates the Member States. Its main objective is to reduce as much as possible the pollutants contained in the atmosphere, in order to prevent more harmful levels on human health and environment. This is pursued by means of a twin-track approach, implementing both air quality standards and emission mitigation controls (EEA Report, 2017).

The Clean Air Package Policy for Europe, published in the late 2013, (COM(2013), 918) aims to achieve specific goals by 2020 and 2030 based on the existing rules. The European Commission has put forward a three-pillar strategy (COM(2018), 171) that comprises the ambient air quality directives (EU, 2004, 2008), the national emission ceilings directive (NEC: EU, 2001, 2016) and the specific directive for the pollution sources: industrial emissions (EU, 2010) power stations (EU, 2010, 2015), vehicles (EU, 2009, 2011), vehicle in real driving conditions (EU, 2016) fuels employed in transport sector (EU, 1997), the energy performance of products (EU, 2009). An additional directive proposal about CO_2 vehicle emissions was presented in 2017 (COM(2017), 767).

The air quality directive (EU, 2008) replaced the five previous laws, with the aim to simplify and make air quality actions more efficient. It is now the basic directive (together with the EU, 2004) for what concerns arsenic, cadmium, mercury, nickel and polycyclic aromatic hydrocarbons. These two laws prescribe standards for measurement methods and pollutant levels evaluation, critical issues, objectives for specific pollutant reductions, requirements in case of exceeding limits, together with guidelines for short and long time plans.

The air quality standards from the UE directives are reported in Table 1.1, while Table 1.2 shows the air quality guidelines (AQGs, 2016) set by the World Health Organisation.

Moreover, annex III (EU, 2008) defines criteria for air quality assessment and the rules for measurement locations and sampling points. The air quality has to be assessed everywhere, except for sites where there is no access for the public. Regarding the sampling points, they must be located in order to protect both the human and the eco-system health. Measurements have to be defined in a different way with the aim to be representative of the macro-scale and the micro-scale. The measurement techniques for each species of contaminant are described in annex VI. In addition to this, the usage of valid models, which make the understanding of what is happening possible or which provide predictions in wider areas, is permitted and their improvement is encouraged.

Pollutant	Averaging period	Legal nature and concentration	Comments
PM_{10}	1 day	Limit value: 50 µg/m³	Not to be exceeded on more than 35 days per year
	Calendar year	Limit value: 40 µg/m³	
$PM_{2.5}$	Calendar year	Limit value: 25 µg/m³	
		Exposure concentration obligation: 20 µg/m³	Average Exposure Indicator (AEI) ([a]) in 2015 (2013-2015 average)
		National Exposure reduction target: 0-20 % reduction in exposure	AEI ([a]) in 2020, the percentage reduction depends on the initial AEI
O_3	Maximum daily 8-hour mean	Target value: 120 µg/m³	Not to be exceeded on more than 25 days/year, averaged over 3 years ([b])
		Long term objective: 120 µg/m³	
	1 hour	Information threshold: 180 µg/m³	
		Alert threshold: 240 µg/m³	
NO_2	1 hour	Limit value: 200 µg/m³	Not to be exceeded on more than 18 hours per year
		Alert threshold: 400 µg/m³	To be measured over 3 consecutive hours over 100 km² or an entire zone
	Calendar year	Limit value: 40 µg/m³	
BaP	Calendar year	Target value: 1 ng/m³	Measured as content in PM_{10}
SO_2	1 hour	Limit value: 350 µg/m³	Not to be exceeded on more than 24 hours per year
		Alert threshold: 500 µg/m³	To be measured over 3 consecutive hours over 100 km² or an entire zone
	1 day	Limit value: 125 µg/m³	Not to be exceeded on more than 3 days per year
CO	Maximum daily 8-hour mean	Limit value: 10 mg/m³	
C_6H_6	Calendar year	Limit value: 5 µg/m³	
Pb	Calendar year	Limit value: 0.5 µg/m³	Measured as content in PM_{10}
As	Calendar year	Target value: 6 ng/m³	Measured as content in PM_{10}
Cd	Calendar year	Target value: 5 ng/m³	Measured as content in PM_{10}
Ni	Calendar year	Target value: 20 ng/m³	Measured as content in PM_{10}

Table 1.1 - Air quality standards from the UE Ambient Air Quality Directives EU, 2004, 2008.

Pollutant	Averaging period	AQG	RL	Comments
PM_{10}	1 day	50 µg/m³		99th percentile (3 days per year)
	Calendar year	20 µg/m³		
$PM_{2.5}$	1 day	25 µg/m³		99th percentile (3 days per year)
	Calendar year	10 µg/m³		
O_3	Maximum daily 8-hour mean	100 µg/m³		
NO_2	1 hour	200 µg/m³		
	Calendar year	40 µg/m³		
BaP	Calendar year		0.12 ng/m³	
SO_2	10 minutes	500 µg/m³		
	1 day	20 µg/m³		
CO	1 hour	30 mg/m³		
	Maximum daily 8-hour mean	10 mg/m³		
C_6H_6	Calendar year		1.7 µg/m³	
Pb	Calendar year	0.5 µg/m³		
As	Calendar year		6.6 ng/m³	
Cd	Calendar year	5 ng/m³ (b)		
Ni	Calendar year		25 ng/m³	

Table 1.2 – WHO air quality guidelines and estimated reference levels (RL) from WHO, 2000, 2006

1.1.2 Air Quality in Urban Planning

Health pollutants effects are related with both short and long term. Short-term is linked to acute health effects, whereas long-term exposure is linked to chronic health effects. The Ambient air quality Directives and the World Health Organisation have respectively defined the air quality standards and the guidelines for the human health protection. Just to keep in mind the order of magnitude of emissions exposure in cities, from the monitoring data reported by the EU-28 (EEA Report, 2017) 19% of urban UE-28 citizens, were found to be exposed to PM_{10} above the UE daily limit (mean values over 2000-2015, with a pick of 43%). Considering the WHO guidelines, population exposed to levels exceeding the annual limit value (20 µm/m^3) was between 50.5 and 92% in the period 2000-2015.

As underlined by a recent report (COM(2018), 330), the UE Commission is seriously concerned by two classes of pollutant, nitrogen dioxide (NO_2) and particulate matter (PM_{10}, $PM_{2.5}$), both very dangerous for the human health. Vehicular traffic is responsible for 40% of the NO_2 emissions and for a great part of PM emissions, together with industrial, agricultural and domestic emissions (EEA Report, 2017).

Technical improvements are essential to prevent traffic emissions, but a new idea of mobility is also requested. As a consequence, two mobility packages were drawn up in 2016 to promote green public transportation, car sharing systems, incentives and infrastructures for zero-emission vehicle adoption. On the same page are the incentives which aim to convert the common energy production systems into greener ones, like solar, wind or hydroelectric energies.

As an example, the Portuguese city of Lisbon has won the European Green Capital Award for 2020, being particularly committed in the field of sustainable land use, urban transportation, green growth and eco-innovation, climate change adaptation and waste treatment. As reported by the European Commission (EGCA, 2020)

- *"*Lisbon was the first capital in Europe to sign the New Covenant of Mayors for Climate Change and Energy in 2016, after achieving a 50% reduction in $C0_2$ emissions (2002-14); reducing energy consumption by 23% and water consumption by 17% from 2007 to 2013
- It has got a clear vision for sustainable urban mobility, with measures to restrict car use and prioritise cycling, public transportation, and walking. In 2017 Lisbon launched a bike-sharing scheme, with electric bikes constituting two thirds of the fleet to encourage cycling in the hilliest parts of the city
- It has got one of the world's largest networks of electric vehicle charging points, while 39% of the municipal car fleet is electric, 93.3% of people in Lisbon live within 300 m of a frequent public transport service and 76% of people live within 300 m of green urban areas
- It has got a strong commitment to sustainable land use with particular focus on establishing green infrastructure, or connected networks of green space, to counteract the effects of climate change, such as drought, extreme heat, and storm flooding"

The research of new ways to prevent and protect air quality the human health in cities is a great responsibility for states, local authorities but also the scientific research. Indeed, research is a crucial tool in urban environment which encompasses a great number of different aspects like air quality and pollutant dispersion, indoor and outdoor ventilation, pedestrian wind comfort, public transportation strategies, etc. As an example, Netherland with its "Dutch standard NEN 8100, (2006) (Wind comfort and wind danger in the built environment)" and the "Dutch practice guideline NPR 6097, (2006)", represents a good integration of scientific research and policy actions. These national laws were draw up in order to prevent the strong winds effect and provide the first case in Europe of a well structure directive on wind for urban planning. They regulate the new-building construction in order to guarantee more liveable cities, by assessing ventilation around buildings. With this objective, the usage of numerical simulations is needed, confirming the importance of research for practical purposes and the feasibility of a smarter urban manufacturing.

Nowadays, a lot of big projects, like the COST Action 732 or HARMO, are involved with the objective to unify research with legislation, to find effective strategies and proposals for regulatory plans and a better way to manage atmosphere and the environment. In particular the COST Action 732 is a project financed by European Commission into the COST programme (European Cooperation in Science & Technology), specifically planned for quality assurance and improvement of micro-scale models to predict flow and transport process in urban or industrial environment. HARMO (Harmonisation within Atmospheric Dispersion Modelling for Regulatory Purposes) is a European initiative born in 1991 and launched to increase cooperation and standardisation of atmospheric dispersion models for regulatory purposes.

1.1.3 Air Quality Modelling

As previous instated, air quality, especially in the urban environment, has become an important research issue, with fundamental applicative implications. The pioneering work of Johnson et al., (1973), Dabberdt et al., (1973), Nicholson, (1975) and others, as discussed in a review paper by Vardoulakis et al., (2003) were able to understand the main features of ventilation and transport in basic element compounding a city, such as the street canyon. However, international directives and the increasing population in cities request a more accurate assessment, to provide previsions of the present and future scenarios, that in turn request to model air quality both at different temporal and spatial different scales (Orlanski, 1975; Schlünzen et al., 2011; Blocken, 2015).

As a matter of fact, spatial scales involved in the Urban Boundary Layer (UBL) that is the region of the Planetary Boundary Layer (PBL) closest to the ground, can vary depending on the study objectives: street scale (of order 10-100 m), neighbourhood scale (100-1000 m) or city scale (1-20 Km). All of them are included in the so called micro-scale range.

For the sake of clarity, the Urban Boundary Layer (UBL) is influenced by a roughness surface corresponding to the urban environment. The latter has got a complex composition, due to the interactions through buildings shapes, different materials, building porosity, etc., making the UBL characterised by a continuous change of roughness, so that flow does not achieve the equilibrium condition.

According to different authors (Barlow, 2014; Zajic et al., 2015) the UBL can be divided into four layers (as shown in Figure 1.):

- Urban Canopy Layer (UCL) is the layer between the surface and the building roofs, very variable in height, where the channelling through streets strongly depends on their orientation with respect to the wind direction
- Roughness Sub-Layer (RSL) just above roofs, is the layer with 2-5H depth (where H is the mean building height), influenced by the drag force of roughness elements and where TKE production and dissipation balance each other
- Inertial Sub-Layer (ISL) is characterised by horizontally homogeneous turbulence and little variation of fluxes with height
- Above the ISL the UBL adopts the structure of the atmospheric boundary layer and it is dominated by entrainment and TKE production

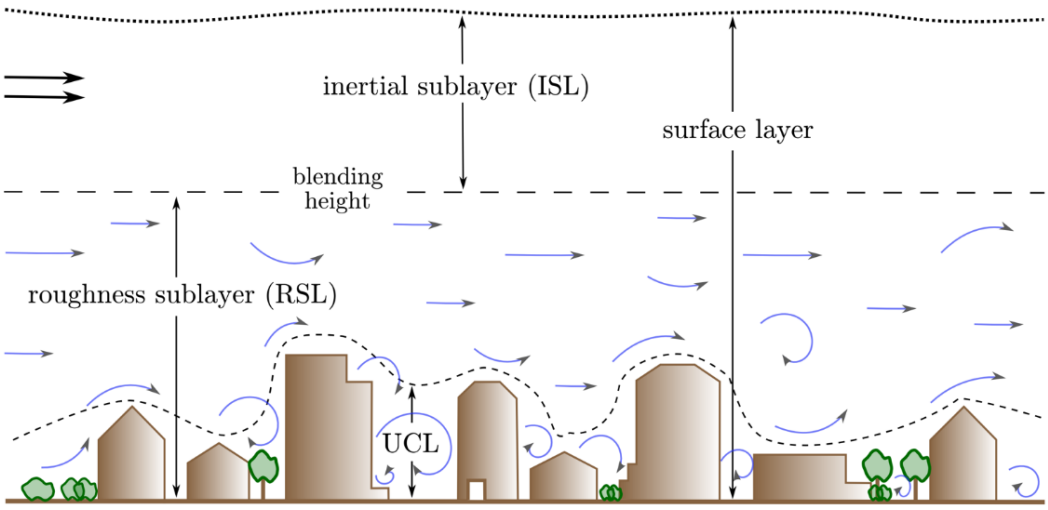

Figure 1.1 – Urban Boundary Layer scheme from Hertwig, (2013). UCL: Urban Canopy Layer; RSL: roughness sub-layer; ISL: inertial sub-layer

Typically, the adiabatic wind speed vertical profile above a roughness canopy, is described by the logarithmic formula:

$$\frac{U(z)}{u_*} = \frac{1}{\kappa} ln(\frac{z-d}{z_0}) \qquad 1.1$$

where d is the displacement height, z_0 the surface roughness, u_* the frictions velocity and κ the Karman constant (Arya, 1999). Another typical formulation is the power law, where α is an empirically derived coefficient depending on the stability condition and δ is the UBL thickness:

$$\frac{U(z)}{u_*} = \left(\frac{z-d}{\delta-d}\right)^{\alpha} \quad \textbf{1.2}$$

However, as defined by Fernando et al., (2010), the flow passing a basic urban unit (e.g. a street canyon) depends on a larger group of fundamental variables, so that the normalised velocity $U(z)$ at a generic downstream x, z position can be written as:

$$\frac{U(z)}{U_H} = f[\frac{h}{l}, \frac{b}{l}, \frac{b}{s}, \frac{b}{w}, \alpha_f, \frac{z}{h}, \frac{x}{h}, Re(=\frac{U_0 H}{\nu})] \quad \textbf{1.3}$$

where U_o is the velocity at the building height H, Re is the Reynolds number and ν the kinematic viscosity. Some of the geometric variables that appear in this equation (Eq. 1.3) can be replaced by the common parameters such as the frontal and the plan area index ($\lambda_f = A_f/A_d$, $\lambda_p = A_p/A_d$) and the frontal solidity ($\lambda_{fs} = A_f/A_T$). All these parameters can be calculated for a real city or district and employed in different ways (see for example Badas et al., 2019).

Time scales are also very important: the traffic concentration and the emissions in general are affected by the economic system of a city, i.e. they are often concentrated in scheduled time frames; therefore the natural daily (or seasonal) variations are influenced by weather patterns, and so by the atmospheric stratification. Moreover, the main problem in urban fluid dynamics remains the turbulence and the big range of scale to be addressed. However, even though technologies are becoming more and more powerful, simplifications in the urban environment fluid dynamics are still necessary for the sake of generalisation. For this reason, simple configurations are extensively applied and their results are very useful to understand and interpret the basic mechanism driving flows in the urban environment.

With such a level of complexity, a multiple approach is suggested by several authors (Macdonald, 2000; Belcher et al., 2003; Baker, 2007; Sabatino et al., 2008; Barlow, 2013; Fernando, 2009; Meroney, 2016), in which each part accounts for the weaknesses of the others.

As for the air quality research studies, the urban environment can be shaped considering two- or three-dimensional basic elements, such as the street canyon configuration or a series of identical parallelepiped elements regularly disposed, or more complex geometries and increasing level of details, depending on the objectives, the simulation method and the available tools. But, of course, the flow dynamics differs substantially if we employ heterogeneous instead of homogeneous, detailed instead of simplified urban canopies, differs substantially (Theurer et al., 1992; Fernando, 2009). However, street canyons or single building arrays are usually preferred to understand the dynamics of basic topics like the influence of geometrical elements (Rafailidis, 1997; Xie et al., 2005; Yassin, 2011) or the stratification (Allegrini et al., 2013; Nazarian et al., 2018) or the basic flow structures and dispersion mechanism around buildings (Coceal et al., 2014; Stabile et al., 2015). More complicated arrays of obstacles are employed with the aim to understand the influence of density in 3D areas or the interaction between different elements, such as the different building heights. Semi-idealised canopy, are employed to understand the mechanisms at street intersections (Carpentieri et al., 2012; Carpentieri and Robins, 2015; Kellnerová and Jaňour, 2008), or more (Kwak et al., 2015; Leo et al., 2018). Finally, very detailed urban models are sometimes employed to study specific cases in cities.

1.2 Objective and Methodology

The present work deals with the influence of some geometrical characteristics of buildings on the flow and dispersion. In particular, the focus is on the building width and the roof shape, that is an interesting topic not yet deeply addressed. To this aim, firstly a 2D street canyon configuration was employed, mainly evaluating the flow in the so called *"skimming flow regime"* and *"wake interference regime"* (Oke, 1988). Secondly, a modelled district of a real city was considered. Both experimental and numerical simulations were here employed:

- ***Water Channel Experiments*** were performed in order to simulate a 2D street canyon with variable aspect ratio in a range from 1 to 6 times the building height (H). Arrays of 20 identical prismatic obstacles, 20x20 mm in section, were employed with either flat or gable roof (45° sloped). The canonical case with 1H canyon spacing was experimented in order to validate the CFD simulations. Velocity fields were measured by the Feature Tracking Velocimetry

- ***CFD Simulations*** were employed for two series of analyses. The first one was aimed at studying the effect of the variability of the building aspect ratio (i.e. the building width, W_B, to height, H ratio) in a virtually infinite array of identical parallelepiped flat roof buildings, by keeping constant the canyon width as 0.5H and 1.0H. The second one aimed at investigating the roof role: the gable roof slope change from 0° to 45° (0°, 10°, 20°, 30°, 45°), and setting the canyon width as 1, 2H. Simulations were carried out by using a Large Eddy Simulations (LES) technique and the open source library OpenFOAM 2.3.x

- ***Wind Tunnel Modelling*** was applied to investigate the effects of roofs on flow and pollutant dispersion at a field study site on the South Bank of the Thames River in London, UK. Analysis were carried out with a 1:200 scale model, by measuring velocities thanks to the Laser Doppler Anemometry and pollutant concentrations with the Fast Flame Ionisation Detection system

1.3 Outline of the Thesis

The thesis is structured into five chapters, as follow:

Chapter 2 presents results of a 2D street canyon analysis of the width building variation, by considering two different canyon spacing, typical of Mediterranean cities. Analysis were elaborated by employing the numerical LES technique;

Chapter 3 is divided into two parts, both dealing with the influence of roof shapes on a 2D street canyon configuration. Section 3.4.2 shows experimental analyses carried out with two roof shapes into the *"skimming flow regime"*, *"wake interference regime"* and the quasi *"isolated roughness regime"* (Oke, 1988) by ranging the canyon width from 1 to 6 times the building height (H). Section 3.4.3 discusses the influence of five roof shapes with the canyon width equal to 1.0 and 2.0H, elaborated with the numerical LES technique;

Chapter 4 presents a wind tunnel investigation carried out at the EnFlo Lab (University of Surrey) on a simplified model of a district in London. This is part of the Managing Air for Green Inner Cities UK project (MAGIC-air.uk). In this part the influence of roof shapes on the model quality results, on ventilation and pollutant dispersion is analysed;

Finally, Chapter 5 presents conclusions, strengths, limitation and further work purposes.

1.4 References

Aarhus, 1998a. Protocol on Heavy Metals - Air Pollution - Environmental Policy - UNECE. https://www.unece.org/env/lrtap/hm_h1.html

Aarhus, 1998b. Protocol on Persistent Organic Pollutants (POPs) - Air Pollution - Environmental Policy - UNECE. https://www.unece.org/env/lrtap/pops_h1.html

Allegrini, J., Dorer, V., Carmeliet, J., 2013. Wind tunnel measurements of buoyant flows in street canyons. Building and Environment 59, 315–326. https://doi.org/10.1016/j.buildenv.2012.08.029

AQGs, 2016. WHO Expert Consultation: Available evidence for the future update of the WHO Global Air Quality Guidelines (AQGs) (2016). http://www.euro.who.int/en/health-topics/environment-and-health/air-quality/publications/2016/who-expert-consultation-available-evidence-for-the-future-update-of-the-who-global-air-quality-guidelines-aqgs-2016

Arya, S.P., 1999. Air Pollution Meteorology and Dispersion. Oxford University Press. ISBN 978-0195073980

Badas, M.G., Salvadori, L., Garau, M., Querzoli, G., Ferrari, 2019. Urban areas parameterisation for CFD simulation and cities air quality analysis. International Journal of Environment and Pollution http://www.inderscience.com/info/ingeneral/forthcoming.php?jcode=ijep

Baker, C.J., 2007. Wind engineering—Past, present and future. Journal of Wind Engineering and Industrial Aerodynamics 95, 843–870. https://doi.org/10.1016/j.jweia.2007.01.011

Barlow, J., 2013. The wind that shakes the buildings: wind engineering from a boundary layer meteorology perspective, in: Owen, J.S., Sterling, M., Hargreaves, D.M., Baker, C.J. (Eds.), Fifty Years of Wind Engineering: Prestige Lectures from the Sixth European and African Conference on Wind Engineering. Birmingham University Press ISBN 978-0704428348.

Barlow, J.F., 2014. Progress in observing and modelling the urban boundary layer. Urban Climate, ICUC8: The 8th International Conference on Urban Climate and the 10th Symposium on the Urban Environment 10, 216–240. https://doi.org/10.1016/j.uclim.2014.03.011

Belcher, S.E., Jerram, N., Hunt, J.C.R., 2003. Adjustment of a turbulent boundary layer to a canopy of roughness elements. Journal of Fluid Mechanics 488, 369–398. https://doi.org/10.1017/S0022112003005019

Blocken, B., 2015. Computational Fluid Dynamics for urban physics: Importance, scales, possibilities, limitations and ten tips and tricks towards accurate and reliable simulations. Building and Environment, Fifty Year Anniversary for Building and Environment 91, 219–245. https://doi.org/10.1016/j.buildenv.2015.02.015

Carpentieri, M., Hayden, P., Robins, A.G., 2012. Wind tunnel measurements of pollutant turbulent fluxes in urban intersections. Atmospheric Environment 46, 669–674. https://doi.org/10.1016/j.atmosenv.2011.09.083

Carpentieri, M., Robins, A.G., 2015. Influence of urban morphology on air flow over building arrays. Journal of Wind Engineering and Industrial Aerodynamics 145, 61–74. https://doi.org/10.1016/j.jweia.2015.06.001

CLRTAP, 1979. Convention on Long-Range Transboundary Air Pollution. https://www.unece.org/fileadmin/DAM/env/lrtap/full%20text/1979.CLRTAP.e.pdf

Helsinki, 1985. The Convention and its achievements - Air Pollution - Environmental Policy – UNECE. URL https://www.unece.org/environmental-policy/conventions/envlrtapwelcome/the-air-convention-and-its-protocols/the-convention-and-its-achievements.html

Coceal, O., Goulart, E.V., Branford, S., Glyn Thomas, T., Belcher, S.E., 2014. Flow structure and near-field dispersion in arrays of building-like obstacles. Journal of Wind Engineering and Industrial Aerodynamics 125, 52–68. https://doi.org/10.1016/j.jweia.2013.11.013

COM(2013), 918 European Commission - COM(2013)918 - Register of Commission documents http://ec.europa.eu/transparency/regdoc/index.cfm;jsessionid=3EAB7C00BF4B14D59E2D411F4A3934A7.cfusion14601?fuseaction=list&n=10&adv=0&coteId=1&year=2013&number=918&version=F&dateFrom=&dateTo=&serviceId=&documentType=&title=&titleLanguage=EN&titleSearch=EXACT&sortBy=NUMBER&sortOrder=DESC.

COM(2017), 767. European Commission - COM(2017)767 - Register of Commission documents. http://ec.europa.eu/transparency/regdoc/?fuseaction=list&n=10&adv=0&coteId=1&year=2017&number=767&version=F&dateFrom=&dateTo=&serviceId=&documentType=&title=&titleLanguage=&titleSearch=EXACT&sortBy=NUMBER&sortOrder=DESC2017.

COM(2018), 171, European Commission - COM(2018)171 - Register of Commission documents. http://ec.europa.eu/transparency/regdoc/?fuseaction=list&n=10&adv=0&coteId=1&year=2018&number=171&version=F&dateFrom=&dateTo=&serviceId=&documentType=&title=&titleLanguage=&titleSearch=EXACT&sortBy=NUMBER&sortOrder=DESC2018.

COM(2018), 330, European Commission - COM(2018)330 - Register of Commission documents http://ec.europa.eu/transparency/regdoc/?fuseaction=list&n=10&adv=0&coteId=1&year=2018&number=330&version=F&dateFrom=&dateTo=&serviceId=&documentType=&title=&titleLanguage=&titleSearch=EXACT&sortBy=NUMBER

COST | Quality Assurance and Improvement of Microscale Meteorological Models. http://www.cost.eu/COST_Actions/essem/732

COST Action 732. COST. https://www.cost.eu/actions/732/#tabs|Name:overview.

Dabberdt, W.F., Ludwig, F.L., Johnson, W.B., 1973. Validation and applications of an urban diffusion model for vehicular pollutants. Atmospheric Environment (1967) 7, 603–618. https://doi.org/10.1016/0004-6981(73)90019-X

EEA Report | No 13/2017, 2017. Air quality in Europe — 2017 report. Publications Office of the European Union, Luxembourg. https://doi.org/10.2800/850018

EGCA, 2020. European Green Capital. http://ec.europa.eu/environment/europeangreencapital/lisbon-is-the-2020-european-green-capital-award-winner/

EMEP - European Monitoring and Evaluation Programme. http://www.emep.int/

EU, 2016a. Directive 2016/2284/EU, of the European Parliament and of the council of 14 Dec 2016 on the reduction of national emissions of certain atmospheric pollutants, amending Directive 2003/35/EC and repealing Directive 2001/81/EC. L. 344, V. 59. https://eur-lex.europa.eu/legal-content/EN/TXT/?uri=OJ:L:2016:344:TOC

EU, 2016b. Commission Regulation 2016/427/EU of 10 March 2016 amending Regulation (EC) No 692/2008 as regards emissions from light passenger and commercial vehicles (Euro 6). L. 82, V. 59. https://eur-lex.europa.eu/legal-content/EN/TXT/?uri=OJ:L:2016:082:TOC

EU, 2015. Directive 2015/2193/EU of the European Parliament and of the Council of 25 November 2015 on the limitation of emissions of certain pollutants into the air from medium combustion plants. L. 313, V. 58. https://eur-lex.europa.eu/legal-content/EN/TXT/?uri=OJ:L:2015:313:TOC

EU, 2011. Regulation (EC) No 510/2011 of the European Parliament and of the Council of 11 May 2011 setting emission performance standards for new light commercial vehicles as part of the Union's integrated approach to reduce CO2 emissions from light-duty vehicles. L. 145 , V. 54. https://doi.org/10.3000/17252555.L_2011.145.eng

EU, 2010. Directive 2010/75/EU of the European Parliament and of the council of 24 November 2010 on industrial emissions. L. 334, V. 53. https://doi.org/10.3000/17252555.L_2010.334.eng

EU, 2009a. Regulation (EC) No 443/2009 of the European Parliament and of the Council of 23 April 2009 setting emission performance standards for new passenger cars as part of the Community's integrated approach to reduce CO2 emissions from light-duty vehicles, OJ L. https://doi.org/10.3000/17252555.L_2009.140.eng

EU, 2009b. Directive 2009/125/EC of the European Parliament and of the Council of 21 October 2009 establishing a framework for the setting of eco-design requirements for energy-related products. https://doi.org/10.3000/17252555.L_2009.285.eng

EU, 2008. Directive 2008/50/EC of the European Parliament and of the council of 21 May 2008 on ambient air quality and cleaner air for Europe. L. 152 V. 51. https://eur-lex.europa.eu/legal-content/EN/TXT/?uri=OJ:L:2008:152:TOC

EU, 2004. Directive 2004/107/EC of the European Parliament and of the council of 15 Dec 2004 relating to arsenic, cadmium, mercury, nickel and polycyclic aromatic hydrocarbons in ambient air. L. 23 V. 48. https://eur-lex.europa.eu/legal-content/EN/TXT/?uri=OJ:L:2005:023:TOC

EU, 2001. Directive 2001/81/EC, of the European Parliament and of the Council of 23 October 2001 on national emission ceilings for certain atmospheric pollutants. L. 309 V. 44. https://eur-lex.europa.eu/legal-content/EN/TXT/?uri=OJ:L:2001:309:TOC

EU, 1997. Council Directive 97/70/EC of 11 December 1997 setting up a harmonised safety regime for fishing vessels of 24 metres in length and over. L. 34 V. 41. https://eur-lex.europa.eu/legal-content/EN/TXT/?uri=OJ:L:1998:034:TOC

Fernando, H. j. s., 2009. Fluid Dynamics of Urban Atmospheres in Complex Terrain. Annu. Rev. Fluid Mech. 42, 365–389. https://doi.org/10.1146/annurev-fluid-121108-145459

Fernando, H.J.S., Zajic, D., Di Sabatino, S., Dimitrova, R., Hedquist, B., Dallman, A., 2010. Flow, turbulence, and pollutant dispersion in urban atmospheres. Physics of Fluids 22, 051301. https://doi.org/10.1063/1.3407662

Geneva, 1991. Protocol concerning the Control of Emissions of Volatile Organic Compounds - Air Pollution - Environmental Policy - UNECE . https://www.unece.org/env/lrtap/vola_h1.html

Gothenburg, 1999. Protocol to Abate Acidification, Eutrophication and Ground-level Ozone - Air Pollution - Environmental Policy - UNECE. https://www.unece.org/env/lrtap/multi_h1.html

HARMO - Harmonisation within Atmospheric Dispersion Modelling for Regulatory Purposes. http://www.harmo.org/default.asp

Hertwig, D., 2013. On Aspects of Large-Eddy Simulation Validation for Near-Surface Atmospheric Flows (PhD Thesis). Universität Hamburg, Von-Melle-Park 3, 20146 Hamburg. http://ediss.sub.uni-hamburg.de/volltexte/2013/6289.

IPCC - Intergovernmental Panel on Climate Change. https://www.ipcc.ch/

Johnson, W.B., Ludwig, F.L., Dabberdt, W.F., Allen, R.J., 1973. An Urban Diffusion Simulation Model For Carbon Monoxide. Journal of the Air Pollution Control Association 23. https://doi.org/10.1080/00022470.1973.10469794

Kellnerová, R., Jaňour, Z., 2008. The flow instabilities within an urban intersection. Hrvatski meteorološki časopis 43, 675–679. https://hrcak.srce.hr/64341

Kwak, K.-H., Baik, J.-J., Ryu, Y.-H., Lee, S.-H., 2015. Urban air quality simulation in a high-rise building area using a CFD model coupled with mesoscale meteorological and chemistry-transport models. Atmospheric Environment 100, 167–177. https://doi.org/10.1016/j.atmosenv.2014.10.059

Leo, L.S., Buccolieri, R., Sabatino, S.D., 2018. Scale-adaptive morphometric analysis for urban air quality and ventilation applications. Building Research & Information 46, 931–951. https://doi.org/10.1080/09613218.2018.1501797

Macdonald, R.W., 2000. Modelling The Mean Velocity Profile In The Urban Canopy Layer. Boundary-Layer Meteorology 97, 25–45. https://doi.org/10.1023/A:1002785830512

MAGIC-air.uk. URL http://magic-air.uk/home.html

Meroney, R.N., 2016. Ten questions concerning hybrid computational/physical model simulation of wind flow in the built environment. Building and Environment 96, 12–21. https://doi.org/10.1016/j.buildenv.2015.11.005

Nazarian, N., Martilli, A., Kleissl, J., 2018. Impacts of Realistic Urban Heating, Part I: Spatial Variability of Mean Flow, Turbulent Exchange and Pollutant Dispersion. Boundary-Layer Meteorol 166, 367–393. https://doi.org/10.1007/s10546-017-0311-9

NEN 8100, 2006. Wind comfort and wind danger in the built environment. NEN 8100:2006. Dutch Standard.

Nicholson, S.E., 1975. A pollution model for street-level air. Atmospheric Environment (1967) 9, 19–31. https://doi.org/10.1016/0004-6981(75)90051-7

NPR 6097, 2006. Application of mean hourly wind speed statistics for the Netherlands. NPR 6097:2006. Dutch Practice Guideline.

Oke, T.R., 1988. Street design and urban canopy layer climate. Energy and Buildings 11, 103–113. https://doi.org/10.1016/0378-7788(88)90026-6

Orlanski, I., 1975. A Rational Subdivision of Scales for Atmospheric Processes. Bulletin of the American Meteorological Society 56, 527–530. https://www.jstor.org/stable/26216020

Oslo, 1994. Protocol on Further Reduction of Sulphur Emissions - Air Pollution - Environmental Policy - UNECE. https://www.unece.org/env/lrtap/fsulf_h1.html

Rafailidis, S., 1997. Influence of Building Areal Density and Roof Shape on the Wind Characteristics Above a Town. Boundary-Layer Meteorology 85, 255–271. https://doi.org/10.1023/A:1000426316328

Sabatino, S.D., Buccolieri, R., Pulvirenti, B., Britter, R.E., 2008. Flow and Pollutant Dispersion in Street Canyons using FLUENT and ADMS-Urban. Environ Model Assess 13, 369–381. https://doi.org/10.1007/s10666-007-9106-6

Schlünzen, K.H., Grawe, D., Bohnenstengel, S.I., Schlüter, I., Koppmann, R., 2011. Joint modelling of obstacle induced and mesoscale changes—Current limits and challenges. Journal of Wind Engineering and Industrial

Aerodynamics, The Fifth International Symposium on Computational Wind Engineering 99, 217–225. https://doi.org/10.1016/j.jweia.2011.01.009

Sofia, 1988. Protocol concerning the Control of Emissions of Nitrogen Oxides - Air Pollution - Environmental Policy - UNECE. https://www.unece.org/env/lrtap/nitr_h1.html

Stabile, L., Arpino, F., Buonanno, G., Russi, A., Frattolillo, A., 2015. A simplified benchmark of ultrafine particle dispersion in idealized urban street canyons: A wind tunnel study. Building and Environment 93, 186–198. https://doi.org/10.1016/j.buildenv.2015.05.045

Theurer, W., Baechlin, W., Plate, E.J., 1992. Model study of the development of boundary layers above urban areas. Journal of Wind Engineering and Industrial Aerodynamics 41, 437–448. https://doi.org/10.1016/0167-6105(92)90443-E

Thunis, P., Degraeuwe, B., Pisoni, E., Trombetti, M., Peduzzi, E., Belis, C.A., Wilson, J., Vignati, E., 2017. Urban PM2.5 Atlas: Air Quality in European cities, EUR 28804 EN. Publications Office of the European Union, Luxembourg. https://doi.org/10.2760/336669

UNECE. Protocols - Air Pollution - Environmental Policy - UNECE. http://www.unece.org/env/lrtap/status/lrtap_s.html

UNFCCC. United Nations Framework Convention on Climate Change. https://unfccc.int/

University of Surrey, Facilities | University of Surrey. https://www.surrey.ac.uk/aerodynamics-environmental-flow-group/environmental-flow-research-centre/facilities

Vardoulakis, S., Fisher, B.E.A., Pericleous, K., Gonzalez-Flesca, N., 2003. Modelling air quality in street canyons: a review. Atmospheric Environment 37, 155–182. https://doi.org/10.1016/S1352-2310(02)00857-9

WHO (Ed.), 2006. Air quality guidelines: global update 2005 ; particulate matter, ozone, nitrogen dioxide and sulfur dioxide. WHO Regional Office for Europe, Copenhagen

WHO (Ed.), 2000. Air quality guidelines for Europe, 2. ed., WHO regional publications European series. World Health Organization, Regional Office for Europe, Copenhagen

WHO - World Health Organization. http://www.who.int/

Xie, X., Huang, Z., Wang, J., 2005. Impact of building configuration on air quality in street canyon. Atmospheric Environment 39, 4519–4530. https://doi.org/10.1016/j.atmosenv.2005.03.043

Yassin, M.F., 2011. Impact of height and shape of building roof on air quality in urban street canyons. Atmospheric Environment 45, 5220–5229. https://doi.org/10.1016/j.atmosenv.2011.05.060

Zajic, D., Fernando, H.J.S., Brown, M.J., Pardyjak, E.R., 2015. On flows in simulated urban canopies. Environ Fluid Mech 15, 275–303. https://doi.org/10.1007/s10652-013-9311-6

Chapter 2

2D street Canyon: influence of building aspect ratio

Most part of this chapter has been accepted for publication as:

Garau, M., Badas, M.G., Ferrari, S., Seoni, A., Querzoli, G., 2019. Air Exchange in urban canyons with variable building width: a numerical approach. International Journal of Environmental and Pollution, Special Issue: HARMO18.

2.1 Summary

The aim of this chapter is to gain further insight into the role played by the building aspect ratio (AR_B, i.e. the ratio of the building width, W_B, to the building height, H) and its influence on the street canyon flow. By employing the Large Eddy Simulation technique with virtually infinite array of identical obstacles immersed in a neutrally-stratified boundary layer, ideal two-dimensional street canyons with various AR_B and AR_C were evaluated (AR_C, i.e. the ratio of the street width, W_B, to the building height, H). A wide series of data with AR_C equal to 0.5 and 1, and 8 different AR_B (from 0.1 to 2), were employed for a total number of 16 different cases analysed. Results were validated for the configuration with a AR_B = 1.0, AR_C = 1.0 with experimental data, obtained in a water channel with regular array of 20 identical buildings, and with other literature data. Results were found strongly dependent on the building aspect ratio related with the street canyon width. The highest turbulence levels and mean vertical velocities were found when the buildings are narrow, irrespective of the canyon shape. Analysis of the exchange rates between the canyon and the overlaying boundary layer, indicated that the flow-rate increases for narrow buildings, and the minimum value is observable for AR_B = 1.5. Finally, in the case of unitary canyon width, the residence time (T_r) is linearly proportional to the building aspect ratio for the whole extent of the investigated rate, while in the narrow canyon case the T_r shows a not obvious trend. However, the mean trends are characterised by a different slope. Concluding, even if results are affected by the simplifications employed in these analyses, they suggested that the building aspect ratio is a crucial parameter when predicting pollutant removal from urban canyons and in the modelling of the urban boundary layer characteristics.

2.2 Introduction

The urban canopy is characterized by a complex geometry that interacts with the fragile equilibrium governing atmosphere, soil and subsoil system. Cities are usually characterized by elevated sources of heat and pollutants, and high levels of PM10 and PM2.5, NO2, SO2, carcinogenic hydrocarbons, etc., which are potentially dangerous for human health. There are many geometrical factors that can influence the fluid dynamic in urban environment and a great amount of work and research has been done in order to understand the influence of each one and the interactions through them. A range of numerical model and experimental techniques can be used to measure, monitor and predict the pollutant concentration in urban context (Vardoulakis et al., 2003) and they are related to the observation scale. Idealized and simplified geometries are often preferred to focus on the influence of individual components of the problem and to reveal the mechanism driving air ventilation and mixing process. Indeed, ventilation has a crucial role against pollutant retention in the urban canopy layer: it promotes the removal of pollutants and heat by means of both the mean flow and the turbulence. The street canyon is the basic urban unit and a lot of analyses are performed with its modelling. It has been used in order to understand basic air flow mechanism, the influence of geometric variations, pollutant release and distribution, etc. For instance, Ferrari et al., (2017) made use of arrays of identical prismatic buildings and canyons, to study the influence of different roof shapes on turbulence and ventilation; Murena and Mele, (2016) identified the negative effects of balconies on air quality inside deep street canyons, by inducing a general decrease of turbulence; Li et al., (2010) investigated the flow field and pollutant distribution by a LES model within the unstable thermal stratification produced by different ground heating intensities.

Focusing on the two-dimensional street canyon configuration, the majority of literature works, both numerical (e.g. Chung and Liu 2012; Wong and Liu 2012) and experimental (Brown et al. 2000; Neophytou et al. 2014; Bernardino et al. 2015), employed square buildings with the aspect ratio equal to $AR_B = 1$ (defined as the ratio of the building width, W_B, to its height, H, see Figure 1), and with the canyon aspect ratio $AR_C = 1, 2$ (defined as the ratio of the canyon width, W, to the building height, H). In general, so much attention was spent in varying the AR_C and other characteristics respect to the AR_B. For example, by fixing the building aspect ratio, Li et al., (2009) focused on the transport of a passive and inert pollutant emitted from a line source at the ground level by using very narrow canyons (AR_C = 0.33, 0.2, 0.1) while Xie and Huang, (2007) varying the AR_C from 0.5 to 10, investigated the impacts of surface heating on pollutant transport and Air Exchange Rate. On the other hand, wider canyons, corresponding to the wake interference and isolated building regimes (Oke 1988), were analysed by other authors with different objectives (i.e. Badas et al., 2017; Garau et al., 2018).

As regards studies about the building aspect ratio (AR_B), the majority of authors employed 3D configurations in order to gain a deeper insight into the effects of randomness in the obstacle topology and to study the height variability influence on specific characteristics of the flow. As a matter of fact Chan et al., (2003) carried out measurements on arrangements of parallelepiped buildings with different combinations of AR_C (ranging from 0.5 to 3.0) and AR_B (ranging from 0.25 to 2.0), varying the building length in the span-wise. Kanda, (2006) found that the aerodynamic surface properties are too different when there is a variability of building heights, probably due by the differences in interaction between the large scale turbulence organised structures (TOS) and the local disturbance produced by the shear instability along the rooflines. Xie et al., (2008) stated that one individual block can be significantly influenced by a relatively remote blocks with different height.

Evaluations on ventilation performance in high-rise cities (with AR_B = 0.19, 0.25, 0.33 and the area density equal to 25% and 40%) was conducted by Hang and Li, (2011); they concluded that lengths of

high-rise building arrays should be limited especially if there are no parks, gardens, grasslands which may get better ventilation by dividing the city into smaller areas. Cheng and Castro, (2002) by repeating unit over a number of urban roughness with random heights and fixing the plan and frontal area density about 25%, studied the roughness sub-layer (RS) finding that it is thicker in case of the random surface than for the uniform one. For that reason they stated that an inertial sub-layer may not exist in urban areas where the dominant feature are high, irregular and heterogeneous roughness elements. Millward-Hopkins et al., (2011), summarized the overall effect of the area density and building height variability in an idealised city, by using three-dimensional blocks. By employing cuboids with the l/H ratio ranging from 0.3 to 3.0 and W_B/H from 0.5 to 5.0, (where H, W_B and l are respectively, the building height, width and length in the span-wise direction), they ideally described the individual building wakes, calculating the span-wise extent of sheltering (L_W) and the rear reattachment length (L_R). Moreover, they estimated the dependence of roughness length and the zero-plane displacement upon area density, via a quasi-empirical modelling approach.

Focusing on the two-dimensional street canyon configuration, Gerdes and Olivari, (1999) performed wind tunnel experiments with a series of four very narrow buildings (AR_B = 0.033-0.02) and AR_C = 2, 4, in order to understand the pollutant dispersion behaviour. Later, Baik et al., (2000) analysed more cases in a water channel by using AR_C = 1.0, 0.67, 0.5, 0.42, 0.33 and AR_B = 0.625, 0.42 in order to characterised the recirculation region behind an obstacle as a function of the flow speed and obstacle slope. Although, a parametric study about the influence of the AR_B in a 2D street canyon, to avoid the influence educed by other geometrical characteristics, was not yet realised.

Therefore, take into consideration the results of a parametric analysis made for the city of Cagliari (Badas et al., 2019), whose urban morphology is typical of many Mediterranean cities, so much different respect to the northern-Europe and American typical constructions, with very narrow canyons and quite tall buildings, we gave a further insight into the influence of the building shapes on street canyon flow, focusing on the building aspect ratios.

A series of Large Eddy Simulations (LES), with two-dimensional building arrays immersed in a neutral boundary layer, were performed by fixing the building height (H) and varying both the buildings and the canyon aspect ratio (respectively AR_B and AR_C) for a total number of 16 configurations. Results were analysed in terms of velocity statistics, ventilation and mean residence time.

The chapter is organised as follows. Section 2.3 presents the numerical model, computational domain and numerical set-up. In Section 2.4, the validation of the model with literature data, experimental and numerical results of present simulations are discussed. Then, the results are presented and discussed. In Section 2.5 conclusions are drawn, giving an overview about limitations of present works and forthcoming steps.

2.3 Methods

This work focuses on the flow in urban canyons formed by a virtually infinite array of identical obstacles immersed in a neutrally-stratified boundary layer. Two canyon aspect ratios, AR_C = 0.5, 1.0 and eight building aspect ratios, AR_B = 0.1, 0.2, 0.3, 0.4, 0.5, 1.0, 1.5 and 2.0, hence a total number of 16 configurations were simulated. The wind direction was chosen orthogonal to the canyon axis in all the test. A LES model was adopted to resolve the turbulent flow within and above the street canyons, which was validated with our water channel experimental data and other literature data in the cases of AR_B = 1.0 and AR_C = 0.5, 1.0.

2.3.1 Numerical Simulations

The open source library OpenFOAM 2.3.1, which solves the approximate form of the governing equations of the flow by means the finite volume method (FVM), was employed to performed numerical simulations. Simulations were run by employing little cluster at the University of Cagliari and thanks to the biggest cluster of the CRS4 (Centro di Ricerca, Sviluppo e studi superiori in Sardegna). Following the classical LES scheme, the filtered governing equations are risolved using modelled sub-grid scale (SGS) motions for which we have employed the Smagorinsky model (Smagorinsky, 1963). Formally, the LES decomposition into resolved and residual components is achieved by the convolution with a spatial filter function, which depends on the cut-off width Δ. The resulting set of equations consists of the continuity equations Eq. 2.1 and the filtered Navier Stokes equations Eq. 2.2:

$$\frac{\partial \bar{u}_i}{\partial x_i} = 0 \tag{2.1}$$

$$\frac{\partial \bar{u}_i}{\partial t} + \frac{\partial}{\partial x_j}\bar{u}_i\bar{u}_j = -\Delta P \delta_{ij} - \frac{\partial \bar{p}}{\partial x_i} - \frac{\partial \tau_{ij}}{\partial x_j} + \nu \frac{\partial^2 \bar{u}_i}{\partial x_i \partial x_j} \tag{2.2}$$

where $\bar{u}_i$ is the velocity component in the i-direction, ΔP the kinematic pressure gradient, δ_{ij} the Kronecker delta and ν the kinematic viscosity. The SGS Reynold stresses are modelled in the form:

$$\tau_{ij} = -2\nu_{SGS} S_{ij} \tag{2.3}$$

where, ν_{SGS} denotes the SGS viscosity that, in OpenFOAM 2.3.x, is defined by:

$$\nu_{SGS} = C_k \Delta \sqrt{K} \tag{2.4}$$

and C_k = 0.094, Δ is the filter width taken to be the power average of grid sizes in all directions $\Delta = (\Delta_1 \Delta_2 \Delta_3)^{1/3}$ and the SGS kinetic energy K is computed as:

$$K = \frac{2C_K}{C_e}\Delta^2 |S|^2 \tag{2.5}$$

C_k = 0.094 and C_ε = 1.048, are the OpenFOAM default values.

The computational domain consists of three identical idealised street canyons, perpendicularly disposed respect to the wind direction. Domain size results in a 3(W_B + W_C) length in the stream-wise direction, where W_B and W_C are respectively the variable building and canyon widths. The building size is equal to 9H in the span-wise direction. Similarly, the height of the computational domain is 9H, larger than the minimum requested in the best practice guidelines (Tominaga et al., 2008; Franke et al., 2011; Blocken, 2015) schematic representation is reported in Figure 2.1. Employing cyclic boundary conditions at the stream-wise and span-wise faces of the domain, allows us to reproduce series of canyons of indefinite longitudinal length, i.e. an idealised two-dimensional canopy

A structured mesh (hexahedral cells, see Figure 2.2) with grid stretching both in stream-wise and vertical direction was employed. In order to guarantee a high enough resolution near the buildings walls, the domain was discretized with 32 cells per H. An expansion ratio lower than 1.2 was used for both the horizontal and vertical axes (*x* and *z*, respectively), according to the good practice guidelines just mentioned. Therefore, the resolution is Δx = Δz = 0.016 H in the proximity of the building walls

and the ground, whist in the canyon centre cell size is doubled. The span-wise resolution was fixed as $\Delta y = 0.05$ H. As a consequence, the total number of cells ranges from a minimum of $2.33 \cdot 10^6$ (in the case of $AR_B = 0.1$ and $AR_C = 0.5$) up to a maximum of $10.82 \cdot 10^6$ (in the case $AR_B = 2$ and $AR_C = 1.0$).

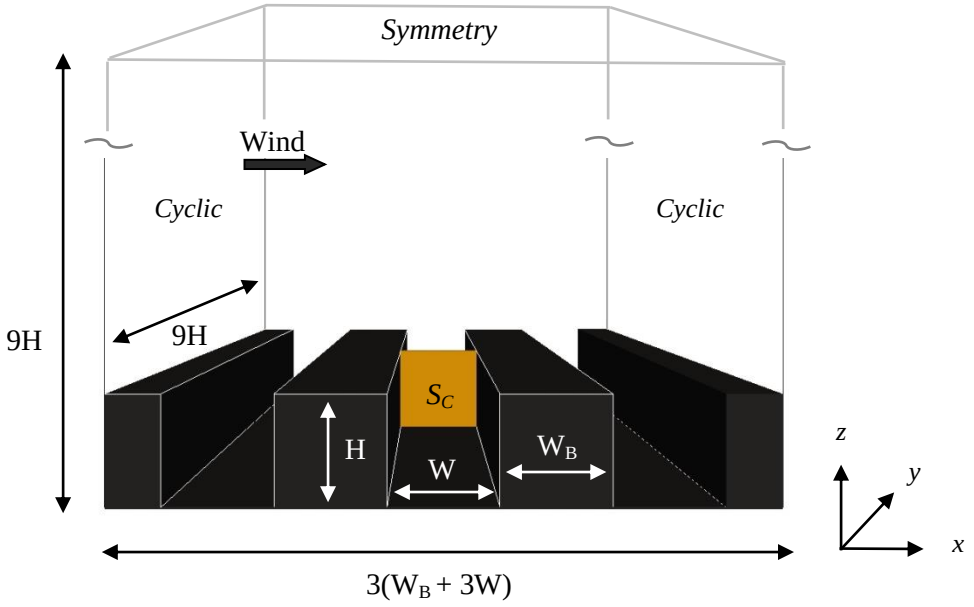

Figure 2.1 - Schematic representation of domain and boundary conditions. H: building height; WB: building width; W: canyon width; Sc: cross-section of the canyon (shaded in yellow). Domain sizes are: x-direction: dependent on W and WB size; z-direction = y-direction: 9H.

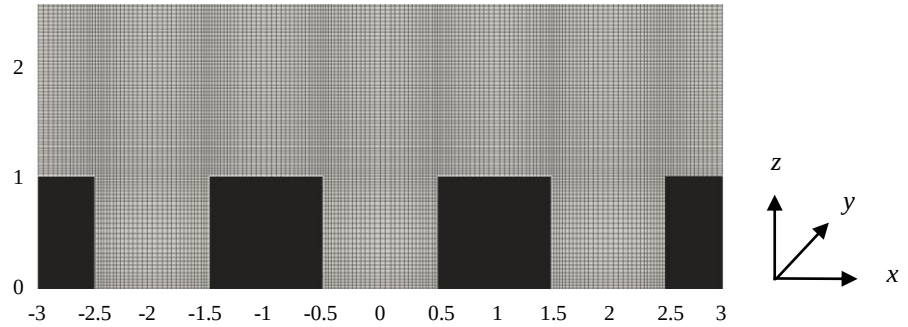

Figure 2.2 - Schematic representation of the structured mesh in a section. $\Delta x = \Delta z = 0.016$ H in the proximity of the building walls and the ground, whist in the canyon centre cell size is doubled. The span-wise resolution is fixed as $\Delta y = 0.05$ H.

All LES runs were initialized by means of a RANS solution, and data used for computing statistics were collected after a sufficient interval of time for the complete development of turbulence. Namely, we chose a transitional time equal to 35 convective times, $T_C = L/U_{mean}$, (T_C is also known as the flow-through time), where L is the domain size in the stream-wise direction (Figure 2.2). An overall time of 70 T_C was used to accumulate the dataset in order to compute the velocity statistics. During the interval time, data was recorded every 0.05 T_C, i.e. a time lapse long enough to ensure a satisfying statistical independence of samples. The mean stream-wise velocity was imposed to obtain a Reynolds number at the building height $Re_H = U_H H/\nu = 7000$, i.e. higher than the minimum value (3400) suggested by Hoydysh et al., (1974) for the flow to be independent of the Reynolds number. The dimensional time-step increment was set in order to assure that the Courant number was always smaller than 0.6 at all grid nodes. The results were averaged both in time, over a minimum of 1350

time steps, and spatially in the span-wise direction in order to enhance the statistical robustness of the dataset.

As regards numerical methods, the second-order-accurate schemes were used for the time and space derivatives. Namely, the backward differencing scheme in the time derivatives, and the central differencing scheme (Gaussian integration with linear interpolation) in the spatial derivatives. The large time-step transient solver for incompressible flow, was applied for the pressure-velocity coupling scheme, by means of the PIMPLE algorithm (merged PISO-SIMPLE). The preconditioned conjugate gradient (PCG) method was used to solve the linear equation system for $\overline{p}$ and the preconditioned bi-conjugate gradient (PbiCG) method for $\overline{u}$.

2.3.2 Experimental Simulations

The experiments conducted in the closed-loop water channel of the Hydraulic Laboratory of the University of Cagliari. Results were employed to validate the numerical outcomes. A neutral boundary layer above a series of 20 identical prismatic obstacles, was employed for two series of data: the first one with the building square section $AR_B = 1.0$ and the second one with a 20×20 mm^2 section resulting in an aspect ratio $AR_B = 0.1$, corresponding to very slender buildings. In both the two cases the canyon aspect ratios were 1.0 and 2.0. The same characteristics of about the facility and the model is here reported, however more details are feasible at the Section 3.3.1 of present work or in Garau et al., (2018).

The water-channel was 8.0 m long and the cross section was 0.40 m wide and 0.50 m high. The array of obstacles, painted in matt black to avoid laser light reflections, were placed 6.0 m downstream from the head of the channel. To allow a complete evolution of the turbulence and to achieve a logarithmic velocity profile, a grid with a honeycomb structure was placed at the head of the channel and a 3 m long series of panels with loose gravel (equivalent diameter: 5 mm) was set on the channel bottom. A sharp-crested weir at the end of the channel regulated the water depth to 0.4 m. The vertical stream-wise mid-plane of the channel was illuminated by a diode laser, 2W in power, emitting green light (2mm thick, 532 nm in wavelength), through an optical system consisting of a cylindrical lens and a mirror. A high-speed camera (2240×1760 pixels resolution) recorded images at a 310 Hz frequency. The images, 150 mm height and 117 mm width, with a spatial resolution about 150px/cm, were recorded in 40 sessions (1200 images in a period of 3.9s each, for a total of 48000 images) separate by a proper time interval that assure the statistical independence, in order to increase the statistical robustness of the velocity dataset. Velocity field was evaluated by tracking neutrally buoyant particles (pine pollen 50μm in diameter) homogeneously dispersed in the flow through an image analysis technique called Feature Tracking Velocimetry. This technique, described in (Besalduch et al., 2013, 2014) is based on: (1) the identification of the particle images on the frames by means of the Harris corner detection algorithm (Harris and Stephens, 1998); (2) the interrogation windows comparisons are made by measuring the dissimilarity between the windows of successive frames; (3) the evaluation of the particles displacement between two successive frames is defined as the displacement minimizing the dissimilarity between interrogation windows. The dissimilarity was determined by the Lorentzian robust estimation (Falchi et al., 2006). Finally, the velocity was obtained as the ratio of the particle displacement to the time interval between frames. the incoming velocity profile follows the typical logarithmic law of the turbulent boundary layer up to about z = 0.14 m (corresponding to 7H), with a maximum velocity of 0.36 m/s, and it was found in good agreement with the data of Farell and Iyengar, (1999). At the building height (H), a Reynolds number $Re_H = U_H H/\nu = 5000$ was obtained, condition that satisfied $Re_H > 3400$ as suggested by Hoydysh et al., (1974). Previous tests, performed on the flow approaching the building series, revealed that, following

the argument proposed by Uehara et al. (2003), only a 1.0 mm deep layer adjacent to the wall is affected by a significant decrease of the velocity because of the viscosity effects. Therefore, the bulk of the flow can be assumed Re independent (Garau et al., 2018).

2.4 Results

2.4.1 Validation

We compared 5 vertical profiles (x/H = -0.4, -0.25, 0, 0.25, 0.4) using 1st and 3rd order of velocity statistics; however, for the sake of brevity, we here show only vertical profiles of the stream-wise velocity (Figure 2.3) and the vertical velocity skewness factor (Figure 2.4) at the canyon central point, x/H = 0, and near the building walls at x/H = ±0.4. These quantities were made non dimensional by the Us velocity, which corresponds to the velocity averaged between z/H = 1 and z/H = 1.5. In addition to the present experimental data, we compared the numerical results with both wind tunnel and LES data available in literature. All the considered works focused on a two two-dimensional street canyon with $AR_B = AR_C = 1.0$ which is the most investigated in literature. The wind tunnel data by Brown et al., (2000) was realised with an array of seven rectangular blocks extended from wall-to-wall in the span-wise direction. It was immersed in a neutral atmospheric boundary layer twelve times high with respect to the building height, the latter perpendicularly disposed respect to the wind direction. A pulsed wire anemometry (PWA), was employed to measure within and near the buildings, with 1200 samples at each point to evaluate velocities, then the turbulent statistics were sampled. For what concerns numerical simulations, Cui et al., (2004) performed an idealised street canyon (CSV81 case) with medium-high mesh resolution (0.3m in x direction and 0.5m in z direction), and by employing a revisited Regional Atmospheric Modelling System (RAMS), originally applied for mesoscale applications, with cyclic boundary conditions, the normal velocity set to zero at walls and the Smagorinsky eddy viscosity model (C_S=0.8-1.2 depending on the location in the street canyon). Comparing results with the wind tunnel data of Brown et al.(2000), the authors found some reasonable dissimilarity related to the limitation of the employed domain (one single canyon) and to the not refined mesh near roofs, where the higher instability occurs. Therefore, Cheng and Liu, (2011) carried out LES by employing three canyons with a 30% coarser mesh resolution in x direction and 20% larger in z direction (particularly at roof level), with respect to the previous LES described. Periodic conditions at the stream-wise and span-wise directions, free-slip boundaries at the top and no-slip at the walls were employed by the authors. The present numerical set up is more similar to the Cheng and Liu, (2011) one, with a coarser mesh resolution (by 10%). The present simulation outcomes are in overall good agreement for both the parameters, even if some differences are visible for the skewness factor at the near wall profiles (Figure 2.4 a, c). A detailed description will be done later. The non-dimensional mean stream-wise velocities well agree with all the other studies inside the canyon, by correctly reproducing the trends, with negative values in the deeper cavity part and the evolution of the shear layer at the rooftop, becoming smoother going downstream. However, present LES results underestimate all the considered values above z/H = 2,while the Cheng and Liu, (2011) data, is in better agreement with the experimental curves (indicated in figure as Lab). This might depend on the higher statistic robustness of laboratory experiments, compared to the numerical ones, that would require longer computational time in order to completely resolve the largest flow structures, located above the canopy. The skewness factor numerically obtained is in good agreement with the experimental data over the whole vertical range for the central profile (Figure 2.4 b). Below z/H = 2.0, it matches also with the other data and between z/H = 0.8 and 1.0, the negative values are correctly reproduced. The most noticeable discrepancy was found at the near wall profiles (x/H = ±0.4): looking at Figure 2.4 a, wind tunnel data seems not clearly identifying the peak, in case of Cui et al, (2004) it

appears amplified while in water channel outcomes it is underestimated. Besides, a good agreement is visible between present and Cheng and Liu, (2011) LES, apart for the upper profile. Similarly, the two LES series are comparable in Figure 2.4 c. Differences might be referred to the difference in the mesh resolution and input parameters, in case of numerical set up, and to the limitation of the experimental techniques in the near wall flow (for example the reflection problem in the water channel visualisations). Therefore, it is convenient to remember the importance of employing a large amount of data for good high moment statistics.

A qualitative comparison was also done for the configuration AR_C = 0.5, AR_B = 0.5 with data reported in Zhong et al., (2015), Zhong, (2016). The field topology, reported in Figure 2.5 (right panel) show the same structure with two main counter-rotating vortexes identified also by other authors (Hoydysh and Dabberdt 1988; Hassan and Crowther 1998; Soulhac 2000). The main vortex central point is sited at the same x/H and height position; in addition to this, the shape of two vortexes are too similar not only in the central part of the canyon, but also near walls and corners, with the main velocities in the upper part of the field closed to the leeward wall. Results are in good agreement with results obtained by Kovar et al, (2002) too.

On the left side of the Figure 2.5 comparison for the mean vertical velocity variance is reported. Maps display similar shapes with a higher values tongue that come into the canyon, closed to the leeward wall. However local differences are visible and they should be done by differences occurring in the walls boundary conditions employed for the numerical set-up.

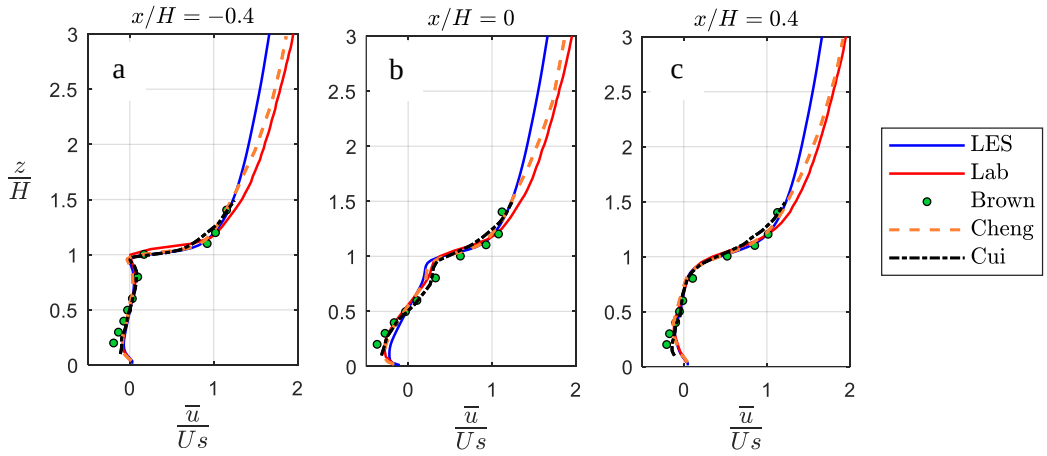

Figure 2.3 – Vertical profiles of the stream-wise velocity for x/H = -0.4 (a), x/H = 0 (b), x/H = 0.4 (c), made non dimensional by using Us (averaged mean velocity at 1<z/H<1.5).Configuration with AR_C = AR_B = 1. Present numerical simulation: solid blue line; experimental simulation: solid red line; numerical simulation from Cheng and Liu, (2011): dashed orange line; numerical results from Cui et al., (2004): dashed black line; experimental results from Brown et al., (2000): green circles.

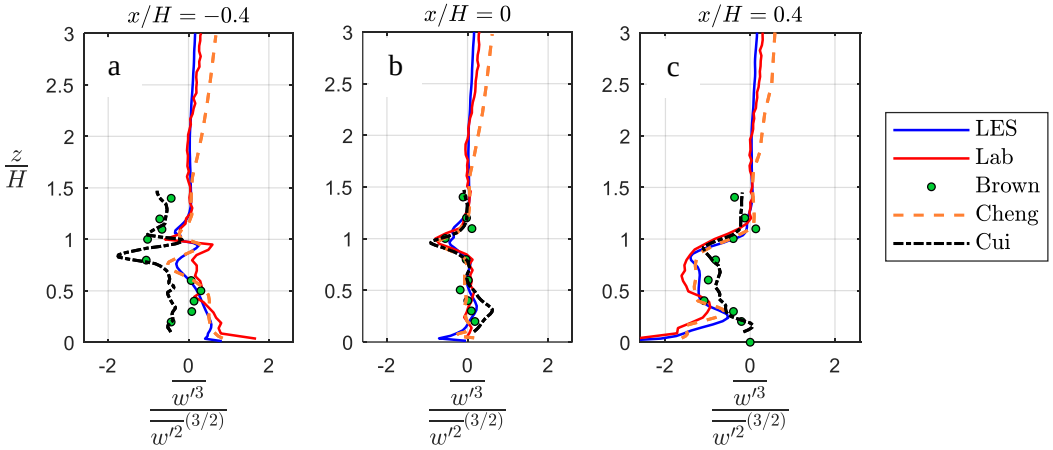

Figure 2.4 - Vertical profiles of the skewness of the vertical velocity for x/H = -0.4 (a), x/H = 0 (b), x/H = 0.4 (c), made non dimensional by using Us (averaged mean velocity at 1.0<z/H<1.5).Configuration with AR_C = AR_B = 1.0. Present numerical simulation: solid blue line; experimental simulation: solid red line; numerical simulation from Cheng and Liu, (2011): dashed orange line; numerical results from Cui et al., (2004): dashed black line; experimental results from Brown et al., (2000): green circles.

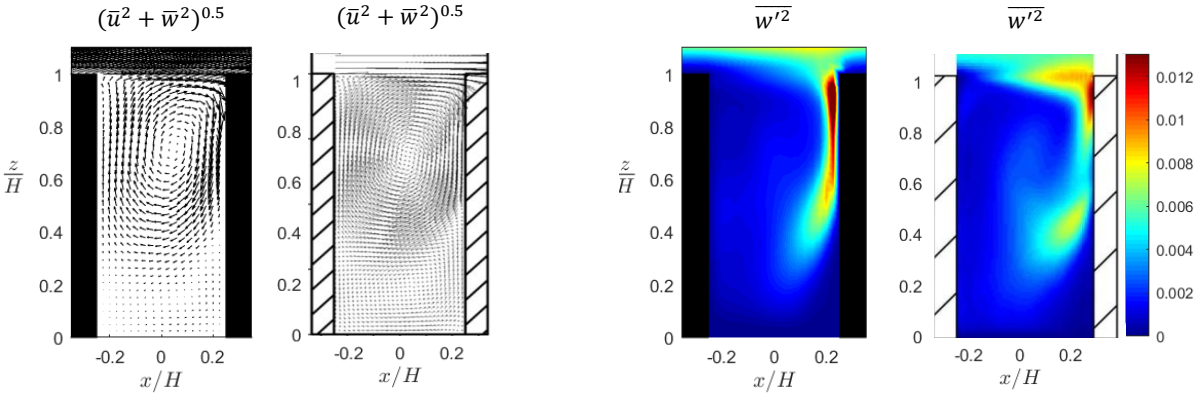

Figure 2.5 – Left panel: comparison of vortex structure between current LES (black buildings)and J.Zhong, (2016) LES (white buildings with stripes); right panel: comparison of the mean vertical velocities variance field between current LES (black buildings)and J.Zhong, (2016) LES (white buildings with stripes).

2.4.2 First and Second order statistics

Qualitative results for the mean velocity magnitude, obtained from numerical simulations (AR_C = 0.5, 1.0 and AR_B = 1.0 respectively in Figure 2.6 a, b), show a completely different behaviour inside the canyon depending on the AR_C parameter: instead of a single main vortex (Figure 2.6 b), two counter-rotating vortexes are shown in the narrower canyon (Figure 2.6 a). This is a consequence of the increasing height respect to the canyon width. Differences at the pedestrian level are relevant: the narrow canyon gives lower velocity values and this could represent a negative aspect for air quality. Looking at the vertical velocity component (Figure 2.7 a, b), which drives the air exchange, it is possible to notice that the entire region included into the lower vortex (for AR_C = 0.5) is characterised by very small values. Furthermore, areas with large vertical velocities are smaller respect to the case with AR_C = 1.0 and lower values are observed at the roof level too. It is well known that the air exchange is mainly controlled by the mixing at the roof level, especially in the skimming flow regime, with a significant effect of the building aspect ratio, AR_B (i.e Soulhac, 2000), while at increasing canyon widths the mixing involves deeper fractions into the canyon. Thus, the air exchange is less dependent on the flow at the roof level, as demonstrated in Badas et al., (2017).

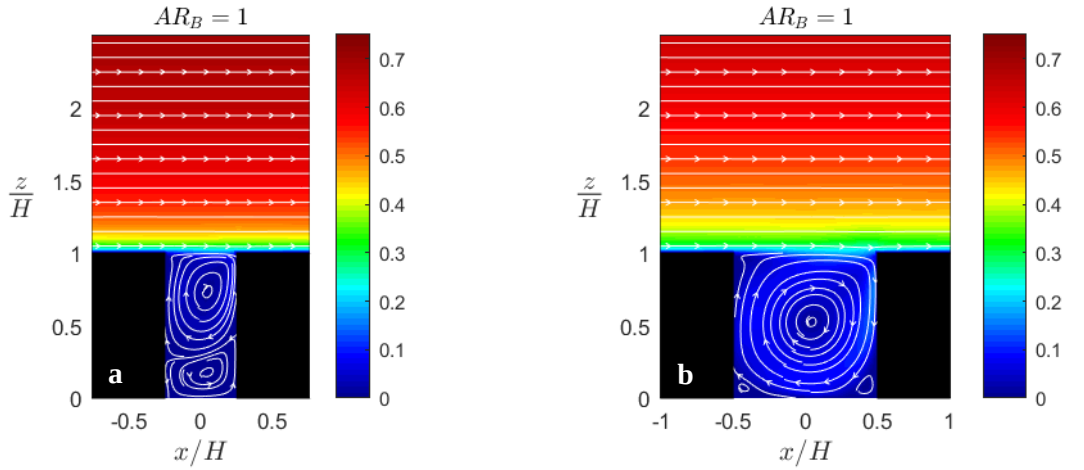

Figure 2.6 – Streamlines of the mean velocity field and mean velocity magnitude, made non dimensional by the free-stream velocity ($\bar{u}/U_{ref}$). Building aspect ratio AR_B = 1.0. Canyon aspect ratios, AR_C = 0.5 (a) and AR_C = 1.0 (b).

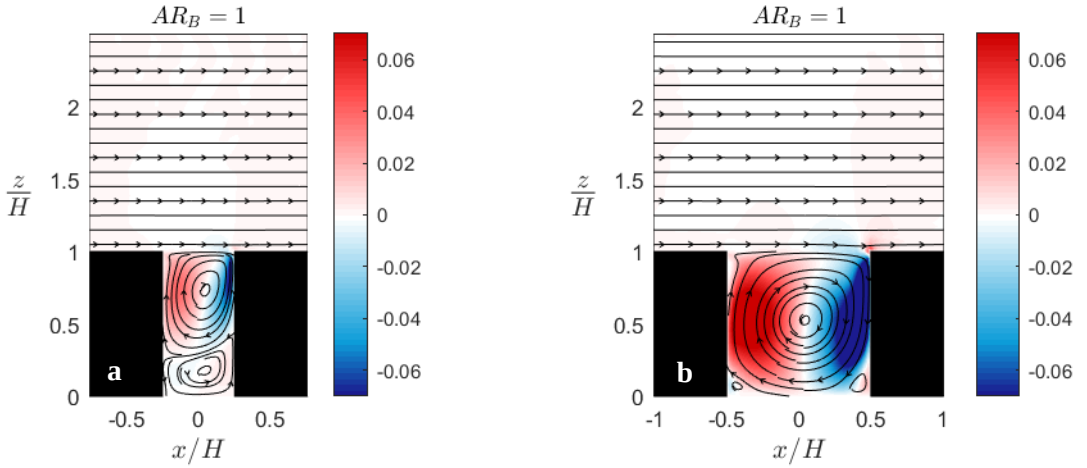

Figure 2.7 - Streamlines of the mean velocity field and mean vertical velocity component, made non dimensional by the free-stream velocity ($\bar{w}/U_{ref}$). Building aspect ratio AR_B = 1. Canyon aspect ratios, AR_C = 0.5 (a) and AR_C = 1.0 (b).

Maps of the variance of the vertical velocity component, made non dimensional by the free-stream velocity $\overline{w'^2}/U_{ref}^2$ and the non-dimensional vertical momentum flux, $\overline{u'w'}/U_{ref}^2$, are presented respectively in Figure 2.8- Figure 2.9. The canyon width variation significantly affects the variance of vertical velocity: for the narrow canyon, only on the top near the downstream wall, values are significantly higher than zero, whilst for AR_C = 1.0, a great amount of the canyon flow exhibits a high level of turbulence, in agreement with other authors statements (e.g. Bernardino et al., 2015). Irrespective of the canyon width, the two series show the same trend, with the maximum achieved around z/H = 1.15, above the roof, because of the effect of the shear layer generated from the building corner. The turbulent momentum flux appears negative outside the canyon and positive for z/H < 0.8 in both the cases. However, the range of flux values is smaller for the narrow canyon (Figure 2.9 a) where the absolute maximum is approximately halved compared to the case AR_C = 1.0. All these considerations converge and underline that a small ventilation is achieved for narrow canyons. Even if the differences observed between the two series, AR_C = 0.5 and AR_C = 1.0, are quite apparent, when we look at the maps of the fields corresponding to different building aspect ratios, at a given canyon shape, it is very difficult to appreciate the existing differences.

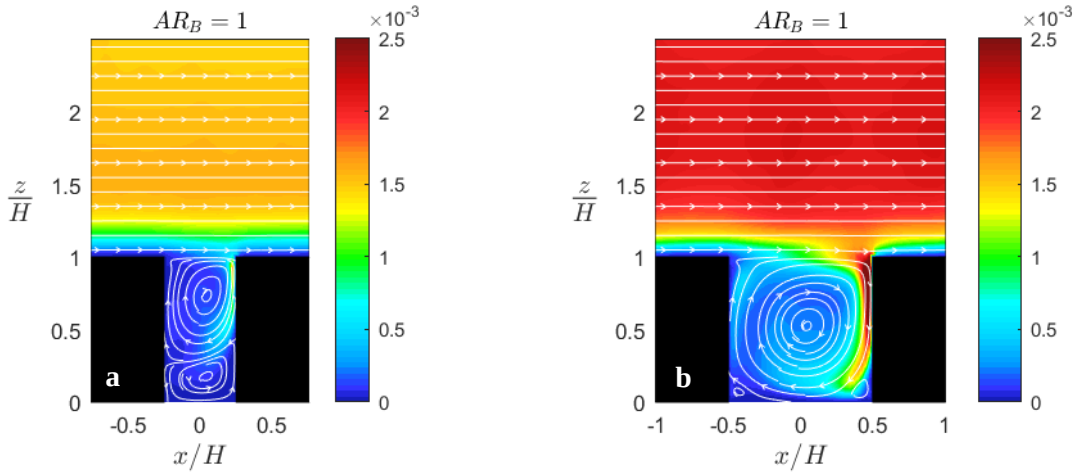

Figure 2.8 – Streamlines of the mean velocity field and variance of the vertical velocity component, made non dimensional by the free-stream velocity ($\overline{w'^2}/U_{ref}^2$). Building aspect ratio AR_B = 1. Canyon aspect ratios, AR_C = 0.5 (a) and AR_C = 1.0 (b).

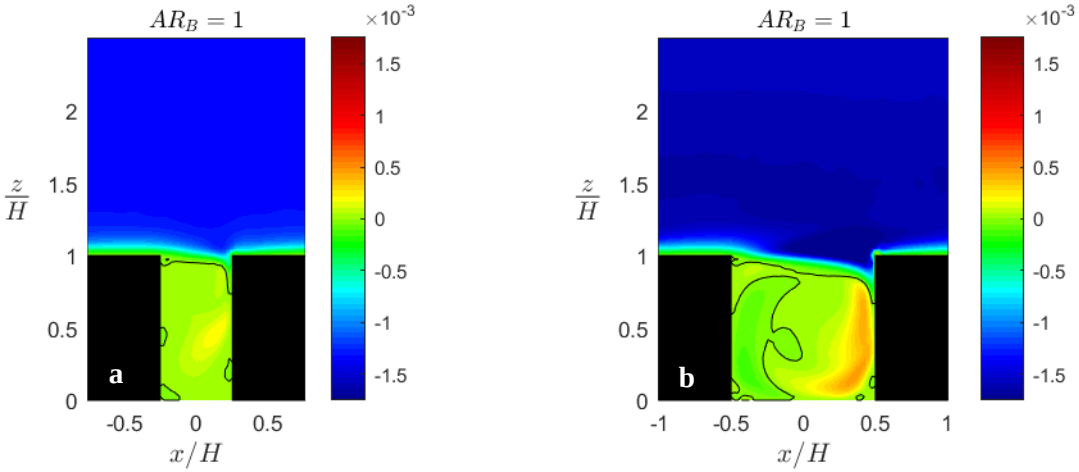

Figure 2.9 – Turbulent momentum flux field, made non dimensional by the free-stream velocity ($\overline{u'w'}/U_{ref}^2$). Building aspect ratio AR_B = 1. Canyon aspect ratios, AR_C = 0.5 (a) and AR_C = 1.0 (b). The black line represents zero values.

As matter of fact, with the aim to synthetically describe the effects due by the building aspect ratio on the flow structure, all the statistics have been horizontally averaged (Eq. 2.6), over one periodical roughness unit: i.e. from the middle point of the upwind building to the middle point of the downwind one, for the full domain height:

$$< \bar{\gamma}(z) >= \frac{1}{\lambda(z)} \int_{\lambda(z)} \bar{\gamma} dx \qquad 2.6$$

where γ is the generic temporally averaged parameter, z is the generic height and λ(z) is the horizontal integration line. The length λ(z) is dependent on the integration height (z): into the canyon is equal to the canyon width; above the canyon is equal to AR_C + AR_B. The resulting vertical profiles, made non-dimensional by the free-stream velocity at z/H = 9, are reported below, divided into two groups corresponding to the canyon width, because of the discussed behaviours. Focusing on the horizontal velocity profiles $\bar{u}/U_{ref}$ (Figure 2.10), differences are more evident above the canopy

where a quite regular increase of the mean velocity by increasing the building width is shown for both the two series.

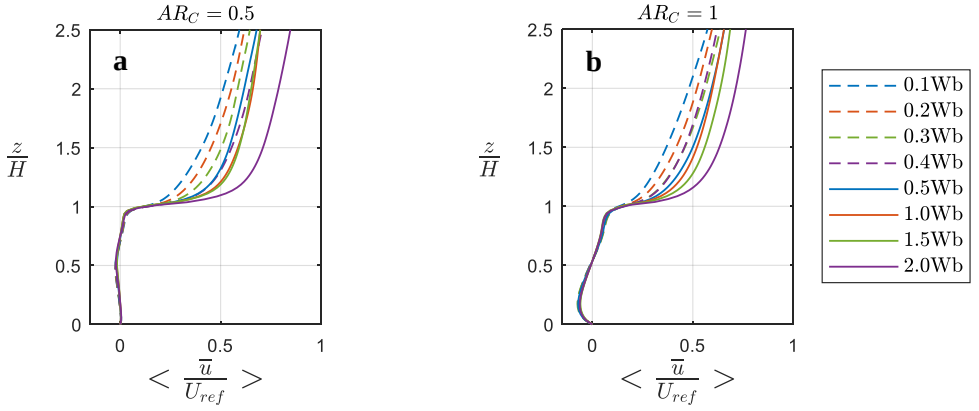

Figure 2.10 – Vertical profiles of the horizontally averaged stream-wise velocity for AR_C = 0.5 case (a) and AR_C = 1.0 (b). Values are made non-dimensional by the free stream velocity at z/H = 9. Different colours and styles indicate different building aspect ratios.

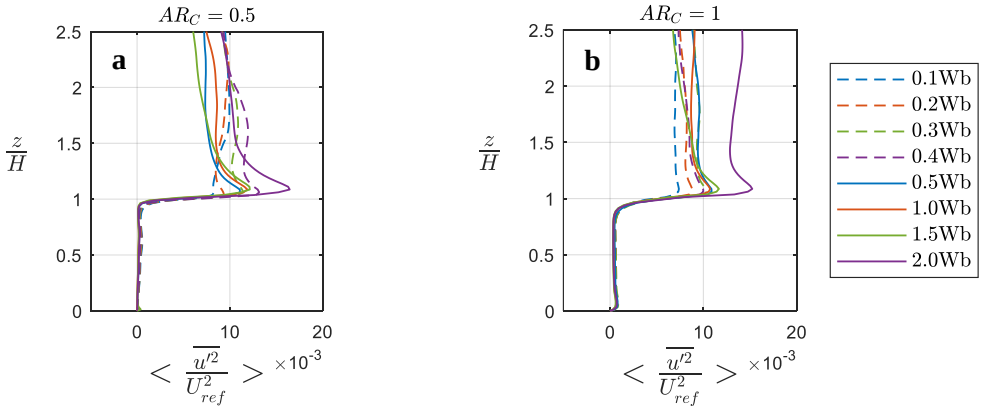

Figure 2.11 - Vertical profiles of the horizontally averaged variance of the vertical velocity for AR_C = 0.5 case (a) and AR_C = 1.0 (b). Values are made non-dimensional by the free stream velocity at z/H = 9. Different colours and styles indicate different building aspect ratios.

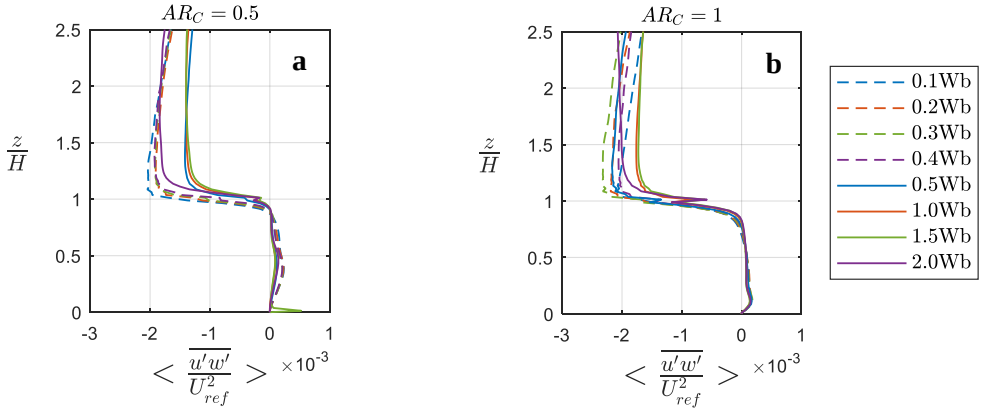

Figure 2.12 - Vertical profiles of the horizontally averaged turbulent momentum flux for AR_C = 0.5 case (a) and AR_C = 1.0 (b). Values are made non-dimensional by the free stream velocity at z/H = 9. Different colours and styles indicate different building aspect ratios.

Indeed, from the inflection point, irrespective of the canyon width, the profiles are characterised by different slopes, but they are all nearly logarithmic as typical of rough-wall boundary layers (Harman and Finnigan, 2007; Pelliccioni et al., 2016). Below this point, profiles seems to collapse in an singular trend: the velocity becomes negative below z/H ≈ 0.8, in narrowest canyons and below z/H ≈ 0.5 in the unitary ones, due to the recirculation mechanism dominating the regions.

About the second order statistics, the variance of the vertical velocity component $\overline{w'^2}/U_{ref}^2$ (Figure 2.11) is significantly affected by the building width especially in two zones: just below the roof level (at around z/H ≈ 0.9 for AR_C = 0.5 and z/H ≈ 0.8 for AR_C = 1.0) and just above, around z/H ≈ 1.2. Here profiles show a trend with decreasing values by increasing the canyons width from W_B = 0.1 to W_B = 2.0. Anyway, both the figures indicate the presence of an intense turbulent layer generated by the two-dimensional roughness just above the canopy. Regarding the internal canyon flow an increasing building width corresponds to a decrease of z position since W_B = 1 for narrow canyon and W_B = 2 for the unitary one.

Influence of AR_B at the horizontally-averaged turbulent momentum flux $\overline{u'w'}/U_{ref}^2$ (Figure 2.12), is mainly apparent outside the canyon cavity, for z/H ≥ 0.9. Indeed above this level, values became negative and they are shifted towards more negative values when cases with increasing AR_C and identical AR_B are considered. The curves present a maximum just above the roof, around the height z/H = 1.15, irrespective of the configuration and the highest values are recorder for AR_B = 0.1-0.3.

Finally, the general variability in turbulent quantities is faster in case of AR_C = 0.5 for the entire profile height. The vertical mean profiles seems to show a general benefit of employing narrow buildings on the ventilation and turbulent quantities, at the roof level, because of the higher interaction between the flow inside the canyon and the overlaying boundary layer. However, the positive or negative effects is strongly dependent on the source position, when a pollutant behaviour is considered.

2.4.3 Flux Exchange Index

As already stated in the previous sections, the bulk air exchange between the canyon and the external boundary layer occurs at the roof level interface and, under the ideal case of a well-mixed box, where the pollutant concentration is assumed constant within the canyon, the outflow rate on the top would be sufficient to describe the phenomenon. The averaged concentration within the canyon in fact, was found strongly dependent on the interaction between the recirculating flow and the incoming flow at the interface (i.e. Soulhac et al., 2008; Salizzoni, 2006). The idea of the well-mixed box model, was already treated by different authors (Fackrell, 1984b; Vincent, 1977; Weitbrecht et al., 2008) and it is here reported in order to clarify the concept. Considering a general tracer and the assumption that the concentration of the external flow is negligible, the mass removal per unit time can be expressed as:

$$\frac{dM}{dt} = -\phi_e C \qquad \textbf{2.7}$$

where M is the mass and $C = M/V_C$ is the concentration of the tracer, ϕ_e is the outflow rate across the interfacial surface and V_c is the volume. Furthermore C is assumed uniform. Dividing the Eq 2.7 by the canyon volume, the concentration can be defined as:

$$\frac{dC}{dt} = -\frac{\phi_e}{V_c} C \qquad \textbf{2.8}$$

Considering the prismatic canyons, like that employed in the present work, the volume can be written as the product of the cross-sectional area and the cross-stream length of the canyon: $V_C = S_C \times L$, thus:

$$\frac{dC}{dt} = -\frac{\varphi_e}{S_c} C \qquad 2.9$$

where φ_e is the outflow rate per unit length ($\varphi_e = \phi_e / L$).

With all these assumptions, the outflow rate per unit length was calculated at the rooftop level considering both the mean values of instantaneous vertical velocities and the contribution of the sole mean velocity field. As matter of fact, the total outflow rate $\varphi_e(z)$ was computed by integrating the absolute value of instantaneous velocity measurements over the line that ideally connect the canyon sidewalls, then it was averaged on the entire number of samples, as reported in Eq. 2.10. Similarly, the mean outflow contribution was evaluated by integrating the absolute values of the mean vertical velocities, over the same line at the rooftop interface, as shown in Eq. 2.11

$$\varphi_e(z) = \frac{1}{2}\overline{\int_{\lambda(z)} |w(t)| dx} \qquad 2.10$$

$$\varphi_{em}(z) = \frac{1}{2}\int_{\lambda(z)} |\overline{w}| dx \qquad 2.11$$

In order to estimate φ_e, was considered that, even if the inflow and outflow are istantaneously variable because of the flow through the cross-stream section, S_c, they are equal on average, since it is a 2D street canyon configuration. Therefore values can be computed by averaging outflow and inflow through the considered horizontal line (Perret et al., 2017; Tuna et al., 2013).

Evaluation for all the examined cases is reported below, in Table 2.1. Mean values for both the two configurations, slowly decrease in case of unitary canyon aspect ratio, from the narrowest buildings to $AR_B = 1.5$. The $AR_C = 0.5$ trend does not appear that clear at all: at narrow buildings it appear to increase together with the building width and from $AR_B = 0.3$, it starts to decrease, then assuming a similar shape respect the previous series. Regarding the mean outflow rate (φ_e), it decreases faster in case of narrow canyon, underlying that a change in buildings width strongly affects the exchange process. In general, as it can be expected, ventilation is higher in case of unitary canyon, but differences became negligible at very narrow buildings.

Table 2.1- Non –dimensional vertical profiles of outflow rates (φ_e and φ_{em} calculated at z/H = 1. Values were made non dimensional by the free stream velocity at z/H = 9 and the canyon width (W)

	AR_b	0.1	0.2	0.3	0.4	0.5	1.0	1.5	2.0
$AR_C = 0.5$	φ_e	0.0145	0.0126	0.0120	0.0107	0.0074	0.0061	0.0055	0.0066
	φ_{em}	0.0031	0.0033	0.0036	0.0034	0.0024	0.0021	0.0020	0.0027
$AR_C = 1.0$	φ_e	0.0162	0.0164	0.0163	0.0149	0.0150	0.0124	0.0116	0.0117
	φ_{em}	0.0051	0.0050	0.0050	0.0045	0.0045	0.0038	0.0036	0.0038

Despite the fact that the air quality within two-dimensional canyons is mainly controlled by the mixing process at the interface with the overlaying flow, the real world is more complex and the

pollutant concentration is far from uniform into the whole canyon: it may vary significantly with height. Therefore, it is useful give a more detailed description of the phenomenon. Indeed, to better understand the capability of air exchange at different canyon z levels, we estimated φ_e(z) and φ_{em}(z) as vertical profiles from the ground to the rooftop, over the 32 horizontal lines connecting the canyon sidewalls. Only φ_e(z) results are here reported (Figure 2.13 a, b, for AR_C = 0.5 and 1.0, respectively). The two series of data, show completely different trends according to the different topology of the flow. Indeed, as it could be expected, in case of narrow canyon the outflow rates are lower and pecks are quite halved respect to the larger canyon widths. For AR_C = 0.5 curves are not monotonic and presented one maximum at around $z/H = 0.7$ and a relative minimum around $z/H = 0.35$. For $z/H < 0.5$ the lower vortex generates only a weak vertical air exchange, and the contribution of the turbulence is predominant. Anyway, in that region, the overall outflow rate is meaningfully smaller compared to the region corresponding to the upper vortex, confirming a poor air ventilation in narrow canyons, especially at the pedestrian level. Analysing the case AR_C = 1.0 (Figure 2.13 b), all configurations have similar trends with a maximum at about z/H = 0.5, corresponding to the centre of the vortex that dominates the canyon.

Despite differences, these two scenarios are highly influenced by the building aspect ratio. Discrepancies are more appreciable at the maximum point and at the roof level and values increase with a decreasing AR_B for the entire canyon depth and even if they are very small, are not negligible.

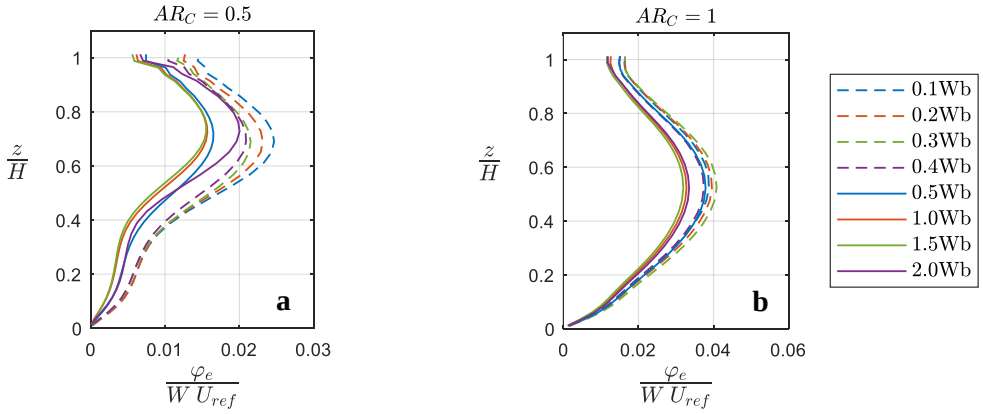

Figure 2.13 – Non-dimensional vertical profiles of exchange fluxes, φ_e calculated for narrow canyon (a) and unitary canyon (b), at different heigth (z/H) inside the canyon. Values were made non dimensionale by the free-stream velocity (U_{ref}) and the canyon width (W). Different colours indicate different canyon aspect ratios.

Anyway, we need to underline that reality is far more complex than this simplified set-up. Thus, for example, the shear layer generated from lateral openings and motions related to the corner vortex mechanism, which are here neglected, play a fundamental role in driving air exchange (i.e. Nosek et al., 2018). In addition to this, the submitted model can be considered valid only in case of uniform pollutant distribution inside the canyon, because of both the convective and total pollutant exchange mechanisms strongly depend on source locations (e.g. Kubilay et al., 2016).
These phenomena may vary in a relevant way with the building aspect ratio variations so that a focus on this could be evaluated in future works.

Finally, the mean residence time T_r was evaluated as a function of the building aspect ratio. In fact, the residence time is the parameter controlling the dynamic of pollutant removal and, referring to Eq. 2.8, $T_r = V_C/\phi_e$ represents its solution. Similarly, $T_r = S_C/\phi_e$, is the solution of the Eq. 2.9. Therefore, the residence time at the roof level was here calculated as defined in Eq. 2.12, where the volume may be rewritten as $V_c = S_c \times L$ and S_c is the cross-sectional area, L is the cross-stream length of the canyon.

$$T_r = \frac{V_C}{L * \varphi_{e(z=H)}} = \frac{S_C}{\varphi_{e(z=H)}} \qquad 2.12$$

Results made non-dimensional by the building height and the free-stream velocity are displayed in Figure 2.14. T_r, increases linearly with AR_B for the entire explored range in case of the unit canyon aspect ratio. Differently, in case of halved canyon width, the residence time increase until AR_B = 1.5, where a maximum was registered (in agreement with the behaviour of the outflow rate reported in Table 2.1). Comparing the two series of data, T_r is quite doubled if the AR_B = 0.1 is considered and then the differences increase achieving the maximum gap for AR_B = 1.5, where the residence time for narrow canyon is 3.5 times higher than the other. This fact underlines two main aspects: the orange series of data is affected by a very low ventilation and in turns, by a very poor capability of pollutant removal; the decreasing of building aspect ratio is more efficient in narrowest canyon, as evidenced by the curves inclination.

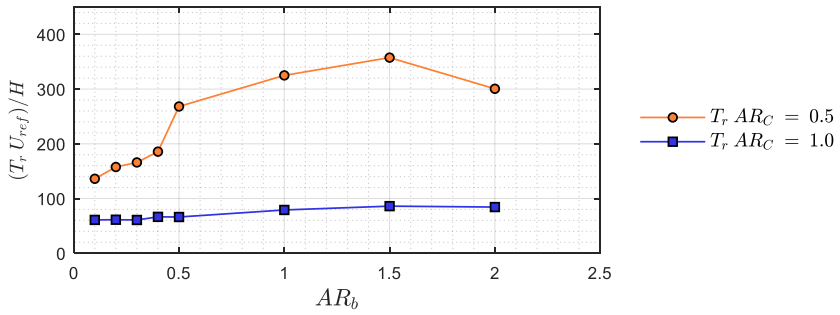

Figure 2.14 – Mean residence time, Tr, as a function of the building aspect ratio for AR_C = 0.5 (orange line with circles) and AR_C = 1.0 (blue line with squares)

2.5 Conclusions

In this chapter the effect of building aspect ratio on street canyon ventilation and turbulent flow characteristics were investigated, by means of a numerical model based on the LES technique. A virtually infinite series of two-dimensional street canyons with rectangular cross section was analysed considering two different canyon aspect ratios (AR_C = 0.5, 1.0), and eight aspect ratios of the buildings (AR_B = 0.1, 0.2, 0.3, 0.4, 0.5, 1.0, 1.5 and 2.0). Results were found strongly dependent on the building aspect ratios related with the canyon aspect ratio, but in the case of narrow buildings, higher turbulence levels and mean vertical velocities were estimated in both the canyon aspect ratios. The analysis of the exchange rates between the canyon and the overlaying boundary layer, indicated that the flow-rate increases for narrow buildings, irrespective of the canyon shape, and the minimum is observable for AR_B = 1.5. Finally, the residence time is linearly proportional to the building aspect ratio for the whole extent of the investigated rate in the case of unitary canyon width, and up to AR_B = 1.5 in the narrowest canyon case. However, the mean trends are characterised by a different slope. Concluding, even if results are affected by the simplifications employed in these analyses, they suggested that the building aspect ratio is a crucial parameter when predicting pollutant removal from urban canyons and in the modelling of the urban boundary layer characteristics.

2.6 References

Badas, M.G., Ferrari, S., Garau, M., Querzoli, G., 2017. On the effect of gable roof on natural ventilation in two-dimensional urban canyons. Journal of Wind Engineering and Industrial Aerodynamics 162, 24–34. https://doi.org/10.1016/j.jweia.2017.01.006

Badas, M.G., Salvadori, L., Garau, M., Querzoli, G., Ferrari, 2019. Urban areas parameterisation for CFD simulation and cities air quality analysis. International Journal of Environment and Pollution. http://www.inderscience.com/info/ingeneral/forthcoming.php?jcode=ijep

Baik, J.-J., Park, R.-S., Chun, H.-Y., Kim, J.-J., 2000. A Laboratory Model of Urban Street-Canyon Flows. J. Appl. Meteor. 39, 1592–1600. https://doi.org/10.1175/1520-0450(2000)039<1592:ALMOUS>2.0.CO;2

Bernardino, A.D., Monti, P., Leuzzi, G., Querzoli, G., 2015. Water-Channel Study of Flow and Turbulence Past a Two-Dimensional Array of Obstacles. Boundary-Layer Meteorol 155, 73–85. https://doi.org/10.1007/s10546-014-9987-2

Besalduch, L.A., Badas, M.G., Ferrari, S., Querzoli, G., 2014. On the near field behaviour of inclined negatively buoyant jets. EPJ Web of Conferences 67, 02007. https://doi.org/10.1051/epjconf/20146702007

Besalduch, L.A., Badas, M.G., Ferrari, S., Querzoli, G., 2013. Experimental Studies for the characterization of the mixing processes in negative buoyant jets. EPJ Web of Conferences 45, 01012. https://doi.org/10.1051/epjconf/20134501012

Blocken, B., 2015. Computational Fluid Dynamics for urban physics: Importance, scales, possibilities, limitations and ten tips and tricks towards accurate and reliable simulations. Building and Environment, Fifty Year Anniversary for Building and Environment 91, 219–245. https://doi.org/10.1016/j.buildenv.2015.02.015

Brown, M.J., Lawson, R.E., Decroix, D.S., Lee, R.L., 2000. Mean Flow and Turbulence Measurements Around a 2-D Array of Buildings in a Wind Tunnel. https://nepis.epa.gov/Exe/ZyPURL.cgi?Dockey=P100G6C6.txt

Chan, A.T., Au, W.T.W., So, E.S.P., 2003. Strategic guidelines for street canyon geometry to achieve sustainable street air quality—part II: multiple canopies and canyons. Atmospheric Environment 37, 2761–2772. https://doi.org/10.1016/S1352-2310(03)00252-8

Cheng, H., Castro, I.P., 2002. Near Wall Flow over Urban-like Roughness. Boundary-Layer Meteorology 104, 229–259. https://doi.org/10.1023/A:1016060103448

Cheng, W.C., Liu, C.-H., 2011. Large-Eddy Simulation of Flow and Pollutant Transports in and Above Two-Dimensional Idealized Street Canyons. Boundary-Layer Meteorol 139, 411–437. https://doi.org/10.1007/s10546-010-9584-y

Chung, T.N.H., Liu, C.-H., 2012. Large-eddy simulation of reactive pollutant dispersion for the spatial instability of photostationary state over idealised 2D urban street canyons. International Journal of Environment and Pollution 50, 411–419. https://doi.org/10.1504/IJEP.2012.051211

CRS4 | centro di ricerca, sviluppo e studi superiori in Sardegna . http://www.crs4.it/it/

Cui, Z., Cai, X., J. Baker, C., 2004. Large-eddy simulation of turbulent flow in a street canyon. Q.J.R. Meteorol. Soc. 130, 1373–1394. https://doi.org/10.1256/qj.02.150

Fackrell, J.E., 1984a. An examination of simple models for building influenced dispersion. Atmospheric Environment (1967) 18, 89–98. https://doi.org/10.1016/0004-6981(84)90231-2

Fackrell, J.E., 1984b. Parameters characterising dispersion in the near wake of buildings. Journal of Wind Engineering and Industrial Aerodynamics 16, 97–118. https://doi.org/10.1016/0167-6105(84)90051-5

Falchi, M., Querzoli, G., Romano, G.P., 2006. Robust evaluation of the dissimilarity between interrogation windows in image velocimetry. Exp Fluids 41, 279–293. https://doi.org/10.1007/s00348-006-0148-3

Farell, C., Iyengar, A.K.S., 1999. Experiments on the wind tunnel simulation of atmospheric boundary layers. Journal of Wind Engineering and Industrial Aerodynamics 79, 11–35. https://doi.org/10.1016/S0167-6105(98)00117-2

Ferrari, S., Badas, M.G., Garau, M., Seoni, A., Querzoli, G., 2017. The air quality in narrow two-dimensional urban canyons with pitched and flat roof buildings. International Journal of Environment and Pollution 62, 347–368. https://doi.org/10.1504/IJEP.2017.089419

Franke, J., Hellsten, A., Schlunzen, K.H., Carissimo, B., 2011. The COST 732 Best Practice Guideline for CFD simulation of flows in the urban environment: a summary. International Journal of Environment and Pollution 44, 419–427. https://doi.org/10.1504/IJEP.2011.038443

Garau, M., Badas, M.G., Ferrari, S., Seoni, A., Querzoli, G., 2018. Turbulence and Air Exchange in a Two-Dimensional Urban Street Canyon Between Gable Roof Buildings. Boundary-Layer Meteorology 167, 123–143. https://doi.org/10.1007/s10546-017-0324-4

Gerdes, F., Olivari, D., 1999. Analysis of pollutant dispersion in an urban street canyon. Journal of Wind Engineering and Industrial Aerodynamics 82, 105–124. https://doi.org/10.1016/S0167-6105(98)00216-5

Hang, J., Li, Y., 2011. Age of air and air exchange efficiency in high-rise urban areas and its link to pollutant dilution. Atmospheric Environment 45, 5572–5585. https://doi.org/10.1016/j.atmosenv.2011.04.051

Harman, I.N., Finnigan, J.J., 2007. A simple unified theory for flow in the canopy and roughness sublayer. Boundary-Layer Meteorol 123, 339–363. https://doi.org/10.1007/s10546-006-9145-6

Harris C., Stephens M.,1988. A combined corner and edge detector. In: Alvey vision conference. Citeseer, pp 10–5244

Hassan, A.A., Crowther J.M., 1998. Modelling of fluid flow and pollutant dispersion in a street canyon. J. Environ Monit Assess (1998) 52: 281. https://doi.org/10.1023/A:1005928630000.

Hoydysh, W.G., Dabberdt W.F., 1988. Kinematics and dispersion characteristics of flows in asymetric street canyons. Atmos Environ 22(12):2677–2689. https://doi.org/10.1016/0004-6981(88)90436-2

Hoydysh, W.G., Griffiths, R.A., Ogawa, Y., 1974. A scale model study of the dispersion of pollution in street canyon. APCA Paper, APCA Paper 74–157. https://doi.org/Presented at the 67th APCA Annual Meeting

Kanda, M., 2006. Large-Eddy Simulations on the Effects of Surface Geometry of Building Arrays on Turbulent Organized Structures. Boundary-Layer Meteorol 118, 151–168. https://doi.org/10.1007/s10546-005-5294-2

Kovar P. A., Louka, P., Sini, J.-F., Savory, E., Czech, M., Abdelqari, A., Mestayer, P.G., Toy, N., 2002. Influence of Geometry on the Mean Flow within Urban Street Canyons – A Comparison of Wind Tunnel Experiments and Numerical Simulations. Water, Air, & Soil Pollution: Focus 2, 365–380. https://doi.org/10.1023/A:1021308022939

Kubilay, A., Neophytou, M.K.-A., Matsentides, S., Loizou, M., Carmeliet, J., 2017. The Pollutant Removal Capacity of an Urban Street Canyon and its Link to the Breathability and Exchange Velocity. Procedia Engineering, International High-Performance Built Environment Conference – A Sustainable Built

Environment Conference 2016 Series (SBE16), iHBE 2016 180, 443–451. https://doi.org/10.1016/j.proeng.2017.04.203

Li, X.-X., Britter, R.E., Koh, T.Y., Norford, L.K., Liu, C.-H., Entekhabi, D., Leung, D.Y.C., 2010. Large-Eddy Simulation of Flow and Pollutant Transport in Urban Street Canyons with Ground Heating. Boundary-Layer Meteorol 137, 187–204. https://doi.org/10.1007/s10546-010-9534-8

Li, X.-X., Liu, C.-H., Leung, D.Y.C., 2009. Numerical investigation of pollutant transport characteristics inside deep urban street canyons. Atmospheric Environment 43, 2410–2418. https://doi.org/10.1016/j.atmosenv.2009.02.022

Millward-Hopkins, J.T., Tomlin, A.S., Ma, L., Ingham, D., Pourkashanian, M., 2011. Estimating Aerodynamic Parameters of Urban-Like Surfaces with Heterogeneous Building Heights. Boundary-Layer Meteorol 141, 443–465. https://doi.org/10.1007/s10546-011-9640-2

Murena, F., Mele, B., 2016. Effect of balconies on air quality in deep street canyons. Atmospheric Pollution Research 7, 1004–1012. https://doi.org/10.1016/j.apr.2016.06.005

Neophytou, M.K.-A., Markides, C.N., Fokaides, P.A., 2014. An experimental study of the flow through and over two dimensional rectangular roughness elements: Deductions for urban boundary layer parameterizations and exchange processes. Physics of Fluids 26, 086603. https://doi.org/10.1063/1.4892979

Nosek, Š., Fuka, V., Kukačka, L., Kluková, Z., Jaňour, Z., 2018. Street-canyon pollution with respect to urban-array complexity: The role of lateral and mean pollution fluxes. Building and Environment 138, 221–234. https://doi.org/10.1016/j.buildenv.2018.04.036

Oke, T.R., 1988. Street design and urban canopy layer climate. Energy and Buildings 11, 103–113. https://doi.org/10.1016/0378-7788(88)90026-6

Pelliccioni, A., Monti, P., Leuzzi, G., 2016. Wind-Speed Profile and Roughness Sublayer Depth Modelling in Urban Boundary Layers. Boundary-Layer Meteorol 160, 225-248.https://doi.org/10.1007/s10546-016-0141-1

Perret, L., Blackman, K., Fernandes, R., Savory, E., 2017. Relating street canyon vertical mass-exchange to upstream flow regime and canyon geometry. Sustainable Cities and Society 30, 49–57. https://doi.org/10.1016/j.scs.2017.01.001

Salizzoni, P., 2006. Mass and momentum transfer in the urban boundary layer. Thèse de doctorat dirigée par Perkins, Richard Mécanique des fluides Ecully, Ecole centrale de Lyon, pp 177. http://www.theses.fr/2006ECDL0015.

Smagorinsky, J., 1963. General circulation experiments with the primitive equations. Mon. Wea. Rev. 91, 99–164. https://doi.org/10.1175/1520-0493(1963)091<0099:GCEWTP>2.3.CO;2

Soulhac, L., 2000. Modélisation de la dispersion atmosphérique à l'intérieur de la canopée urbaine. Thèse de doctorat dirigée par Perkins, Richard Mécanique Ecully, Ecole centrale de Lyon, pp 345. http://www.theses.fr/2000ECDL0007

Soulhac, L., Perkins, R.J., Salizzoni, P., 2008. Flow in a Street Canyon for any External Wind Direction. Boundary-Layer Meteorology 126, 365–388. https://doi.org/10.1007/s10546-007-9238-x

Tominaga, Y., Mochida, A., Yoshie, R., Kataoka, H., Nozu, T., Yoshikawa, M., Shirasawa, T., 2008. AIJ guidelines for practical applications of CFD to pedestrian wind environment around buildings. Journal of Wind Engineering and Industrial Aerodynamics, 4th International Symposium on Computational Wind Engineering (CWE2006) 96, 1749–1761. https://doi.org/10.1016/j.jweia.2008.02.058

Tuna, B.A., Tinar, E., Rockwell, D., 2013. Shallow flow past a cavity: globally coupled oscillations as a function of depth. Exp Fluids 54, 1586. https://doi.org/10.1007/s00348-013-1586-3

Uehara, K., Wakamatsu, S., Ooka, R., 2003. Studies on critical Reynolds number indices for wind-tunnel experiments on flow within urban areas. Boundary-Layer Meteorology 107, 353–370. https://doi.org/10.1023/A:1022162807729

Vardoulakis, S., Fisher, B.E.A., Pericleous, K., Gonzalez-Flesca, N., 2003. Modelling air quality in street canyons: a review. Atmospheric Environment 37, 155–182. https://doi.org/10.1016/S1352-2310(02)00857-9

Vincent, J.H., 1977. Model experiments on the nature of air pollution transport near buildings. Atmospheric Environment (1967) 11, 765–774. https://doi.org/10.1016/0004-6981(77)90186-X

Weitbrecht, V., Socolofsky, S.A., Jirka, G.H., 2008. Experiments on Mass Exchange between Groin Fields and Main Stream in Rivers. Journal of Hydraulic Engineering 134, 173–183. https://doi.org/10.1061/(ASCE)0733-9429(2008)134:2(173)

Wong, C.C.C., Liu, C.-H., 2012. Pollutant dispersion over two-dimensional idealised urban roughness: a large-eddy simulation approach. International Journal of Environment and Pollution 50, 64–74. https://doi.org/10.1504/IJEP.2012.051181

Xie, X., Huang, Z., 2007. Impact of aspect ratio and surface heating on pollutant transport in street canyons. J Mech Sci Technol 21, 1781. https://doi.org/10.1007/BF03177433

Xie, Z.-T., Coceal, O., Castro, I.P., 2008. Large-Eddy Simulation of Flows over Random Urban-like Obstacles. Boundary-Layer Meteorol 129, 1. https://doi.org/10.1007/s10546-008-9290-1

Zhong, J., 2016. Modelling air pollution within a street canyon. Ph.D. thesis, University of Birmingham. http://ethese.bham.ac.uk/6491/

Zhong, J., Cai, X.-M., Bloss, W.J., 2015. Modelling the dispersion and transport of reactive pollutants in a deep urban street canyon: Using large-eddy simulation. Environmental Pollution 200, 42–52. https://doi.org/10.1016/j.envpol.2015.02.009

Chapter 3

2D street Canyon: influence of roof shape

Part of this chapter was published as:

Garau, M., Badas, M.G., Ferrari, S., Seoni, A., Querzoli, G., 2018. Turbulence and Air Exchange in a Two-Dimensional Urban Street Canyon Between Gable Roof Buildings. Boundary-Layer Meteorology, vol. 167, n. 1, pp. 123–143.

3.1 Summary

In this chapter the effect of a typical building covering with gabled roofs, was experimentally and numerically investigate for a wide range of configurations. Despite the variety and complexity of the urban canopy, we focus on a simple, prototypal shape, the two-dimensional canyon, with the aim of elucidating some fundamental phenomena driving the street-canyon ventilation. Experimental simulations were performed in a water channel, over an array of identical prismatic obstacles representing a urban canopy. The aspect ratio, i.e. canyon-width to building-height ratio (AR_C), ranges from 1 to 6 and gable roof buildings with 1:1 pitch (45° slope) were compared with flat roofed buildings (0° slope). Numerical simulations were employed in order to study the variability of gable roof slopes, from 0° to 45° (0°, 10°, 20°, 30°, 45°), by choosing the most common configurations with AR_C = 1, 2. Flow dynamics were discussed in terms of mean flow and second and third order statistical moments of the velocity. The well mixed-box theory was employed to estimate the air exchange mechanism, by computing the outflow rate and mean residence time. Results show that gable roofs tend to delay the transition from the skimming-flow to the wake-interference regime and promote the development of a deeper and more turbulent roughness layer. The presence of a gable roof significantly increases the momentum flux, especially for high packing density. The air exchange is improved compared to the flat roof buildings, and the beneficial effect is more significant for narrow canyons. However, not every roof shape positively effects ventilation, so that an optimum should be identified with reference to the considered flow regime.

3.2 Introduction

Poor air quality is a serious problem especially in modern, large cities and it is responsible for chronic and acute damages on human health. This phenomenon is mainly associated by motor vehicles emissions that effect the atmosphere mainly within the space among buildings. The interaction between the characteristics of the flow and the urban canopy is the key problem since these effect the air quality both outdoor and indoor. Typically, the urban scenario is very complex and heterogeneous with different parameters and variables such as building arrangements, orientation and shape, green areas, terrain structure, vehicle traffic, etc. For this reason is quite impossible to understand the influence of every element unless simplifications are taken into account. As matter of fact site-specific investigations can be performed by means detailed numerical simulations or reduce-scale models, including all the detailed of the specific city portion, even if they are computationally expansive (Blocken et al., 2012; Carrasco-Hernandez et al., 2015; Janssen et al., 2013; Kastner-Klein and Rotach, 2004). Several studies have been undertaken, both experimentally and numerically, to investigate dispersion in the urban boundary layer from the street-scale (∼100–200 m) to the district-scale (∼1–2 km), (Britter and Hanna, 2003) and with different specific objectives. Most of them, are made on single blocks (Castro and Robins, 1977; Martinuzzi and Tropea, 1993; Sousa and Pereira, 2004; Tominaga et al., 2015) or identical array of them (Brown et al., 2000; Neophytou et al., 2014; Bernardino et al., 2015). However it is well known that geometries influence in different ways fluid dynamics. In order to model pollutant transport and energy balance in an urban environment, several physically based urban canyon models have been developed and are included in many micro-scale meteorological and dispersion model (Amicarelli et al., 2012; Fallah-Shorshani et al., 2017; Pelliccioni et al., 2015). Hence investigation on simple, basic configurations may provide important contribution on basic phenomena comprehension.

The air quality within the street canyons depends on the air exchange with the overlaying atmosphere, which, in turn, is driven by the shear layer generated at the roof level. As a consequence, the roof shape causes deep modification in the urban roughness sub-layer and have a key role in the canyon ventilation. Rafailidis, (1997) performed wind tunnel experiments with two different packing densities with flat and pitched roofs with 45° slope, and found that ventilation in the higher part of the canyon is strongly dependent on the roof shape. Afterwards, several experimental (Kastner-Klein and Plate, 1999; Kellnerová et al., 2014) and numerical simulation (Nosek et al., 2017; Takano and Moonen, 2013; Xie et al., 2005; Yassin, 2013) suggested that the shape of adjacent buildings could be an effective element to reduce pollution within street canyons. Recently, Ozmen et al., (2016) investigated isolated buildings with three different pitches angles and described differences occurring in recirculation regions, in the kinetic energy and in the pressure fields. Therefore, their results are limited on one of the three flow regimes defined by Oke, (1988). In a previous work (Badas et al., 2017), by using RANS numerical modelling, a systematic analysis of the effect of the roof slope and canyon aspect ratio on air exchange between the street canyon and the overlaying atmospheric boundary layer, was performed. A single linear relation was founded between the square root of the friction coefficient and the turbulence-driven ventilation, despite the roof pitch. However, due to the numerical model adopted, they could not give detailed information about turbulent quantities and structures. Some other very specific studies were arranged to analyze practical problem, as tornado (Hu et al. 2011) or buildings with particulars (i.e. Perén et al. 2016). Among these, a meaningful branch, that is important to cite, concerns about roof mounting wind turbines (i.e. Abohela et al. 2013).

Actually, despite these works suggest the importance of the roof shape, there is no systematic investigation on turbulent characteristics of the flow in street canyons between gable roof buildings has been carried out. Therefore, in order to reveal how the presence of gable roofs affects the turbulent

characteristics of the flow and ventilation in both the skimming flow and the wake interference regimes (Oke, 1988), two series of data were performed. Indeed, two series of complementary simulations were performed: the first one is about experimental simulations carried out in a water channel, with arrays of identical two-dimensional street canyons with variables aspect ratios, i.e. canyon-width to building-height ratio (AR_C = W/H = 1, 2, 3, 4, 6), and gable roof buildings with 1:1 pitch (45° slope), compared with flat roofed buildings (0° slope); the second one is about numerical simulations (LES) made in order to study the variability of gable roof slopes, from 0° to 45° (0°, 10°, 20°, 30°, 45°) with aspect ratios AR_C = 1, 2. . Results are described in terms of mean flow, second and third order statistics of the velocity. Moreover, the air exchange mechanism and the mean residence time were evaluated.

The chapter is organised as follows. Section 3.3 presents the numerical model, computational domain and numerical set-up. In section 3.4, experimental (3.4.2) and numerical (3.4.3) results are discussed. Then, in section 3.5 conclusions are drawn, giving an overview about limitations of present works and forthcoming steps.

3.3 Methods

As previously stated, flow was investigated with both laboratory and numerical simulations. The two-dimensional street canyons configuration, formed by identical buildings with flat or symmetrical dual-pitched roofs, was adopted varying the roof slope and the canyon aspect ratio, by fixing the wind flow perpendicular to the canyon axis, which is the worst condition for air ventilation and pollution removal from the canyon. The employed techniques and set-up are discussed below.

3.3.1 Experimental Simulations

The experiments were carried out in a closed-loop water channel at the University of Cagliari. The channel, schematically represented in Figure 3.1 is 8.0 m long, 0.40 wide and 0.50 m deep and fed by a constant head reservoir (1), with the mean flow rate regulated by a sharp-crested weir at the discharge and (2). During the experiments, the weir height was regulated so that the water depth was h = 0.42 m and the free-stream velocity $U_{ref} = 0.36\ m/s$, with a 0.10 m thick honeycomb (3) placed at the inlet of the channel as a flow straightener. A series of 20 equidistant, prismatic obstacles representing the buildings (4) was placed at the end of the channel; the obstacles consisted of 20x20 mm^2 squared section bars, eventually equipped with an additional triangular prism representing a 45° slope gable roof. The bars are hooked to a sheet and everything is painted in black to avoid laser reflections. Obstacles spanned through the whole width of the channel, in order to represent an idealised two-dimensional canopy. Measurements were performed on a 17^{th} canyon, which was located 6.15 m downstream from the honeycomb. The 16 identical canyons upstream from the test section ensured that the roughness layer generated by the building series reached its equilibrium (Brown et al., 2000; Llaguno-Munitxa et al., 2017). As a consequence, the flow in the investigated region was representative of a roughness layer over a virtually infinite series of canyons and weakly dependent on the flow upstream from the buildings. Nonetheless, to promote the rapid development of the turbulent boundary layer upstream from the obstacles, irregularly distributed pebbles (5) with 5 mm in diameter, were glued to the bottom of the channel downstream from the honeycomb grid for a total length of 3.0 m. Measurements were performed by means of a two-frame particle tracking velocimetry developed in-house in order to be robust to high velocity gradients and seeding density variations (Besalduch et al., 2014, 2013). Pine pollen particles (20-µm mean diameter) were uniformly dispersed in the working fluid before the experiments and the vertical stream-wise mid-plane of the channel was illuminated by a 2-mm thick light sheet generated by o diode laser (6), 532 nm in wavelength and 2 W

in power, through an optical system consisting of a cylindrical lens and a mirror. A high-speed camera (2240x1740 pixels in resolution), placed orthogonal to the measurement plane recorded 310 frames per second (7). The framed area was 0.15 m x 0.12 m, with a resulting spatial resolution of 67 μm per pixel, and centred on the last but two canyon, as above mentioned. The velocity field was obtained by comparing pairs of successive frames. Firstly, particles were identified on the first frame as regions with high intensity gradients by means of the Harris detector (Rosten and Drummond, 2006). Secondly, interrogation windows centred on particle positions in the first frame were compared with shifted windows in the second frame for a range of possible displacements. For each displacement, the dissimilarity between windows was determined by means of the Lorentzian estimator (Falchi et al., 2006) and the particle velocity was obtained as the displacement that minimized the dissimilarity divided by the time interval between frames. For each configuration, 48.000 velocity fields were measured; velocity fields were acquired in 40 separated recording session (1200 fields at 310 Hz each) in order to increase the statistical independence of the dataset. Uncertainty in the evaluation of the statistics presented in the following has been estimated from their standard deviation computed over the 40 recording sessions (Bendat and Piersol, 2011) and is reported in the captions of the corresponding figures. The height, H, of the eaves was chosen as a length scale and kept constant in all configurations (H = 20 mm), (Figure 3.2). Five different values of AR_C = W/H, were explored (AR_C = 1, 2, 3, 4, 6) by varying the canyon width, W, from 20 mm up to 120 mm.

For each aspect ratio, two building shapes were compared: gable roof with 45° slope and flat roof with the same eaves height (H). The building width was W = H = 20 mm in all cases. It should be noted that, equivalently, also the total height of the building could have been chosen as a length scale: however the eaves height was chosen in order to keep the habitable volume of the building constant, which is the most significant parameter in urban planning. As a results, obstacles of different overall heights were compared and some variations in the flow could be ascribed to that discrepancy.

A preliminary study characterizing the approaching flow were conducted by measuring the profile just upstream from the first prismatic obstacle. The left panel of Figure 3.3 show the vertical profile of the stream-wise component of the mean velocity, with the logarithmic law: $\bar{u} = (u_*/k)\ln(z/z_0)$ superimposed;where $u_* = 20\,mm/s$ $(u_*/U_{ref} = 0.055)$ and $z_0 = 0.152\,mm$ $z_0/H = 0.0076$ are the best fitting values of the friction velocity and roughness length, respectively, and k = 0.4 is the von Karman constant. Comparison of the experimental data points with their best fit line demonstrates that the incoming velocity profile follows the typical logarithmic law of the turbulent boundary layer up to about $z = 7H$, even if a small deviation is observed from $4H$. This height is always much larger than the building height, but becomes comparable to the canyon width for the largest aspect ratios. The right panel of Figure 3.3 reports the non-dimensional standard deviations of the stream-wise and vertical velocity components, made non-dimensional by the free-stream velocity U_{ref}. Values on the ground are low compared to atypical atmospheric boundary layer, presumably because of the characteristics of the bottom surface upstream from the buildings. However, as above mentioned, the boundary layer was here investigated only after it reached its equilibrium over the virtually infinite series of obstacles, where the flow mainly depends on the packing density and shape of the obstacles and it is nearly independent of the upstream conditions. Due to the reached equilibrium, the inflow conditions of the test section are about the same as those presented in the results. The Reynolds number based on the free-stream velocity and the building height, H, was found equal to $Re = U_{ref}H/\nu = 7000$, well above the threshold for the incoming velocity profile and large turbulence structures of the flow to be independent of Reynolds number. In addition to the above criterion, in order to ensure the Reynolds-number independency also between the roughness elements,

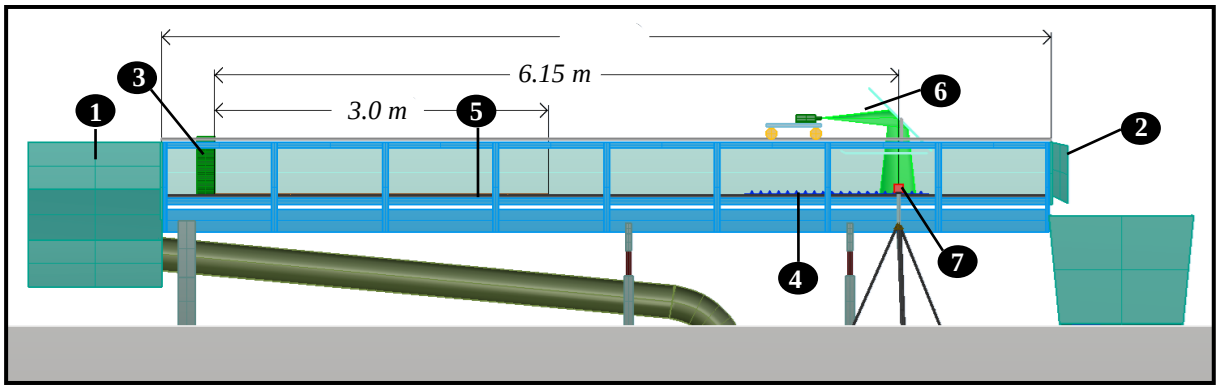

Figure 3.1- Water channel facility representation. (1) Constant head reservoir; (2) sharp-edged weir; (3) honeycomb; (4) array of 20 buildings; (5) 3 m pebbles panels; (6) laser and mirror; (7) high-speed camera.

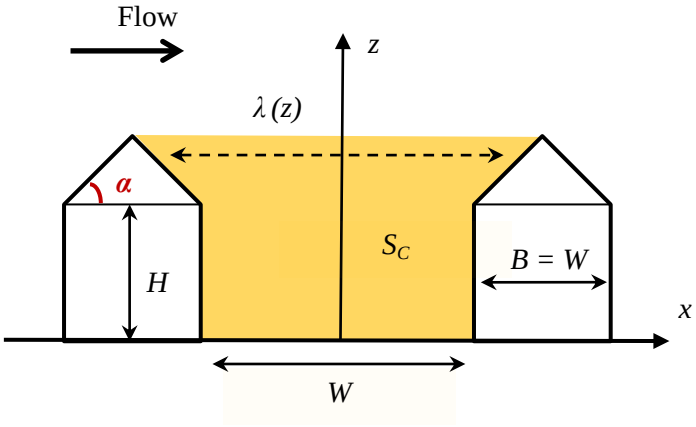

Figure 3.2 – Schematic representation of urban canyon geometry with gable roofs. H: eave height; B: building width; W: canyon width; λ(z): line between buildings at a generic height z; S_C: cross-section of the canyon (shaded in yellow).

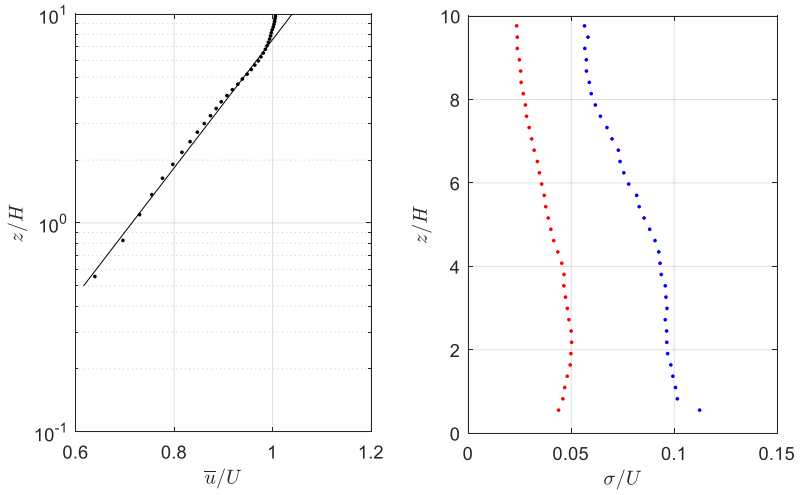

Figure 3.3 - Left panel: vertical profile of the mean stream-wise velocity component made non-dimensional by the free-stream velocity, $U=U_{ref}$ (dots) measured just upstream of the buildings. The straight line represents the logarithmic best fit line. Right panel: Standard deviation, σ, of the stream-wise (blue dots) and vertical (red dots) velocity component made non-dimensional by the free-stream velocity, U. Maximum uncertainty in the estimation of the mean velocity is ± 0.5×10^{-4} U_{ref}, while the uncertainty in the estimation of the standard deviation for the given finite-size dataset (48000 samples) is ± 0.3% (Bendat and Piersol, 2011).

Uehara et al., (2003), propose to check that the fluid velocity decrease due to the viscous stress in the canyon is negligible. They indicate that the velocity decrease exceeds 10% when $z_+ = zu_*/\nu < 20$, i.e. in our case, $z < 1$ mm. Therefore, in the bulk of the canyon the flow can be assumed Re independent.

Before running the experiments, preliminary series of measurements were performed in order to verify that the characteristics of the flow within the canyon were laterally homogeneous within a range of 50 mm from the symmetry, vertical plane. They were also carried out with the aim to assure that the mean flow was actually aligned with the channel main axis and no significant secondary flows were present, and that characteristics of the flow within the upstream and downstream canyons were the same as in the test canyon.

Finally, it should be mentioned that the present results are obtained with steady boundary conditions and do not include the natural time variability in wind speed and direction of the atmospheric boundary layer.

3.3.2 Numerical Simulations

The Large Eddy Simulation technique with the Smagorinsky sub-grid scale model (Smagorinsky, 1963) was used in order to perform numerical simulations, making use of the OpenFoam 2.3.1, which solves the approximate form of the governing equations by means of the finite volume method (FVM). Second-order-accurate schemes were used for the time and space derivatives. The large time-step transient solver for incompressible flow, was employed for the pressure-velocity coupling scheme, using the PIMPLE algorithm (merged PISO-SIMPLE). All LES simulations were initialised with the solution of a preliminary series of RANS simulations (Reynolds-Averaged Navier-Stokes). Ten different building configurations were performed by setting periodic boundary conditions both in the stream-wise and in the span-wise direction, in order to mimic a series of idealised 2D street canyons. The spatial domain, which consist of 3 canyons and 4 buildings (the side buildings are halved), is 9H in the vertical direction (z axis) and 9H in the span-wise one (y axis). Is important to underline that 9 times the building length scale (H) is the minimum requested by the guidelines (see Blocken, 2015; Franke et al., 2011; Tominaga et al., 2008), taking into account that where gabled roofs are employed, the maximum building height is 1.5H for α = 45°. Domain size in the stream-wise direction (x axis), measured in building width units, ranges from 6H to 9H, depending on the canyon width. Structured mesh with grid stretching both in stream-wise and vertical direction, was employed in order to discretised the domain: a higher resolution was imposed near building walls and the ground (Δx=Δy=0.016H), whilst at the canyon centre the cell size was doubled. The mean stream-wise velocity has been chosen in order to obtain a Reynolds number higher than the minimum of 3400 at the building height ($Re = U_{ref}H/\nu = 7000$). The dimensional time-step increment was set in order to assure that the Courant number was always smaller than 0.6 at all grid points. The results were averaged over a minimum of 1350 time steps, as well as in the span-wise direction, verifying that the simulation time was sufficient to obtain statistically-steady and representative results. Further information about numerical set-up was deeper described in Section 2.3.1 of this thesis.

3.4 Results

3.4.1 Validation

Numerical and experimental results were compared together and with literature works, by measuring 5 vertical (x/H = -0.4, -0.25, 0, 0.25, 0.4) from the 1st to the 3rd order velocity statistic. Results for the most common configuration ($AR_B = AR_C = 1$). are reported in Section 2.4.1.

3.4.2 Flat and gabled roofs for different flow regimes

3.4.2.1 Mean and turbulent flow fields

Qualitative analysis of the flow at different aspect ratios, immediately shown differences occurring between the two roof configurations (flat and gabled).

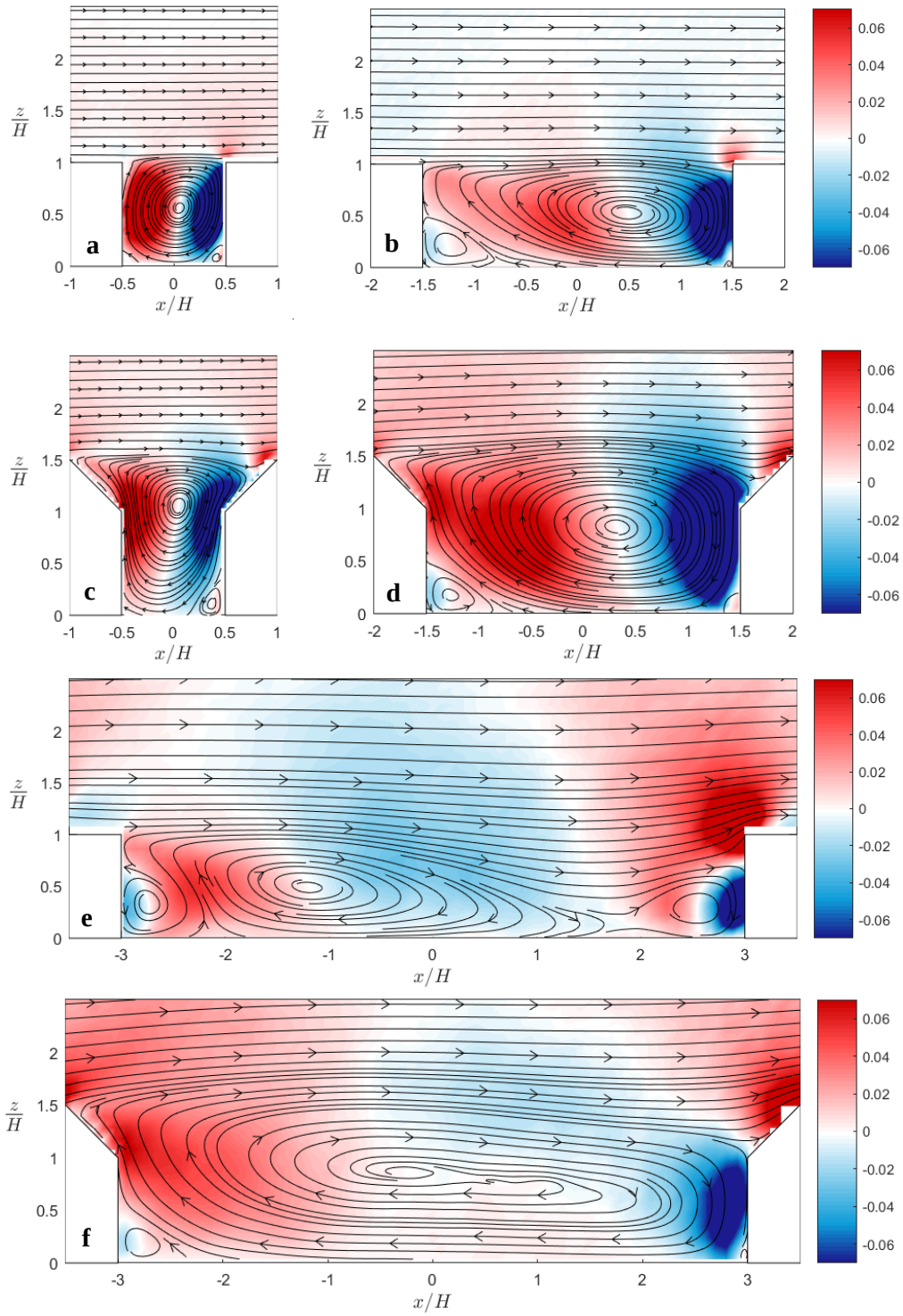

Figure 3.4 - Streamlines of the mean velocity field and mean vertical velocity component, made non dimensional by the free-stream velocity ($\overline{w}/U_{ref}$). Canyon aspect ratios, AR_C = 1, α = 0° (a); AR_C = 3, α = 0° (b); AR_C = 1, α = 45° (c); AR_C = 3, α = 45° (d); AR_C = 6, α = 0° (e); AR_C = 6, α = 45° (f). Colour scale is common for all the panels. Maximum uncertainty in the mean velocity estimation over the maps is ± 5.0 × 10^{-3} U_{ref}

In Figure 3.4 the streamlines are superimposed on the vertical velocity component ($\overline{w}/U_{ref}$) colour map; they show the overall structure of the flow for the different flow regimes, i.e. the skimming flow regime (Figure 3.4 a) the wake interference regime (Figure 3.4 b) and the upcoming isolated roughness regime (Figure 3.4 e), as defined by Oke, (1988) for flat roofs configuration. In order to assess the changes driven by the roof slope on the flow pattern, flat ad gable roofs are presented for the identical aspect ratios.

Results for AR_C = 1 (Figure 3.4 a, c) present the typical structure of the skimming flow regime, with a unique big vortex and two small recirculating vortexes at the lower corners on the ground. However, a few differences arise between them: the main vortex centre move up in case of gable roof (from z/H ≈ 0.55 to z/H ≈ 1.05 for flat and gable roofs respectively). The upward shift is larger than that justified by the overall building height increase since the centre moves a mid-height of the canyon (i.e. z/H ≈ 0.75). This mean that differences are only in part due to the increased total height of the buildings. In addition to this, also at the interface region roofs affect the flow, thus the streamlines appear strongly perturbed and a region of downward flow extends out of the canyon in the downwind half of the interface. Differently, at the flat roof interface, streamlines appear undisturbed. The reattachment point that in case of flat roof is close to the eaves at the windward building corner, in case of roofs is located at 2/3 of the windward pitch length, above the eaves (x/H = 0.8, z/H = 1.3). Vertical velocities appear higher in the second upper part of the canyon with gable roof and extended up to the eaves level, causing the perturbation at interface. In the meantime, very low values are visible at pedestrian level.

For AR_C = 3 (Figure 3.4 b, d) the flow inside the canyon, is characterised by two counter-rotating vortexes, well evident in case of flat roof and less developed for the other configuration. The transition between the two regimes (skimming flow and wake interference regimes) individuated at AR_C ≈1.5 for idealised two-dimensional street canyon (Sini et al., 1996; Ngan and Lo, 2016) was respected by present experiments. As matter of fact, for flat roofs and AR_C = 2, not reported here for a sake of brevity, two counter rotating vortexes are well represented (see Garau et al., 2018). For gable roof case, this transition is delayed, thus for AR_C = 3 appears not yet developed. Also in this aspect ratio, the streamlines at the interface are highly perturbed respect to the counterpart. The reattachment point on the downwind building remains nearly at the same position than in AR_C = 1 case, for flat roofs, whereas it shifts downwards about 1/3 of the windward pitch, in case of gable roof (x/H = 1.6, z/H = 1.1). With the roof presence, vertical velocities are more intense not only inside the canyon but also above the interface; the regions with higher values are more extent all over inside the canyon.

For AR_C = 6 the external flow between flat roof buildings inflects significantly below the height of the eaves (Figure 3.4 e). The flow within the canyon consist of a main vortex with the centre at x/H ≈ -1.1, z/H ≈ 0.5, and two counter-rotating vortexes at the leeward and windward walls. The flow pattern indicating the upcoming isolated interference flow regime, which has been observed to occur for AR_C > 9 (Sini et al., 1996). Conversely, in case of gable roof, the flow is still organised in a single main vortex and a single secondary vortex near the leeward wall. The reattachment point is at x/H = 3.1, z/H = 1.1, shifted downward respect to the previous analysed canyon width. Vertical velocities appear highest at the upwind pitch and windward wall corner respectively for gable and flat roofs. Differences can be notice close to the leeward walls and at upper levels.

As regards the second order statistics, map of turbulent momentum flux, $\overline{u'w'}/U_{ref}^2$, made non dimensional by the square of the free stream velocity, were here reported in Figure 3.5 for AR_C = 1, 3, 6. Differences in turbulence exchange occur across the roughness sub layer: for both the two roof shapes, in case of AR_C = 1 (Figure 3.5 a, c), the turbulent flux is positive in most of the canyon and negative outside, with a sharp negative ripple marking the shear layer at interface.

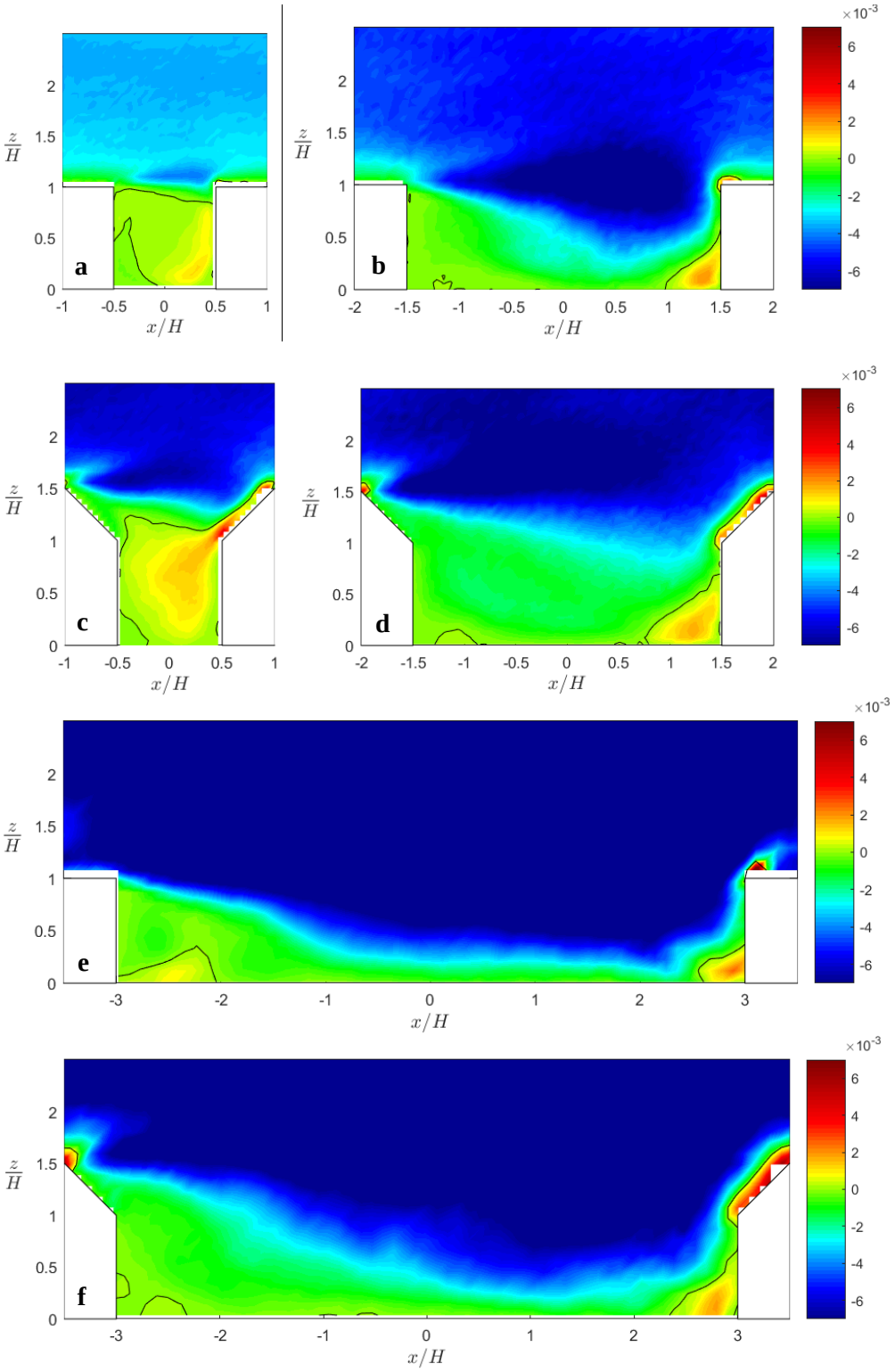

Figure 3.5 – Turbulent momentum flux made non dimensional by the free-stream velocity ($\overline{u'w'}/U_{ref}^2$). Canyon aspect ratios, AR_C = 1, α = 0° (a); AR_C = 3, α = 0° (b); AR_C = 1, α = 45° (c); AR_C = 3, α = 45° (d); AR_C = 6, α = 0° (e); AR_C = 6, α = 45° (f). Colour scale is common for all the panels. The black line marks the transition from negative to positive values. Maximum uncertainty over the maps is ± 0.4 × $10^{-3}U_{ref}^2$.

The transition from negative to positive values is marked in pictures by a black lines that is equal to the zero values set. Moreover, in case of roofs intensities are higher (both positive and negative),

underlying the increasing level of turbulence due by the presence of corners and pitches, as was already stated in a previous numerical work (Badas et al., 2017). This is particularly evident in the corner of the downwind wall of the Figure 3.5 c, under which a tongue with higher positive value come into the canyon.

As the flow changes to the wake interference regime, the negative region rapidly extent into the canyon. This is particularly evident in case of flat roof buildings, for AR_C = 3 (Figure 3.5 b), where the negative ripple come from the leeward building corner close to the ground near the windward wall. Differently, in case of gable roofs (Figure 3.5 d) it go with a more higher trajectory, from the top of the first building to the pitch of the second one. Positive values are observable only in small areas in proximity of the lower windward building corners. Another thin region of positive flux is found on the windward pitch of the gable roofs.

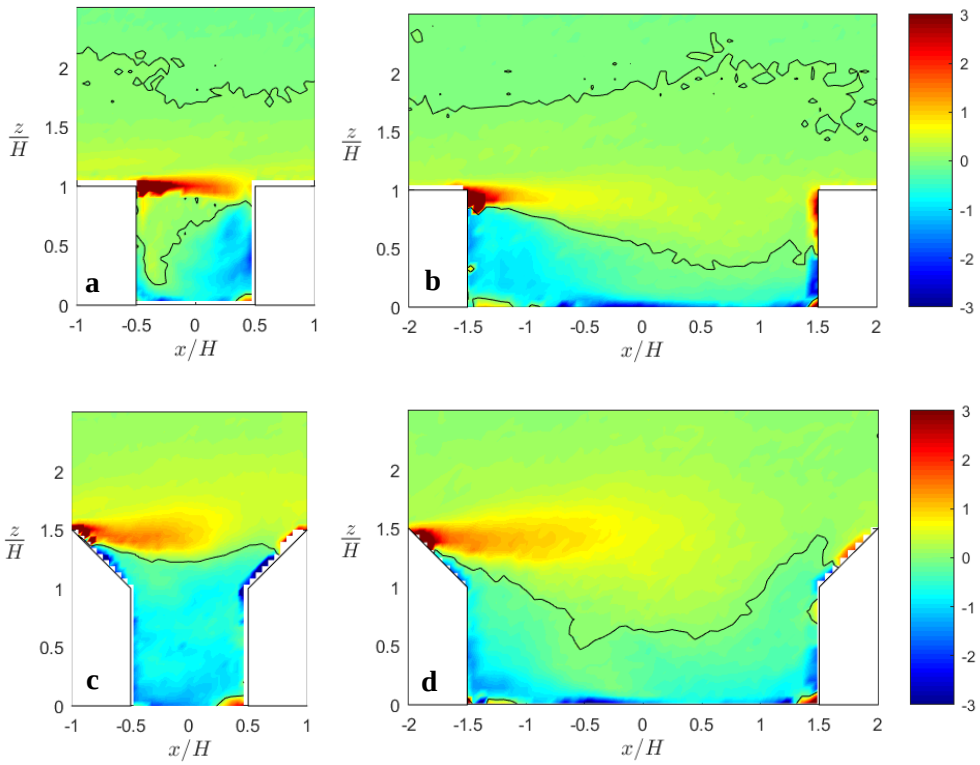

Figure 3.6 – Skewness factor of the non-dimensional stream-wise velocity component $(\overline{u'^3}/\sqrt{(\overline{u'^2})^3})$. Canyon aspect ratios, AR_C = 1, α = 0° (a); AR_C = 3, α = 0° (b); AR_C = 1, α = 45° (c); AR_C = 3, α = 45° (d). Colour scale is common for all the panels. The black line marks the transition from negative to positive values. Maximum uncertainty in the evaluation of the third moment over the maps is ± 0.15 × $10^{-3}U_{ref}^3$.

The third-order moments of the velocity components, play a relevant role in pollutant dispersion, and are among the parameters needed for its Lagrangian stochastic modelling (Monti and Leuzzi, 1996). The spatial distribution of the skewness factor of the stream-wise and vertical velocity components $(\overline{u'^3}/\sqrt{(\overline{u'^2})^3}, \overline{w'^3}/\sqrt{(\overline{w'^2})^3})$, are respectively represented in Figure 3.6 Figure 3.7, for AR_C = 1, 3. The transition from negative to positive values is marked with a black line representing the zero values. Irrespective of the roof shape, the skewness of the stream-wise velocity component, show high, positive value at the shear layer, developing from the upwind building edge, at the top of the building. The positive layer extent up to the doubled building height (i.e z/H ≈ 2 for flat roofs).

The skewness of the vertical velocity, is negative inside the canyon, especially in the downstream part, where the shear layer penetrates down. Values are positive in most of the overlaying boundary layer and in the upstream portion of the canyon. The negative region is that where the external flow come into the canyon, refreshing its air, thus the region where the air exchange occur typically by means of intense and sporadic downwash events. As an example, one of this event was captured in three snapshot for each roof shape in case of $AR_C = 1$ and reported in Figure 3.8 (a, b, c and e, f, g respectively for flat and roof cases).

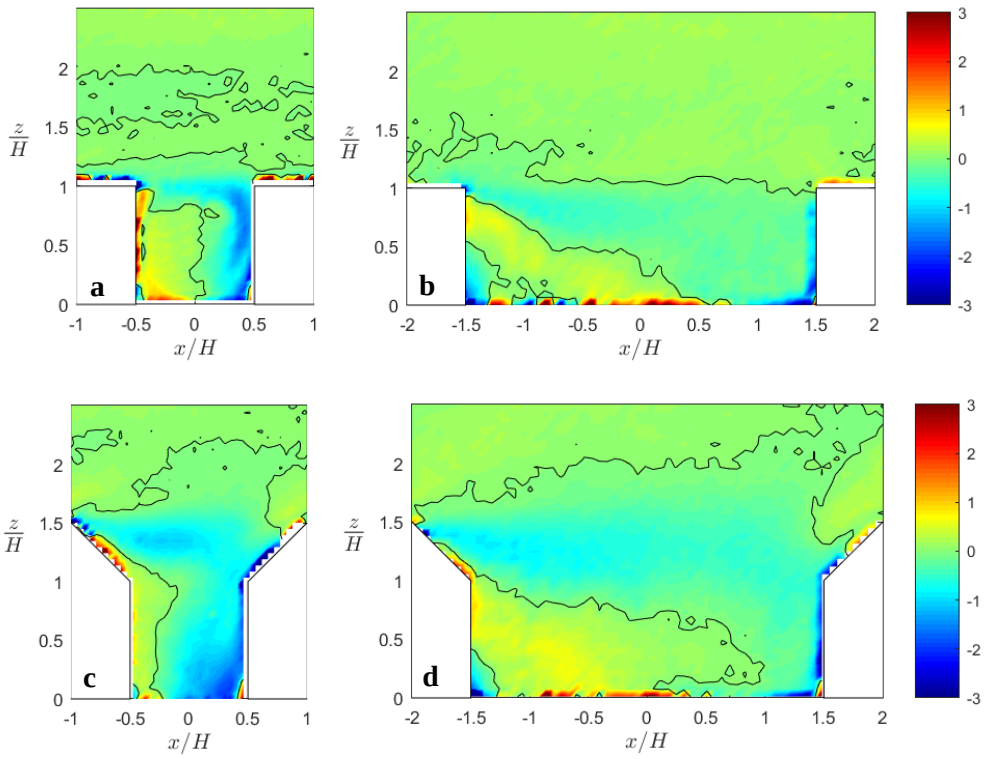

Figure 3.7 – Skewness factor of the non-dimensional vertical velocity component $(\overline{w'^3}/\sqrt{(\overline{w'^2})^3})$. Canyon aspect ratios, $AR_C = 1$, $\alpha = 0°$ (a); $AR_C = 3$, $\alpha = 0°$ (b); $AR_C = 1$, $\alpha = 45°$ (c); $AR_C = 3$, $\alpha = 45°$ (d). Colour scale is common for all the panels. The black line marks the transition from negative to positive values. Maximum uncertainty in the evaluation of the third moment over the maps is $\pm 0.05 \times 10^{-3} U_{ref}^3$.

The instantaneous velocity vector representation makes clear the regions where the phenomenon is more intense and the differences existing between the two roof shapes. It develops from the higher corner of the windward building (Figure 3.8 a) and continues along the building wall and the ground (Figure 3.8 b), then the air gets out into the upper layers. This events happen following the recirculation vortex shape in a very ordered way. Differently, the scenario with gable roofs appear more intense along the walls, where the entrance of fresh air come from the windward pitch (Figure 3.8 d, e, f) when the main vortex crash to the building wall losing the mean shape discussed above and shown in Figure 3.4 a. This is more evident in panel f, where the flux seems do not have a precise order: this is the proper condition for which air go to the overlaying boundary layer by moving up along the entire leeward wall.

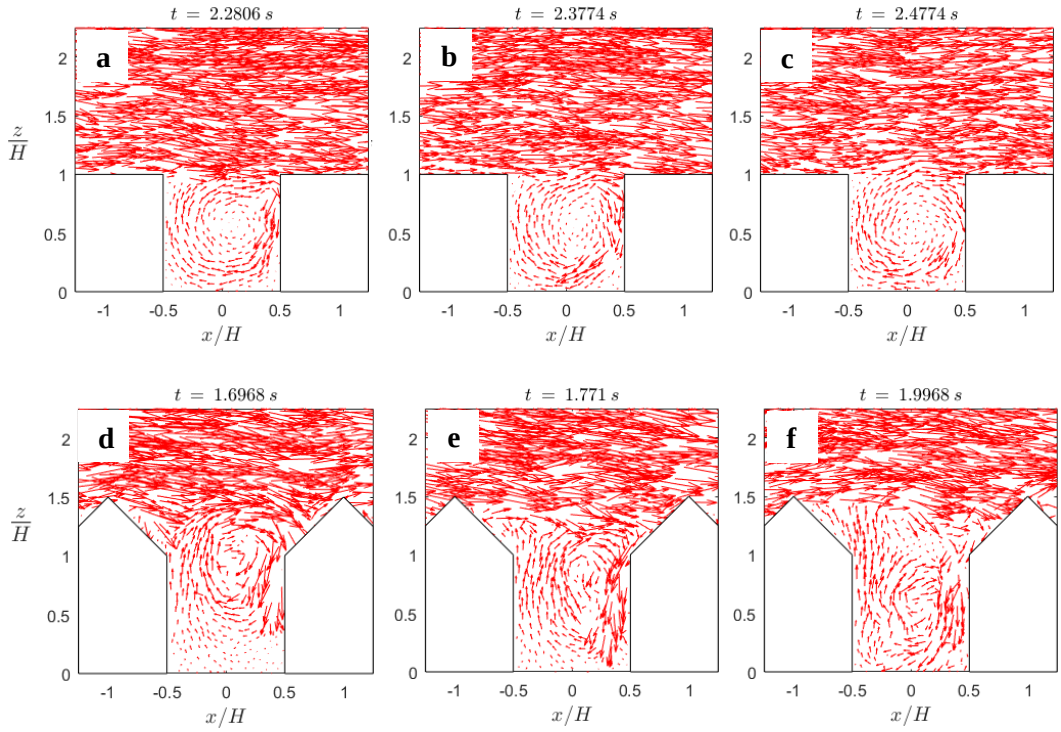

Figure 3.8 - Vector field velocity representation of a downwash event evolution in case of flat roofs (a, b, c) and gable roof (d, e, f) buildings.

3.4.2.2 Mean and turbulent vertical profiles

In order to synthetically analyse the effects due by the roof shape with variable canyon widths, on the flow structure, all the statistics have been horizontally averaged (Eq. 3.1), over one periodical roughness unit: i.e. from the middle point of the upwind building to the middle point of the downwind one, for the full domain height:

$$< \bar{\gamma}(z) >= \frac{1}{\lambda(z)} \int_{\lambda(z)} \bar{\gamma} dx \qquad 3.1$$

where γ is the generic temporally averaged parameter, z is the generic height and λ(z) is the horizontal integration line. The length of λ varied with the canyon width variation and with the integration height, which in case of gable roofs, depends on the pitches slope. The resulting vertical profiles are presented in Figure 3.9 -Figure 3.10.

The mean stream-wise velocity component, made non dimensional by the free stream velocity is presented in Figure 3.9 a. The graphs report results for five aspect ratios (different colours) and two roof shapes (different line styles). All the curves show an inflection point at the overall building height, irrespective of the roof and canyon variation. Above this point the curves are pretty logarithmic correspondent to the typical rough-wall boundary layer, even if it is characterised by different slopes. Under the inflection point, curves for gable roof cases collapse in a unique one for AR_C >1, in agreement with Florens et al., (2013), for which velocities are negative below z/H = 0.85. In case of AR_C = 1, velocities became negative for z/H < 1.2, depending on the main vortex shape and on its centre position. Conversely, flat roof outcomes show similar behaviour for the entire AR_C investigated range and, for a large fraction of the canyon height, they collapse together, except for the AR_C = 6 case, which present a more gentle trend in the transition from the internal to the external flow. The horizontally-averaged turbulent momentum flux (Figure 3.9 b), only in the narrow canyon case,

exhibits positive values in most of the canopy depth, while, for the larger ones, it is negative for the entire investigated height range, with a maximum (absolute value) above the canopy at z/H ≈ 2, 3 respectively for flat and roofed configurations. Positive flux in the unitary canyon case is below z/H = 0.9 for flat roofs and z/H = 1.15 for the gabled ones. The maximum value for larger canyons increase with the increase of the canyon width, continuously for flat roofs whilst, in case of roofs, it becomes nearly constant for 1 < AR > 4. Finally, the roof presence seems to have two significant effects: the momentum flux increase even if the phenomenon decrease with the packing density, thus for AR_C = 6, the flux is no more effected by the presence of roofs. Furthermore, the high-flux layer above the buildings is always deeper in case of gabled roofs.

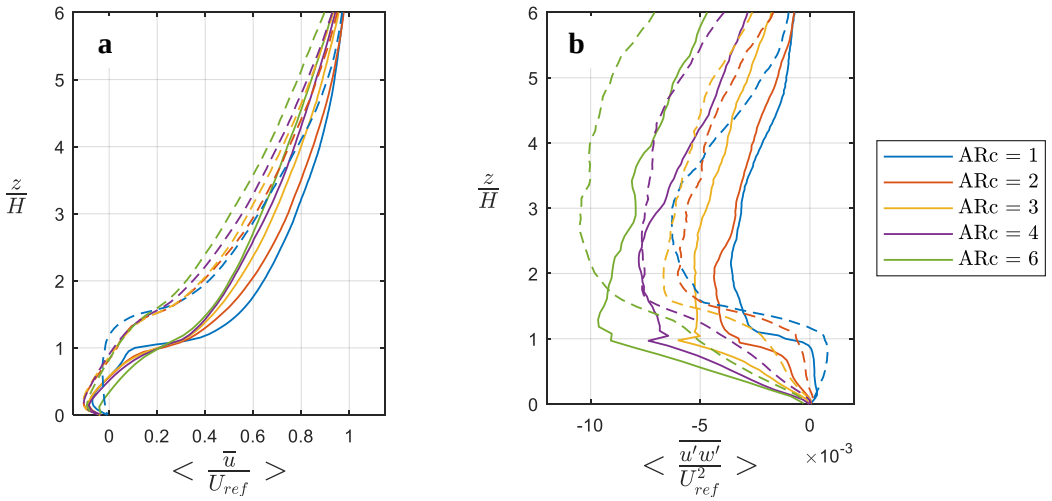

Figure 3.9 - Vertical profiles of the horizontally averaged stream-wise velocity (a) and turbulent momentum flux (b). Values are made non-dimensional by the free stream velocity at U_{ref}. Different colours indicate different building aspect ratios and styles indicates flat (solid lines) and gable roofs (dashed lines).

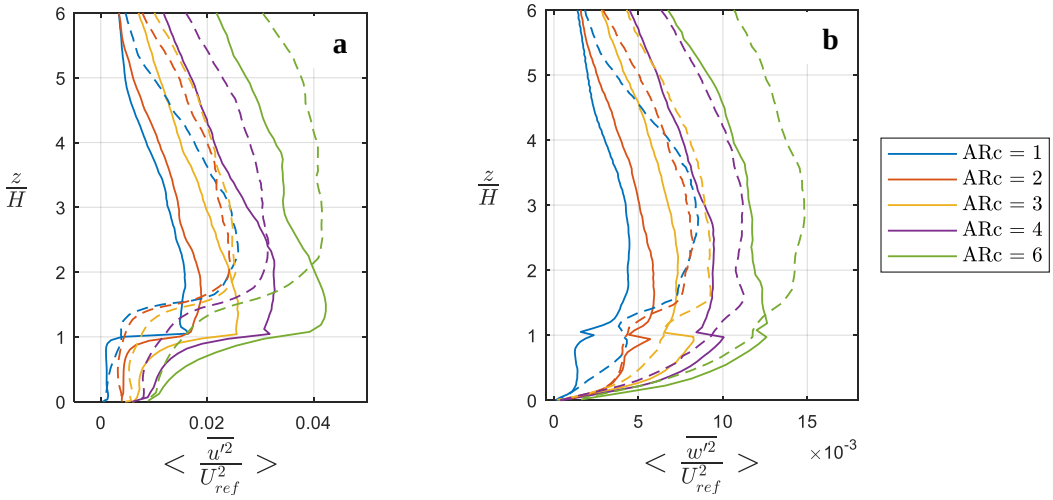

Figure 3.10 - Vertical profiles of the horizontally averaged variance of the stream-wise velocity (a) and the vertical velocity (b). Values are made non-dimensional by the free stream velocity at U_{ref}. Different colours indicate different building aspect ratios and styles indicates flat (solid lines) and gable roofs (dashed lines).

Figure 3.10 exhibit the vertical profiles of the horizontally-averaged variance of the stream-wise velocity (a) and the vertical velocity (b) components. Both the two quantities suggest the presence of an intense turbulence layer just above the canopy. This is due by the presence of the roughness

element and with the decreasing packing density, the variance increase systematically in case of flat roofs. On the contrary, if roofs are gabled, this behaviour is not visible: high values are attained starting from AR_C = 1 and then remain nearly constant, with a significant increase for AR_C = 6. The depth of the high-turbulence layer increases with aspect ratio.

3.4.2.3 Flux Index Exchange

The air exchange mechanism was already mentioned in the previous paragraphs and a series of velocity snapshots of the phenomenon was presented in Figure 3.8. This air exchange between the canyon and the external boundary layer occurs at the interfacial surface, that can be individuated at the roof level and, under the ideal case of a well-mixed box, where the pollutant concentration is assumed constant within the canyon, the outflow rate on the top would be sufficient to describe the phenomenon. The well-mixed box theory was treated in Section 2.4.3.

In reality, this mechanism is highly more complicated and the pollutant concentration may vary significantly with height. Therefore, in order to give a more detailed description of the phenomenon and to better understand the capability of air exchange into the canyon, we estimated φ_e(z) and φ_{em}(z) (respectively in Eq. 3.2 and Eq. 3.3) as functions of the height. φ_e(z) corresponds to the outflow rate across a generic horizontal section of the canyon at the height z. It was computed by integrating the instantaneous vertical velocity fields, over the line λ(z), that ideally connect the canyon sidewalls, then it was averaged on the whole sample amount. The integration line is z dependent. Likewise, the contribution of the sole mean velocity field φ_{em}(z), was evaluated.

$$\varphi_e(z) = \frac{1}{2}\overline{\int_{\lambda(z)} |w(t)|dx} \qquad 3.2$$

$$\varphi_{em}(z) = \frac{1}{2}\int_{\lambda(z)} |\overline{w}|dx \qquad 3.3$$

Results in Figure 3.11Figure 3.11 were separately displayed for flat roof (a) and gable roof (b) considering that the canyon section S_C varied, as the number of integration line along the canyon depth, from the top of the building to the ground. For flat roof building, results of both the quantities in case of $AR_C \leq 2$, show the maximum at z/H ≈ 0.5, where the main velocities are mainly vertical. As matter of fact, at the roof level values are quite halved respect to maximum. Considering $AR_C > 2$, values continuously increase with the height (z) and from the ground to the rooftop, the exchange rate became more and more higher with increasing canyon width. This is a consequence of the increasing contribution of the turbulent mixing at the interfacial shear layer.

A completely different behaviour is visible in panel b, regarding the 45° sloped roof results. Indeed, trends for AR_C = 1 do not present a maximum at the medium height of the building, showing a quasi linear increase with height since the rooftop in case of φ_e(z) and since z/H ≈ 1.15 in case of φ_{em}(z), while for AR_C = 2 there is a maximum around z/H ≈ 0.8. Despite of this at the roof top the discrepancies between the mean contribution and the total outflow rate, appear higher in gable roof case for the whole investigated aspect ratio range. The remaining curves show similar trend in both the roof configuration.

Quantitative comparison between the two configurations, highlight that flat roofs give slightly greater mixing at lower levels, whilst for z/H > 0.75, φ_e(z) is higher for gable roofs: gable roof

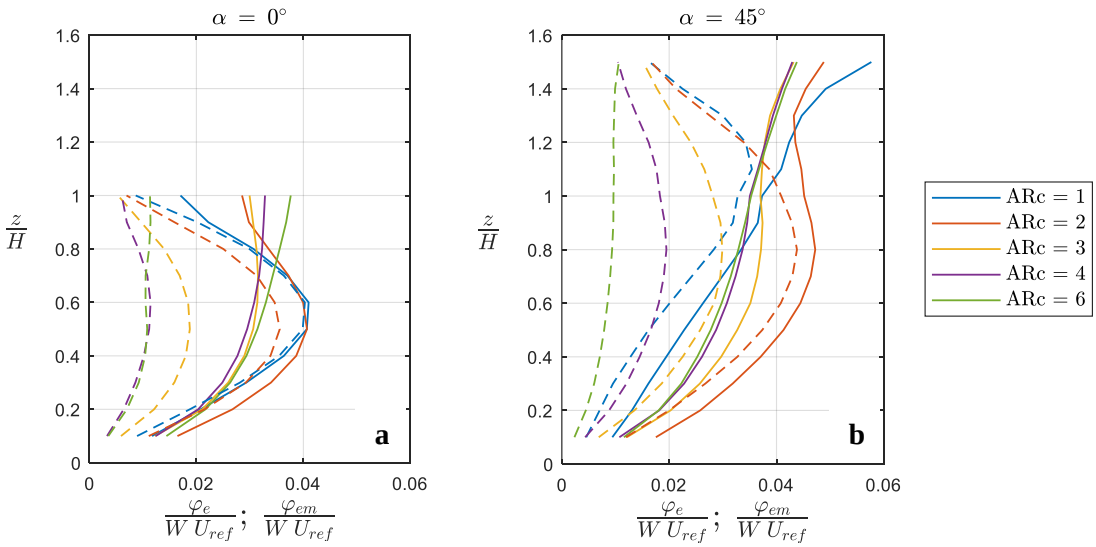

Figure 3.11 - Non-dimensional vertical profiles of exchange fluxes, φ_e (solid lines) and φ_{em}(dashed lines) calculated for flat roof (a) gable roof (b cases), at different heigth (z/H) inside the canyon. Values were made non dimensionale by the free-stream velocity (U_{ref}) and the canyon width (W). Different colours indicate different canyon aspect ratios.

promotes a considerable turbulent mixing above the height of the eaves, which plays a key role in increasing the exchange flux at the canyon interface.

In order to better understand the ventiltion dynamics, the istantaneous exchange fluxes at the rooftop (Eq. 3.4) was considered to compute the Probability Density Function (PDF).

$$\varphi_i(z) = \frac{1}{2}\int_{\lambda(z)} |w(t)|dx \qquad 3.4$$

In agreement with Perret et al., (2017), results Figure 3.12 show positive skewed PDF values and the width increase with the aspect ratio. Flat roofs (a), present wider and more positive skewed values, compared to the gabled roofs (a). The higher right tail of the PDF distribution indicates that the more effective mixing induced by the roof slope is doinated by relatively low mixing, occasionally interrupted by few, intense mixing events. Additionally, it is worth noting that the flat-roof cases show an increase in the right tail and width of the distribution with the aspect ratio. Conversely, with gable roofs the widest and most heavy-tailed distributions are found for the lowest value of AR_C, a signature of itense turbulent mixing events driven by the pitched roof especially for small aspect ratios.

Finally, the mean residence time Tr was evaluated as a function of the building aspect ratio (Figure 3.13) made non dimensional by the building height and the free stream velocity, and it is reported within the outflow rate at the rooftop level. The residence time, computing as in Eq. 3.5, represents the parameter controlling the dynamic of pollutant removal.

$$T_r = \frac{S_C}{\varphi_{e(z=H)}} \qquad 3.5$$

The mean residence time in case of flat roofs, as can be expected, decrease with the increasing of canyon width, faster in the transition from the skimming flow to the wake interference regime (from AR_C = 1, to AR_C = 2). The mean residence time in gable roof building configuration, is always lower

compared to its flat-roof counterparts and it exhibit a very weak dependence on the aspect ratio, more evident through the narrower canyons.

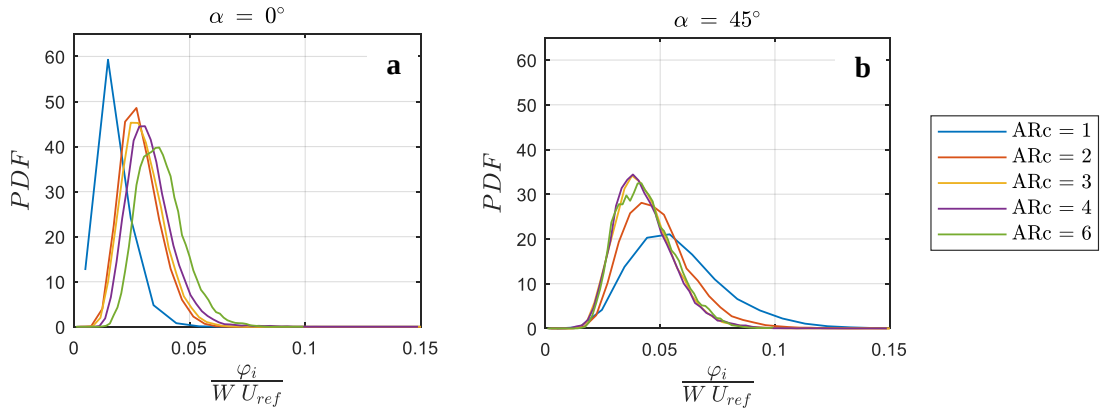

Figure 3.12 – Probability density function of the instantaneous exchange flux φ_i at the rooftop,made non dimensional by the canyon width and the free stream velocity, for flat roof (a) and gable roof (b) buildings.

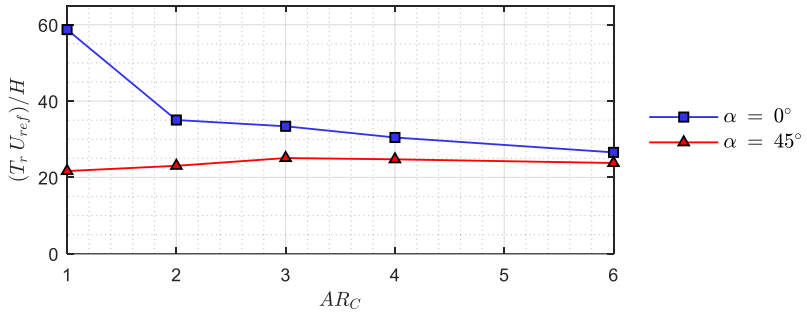

Figure 3.13 - Mean residence time, Tr, as a function of the building aspect ratio for α = 0° (blue line with square) and α = 45° (red line with triangles).

3.4.3 Gabled roofs with different slopes

3.4.3.1 Mean and turbulent flow fields

The vertical velocity field with variable roof pitch slope are reported in Figure 3.14-Figure 3.15, respectively for the two series of data with the canyon aspect ratio equal to 1 and 2. The streamlines are superimposed on the velocity component ($\overline{w}/U_{ref}$) colour map and show the flow structure that varied from the flat roof to the 45° sloped in both the two canyon width, but with different mechanism.

In case of unitary aspect ratio (skimming flow regime), a unique main vortex with two small recirculation vortexes is everywhere present. As already stated in Section 3.4.2.1, the main vortex centre move up in from z/H ≈ 0.55 in the flat roof case to z/H ≈ 1.05 the 45° slope roof configuration, where the difference do not appear justifiable with the increased building height. However, looking at the entire series, the increasing height of the vortex centre appears moving up regularly with the increasing height of the building since the 30° sloped roof Indeed the ratio between the centre and the edifice heights was estimated around $z_c/h_{tot} \approx 0.5$ from flat roof to 30° sloped and $z_c/h_{tot} \approx 0.75$ for the 45° sloped case. Regarding the interface flow, between the canyon and the overlaying air, the streamlines appear more and more perturbed with the increasing slope of pitches. The higher perturbation is sit in the downwind building, where the reattachment point gradually move up from the windward building corner (flat roofs), to the windward pitch above the eaves.

Looking at the vertical velocity fields, another big difference is visible between the 45° sloped roof and all the other cases: the lowest quantities are registered at pedestrian levels, and the highest velocity areas are smaller, positioned around both the downwind and the upwind eave corners. Moreover, down to the 30° slope, the extension of these areas decrease with the slope but remains significant at pedestrian levels. Quantitative differences will be shown in next analyses.

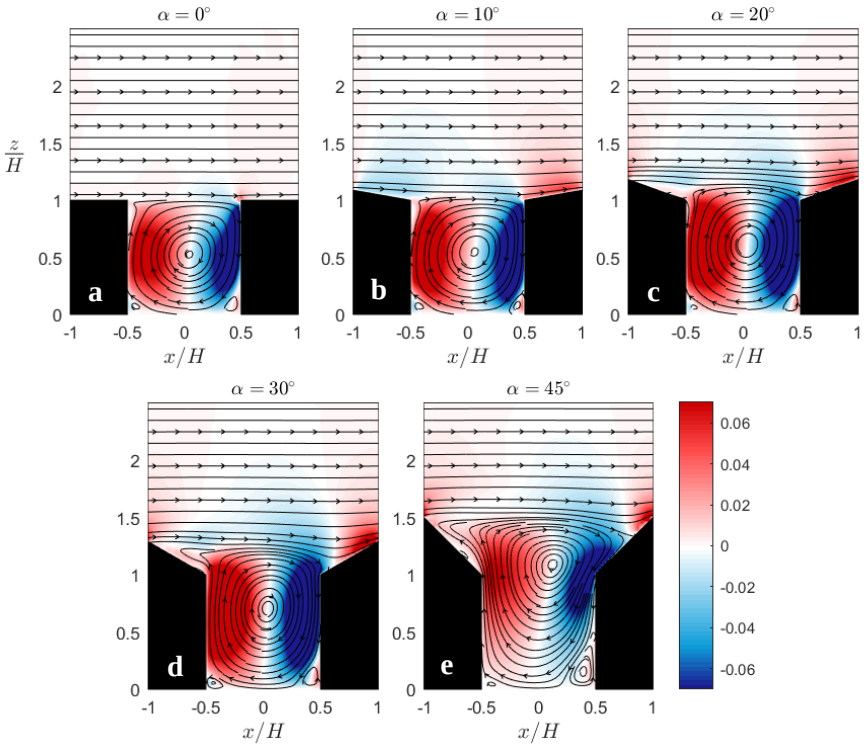

Figure 3.14 - Streamlines of the mean velocity field and mean vertical velocity component, made non dimensional by the free-stream velocity ($\overline{w}/U_{ref}$). Canyon aspect ratios, AR_C = 1, α = 0° (a); α = 10° (b); α = 20° (c); α = 30° (d); α = 45° (e). Colour scale is common for all the panels.

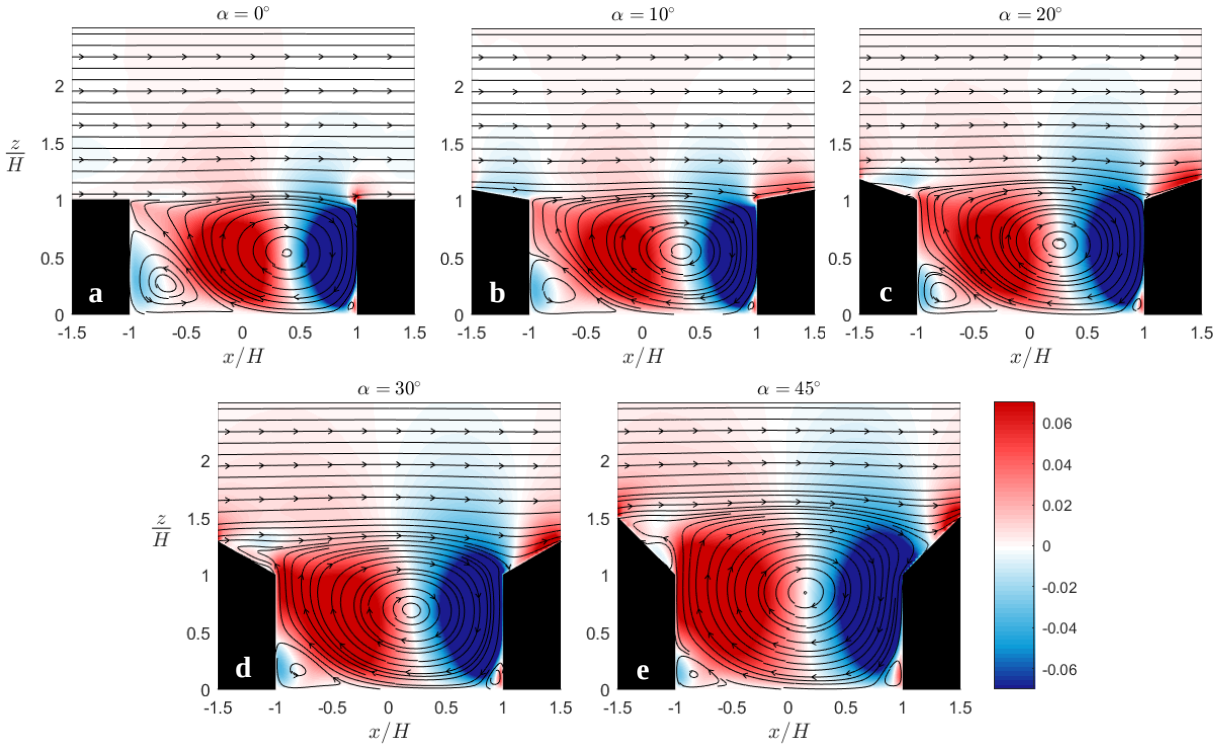

Figure 3.15 - Streamlines of the mean velocity field and mean vertical velocity component, made non dimensional by the free-stream velocity ($\overline{w}/U_{ref}$). Canyon aspect ratios, AR_C = 2, α = 0° (a); α = 10° (b); α = 20° (c); α = 30° (d); α = 45° (e). Colour scale is common for all the panels.

In case of wake interference regime (AR_C = 2), streamlines correctly shown the two counter rotating vortexes. The main vortex centre shown smaller variation in z/H position, respect to the previous configuration, albeit with the same gap between the 45° roof and the others. Instead, higher differences are visible in x/H centre position, had to the vortexes shape variation. It is well evident that the typical wake interference regime structure dwindles with the increasing roof slopes i.e. with the increasing total building height. Indeed, considering the total height of the building, instead of the eaves level, the canyon aspect ratio varies from 2 (flat roof case) to 1.33 in case of the maximum pitch. Considering that the standard transition point between the two regimes is individuate when $AR_C \approx 1.5$ (Ngan and Lo, 2016; Sini et al., 1996), there are two possible explanation to this behaviour: the canonical transition limits for the flow regimes have to been revisited in case of different building shape, or the correct way to define the flow regime in case of various roof shape, is to evaluate the aspect ratio respect to the total height of the building. However this answer is far from being obvious and next analysis will be useful to explain it.

Focusing on vertical velocities, intensities do not show big differences at the pedestrian level. On the contrary at the interface the flow appear more and more disturbed when the pitches slope is higher, and the reattachment point assumes a similar behaviour than in the skimming flow regime.

For a sake of continuity with the previous sections, fields of turbulent momentum flux, $\overline{u'w'}/U_{ref}^2$, through the second order statistics, were chosen to be here reported. Fields made non dimensional by the square of the free stream velocity, are shown in Figure 3.16 - Figure 3.17 respectively for AR_C = 1, 2, only for fields that were not reported in Section 3.4.2.1, because results are extremely similar. Thus, looking at the Figure 3.16, the evolution of turbulence level occurring across the roughness sub-layer where the negative ripple marking the shear layer, move from the downwind corner, to the upwind pitch, when the roof slope increase. In the meantime turbulence level in the ripple and upper became

higher. Also the positive values inside the canyon change with the roof slope, becoming more spaced with the highest values visible near the downwind wall and pitch.

Positive values are reduced in the downwind corner of the canyon and close to the ground in case of AR_C = 2 and the area is different just in case of 45° slope. The difference in the roughness sub-layer too, are not great: like in the skimming flow case the ripple moves from one corner to the other, upwind, but both shape and intensities do not change in a substantial way, a part for the 45° slope. Previous RANS (Reynolds Average Navier Stokes) simulation (Badas et al., 2017), analysis on variable roof slopes showed results from 0° to 40° cases, without identify a so particular variation. All these suggested that the 45° pitched roof may represent a critical tilt angle, from which a different flow dynamic behaviour is established.

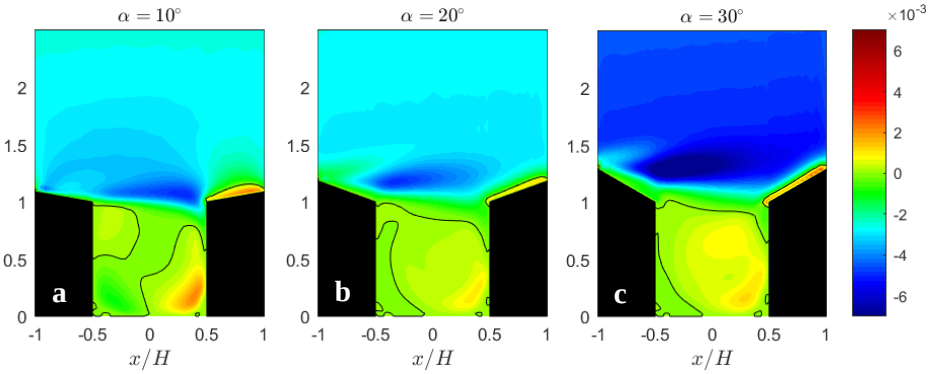

Figure 3.16 – Turbulent momentum flux, made non dimensional by the free-stream velocity ($\overline{u'w'}/U_{ref}^2$). Canyon aspect ratios, AR_C = 1, α = 10° (a); α = 20° (b); α = 30° (c). Colour scale is common for all the panels.

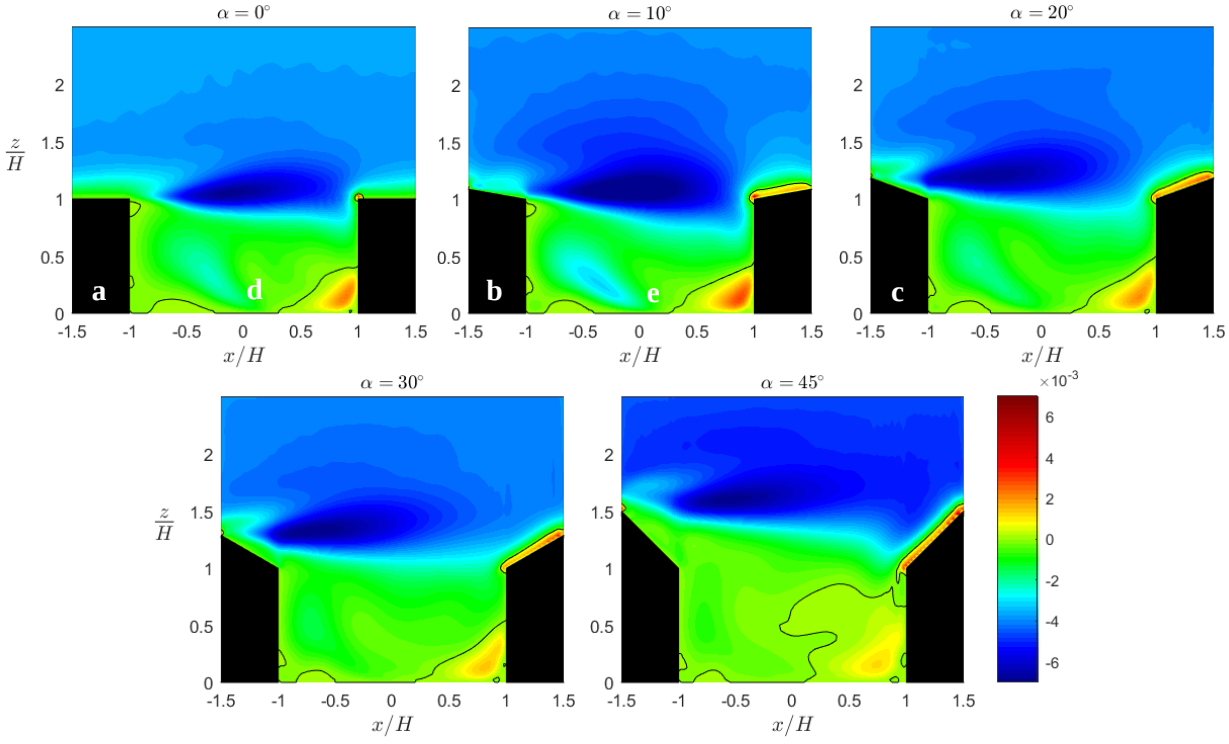

Figure 3.17 - Turbulent momentum flux, made non dimensional by the free-stream velocity ($\overline{u'w'}/U_{ref}^2$). Canyon aspect ratios, AR_C = 2, α = 0° (a); α = 10° (b); α = 20° (c); α = 30° (d); α = 45° (e). Colour scale is common for all the panels.

3.4.3.2 Mean and turbulent vertical profiles

The horizontally averaged profiles for every quantities, were evaluated by mean the Eq.2.6, which integrate the variable over one periodical roughness unit. The resulting vertical profiles are here presented by dividing results respect to the canyon width. Stream-wise velocities for the skimming flow (Figure 3.18 a), show little variation inside the canyon (z/H <1) from 0° to 30°, whit the increasing vortex height, while in case of 45° slope, the curve seems very different: inside the canyon velocities are everywhere negative down to the z/H < 1.2 where values became positive. Up to the eaves level (z/H = 1) curves became pretty logarithmic, with different slopes. In case of AR_C = 2, (Figure 3.18 b), curves shown a more similar trend, with a decreasing inclination with the increase roof slope and a higher position of the transition point from negative to positive values.

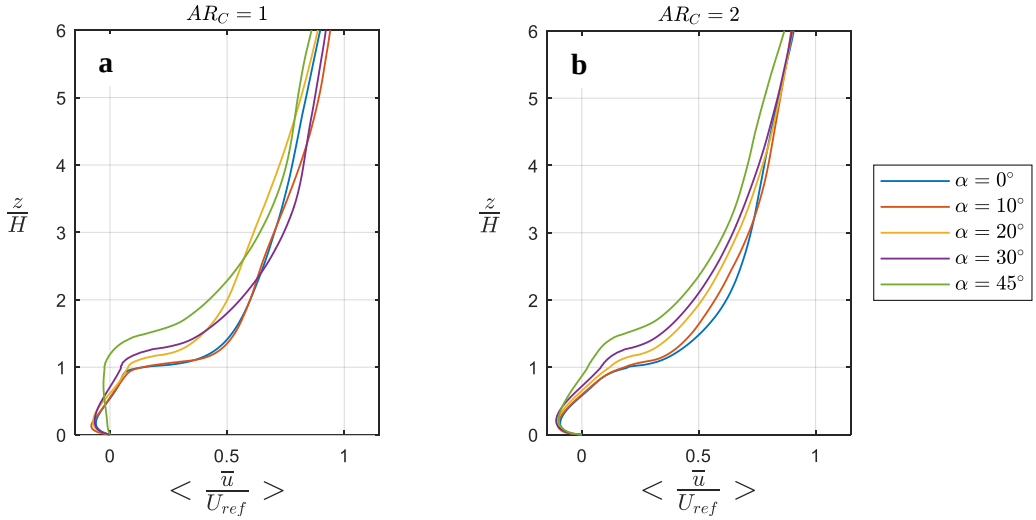

Figure 3.18 - Vertical profiles of the horizontally averaged stream-wise velocity for configurations with AR_C = 1 (a) and AR_C = 2 (b). Values are made non-dimensional by the free stream velocity at U_{ref}. Different colours indicate different roof slopes.

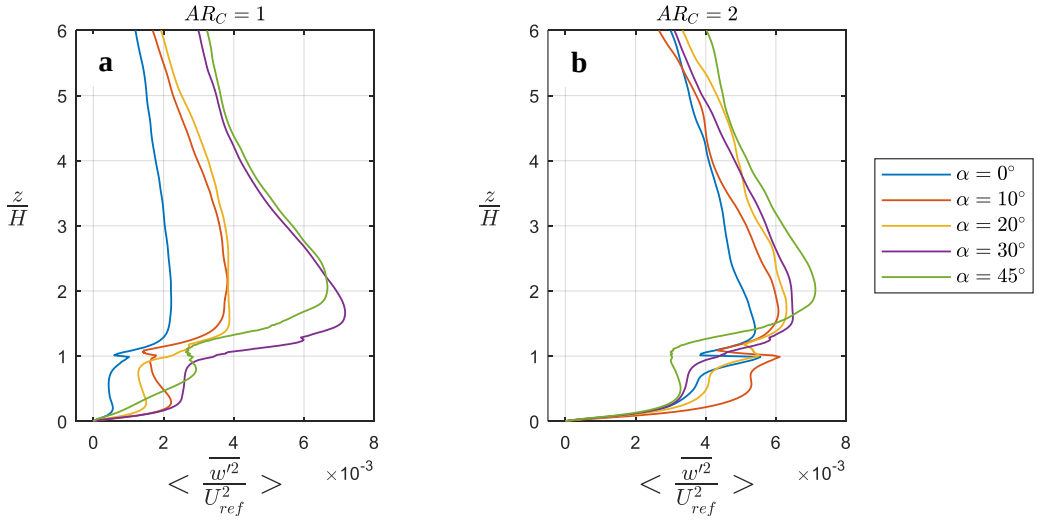

Figure 3.19 - Vertical profiles of the horizontally averaged variance of the vertical velocity for configurations with AR_C = 1 (a) and AR_C = 2 (b). Values are made non-dimensional by the free stream velocity at U_{ref}. Different colours indicate different roof slopes.

Figure 3.19 exhibit the vertical profiles of the horizontally-averaged variance of the vertical velocity components in case of AR_C = 1 (a) and 2 (b). The increase in turbulence with the roof slope,

is impressive: from 0° to 30° the maximum, which varied in height, is quite quadrupled above the roof level, and under it, value remain sensible higher for all the canyon depth by employing the gable roof. In the case of 45° slope, into the canyon turbulence continuously increase with a different trend respect to the others. More or less the same differences can be described in the highest canyon case, even if the variance of vertical velocity show higher values into the canyon with respect to the previous case, and differences through roof shape variation are limited.

Similar behaviour are visible in Figure 3.20 a, b, where the turbulent momentum fluxes are synthetized: only the narrow canyon case exhibit the positive values in most of the canopy depth and up to z/H = 0.9 became negative. The positive maximum is registered in the green line at z/H ≈ 0.9 and the negative maximum is in a range between z/H ≈ 1.75 and z/H ≈ 1.0 (Figure 3.20 a). A smoother behaviour was found in the wake interference regime, where only the 45° slope seems shift up respect the other, maintaining the same trend.

Furthermore, the second order statistics highlight the importance of roofs to make higher the turbulence, that is the main contribution driving the ventilation and pollutant dispersion in the street canyon unit (Badas et al., 2017; Ho et al., 2015).

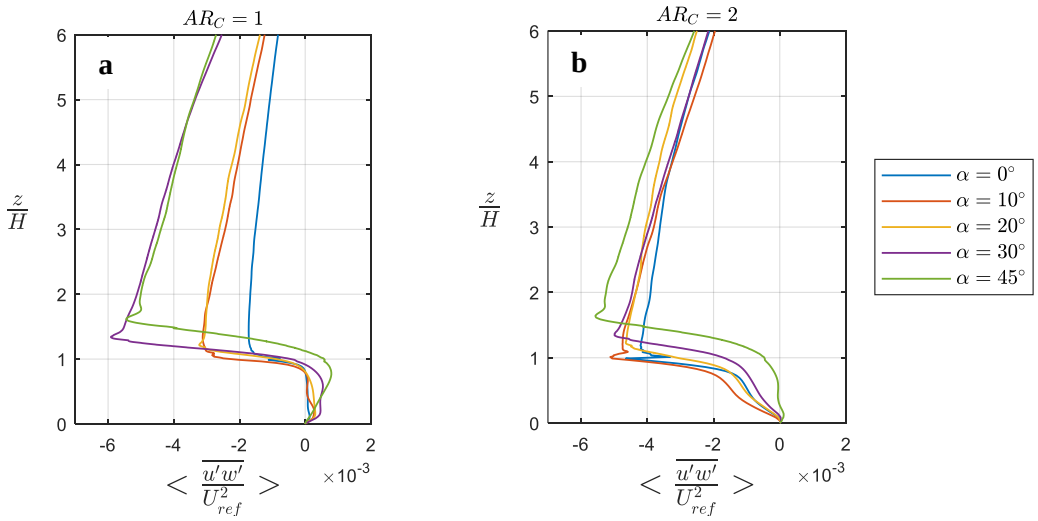

Figure 3.20 - Vertical profiles of the horizontally averaged turbulent momentum flux for configurations with AR_C = 1 (a) and AR_C = 2 (b) Values are made non-dimensional by the free stream velocity at U_{ref}. Different colours indicate different roof slopes.

3.4.3.3 Flux index exchange

In order to see how roofs effect ventilation mechanism, the medium and total flux exchange indexes were evaluated with Eq. 2.10- 2.11. Results are reported in Figure 3.21 divided by aspect ratio width, where the z position are made non-dimensional respect to the eaves level H. Results confirmed the positive effect on ventilation, not only at the roof level, but also into the canyon. Although quantities are very small, differences may be relevant for ventilation especially in narrowest canyon, where a substantial reduction of air exchange was demonstrate and discussed (see Section 2.4.3, Figure 2.13).

As matter of fact, looking at solid lines in Figure 3.2 a, a little slope in roofs (orange line) seems able to increase ventilation around the 23% considering the maximum point at z/H ≈ 0.55. By increasing the slope, differences grow up in the upper part of the canyon since the 30° sloped roof, for which the maximum is reached at z/H ≈ 0.7 and it is 40% higher than the flat roof case. Down to the maximum, Differences tends to be minimised and at z/H ≈ 0.35, curves from 10° to 30° overlap each other in a singular line, with a smaller and smaller gap respect to flat roofs. Above the maximum point, where turbulence level became significant (see the differences occurring between the dashed

and the solid lines), differences grow up faster and at roof top the higher discrepancy is registered between flat roof and 30° tilt angle, approximately equal to 75%. Similar observation can be done by focusing on the eaves level, for which the viola line appear around 43% higher than the blue one. The green lines representing the 45° roof case, completely differs from the others, assuming a quite linear trend, with increasing values from the ground to the half part of pitches for both the two quantities (medium and total exchange fluxes respectively represented with dashed and solid line). This curves intersect the flat roof lines (blue) only around z/H ≈ 0.75 and above eaves became similar to the 30° case (viola).

This behaviour confirmed the previous analysis and support the idea that the 45° slope represent a critical case for which a different flow regime have to be identified. In addition to this this is the only configuration in which differences between medium and total quantities substantially differs for the entire canyon depth.

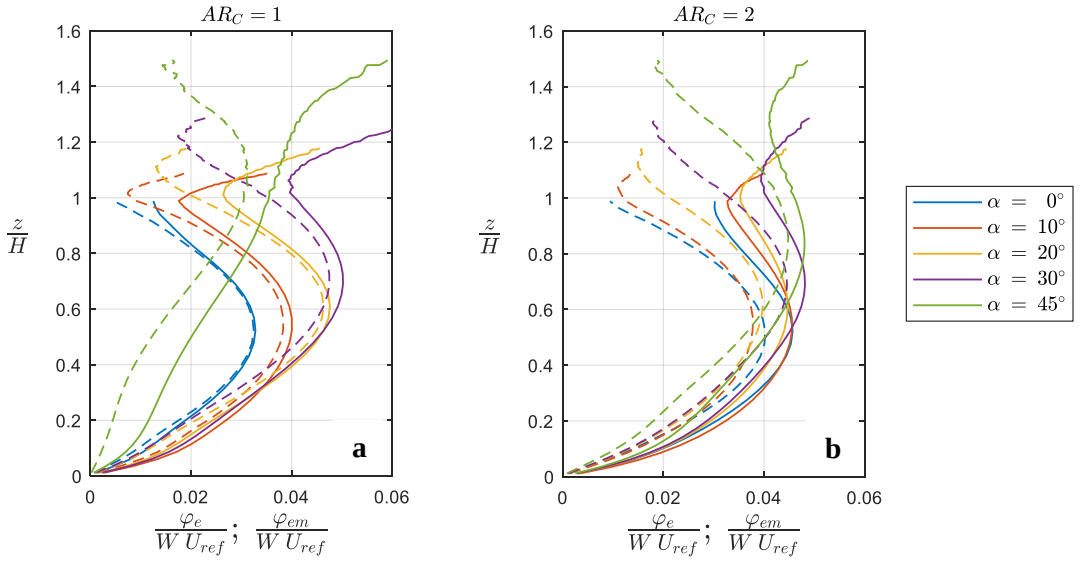

Figure 3.21 - Non-dimensional vertical profiles of exchange fluxes, φ_e (solid lines) and φ_{em}(dashed lines) calculated for flat roof with variable slope in case of AR_C = 1 (a) and 2 (b), at different heigth (z/H) inside the canyon. Values were made non dimensionale by the free-stream velocity (U_{ref}) and the canyon width (W). Different colours indicate different canyon aspect ratios.

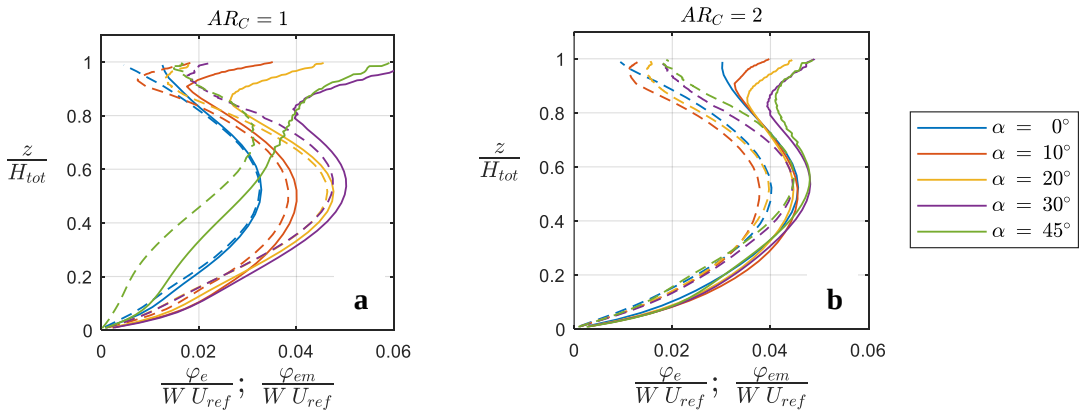

Figure 3.22 - Non-dimensional vertical profiles of exchange fluxes, φ_e (solid lines) and φ_{em}(dashed lines) calculated for flat roof with variable slope in case of AR_C = 1 (a) and 2 (b), at different heigth (z/H_{tot}) inside the canyon. Values were made non dimensionale by the free-stream velocity (U_{ref}) and the canyon width (W). Different colours indicate different canyon aspect ratios.

Looking at the larger canyon configurations (Figure 3.21 b), trends became more similar and regular, reducing discrepancies for the entire profile height. The 45° case tend to the others even if registered the minimum flux index values since z/H ≈ 0.5. Turbulence levels, which can be identify by the differences occurring between dashed and solid lines, do not substantially varied up to the eaves level with the increasing roof slopes.

If we make the heights non dimensional by the top level instead of the eaves level Figure 3.22, the main observations previously discussed, do not change. However differences for the maximum values and at the top can be better visualised, for both the canyon widths. The better shape solution that maximize ventilation appear the 30° slope one and the worst is the 45° for narrow canyon. This last one do not brings benefits in the larger canyons.

3.5 Conclusions

In this work the flow above an array of two-dimensional, prismatic obstacles was analysed with the aim of highlighting the effect of the presence of a gable roof as building covering. Experimental results show a delay in transition from one flow regime to the other (skimming flow vs. wake interference regime and wake interference regime vs. isolated roughness regime). In fact the morphology seems to be affected by the overall height of the building (Figure 3.4) even if the effect rapidly decreases with the increasing canyon width. However, numerical results for AR_C = 1, 2 demonstrate that the 45° gable roof behaviour is quite far from the others and it has to be considered as a particular case. As a matter of fact, the centre of the vortex is shifted up to the initial position (z/H ≈ 0.55 for flat roofs where H is the eaves height) from 0° to 45° slope, with a consequent stretch of the main vortex, but in the 45° slope, the vortex shape and its centre position extremely differs from the 30° sloped roofs. The vertical centre coordinate was estimated around $z_c/h_{tot} \approx 0.5$ for all cases, apart from the 45° sloped pitches, for which $z_c/h_{tot} \approx 0.75$ (where h_{tot} is the total building height). In addition to this, the slope of the roof perturbs a larger portion of flow above the canopy, as can be observed both by the streamlines (Figure 3.4-Figure 3.14) and in the vertical mean velocity profiles (Figure 3.9 a, Figure 3.18).

Pitched roofs generate also a thicker and more intense turbulent layer just above the buildings, characterized by larger momentum fluxes (Figure 3.9 b - Figure 3.20) and velocity variances (Figure 3.10 -Figure 3.19) that show the maximum quite quadrupled above the roof level (Figure 3.19 a), going from 0° to 45°. The turbulent shear layer grows between the top building and the eaves levels.

Analysis of the exchange flow rate at different heights, for the entire canyon depth $\varphi_e(z)$ made on the experimental series results, attested that the mean flow contribution to the exchange rate is around the vortex centre height. Indeed, in case of gable roofs this point shifts upwards, whereas the mixing is slightly decreased in the lower portion of the canyon (Figure 3.11). The overall exchange flux rate increases especially in the upper part of the canyon; this trend is more evident for the narrower canyons. If this is true, then a little gable roof slope variability (Figure 3.22a) produces a considerable ventilation increase. By increasing the slope, differences grow up in the upper part of the canyon up to the 30° sloped roof, for which the maximum is reached at z/H ≈ 0.7 and its value is 40% higher than the flat roof case. Noticeably, the 45° roof case completely differs from the others, assuming a quite linear trend, with increasing values from the ground to the half part of pitches for both quantities (i.e. mean and total exchange flux rates).

The residence time increases by about 30% when the aspect ratio decreases from 6 to 2 and a further 70% increase is visible as AR_C become 1. When gable roofs are employed, the mean residence time is always lower compared to the flat-roof counterpart, which exhibits a very weak dependence on

the aspect ratio (Figure 3.13). However, for a 45° sloped roof this behaviour should not be guaranteed at the pedestrian levels, as shown by the flux exchange index, but other tilts have to be employed.

These result are particularly significant in densely urbanized areas, or in an old town, where street canyons are typically narrow. Further developments of this work, which is mainly focussed on the statistical description of the phenomenon, may include the extension to three-dimensional arrangements of buildings, or to more realistic roof shapes. The analysis of the time-dependent behaviour of the flow, for example sweep and ejection events and how these are affected by the roof shape, may also be carried out.

3.6 References

Abohela, I., Hamza, N., Dudek, S., 2013. Effect of roof shape, wind direction, building height and urban configuration on the energy yield and positioning of roof mounted wind turbines. Renewable Energy 50, 1106–1118. https://doi.org/10.1016/j.renene.2012.08.068.

Amicarelli, A., Leuzzi, G., Monti, P., 2012. Lagrangian micromixing models for concentration fluctuations: an overview. American Journal of Environmental Sciences 8, 577–590. http://doi.org/10.3844/ajessp.2012.577.590

Badas, M.G., Ferrari, S., Garau, M., Querzoli, G., 2017. On the effect of gable roof on natural ventilation in two-dimensional urban canyons. Journal of Wind Engineering and Industrial Aerodynamics 162, 24–34. https://doi.org/10.1016/j.jweia.2017.01.006

Bendat, J.S., Piersol, A.G., 2011. Random Data: Analysis and Measurement Procedures. John Wiley & Sons, 2011, Fourth Edition, First published in 1971. pp 467, ISBN 978-1-118-21082-6

Bernardino, A.D., Monti, P., Leuzzi, G., Querzoli, G., 2015. On the effect of the aspect ratio on flow and turbulence over a two-dimensional street canyon. International Journal of Environment and Pollution 58, 27–38. https://doi.org/10.1504/IJEP.2015.076581

Besalduch, L.A., Badas, M.G., Ferrari, S., Querzoli, G., 2014. On the near field behavior of inclined negatively buoyant jets. EPJ Web of Conferences 67, 02007. https://doi.org/10.1051/epjconf/20146702007

Besalduch, L.A., Badas, M.G., Ferrari, S., Querzoli, G., 2013. Experimental Studies for the characterization of the mixing processes in negative buoyant jets. EPJ Web of Conferences 45, 01012. https://doi.org/10.1051/epjconf/20134501012

Blocken, B., 2015. Computational Fluid Dynamics for urban physics: Importance, scales, possibilities, limitations and ten tips and tricks towards accurate and reliable simulations. Building and Environment, Fifty Year Anniversary for Building and Environment 91, 219–245. https://doi.org/10.1016/j.buildenv.2015.02.015

Blocken, B., Janssen, W.D., van Hooff, T., 2012. CFD simulation for pedestrian wind comfort and wind safety in urban areas: General decision framework and case study for the Eindhoven University campus. Environmental Modelling & Software 30, 15–34. https://doi.org/10.1016/j.envsoft.2011.11.009

Britter, R.E., Hanna, S.R., 2003. Flow and Dispersion in Urban Areas. Annual Review of Fluid Mechanics 35, 469–496. https://doi.org/10.1146/annurev.fluid.35.101101.161147

Brown, M.J., Lawson, R.E., Decroix, D.S., Lee, R.L., 2000. Mean Flow and Turbulence Measurements Around a 2-D Array of Buildings in a Wind Tunnel. https://nepis.epa.gov/Exe/ZyPURL.cgi?Dockey=P100G6C6.txt

Carrasco-Hernandez, R., Smedley, A.R.D., Webb, A.R., 2015. Using urban canyon geometries obtained from Google Street View for atmospheric studies: Potential applications in the calculation of street level total shortwave irradiances. Energy and Buildings 86, 340–348. https://doi.org/10.1016/j.enbuild.2014.10.001

Castro, I.P., Robins, A.G., 1977. The flow around a surface-mounted cube in uniform and turbulent streams. Journal of Fluid Mechanics 79, 307–335. https://doi.org/10.1017/S0022112077000172

Falchi, M., Querzoli, G., Romano, G.P., 2006. Robust evaluation of the dissimilarity between interrogation windows in image velocimetry. Exp Fluids 41, 279–293. https://doi.org/10.1007/s00348-006-0148-3

Fallah-Shorshani, M., Shekarrizfard, M., Hatzopoulou, M., 2017. Integrating a street-canyon model with a regional Gaussian dispersion model for improved characterisation of near-road air pollution. Atmospheric Environment 153, 21–31. https://doi.org/10.1016/j.atmosenv.2017.01.006

Florens, E., Eiff, O., Moulin, F., 2013. Defining the roughness sublayer and its turbulence statistics. Exp Fluids 54, 1500. https://doi.org/10.1007/s00348-013-1500-z

Franke, J., Hellsten, A., Schlunzen, K.H., Carissimo, B., 2011. The COST 732 Best Practice Guideline for CFD simulation of flows in the urban environment: a summary. International Journal of Environment and Pollution 44, 419–427. https://doi.org/10.1504/IJEP.2011.038443

Garau, M., Badas, M.G., Ferrari, S., Seoni, A., Querzoli, G., 2018. Turbulence and Air Exchange in a Two-Dimensional Urban Street Canyon Between Gable Roof Buildings. Boundary-Layer Meteorol 167, 123–143. https://doi.org/10.1007/s10546-017-0324-4

Ho, Y.-K., Liu, C.-H., Wong, M.S., 2015. Preliminary study of the parameterisation of street-level ventilation in idealised two-dimensional simulations. Building and Environment 89, 345–355. https://doi.org/10.1016/j.buildenv.2015.02.042

Hu, H., Yang, Z., Sarkar, P., Haan, F., 2011. Characterization of the wind loads and flow fields around a gable-roof building model in tornado-like winds. Exp Fluids 51, 835. https://doi.org/10.1007/s00348-011-1102-6

Janssen, W.D., Blocken, B., van Hooff, T., 2013. Pedestrian wind comfort around buildings: Comparison of wind comfort criteria based on whole-flow field data for a complex case study. Building and Environment 59, 547–562. https://doi.org/10.1016/j.buildenv.2012.10.012

Kastner-Klein, P., Plate, E.J., 1999. Wind-tunnel study of concentration fields in street canyons. Atmospheric Environment 33, 3973–3979. https://doi.org/10.1016/S1352-2310(99)00139-9

Kastner-Klein, P., Rotach, M.W., 2004. Mean Flow and Turbulence Characteristics in an Urban Roughness Sublayer. Boundary-Layer Meteorology 111, 55–84. https://doi.org/10.1023/B:BOUN.0000010994.32240.b1

Kellnerová, R., Fuka, V., Kukačka, L., Uruba, V., Štěpán Nosek, Zbyněk Jaňour, 2014. Street Canyon Ventilation of Traffic Pollution: Comparison Between Experiment and LES. Conference paper: VI. International Symposium on Computational Wind Engineering https://doi.org/10.13140/2.1.1153.8883

Llaguno-Munitxa, M., Bou-Zeid, E., Hultmark, M., 2017. The influence of building geometry on street canyon air flow: Validation of large eddy simulations against wind tunnel experiments. Journal of Wind Engineering and Industrial Aerodynamics 165, 115–130. https://doi.org/10.1016/j.jweia.2017.03.007

Martinuzzi, R., Tropea, C., 1993. The Flow Around Surface-Mounted, Prismatic Obstacles Placed in a Fully Developed Channel Flow (Data Bank Contribution). J. Fluids Eng 115, 85–92. https://doi.org/10.1115/1.2910118

Monti, P., Leuzzi, G., 1996. A closure to derive a three-dimensional well-mixed trajectory-model for non-Gaussian, inhomogeneous turbulence. Boundary-Layer Meteorol 80, 311–331. https://doi.org/10.1007/BF00119421

Neophytou, M.K.-A., Markides, C.N., Fokaides, P.A., 2014. An experimental study of the flow through and over two dimensional rectangular roughness elements: Deductions for urban boundary layer parameterizations and exchange processes. Physics of Fluids 26, 086603. https://doi.org/10.1063/1.4892979

Ngan, K., Lo, K.W., 2016. Revisiting the flow regimes for urban street canyons using the numerical Green's function. Environ Fluid Mech 16, 313–334. https://doi.org/10.1007/s10652-015-9422-3

Nosek, Š., Kukačka, L., Jurčáková, K., Kellnerová, R., Jaňour, Z., 2017. Impact of roof height non-uniformity on pollutant transport between a street canyon and intersections. Environmental Pollution 227, 125–138. https://doi.org/10.1016/j.envpol.2017.03.073

Oke, T.R., 1988. Street design and urban canopy layer climate. Energy and Buildings 11, 103–113. https://doi.org/10.1016/0378-7788(88)90026-6

Ozmen, Y., Baydar, E., van Beeck, J.P.A.J., 2016. Wind flow over the low-rise building models with gabled roofs having different pitch angles. Building and Environment 95, 63–74. https://doi.org/10.1016/j.buildenv.2015.09.014

Pelliccioni, A., Monti, P., Leuzzi, G., 2015. An alternative wind profile formulation for urban areas in neutral conditions. Environ Fluid Mech 15, 135–146. https://doi.org/10.1007/s10652-014-9364-1

Perén, J.I., van Hooff, T., Leite, B.C.C., Blocken, B., 2016. CFD simulation of wind-driven upward cross ventilation and its enhancement in long buildings: Impact of single-span versus double-span leeward sawtooth roof and opening ratio. Building and Environment 96, 142–156. https://doi.org/10.1016/j.buildenv.2015.11.021

Perret, L., Blackman, K., Fernandes, R., Savory, E., 2017. Relating street canyon vertical mass-exchange to upstream flow regime and canyon geometry. Sustainable Cities and Society 30, 49–57. https://doi.org/10.1016/j.scs.2017.01.001

Rafailidis, S., 1997. Influence of Building Areal Density and Roof Shape on the Wind Characteristics Above a Town. Boundary-Layer Meteorology 85, 255–271. https://doi.org/10.1023/A:1000426316328

Rosten, E., Drummond, T., 2006. Machine Learning for High-Speed Corner Detection, in: Leonardis, A., Bischof, H., Pinz, A. (Eds.), Computer Vision – ECCV 2006: 9th European Conference on Computer Vision, Graz, Austria, May 7-13, 2006. Proceedings, Part I. Springer Berlin Heidelberg, Berlin, Heidelberg, pp. 430–443. https://doi.org/10.1007/11744023_34

Sini, J.-F., Anquetin, S., Mestayer, P.G., 1996. Pollutant dispersion and thermal effects in urban street canyons. Atmospheric Environment 30, 2659–2677. https://doi.org/10.1016/1352-2310(95)00321-5

Smagorinsky, J., 1963. General circulation experiments with the primitive equations. Mon. Wea. Rev. 91, 99–164. https://doi.org/10.1175/1520-0493(1963)091<0099:GCEWTP>2.3.CO;2

Sousa, J.M.M., Pereira, J.C.F., 2004. DPIV study of the effect of a gable roof on the flow structure around a surface-mounted cubic obstacle. Exp Fluids 37, 409–418. https://doi.org/10.1007/s00348-004-0830-2

Takano, Y., Moonen, P., 2013. On the influence of roof shape on flow and dispersion in an urban street canyon. Journal of Wind Engineering and Industrial Aerodynamics 123, 107–120. https://doi.org/10.1016/j.jweia.2013.10.006

Tominaga, Y., Akabayashi, S., Kitahara, T., Arinami, Y., 2015. Air flow around isolated gable-roof buildings with different roof pitches: Wind tunnel experiments and CFD simulations. Building and Environment 84, 204–213. https://doi.org/10.1016/j.buildenv.2014.11.012

Tominaga, Y., Mochida, A., Yoshie, R., Kataoka, H., Nozu, T., Yoshikawa, M., Shirasawa, T., 2008. AIJ guidelines for practical applications of CFD to pedestrian wind environment around buildings. Journal of Wind Engineering and Industrial Aerodynamics, 4th International Symposium on Computational Wind Engineering (CWE2006) 96, 1749–1761. https://doi.org/10.1016/j.jweia.2008.02.058

Uehara, K., Wakamatsu, S., Ooka, R., 2003. Studies on critical Reynolds number indices for wind-tunnel experiments on flow within urban areas. Boundary-Layer Meteorology 107, 353–370. https://doi.org/10.1023/A:1022162807729

Xie, X., Huang, Z., Wang, J., 2005. Impact of building configuration on air quality in street canyon. Atmospheric Environment 39, 4519–4530. https://doi.org/10.1016/j.atmosenv.2005.03.043

Yassin, M.F., 2013. Numerical modelling on air quality in an urban environment with changes of the aspect ratio and wind direction. Environ Sci Pollut Res 20, 3975–3988. https://doi.org/10.1007/s11356-012-1270-9

Chapter 4

3D simulations: influence of roof shape at a field study site in London

This chapter has been part of the main project MAGIC air UK:

This work represents the outcomes of a wonderful and fruitful collaboration at University of Surrey and at the MAGIC (Managing Air for Green Inner Cities) team. It was realisable thanks to a six months Erasmus+ traineeship fellow.

4.1 Summary

The aim of this work is to investigate the effects of roofs on flow and pollutant dispersion at a field study site on the South Bank of the Thames River in London UK. It is part of the Managing Air for Green Inner Cities (MAGIC) project being carried out by the university of Cambridge, Imperial College London, London South Bank University and the University of Surrey. The experiments were carried out in the EnFlo meteorological wind tunnel at the University of Surrey (Mechanical Engineering Sciences Department). In the first step a preparatory work was done by analysing the real roof shapes and identifying modelling criteria; in the second step three different configurations for the model (with some roofs, with all the roofs in the district or without roofs) were analysed in order to understand if roofs could influence the flow only locally or also at greater distances; in the third step two configurations (with all roofs and without roofs) were used to deeply investigate the local effects of roofs, considering two different flow regimes (skimming flow or wake interference). Pollutant dispersion was considered only in the third step. Results show that turbulence quantities around flat roofs and around sloped roofs greatly varied and that a general improvement in air quality is achieved for both analysed flow regimes, not only above roof level but also at pedestrian level,.

4.2 Introduction

The urban canopy is characterized by a wide range of elements and geometrical shapes interacting with the atmosphere. It is well known that ventilation plays a key role in transporting pollutants from the street level to the overlying air and, as a consequence, its correct prediction plays a crucial role in planning of healthy urban areas. Several experimental and numerical studies dealt with urban flows over both schematic and complex building geometries, focusing on different with spatial scales. A recent work of Ricci et al. (2017) highlights the differences in urban area models, respect to the employed level of modelling detail. They evaluated deviations caused by geometrical simplifications in a district of Livorno in terms of differences between mean velocity ratios (calculating the Fractional Bias, the normalized Mean Square Error, the correlation coefficient and the Fraction of data within a factor of 1.3). Nevertheless, this underlined the huge computational power required for numerical simulations of architectural or urban details at the level of parapets, street furniture, etc. As matter of fact, detailed configurations are usually performed for a single building or small areas by means of RANS models (see e.g. van Hooff and Blocken, 2010). With the aim to understand the urban fluid dynamics in depth, a great et extent of elements should be considered. Moreover idealised and simplified geometries are preferred to focus on the influence due to simplified components of the problem and to reveal the mechanism driving air ventilation and mixing processes. Thus much attention was paid in the literature to simple building configurations like the street canyon unit.

Regarding roofs, several authors evaluated the influence of different shapes on in-canyon wind flow and pollutant distribution patterns. Rafailidis (1997) compared two street canyons with aspect ratio of 1 and 2 (defined as the ratio between the street width and the height of the reference building AR_C = W/H), by using flat and gable roofs with 45 slopes. He concluded that roof shapes play a central role in ventilation, especially in the upper part of the urban canyons. Later other authors focused on the influence of gabled roofs by using both 2D street canyons (e.g. Xie et al., 2005; Yassin, 2011) and a single 3D building (e.g. Tominaga et al., 2015). A more systematic analyses was made at the University of Cagliari by both numerical (Badas et al., 2017) and experimental simulations (Garau et al., 2018). In these works a large range of canyon aspect ratios and different roof slopes were studied comparing flat and gabled roofs in terms of first and second order statistics and exchange fluxes. With the 2D street canyon configuration and the wind direction perpendicular to the building walls, they stated that the presence of any sloped roof could influence in a positive way the ventilation (calculated as the Air Exchange Flux at different canyon heights) not only in the flow above roofs, but also at pedestrian level. As already demonstrated by Ho et al. (2015), this is related to the increase of turbulent quantities in the entire field.

To study different shapes from the gabled one several authors considered isolated buildings to evaluate the impact of velocity field, surface pressure and pollutant dispersion. For example Xu and Reardon (1998) employed hip roofs and Natalini et al. (2013) vaulted ones. Huang et al., (2009) through several other authors, employed wedge-shaped roofs finding that the height of a wedge-shaped roof peak is a crucial parameter determining the vortex structure inside the canyon and influencing the pollutant distribution pattern; higher pollutant levels are observed for step-down canyons. This topic has particularly been studied with regards to siting roof-mounted micro turbines (e.g. Ledo et al., 2011; Abohela et al., 2013), but the analyses are usually made with the objective to identify the best installation point for maximum wind-turbine efficiency.

However, as stated before, real fluid dynamics behaviour in urban patterns is more complicated and other parameters like the variability of building height and shapes, intersections, presence of trees, influence the flow. Along this route, a more realistic model was considered in DAPPLE (Dispersion of Air Pollutants and their Penetration into the Local Environment). By a model of the real street network

at 1:200 scale and flat roof buildings of varying height, the mechanism of pollutant exchange within intersections was described in Carpentieri et al. (2012), Carpentieri and Robins (2015) or Soulhac et al., (2009). Measurements at several intersections, but using only one wind direction, reported in (Carpentieri et al., 2012), shown heterogeneous behaviour confirming the increased complexity of real intersection geometries. In these particular locations, the horizontal turbulent mass fluxes were found to be negligible respect to the mean fluxes; vertical fluxes indicated an increasing turbulent exchange at roof level at the intersection, highlighting the importance in exchange between canopy and external flow. The estimation of a proportionality between turbulent fluxes and concentration gradients showed a huge variability, suggesting that models can under-estimate turbulent fluxes where the velocity field is more complex.

This specific topic was also studied at the Czech Academy of Sciences by a module geometry. With relevance to the typical patterns of the central European cities, Nosek et al. (2016) modelled the urban site as a series of courtyards with different configurations: gable roofs at 45 slope above uniform building height or above varying building heights. By means of wind tunnel facilities they considered three different street canyon configurations, with AR_C = 0.8, and a line pollutant source in order to evaluate the correlations between ventilation process and concentrations. They found high correlation coefficient (>0.5) at roof level, irrespective of the canyon model and wind direction. Regarding roof height variability they stated that generally more pollutant is removed to the flow aloft from the non-uniform canyon and, in particular, the configuration in which the average height of the upstream building is higher than the downstream building achieved the best ventilation performance and the lowest spatially-averaged concentrations. Their study was later implemented in Nosek et al. (2017) focusing on the intersection flow behaviour. They highlighted that with the perpendicular wind direction, if the tallest building in the final part of the canyon is positioned up-stream, then the lateral exchange between canyon and intersections increased. For oblique wind direction, increasing height for up-stream buildings produced a stronger lateral ventilation. This reason emphasises that more realistic building shapes considerably change the flow and the consideration about pollutant dispersion behaviour in the urban pattern. However, it still remain to understand if the results are useful also in complex urban environments where a great amount of elements complicate the flux.

In this study attention is concentrated on the influence of roofs on a modelled site investigated by wind tunnel measurements. The work was part of the MAGIC (Managing Air for Green Inner Cities) project. It considers a real urban area of 500 m radius from St George's Circus, in South London. The goal of the MAGIC project is to understand the flow and pollutant behaviour, at first in the specific site mentioned above, and to propose solutions in order to develop cities with lower pollution level or heat island effect.

The present work aims to understand if in a real urban pattern (buildings with different height and width; streets with various canyon depth and aspect ratio; non uniform intersections; etc.), differences between flat roof model and shaped roof model exist in terms of ventilation and pollutant removal, not only in the flow above buildings, but also at pedestrian level. Understanding the impact of architectural elements as roofs on urban flow behaviour may positively contribute to a more responsible and efficient urban plan. In pursuit of this, the work was divided into three main steps: first step consists of a preparatory work analysing the roof shapes and choosing criteria to put to include them in the original site model; in the second step three different configurations (with some roofs, with all roofs and without roofs), were analysed in order to understand if roofs could influence the flow near buildings or also at larger distances; third step treats only two configurations (with all roofs and without roofs) used to investigate deeply the local effects of roofs, with reference to the so called skimming flow and wake interference regimes (Oke, 1988). Pollutant dispersion was considered only in the third step. Analysis made by coupled LDA (Laser Doppler Anemometry) and FFID (Fast

Flame Ionization Detector) technologies, are here presented in terms of first and second order statistics, including correlations between velocity and pollutant concentrations. For a series of selected points the joint probability function (JPDF) and the quadrant analysis were made.

The chapter is organised as follow: Section 4.2 summarises the literature survey which specifically introduces the main objective, works that deal with the influence of roof shape and the aim of present work. Furthermore the outstanding issues with respect to the roof usage in models are introduced. Section 4.3 focuses on the EnFlo Wind Tunnel facilities and the methods employed for measurements and post-processing. Section 4.4 outlines criteria and procedures applied to build the MAGIC model with flat roof, and the roofs in the existing model, and the characteristic of the boundary layer. Section 4.5 presents the results of the study carried. Finally, Section 4.6 reports conclusions of the work.

4.3 Methods

4.3.1 EnFlo Wind Tunnel

The experiments were conducted under neutral boundary layer conditions in the meteorological wind tunnel of the Environmental Flow Research Centre (EnFlo) at the University of Surrey, UK. The facility, reported in Figure 4.1, is a suck-down open circuit wind tunnel with a working section 20 m long (x-direction), 3.5 m wide (y-direction) and 1.5 m high (z-direction). The wind speed could be set in the range 0.3-3.0 m/s driven on two fans and the facility is capable of simulating both stable and unstable atmospheric conditions, by means of 15 vertically aligned heaters at the inlet section, combined with the floor cooling/heating system. However, this feature was not used in this study. The wind tunnel and its associated instrumentations were fully automated and controlled using virtual instrument software created by the EnFlo research staff using LabVIEW. The laboratory temperature was constantly monitored by thermistor rakes positioned downstream of to the inlet section and in each tunnel wall panel: an optimum temperature was imposed and maintained in order to assure a uniform inlet temperature profile both in the x and y direction. When temperatures were outsides of the acceptable range, the laboratory control system activated water-cooled heat exchangers, that cooled the air coming out the test section, together with fans placed on the laboratory ceiling, which mixed the air and reduced the natural stratification in the laboratory. The temperature deviation in the results here reported was of the order of ±0.5° C across the inlet.

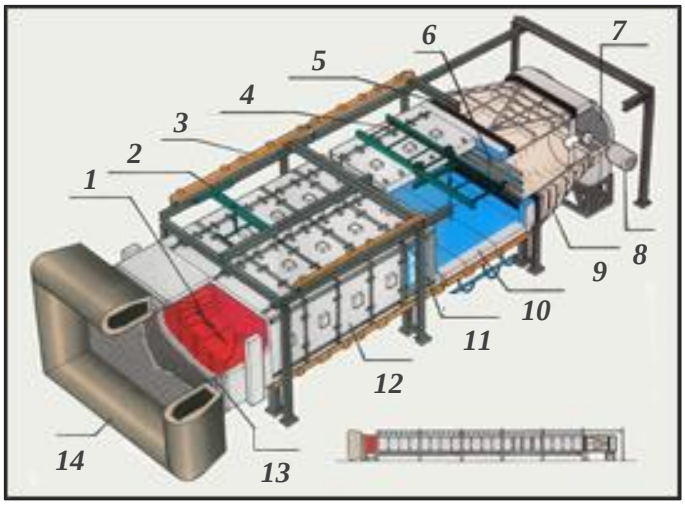

Figure 4.1 – EnFlo wind-tunnel facility scheme: (1) 405 kW heater; (2) Panel transfer trolley; (3) Bus bar; (4) traversing mechanism; (5) Flexible coupling; (6) Cooler; (7) Honeycomb screen; (8) Motor; (9) Transition duct; (10) Cooling panel; (11) Viewing panel; (12) Heating panel; (13) Smoothing screens.

An automated traverse system allowed three dimensional movements of the measurement equipment in the range of about x = 10 m, y = 2 m, z = 1 m. The origin of axis is usually defined at the centre of the measuring section at the ground, coincident with the turntable central point.

Other important tools were available in the EnFlo LabVIEW software, not only to control and optimise the measurements, but also for safety requirements. An example is the collision detector system that automatically calculated the best way to reach a desired measuring position in the model, avoiding undesired collisions of the probe with the model. Further characteristics of the facility are reported in Table 4.1.

Table 4.1 – Meteorological EnFlo Wind Tunnel Characteristics (Facilities | University of Surrey)

SPECIFICATIONS	• **Thermally stratified** • **Twin fans, suck through**
DIMENSIONS	• Working section: 20L x 3.5W x 1.5H m • Overall length: 27.2 m
AIR SPEED RANGE	• 0.3 to 3.0 m/s
INLET HEATER	• Number of layers: 15 at 0.1 m spacing • Maximum heating rate: 400 kW • Maximum temperature gradient: 80 °C/m • Maximum bulk temperature rise: 80 °C
ROOF/FLOOR PANEL PERFORMANCE	• Maximum heating rate: 2 kW/sq. m • Maximum surface temperature: 120 °C • Maximum cooling rate: 1 kW/sq. m • Minimum surface temperature: 5 °C
SIDE PANEL PERFORMANCE	• Number of heating zones: 3 at 0.5 m • Maximum heating rate: 0.2 kW/sq m

The boundary layer upstream of the model was shaped by means of a set of Irwin spires and a series of rectangular-shape roughness elements positioned between the Irwin's spires and the measurement section. This type of spire, extensively used in previous experiments at the EnFlo laboratory, is characterised by a triangular flat front plate, normal to the flow, with a splitter triangular plate on the downwind side (Figure 4.2). They are normally placed in a lateral row immediately after the inlet section, as shown in Figure 4.2 a. The design process for neutral stratification is detailed in Irwin (1981).

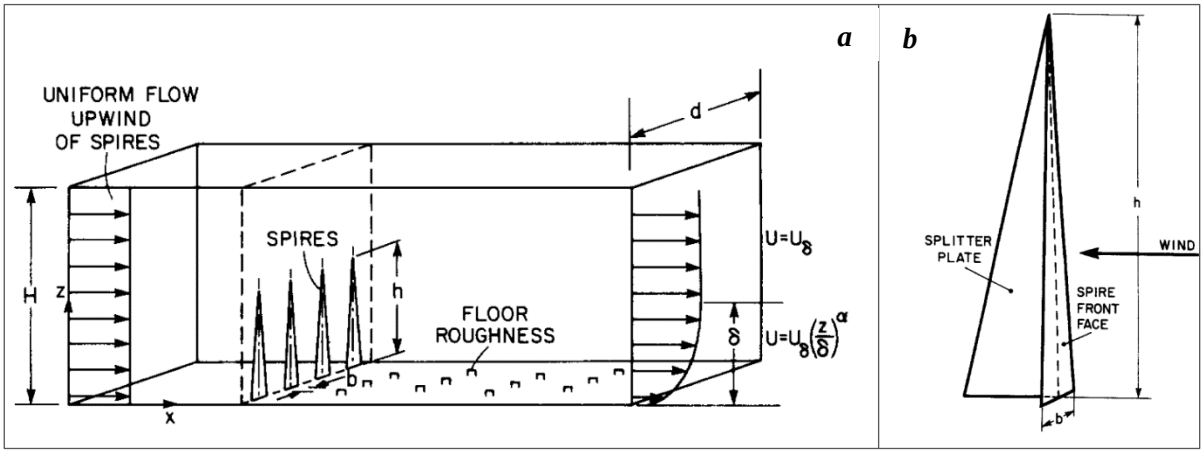

Figure 4.2 – Panel a: spires and roughness elements scheme from Irwin, (1981); panel b: spire scheme with triangular section and splitter plate.

In order to simulate the urban boundary layer like a NBLs (Neutral Boundary Layers), in this work the configuration extensively employed in the EnFlo laboratory was used. It consists of a set of five Irwin's spires 1.26 m height and 0.17 m wide at the basement, spaced laterally 0.63 m. Spires dimension was obtained by the previous formula, imposing $h = 1$ m and $\alpha = 0.21$, being $H = 1.5$ m. Roughness elements, employed to control and maintain the surface friction and drag, are formed by thin plates rectangular-shaped 80 mm x 20 mm (width and high respectively), 240 mm spaced in both x and y Figure 4.3. They are distributed along the first 12 m fetch of the wind tunnel.

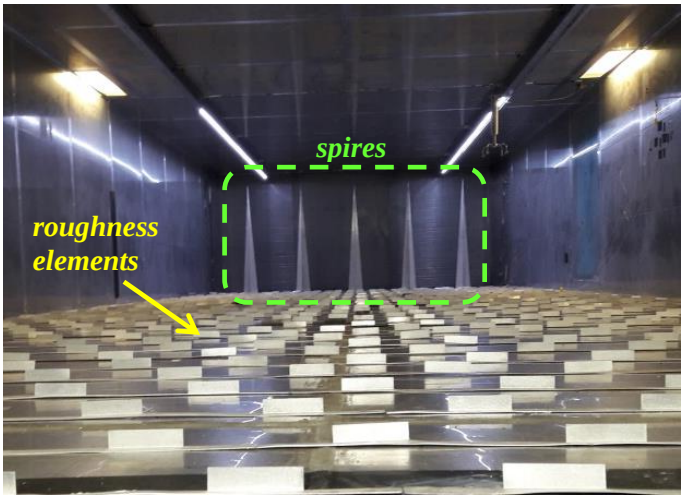

Figure 4.3 – Wind tunnel overview with the facilities employed to develop the neutral boundary layer upstream to the measurement section.

4.3.2 Laser Doppler Anemometry system (LDA)

The LDA technique (shown schematically in Figure 4) was used in the present set-up to measure the instantaneous velocities. This is an ideally non-intrusive optical method based on the Doppler effect, which is associate with the light propagation and accounts for the frequency shift observed whenever a wave (in this case the light source) is moving or is reflected off a moving surface.

The currently used dual-beam is configured with two in-going laser beams crossing at the intersection angle are used to form a measurement volume and the scattered light from bottom beams is collected in a single detector. The basic principle of the technique employed the Doppler effect twice: when the incident laser light impinges on a moving tracer particle and when light is scattered from the moving tracer particle. The detected frequency of scattered light is reported in the equation below:

$$f_r = f_b \frac{\left(1 - \frac{v_p e_b}{c}\right)}{\left(1 - \frac{v_p e_{pr}}{c}\right)} \approx f_b + v_p \frac{\left(e_{pr} - e_b\right)}{\lambda_b} \qquad 4.1$$

Where f_r is the receiver frequency, $f_b$is the beam frequency, f_p is the particle frequency, c is the light speed, v_p is the particle velocity, λ_b the light wavelength and $v_p\left(e_{pr} - e_b\right)/\lambda_b$ is the Doppler shift of the incident wave frequency. This relation is valid for $\left|v_p\right| \ll c$, where $c = f_b\lambda_b$. Thus the Doppler shift is linearly dependent on the velocity of the particle and to the difference between the normal vectors which appears when the direction of propagation between the incident and scattered waves differs. To resolve the Doppler shift directly, the most common approach is the dual-beam

configuration (Figure 4.4 a). In this way at the two waves intersection the measurement volume is formed and scattered waves are detected with a single detector. The frequency difference between the two waves, expressed in terms of velocity and direction φ can be written as:

$$f_D \approx \frac{2sen(\frac{\varphi}{2})}{\lambda_b}|v_p|\cos(\alpha) \qquad 4.2$$

The hardware of an LDA system consist of transmitting and receiving units. The optical component in the transmitting unit commonly counts the laser, the laser beam transmitter including the Bragg cells and splitters, the fibre and the LDA-head, as shown in Figure 4.4 b (Zhang, 2010). A COHERENT Genesis MX-STM laser with a 40 MHz frequency-shifted Bragg cell was here employed. The green light had a wavelength equal to 514.5 nm and the blue 488 nm. Both were conveyed by means of a Dantec Dynamics 27 mm Fibre-flow probe with a focal analyser (BSA).

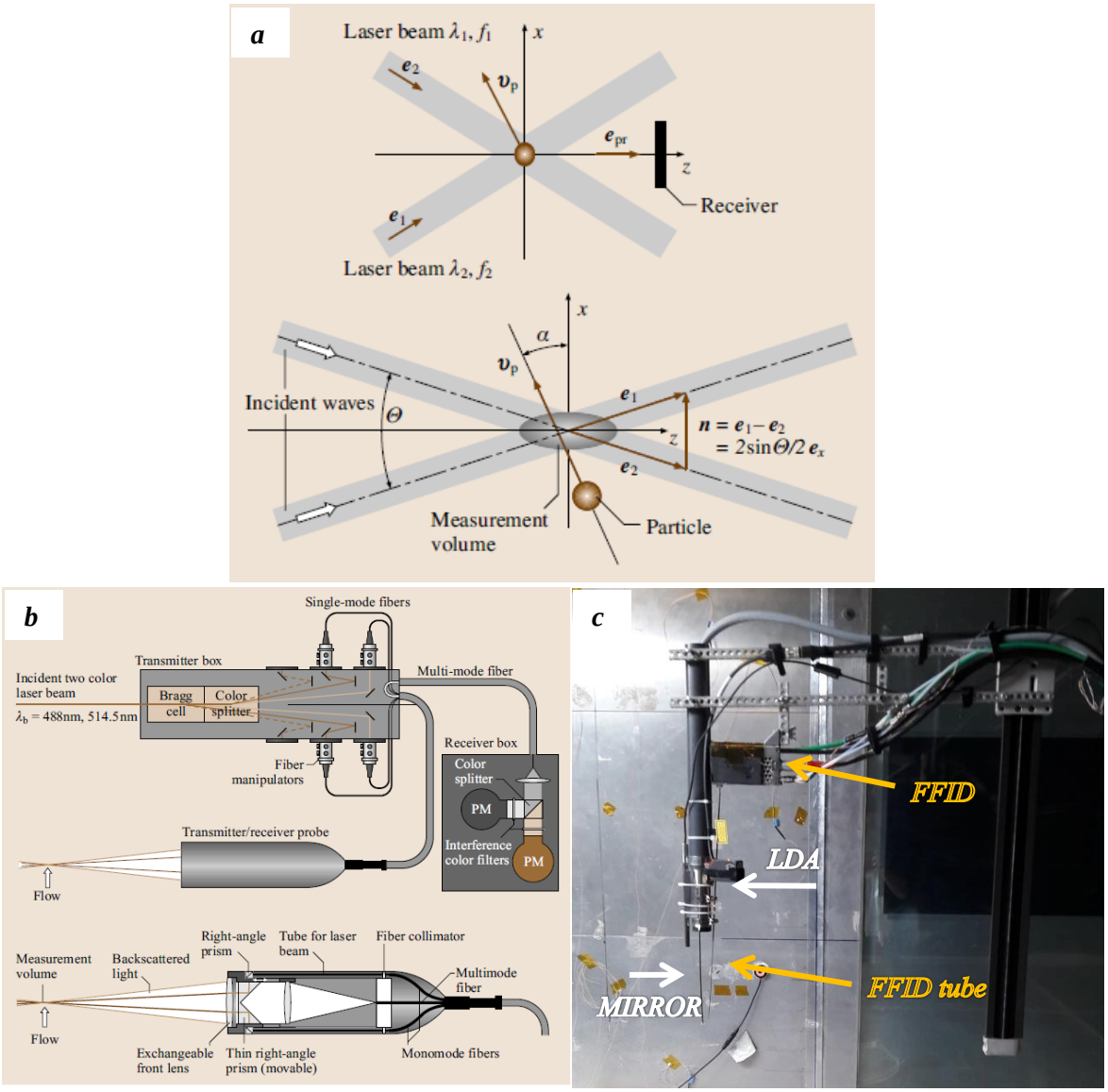

Figure 4.4 – Panel a: dual-beam configuration and vector relations relevant to determining the DOPPLER frequency (Tropea et al., 2007); Panel b: generic scheme for the LDA system suitable for measuring two velocity components (Tropea et al., 2007). Panel c: set-up used for the present work, with a coupled system LDA FFID.

After getting into the transmitter, the laser is separated and split into a pair of green and pair of blue beams. In order to resolve velocity directions, the Bragg cell is employed to shift one green and one blue beams. The four laser beams are then conducted into four fibres connected to the LDA head. This arrangement allow to measure two perpendicular velocity components simultaneously. The front lens on the LDA head enables all four laser beams to be focused at a unique point for forming the LDA measurement volume.

Two configurations were employed: the first configuration allowed the measurement of the stream-wise and lateral component of the velocity (u and v), for which the LDA probe was vertically mounted with a mechanical arm on the traverse. In the second configuration, used to measure the stream-wise and vertical component (u and w, respectively), a mirror was added to deflect the laser beams. The latter was 6 mm in diameter, positioned 145 mm below the probe lens and 15 mm from the measuring volume. The set-up is reported in Figure 4.4 c, together with the FFID (Fast Flame Ionisation Detector) system that is described later. For each measurement point the acquisition time was 150 seconds with a target acquisition frequency of 100 Hz. The latter, depending on the seeding rate, was variable; hence for time series analysis, the data resampling was necessary.

The LDA technique requires the presence of seeding particles, thus a sugar solution aerosol was employed, producing particles of nominal diameter 1 μm. A hydro-sonic pump generates the aerosol, while the seeding rate is regulated according to the difference between the desired and measured LDA sampling rate. The data collection times was chosen as 2.5 min in order to control the standard error in results, which was estimated as 3% in $\bar{u}$, 5% in $\bar{w}$, $\bar{v}$ 10 % in $\overline{u^2}$, 8% in $\overline{w^2}$, 14% in $\overline{uw}$.

4.3.3 Fast Flame Ionisation Detector system (FFID)

The HFR400 Fast FID (Flame Ionisation Detector) was employed for concentration measurements. The system produces an output signal that varies quite linearly with the volumetric hydrocarbon content of a gas, across a wide dynamic range. Basic operating principles are described below, further details can be found in Cheng et al., (1998).

The flame ions are collected by an electrode negatively based at 150-200 volts with respect to the burner, located below the electrode. Thermal ionisation can be consider negligible with respect to charge production from the chemical process. The chemical reaction is quite complex but the general process is $CH + O = CHO^+ + e^-$ $CH + O = CHO^+ + e^-$. For a hydrocarbon with molecular formula C_nH_m, the current collected by the electrode, i (A), is given by $i = r[C_nH_m]Q$, where the C_nH_m is the molar concentration $[mol\ cm^{-3}]$ and Q the sample volume flow rate through the detector $[cm^3s^{-1}]$. For aliphatic hydrocarbons the response is proportional to the number of carbon atoms in the molecule.

For the FFID technique, methane or propane are usually employed as a tracer. The pointwise sampling is directly made into the flame avoiding mixing process with the fuel, thus minimizing the transit time. In order to provide a constant mass flow to the FFID, the Ballast Chamber is employed: it maintains a very nearly constant pressure changes and, for this reason, it is also known as constant-pressure chamber. The sample is a through a small diameter transfer tube, connected to a larger tube in the Ballast Chamber. The scheme of the employed FFID system is reported in Figure 4.5. Calibration of the instrument is always necessary and it was achieved by introducing a mixture of gases with known composition into the sampling tube. The temporal response of the FFID depends on the length of the series of tubes between the entry of a sample and the hydrogen flame, but it is also important to take into account the longitudinal mixing of the sample. In this case the frequency response was near 200 Hz. Due to the length of the FFID sample tube, the mean delay in the sampling time, with respect to that of the LDA, was approximately 17 ms, which was used for the synchronisation between the velocity and the concentration time series. The coupled system was introduced by Carpentieri et al.

(2012). The propane (C_3H_8) - 1.8 % propane in air - was employed as a tracer with two kinds of outlet section, in order to represent both a pointwise and linear sources. The standard error in results was estimated as 5% in $\bar{c}$, 10 % in $\overline{c^2}$, and 15% in $\overline{uc}$, $\overline{wc}$.

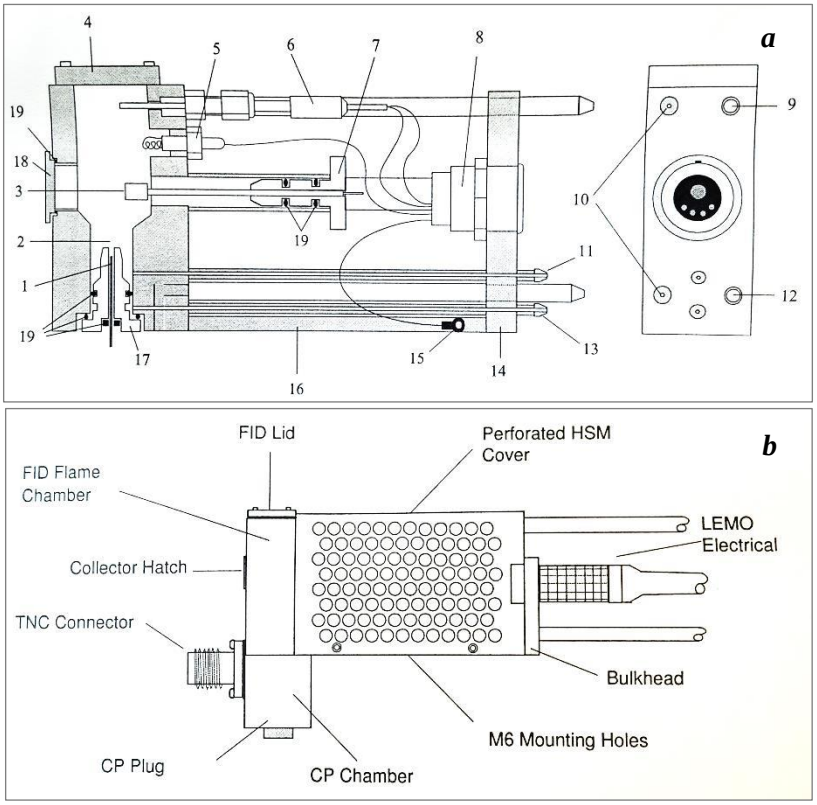

Figure 4.5 - Shematic representation of the Fast response Flame Ionization Detector (FFID). Panel a: (1) FID tube (sample capillary); (2) Flame; (3) Collector electrode; (4) Lid; (5) Glow plug; (6) Thermocouple; (7) Collector insulator assembly; (8) Electrical Connector; (9) FID bleed; (10) Vac supply; (11) Air; (12) CP Bleed; (13) Fuel; (14) Bulkhead; (15) Earth tag; (16) Baseplate; (17) Removable nozzle; (18) Inspection hatch; (19) O rings/seals (HFR400 User Manual, 1998).

4.4 MAGIC wind tunnel model

4.4.1 MAGIC site overview

MAGIC is a EPSRC (Engineering and Physical Sciences Research Council) funded project carried out by the University of Cambridge, the Imperial College London, the London South Bank University and the University of Surrey (MAGIC-air.uk). Its main goal is to understand both outdoor and indoor flow and pollutant behaviour within urban environments, in order to develop cities with lower pollution levels or heat island effect. As a case study, the project considers a real urban area in South London, of 500 m radius from St George's Circus.

A water station was located above a central building. This is used to assimilate meteorological data, compare their with experimental simulation or to use the same as input data in numerical simulations. Barometric pressure, humidity, air temperature, dew point, wind speed and wind direction were monitored with a Gill MetPak instrument. Wind parameters were measured with the Gill WindSonic ultrasonic anemometer aligned with cardinal directions. However is only the horizontal components were measured.The London Heathrow mean wind directions graph (Figure 4.6) was used as reference to understand the more frequent and strong wind direction in London. The more intense and frequent wind direction is from South-West to North-East.

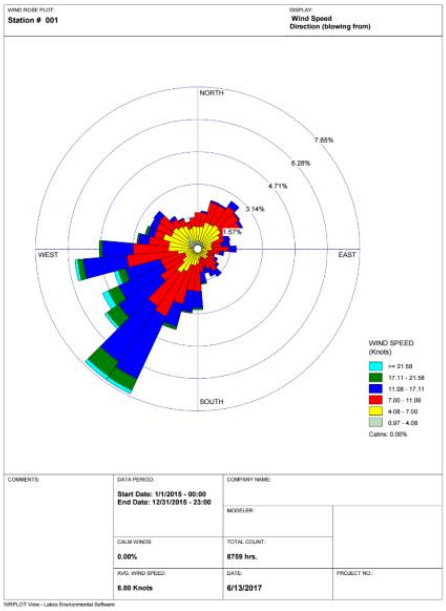

Figure 4.6 - Mean wind direction graph from London Heathrow weather station.

4.4.2 Wind tunnel flat model

The basic 1:200 scale wind tunnel model employed for the experimental campaign was made at the University of Surrey in April 2017 (Figure 4.7). It consists of 150 flat roof buildings, with flat roofs. This model was built with a simplified geometry from the Ordnance Survey (OS) open dataset. The area of interest is sited in the National Grid square TQ37NW (OS Map).

In order to build the model, three open datasets from Ordnance Survey were loaded and elaborated in QGIS, an open-source geographic information system software. The three datasets consist of: the OS Terrain 5 Digital Terrain Model (DTM), with 5 m horizontal resolution; OS Vector Map Local (VML), with the detailed building outlines, paths and street names; the OS Building Height Attribute (BHA) with height attributes for each building in OS Master Map Topography Layer. In OS BHA the heights described at pp. 146-147 of the OS Mastermap Topography Layer user guide (OS MTL guide, 2016) are available. However, details about roofs are not available yet.

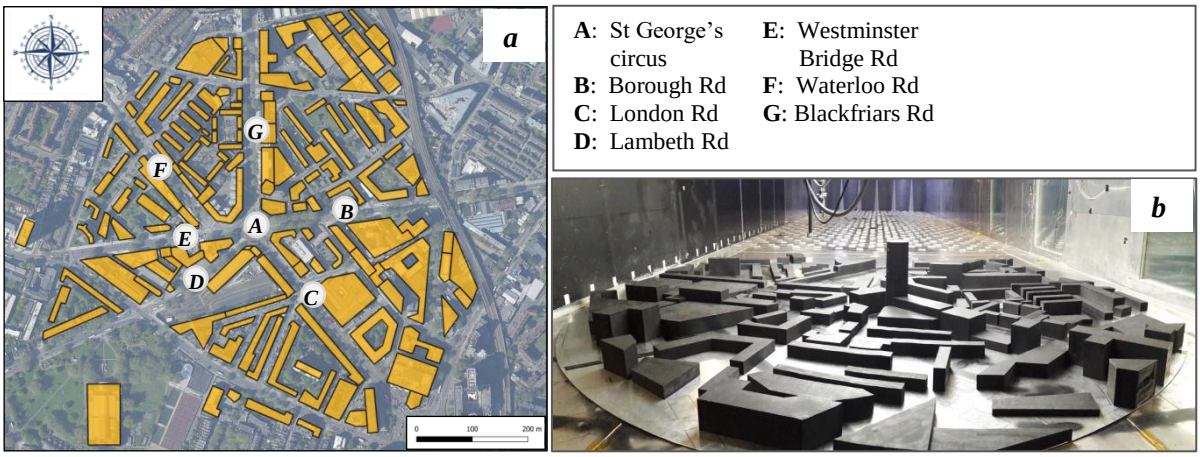

Figure 4.7 - Panel a: Plan view of the MAGIC site in London. The ortho-photo view is overlapped with the 150 model buildings. Panel b: MAGIC model with flat roofs, created for experiments; wind tunnel view on the rotating turntable.

Blocks for wind tunnel model has been built with flat roof and the *RelH2* height which is the building height at the eaves level, above ground. The origin of the coordinates system of the model was chosen to be the obelisk (St George's Circus central point), that corresponds to the central point of the wind tunnel turntable.

4.4.3 Wind tunnel roof model

In order to define the model with roofs, a preliminary study about the distribution, the slope and the shape of roofs at the MAGIC site was conducted by means of maps and geospatial data, already described above.

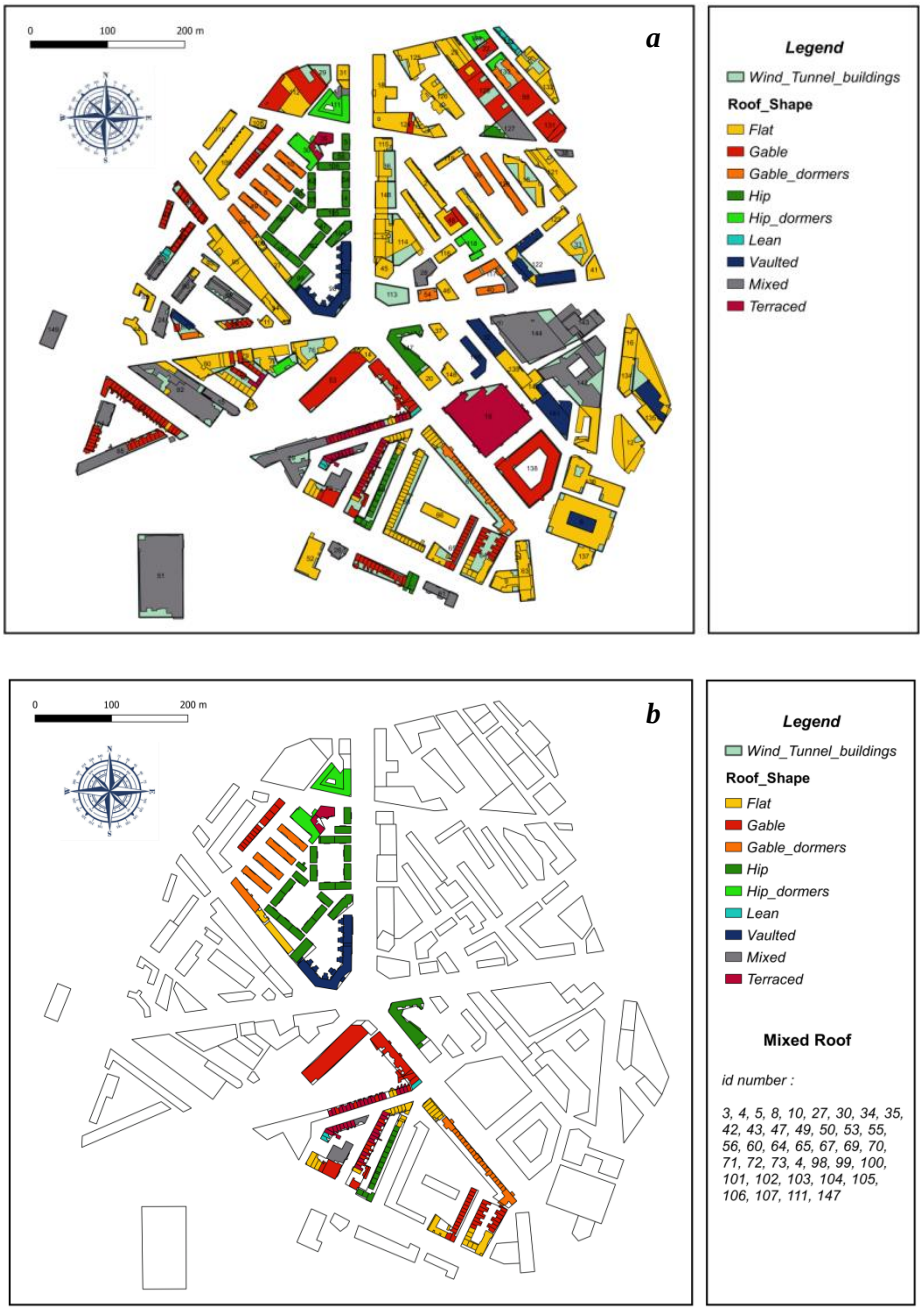

Figure 4.8 – Panel a: distribution of 9 different shapes of roof in the MAGIC site, considering the 150 buildings adopted for the wind tunnel model. Panel b: distribution of building with roofs in the MAGIC wind tunnel model.

By using of the open source GIS software QGIS, a comparison between maps of slope and the satellite images was possible. Then calculating the differences in height between the eaves and the maximum level of every buildings, 9 different shapes of roof were identified. Their distribution is reported in Figure 4.8 a.

In order to perform a preliminary campaign of experiments, a few considerations were taken into account: the North-West part of the model is the denser with respect to the variety of roofs; the main wind direction (more frequent and intense) is around α = 220°; the Clarence Centre at the beginning of London Rd (C in Figure 4.7), near St George's circus (A in Figure 4.7) have a strategic importance respect to the MAGIC project. Consequently to this, only some roofs were built to test the model and the final distribution employed in the wind tunnel, is reported in Figure 4.8 b.

All geometry detail topics as cornices, chimneys, etc., were omitted in this session; however these represent an interesting point for future investigations.

4.4.4 NBLs characteristics

Reference flow conditions were measured by an ultrasonic anemometer sited upstream to the measurement section for which the reference mean wind speed at 1 m height was found equal to $U_{ref} = 2.0\, m/s$, for all the experiments here reported. However the reference wind speed is registered by means an anemometer positioned 5 m downstream to the spires, where the boundary layer is not completely developed yet. For this reason the approaching flow characteristics, reported in the Figure 4.9 (a-f) are affected by a small differences in wind speed at z = 1000 mm, for which the non-dimensional velocity on the top is a little bit higher than the unit (blue line in Figure 4.9 a, underline this fact). The approaching flow characteristics were analysed in previous works (e.g. Marucci et al. 2018) with a series of three profiles in the developed region (y = 0 and x = 12500, 13950, 15400 mm, considering the origin of x axis at the inlet section).

The mean velocity and turbulent quantities profiles at the three locations show no significant variations with x, ensuring sufficient longitudinal uniformity in the analysed region. The combination of spires and roughness elements, allow to obtain a thickness of $\delta \cong 1$ m; other aerodynamic parameters are: roughness length $z_0 = 0.002$ m, the displacement height $d_0 = 0$, the friction velocity $u_* = 0.132$ m/s ($u_*/U_{ref} = 0.066$), for the exponent $\alpha = 0.24$. The Reynolds number based on the roughness length and the friction velocity $Re_* = z_0 u_*/\nu \approx 17.6$ (where $\nu = 1.5 * 10^{-5}$ is the kinematic viscosity of air at standard conditions T ≈ 20°, $P = P_{atm}$) was llarger than the minimum requested for flow fully independent of the Reynolds number, according to (Snyder and Castro, 2002). Reynolds numbers could be also expressed as $Re = \delta U_{ref}/\nu \approx 1.3333e + 05$, well above the threshold for the incoming velocity profile and large turbulence structure of the flow to be independent of Reynolds number Snyder (1981).

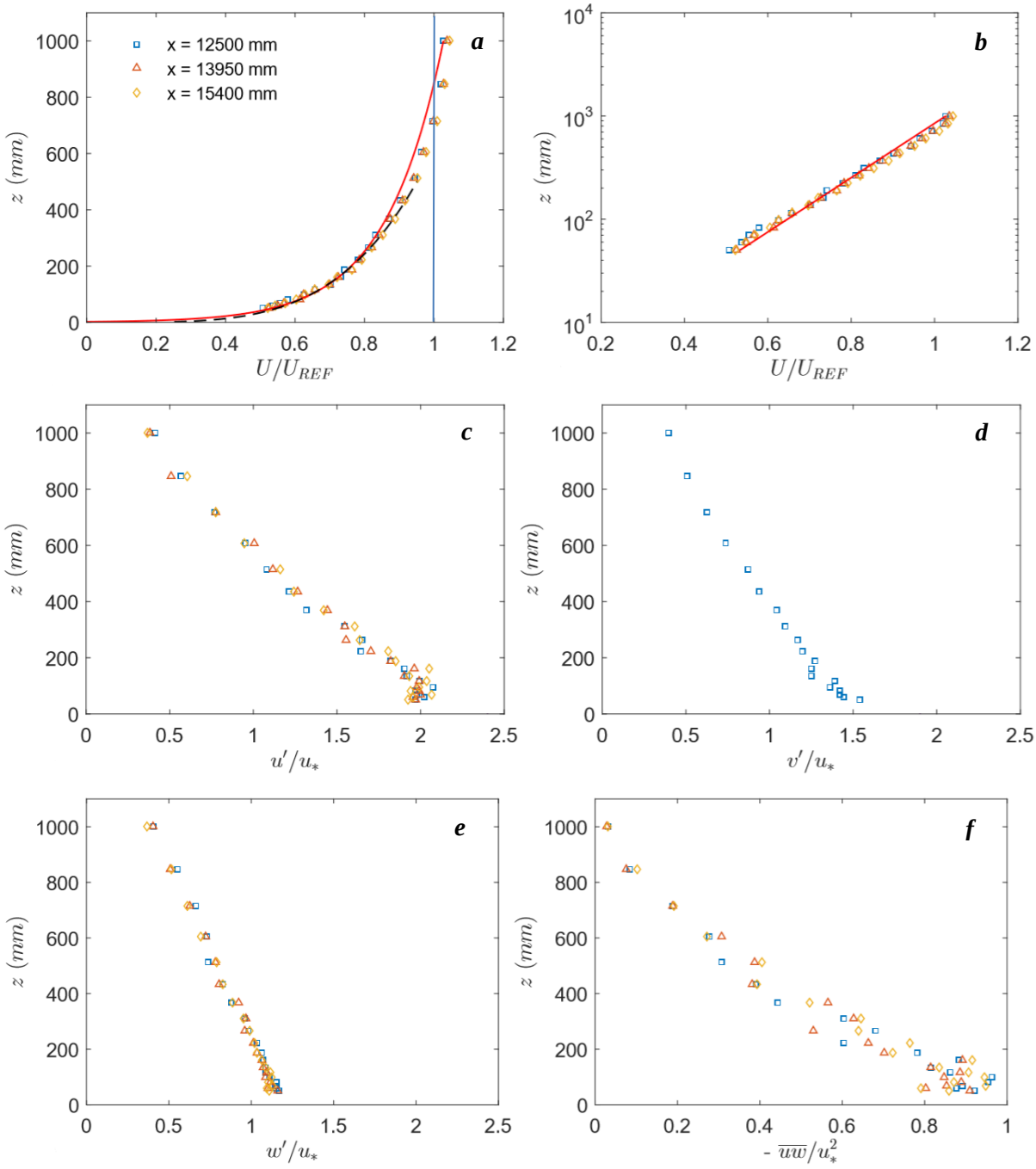

Figure 4.9 - Profiles of mean horizontal velocity, turbulent intensities and Reynolds shear stress, made non dimensional by the friction velocity for the NBL. The continuous red and blacks line in a, b, are respectively logarithmic and power law fitting (Marucci et al., 2018)

4.5 Results and Discussion

A preliminary investigation of the flow was initially performed in order to understand if differences between the flat roof and the no-flat roof model were observable and significant. After this, a more specific analysis was carried out near the building walls, from street level up twice the building height. Moreover, two specific sites were analysed with both point and linear sources, London Rd and Waterloo Rd. The main characteristics of each measurement campaign are reported in the table below (Table 4.2).

Table 4.2 - Characteristics of the four block measurements campaign with analysed parameters, wind directions, related figures in this chapter and objectives.

Analysis Name	Measured Parameters	Met. WD α	Map Fig. n.	Section n.	Description
Preliminary Measurements	u w	310° 130° 220°	4.10-4.16 4.10-4.16 4.10	4.5.1	Distributed profiles to understand the general behaviour and differences between two configurations (with, without roofs)
North-West district	u v w	220°	4.20**Figure 4.20**	4.5.2	Vertical profiles around Clarence Centre (98), along Blackfriars Rd and in three canyons downstream to Waterloo Rd
Waterloo Rd	u w c	220°	4.31Figure 4.30	4.5.3	Analysis made with both linear and pointed source in Waterloo Rd. Vertical profiles in the 2nd canyon downstream between buildings 49-8
London Rd	u w c	230°	4.43	4.5.4	Analysis made with both linear and pointed source in St George's Circus 5 vertical profiles in 4 sections

For each case a table was prepared and measurement points ordered with a progressive number that univocally identifies the locations. In these tables, characteristics of the closest buildings or the street and other details are associated to the measurement points. Points are otherwise plotted in a map with the corresponding number. Results are mainly discussed in terms of first and second order statistics, respect to parameters that were measured for each case. Further analysis was performed for interesting points by using the time series. For this specific analysis, data were post-processed and velocity measurements were resampled by means of an interpolation, in order to obtain the proper constant frequency needed to analyse together concentration, pressure and velocity parameters.

4.5.1 Preliminary measurements on the influence of roofs

Preliminary measurements were fulfilled with 18 points spread out in the entire model, where the flow was evaluated considering three roof configurations (with five roofs above buildings 60, 49, 8, 3, 10; with all roofs as defined in previous paragraphs; without roofs) and three wind directions (met. direction equal to $220°, 130°$ and $130°$). These variables were chosen in order to study the general influence of the increasing number of no-flat roofs on the model and the variation of the angle of incidence on building facades. Additional 15 points allocated in three profiles perpendicularly aligned with respect to the wind direction, were employed at two different heights, in order to verify the increase of turbulence at higher levels.

4.5.1.1 Vertical profile measurements

Measurement points were investigated by means of vertical profiles with a spatial resolution of $\Delta z = 10\,mm$ in z direction, from the minimum height $z = 30\,mm$ to the maximum equal to $z = 160\,mm$ for points 1-10, $z = 330\,mm$ for point 11-13 and $z = 450\,mm$ for points 14-18 (at the model scale). All the measured points are shown in Figure 4.10 and characteristics of the nearest buildings are reported in Table 4.3.

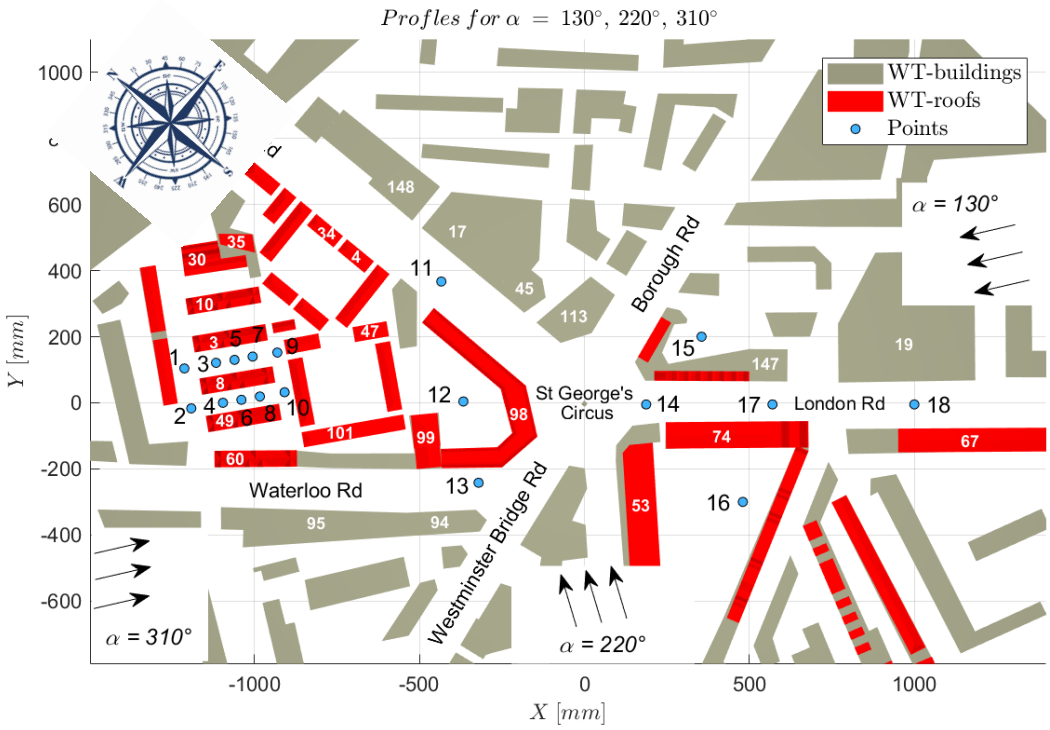

Figure 4.10 - Wind tunnel model: measurement points (blue circles with black number) at MAGIC site for the meteorological wind directions (black arrows on the left side) equal to 130°, 220°, 310°. The most important buildings are numbered in white. Red geometries represent the roofs above buildings.

Table 4.3 - Characteristics of the buildings closest to the measurement points: preliminary analysis with three meteorological wind direction α = 130°, α = 220° and α = 310°.

Point n	Building n	Building + Roof Height	Roof type	Roof Slope α	Comment
1-8	49, 8, 3	80.0 + 17.5	Gabled dormers	35°- 41°	2nd - 3rd street canyons
9-10	103, 101	59 + 12	Hip	28°	Courtyard
11	17, 45	120, 405	Flat	0°	Blackfriars Rd
12-13	98	123.2 + 20.0	Vaulted		Courtyard
14	147, 74	45+10, 46+23	Gabled	29°, 30°	London Rd
15	147	45+10	Gabled	29°	Clarence Centre Courtyard
16	74-73 53	46+23, 39.7+15 28+20	Gabled	30° 20°	Train Station
17	147, 74	45+10, 46+23	Gabled	29°, 30°	London Rd
18	67, 19	38.6+18, 51.5	Gabled, Flat	26°, 0°	London Rd

Considering the wind direction equal to 310°, very small differences were visible in all the results so that a wide comment is not necessary. Such small differences may be justified by the fact that the measurement points were initially chosen at the centre of the street canyon. Indeed if the approaching wind flow direction is parallel to the building walls, in the skimming flow regime (where the width-to-height ratio is less than 1.5) and with the length-to-width ratio higher than 2, the wind flow generates a mean wind along the axis, sometimes uplifting along walls (Ahmad et al. 2005). Nevertheless, it is

interesting to underline a couple of aspects: the flow comparison between point 1 and 2, revealed no large discrepancy meaning that the incoming flow into the third street canyon (between buildings 8 and 3) is very similar to the second one (between buildings 49 and 8). What would have been expected to happen at point 1 was an increase of the vertical velocity component and turbulence, however a deviation from this behaviour might have been caused by the presence of only one pitched roof upstream the points, not very sloped (building 107 with gable roof slope of 15°). Furthermore, the two series of outcomes for the points along the street canyons revealed that going downstream intensity differences grow up at lower levels. This behaviour is visible from point 3 (third canyon) or 4 (second canyon) to points 9, 10 respectively. As an example results for point 7 are reported above (Figure 4.11) looking at the first order statistics, the vertical component shows variations between the configuration without roofs and the two with roofs (*5 Roofs* or *All Roofs* as reported in the legend with green and red symbols, respectively). The last two perfectly overlap each other, underlying that the upstream roof (building 107) is not influent on the flow. Looking at the second order statistics, in the presence of roofs turbulent quantities are lower: it seems that the effect of roofs with dormers on the flow is equivalent to an increase of the total height of the walls for a large part of roof area.

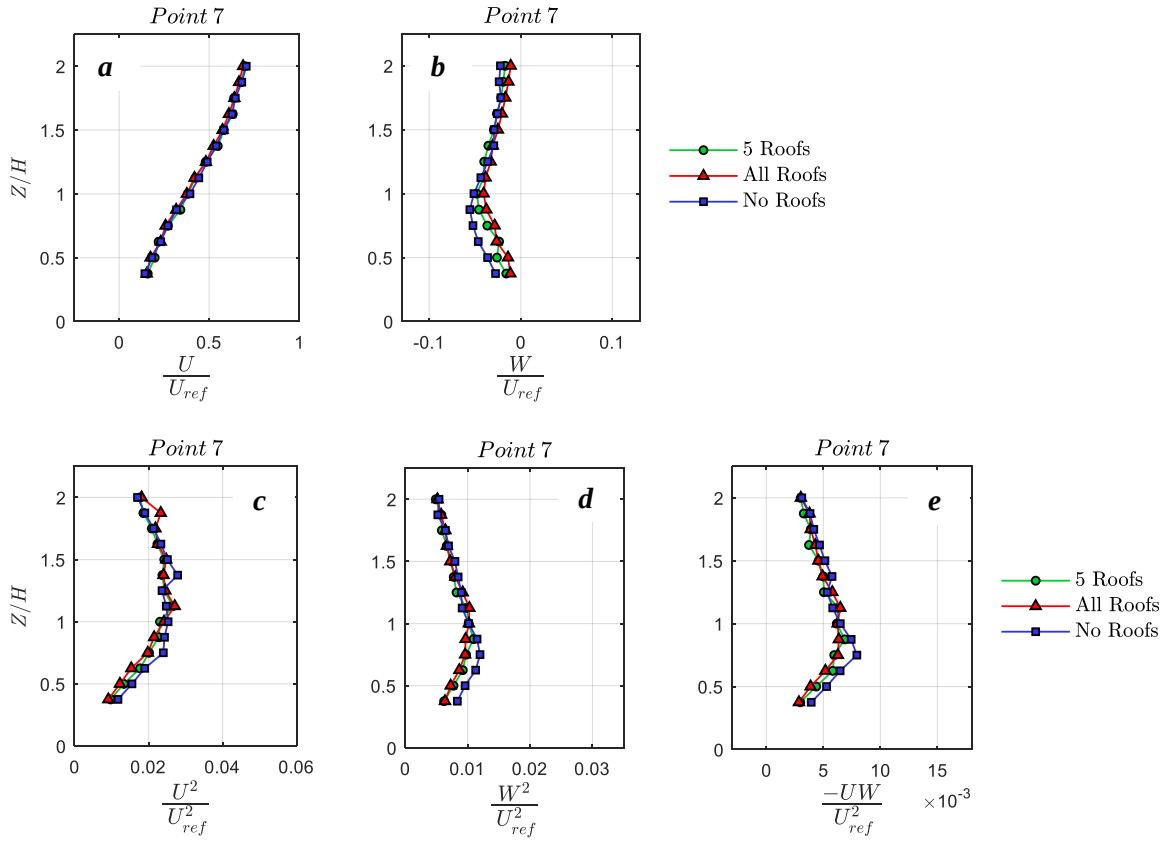

Figure 4.11 - First and second order statistics for point 7: mean stream-wise (a) and vertical (b) velocity components; variance of the mean stream-wise (c) and vertical (d) velocities; Reynolds stress (e) factor. Quantities are made non-dimensional by the free stream velocity U_{ref} , measured at z = 1 m and by the eaves height of buildings 3, 8. The non-dimensional height at the top of the buildings with roof is equal to z/H = 1.22 .

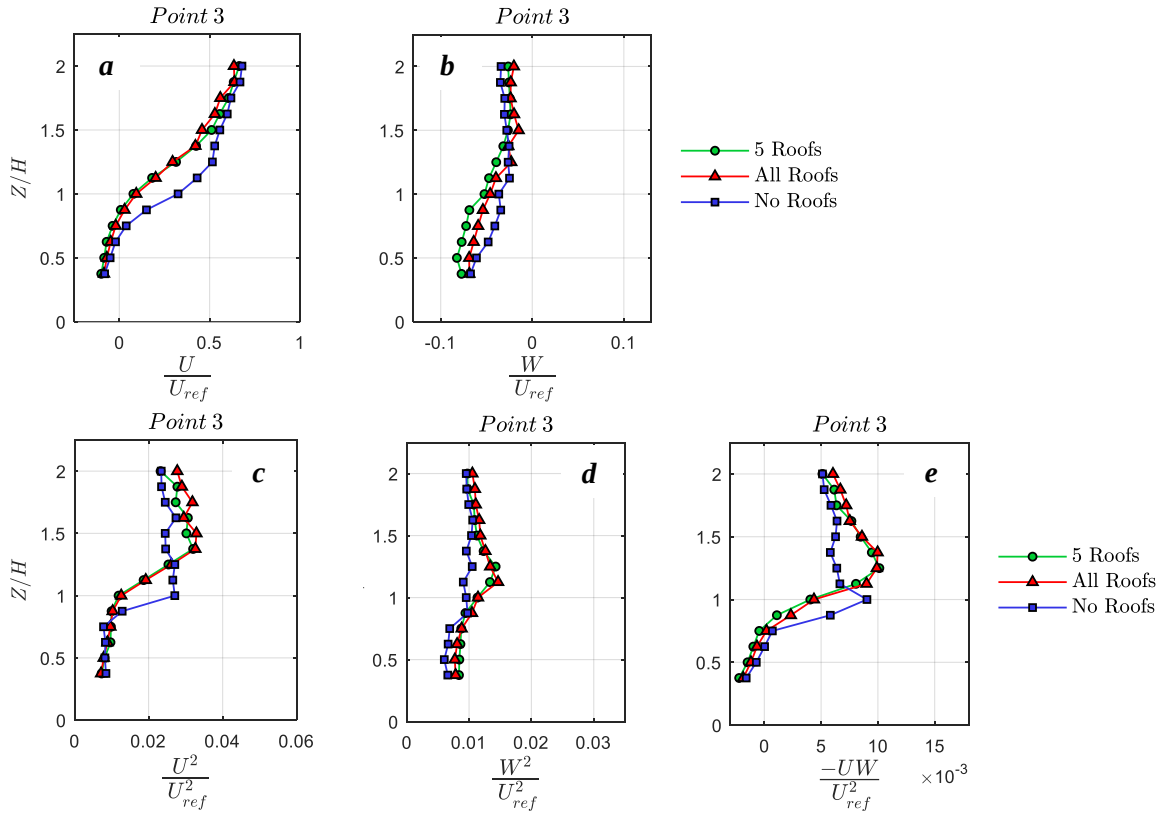

Figure 4.12 - First and second order statistics for point 3: mean stream-wise (a) and vertical (b) velocity components; variance of the mean stream-wise (c) and vertical (d) velocities; Reynolds stress (e) factor. Quantities are non-dimensional by the free stream velocity U_{ref} , measured at z = 1 m and by the eaves height of buildings 3, 8. The non-dimensional height at the top of the buildings with roof is equal to z/H = 1.22 .

Regarding the data acquired with wind direction $\alpha = 220°$ only eight points (3-9 and 4-10) were measured, focusing on the street canyon. When the approaching flow to the buildings array is perpendicular, discrepancies are more significant with respect to the parallel wind direction. A large number of literature works described the flow behaviour in the skimming flow regime for idealised street canyons, both at the central section and at intersections. Here similar trends were found, even though the geometry employed was more complex and varied respect to the majority of the works. As an example, Figure 4.12 shows vertical profiles for both first and second order statistics at point 3 (third canyon external point, Figure 4.10). Profiles are shifted up as a consequence of the increasing height, but quantities decrease around the eaves level in case of stream-wise component and increase for the entire profiles in case of vertical components and Reynolds stress factor. An interesting behaviour is visible for the vertical component comparing the *5 Roof*s and the *All Roofs* configurations, which are not perfectly overlapped: the first one shows higher vertical values in the canyon and despite the small amplitude, they are present in all the external points (3, 4, 7, 8) where the nearby buildings with roofs seems to influence the flow by reducing the vertical component. Therefore near the street canyon borders, the adoption of more detailed models is suggested in order to better estimate the flow behaviour.

The third wind direction employed was $\alpha = 130°$ (Figure 4.10). Among the configurations, differences are visible only for some point into the street canyon, due to the influence of the hip roofs above the buildings that constitute the courtyard agglomerate upstream, and for the point 12, placed at the centre of the courtyard of building 98. About the street canyon, the second (buildings 49, 8) is more influenced than the third one (buildings 8, 3). Odd points from 1 to 9 (third canyon), show

differences in the vertical component of the velocity, less evident for the variance factor. However the larger differences are found for point 9, decreasing until point 1, as show in Figure 4.13.

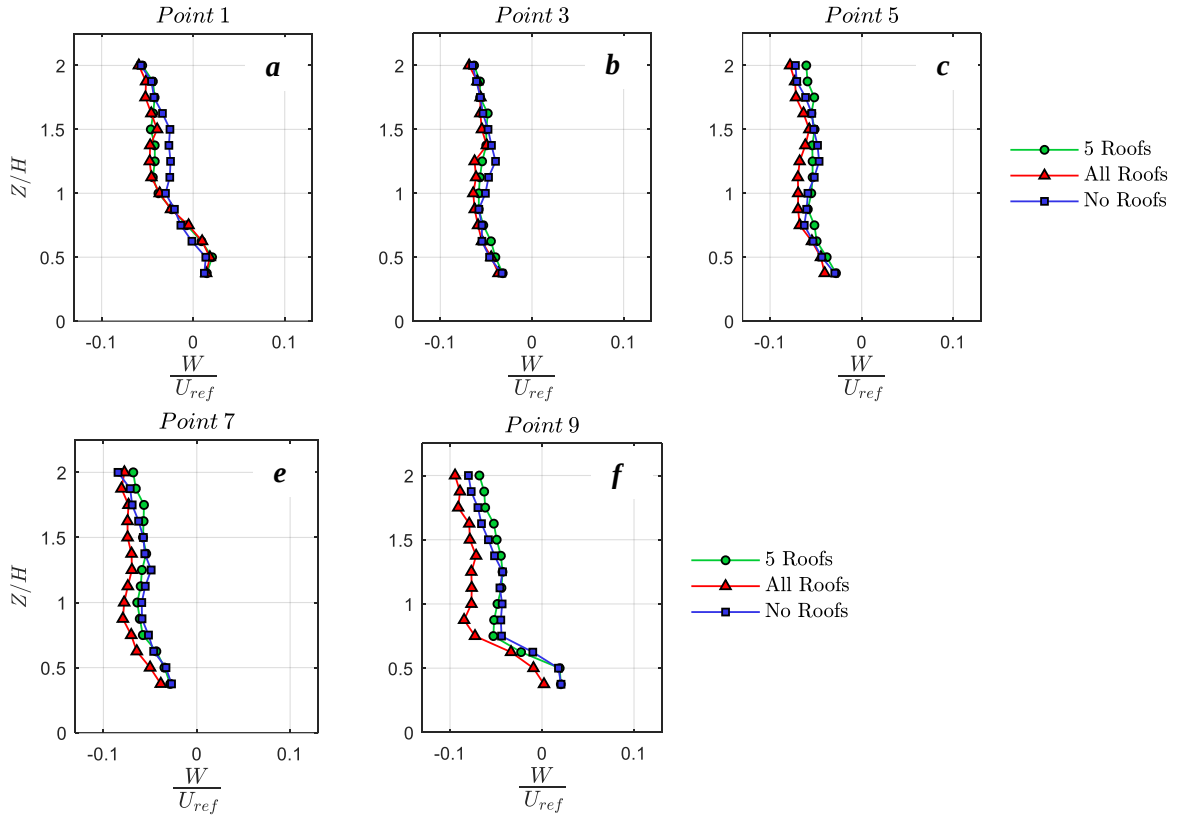

Figure 4.13 - Mean vertical velocity components for measurement points in the third street canyon (see Figure 4.10) between buildings 8 and 3: point 1 (a), point 3 (b), point 5 (c), point 7 (d), point 9 (e). Quantities are non-dimensional by the free stream velocity U_{ref}, measured at z = 1 m and by the eaves height of buildings 3, 8. The non-dimensional height at the top of the buildings with roof is equal to z/H = 1.22 .

Every point (second canyon) shows the same trend with higher differences for point 10, downstream the building with hip roofs and building 98. In this case also the stream-wise velocity component is influenced, with a reduction of velocities from the building high (e.g. Figure 4.14, point 10). Discrepancies registered through the configurations in the second canyon with respect to the third, should be related with a coupled effect of the wind direction, that flows above the buildings with hip roofs forming the courtyard, and the presence of building 98 with a vaulted roof. Indeed the second canyon is perpendicularly invested by the wind which previously flowed on the facades of building 98.

Regarding the 5 Roofs configuration, outcomes show little differences moving from point 9 to point 1 (or from point 10 to point 2); profiles varied not linearly from the No Roofs results to the All Roofs ones. As a consequence it could be stated that where the density of roofs in a district is high, there is an interaction among the various roofs and the effects are generally amplified respect to the case of an isolated roof. Thus, for a correct prediction of the main events on a street, the usage of a more detailed model seems advisable.

Another interesting point is the number 12, reported in Figure 4.15. It exhibits huge differences among the configurations: the shapes of all the profiles remain identical but shifted upwards as effect of the increasing height with the roofs. Lower stream-wise and higher vertical velocities, characterised by opposite directions at lower street canyon levels, are observed for the entire profile.

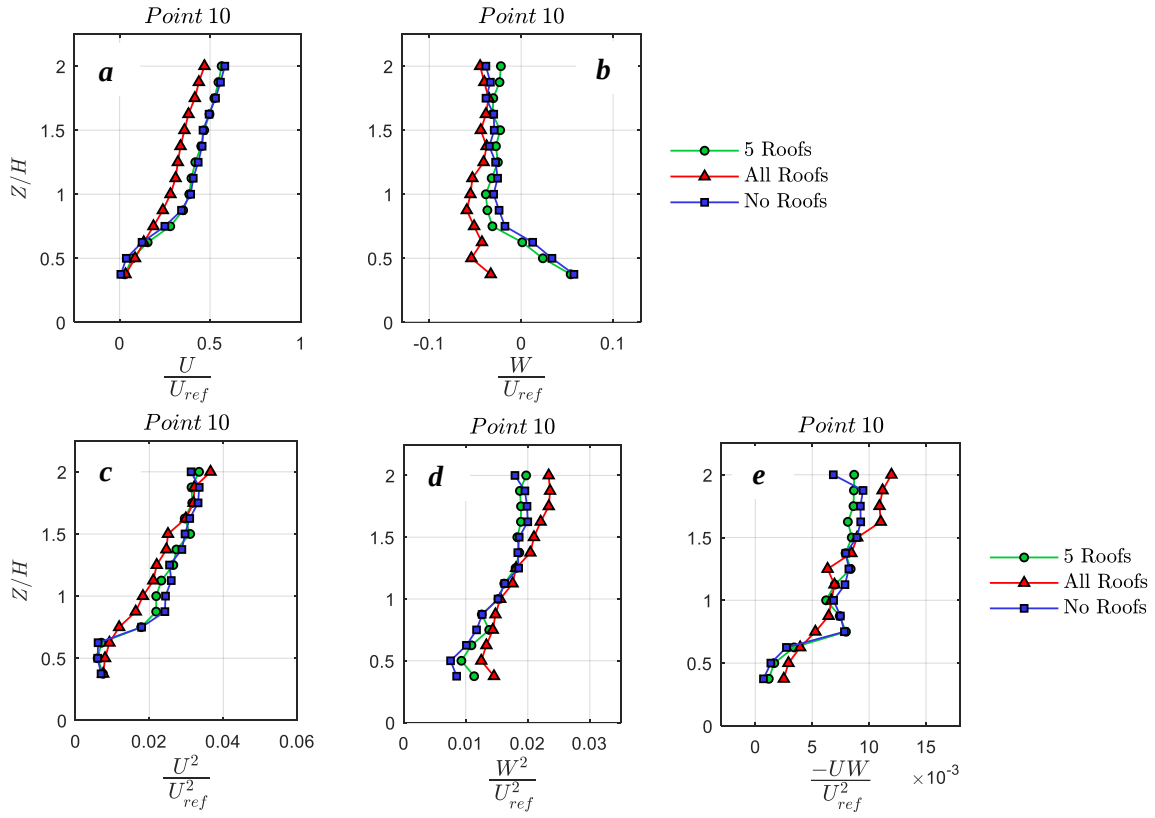

Figure 4.14 - First and second order statistics for point 10, external point in the second street canyon (see Figure 4.10) between buildings 49 and 8: mean stream-wise (a) and vertical (b) velocities components; variance of the mean stream-wise (c) and vertical (d) velocities; Reynolds stress (e) factor. Quantities are non-dimensional by the free stream velocity U_{ref} , measured at z = 1 m and by the eaves height of buildings 8, 49. The non-dimensional height at the top of the buildings with roof is equal to z/H = 1.22 .

In the meantime, the variance of vertical velocity and the Reynolds stress show lower values below the eaves level and higher values above. Furthermore, the maximum value belongs to this height, which is larger in case of roofs, underlying the increase of turbulence in the shear layer. Profiles collapse around 2H level in a unique curve, with the exception of the vertical velocity component.

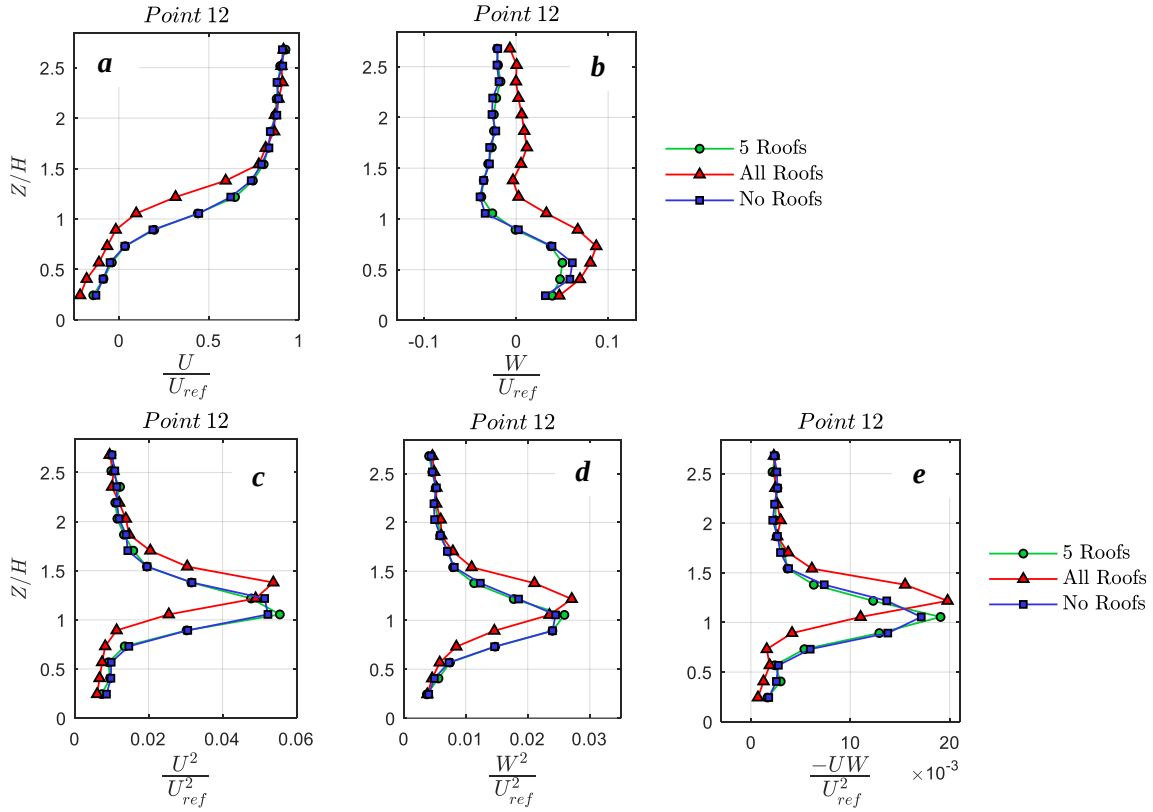

Figure 4.15 - First and second order statistics for point 12 in the centre of the building 98 courtyard: mean stream-wise (a) and vertical (b) velocities components; variance of the mean stream-wise (c) and vertical (d) velocities; Reynolds stress (e) factor. Quantities are made non dimensional by the free stream velocity U_{ref}, measured at z = 1 m and by the eaves height of building 98. The non-dimensional height at the top of the buildings with roof is equal to z/H = 1.16.

4.5.1.2 Lateral profile measurements

In order to verify the influence of roofs above the building height, a series of three lateral profiles (A, B, C with 5 points each one, as shown in Figure 4.16), where measured in the region between building 98 and the 5 buildings with gabled-dormer roofs. Measurement where carried out at z = 120 mm and z = 140 mm (model scale), for which the corresponding non-dimensional heights with respect to the buildings in the district are reported in the table below (Table 4.4). The lowest height was chosen to be approximately twice the height of the shortest building with gentle hip roofs, in order to avoid capturing effects of the latter. The profiles are equally spaced each other 100 mm along the wind direction, while the points are 150 mm far apart in each profile.

Table 4.4 - Non-dimensional heights for buildings above the profiles A, B, C with respect to z = 120 mm and z = 140 mm. H_r is the total height of buildings with roofs, H_e is the eaves heigth.

z model scale [mm]	z/H_r - z/H_e Build. 98	z/H_r - z/H_e Build. 101, 103, 47, 34, 4, etc.	z/H_r - z/H_e Build. 60,49,3,8,10	z/H_r - z/H_e Build. 30
120	0.84 - 0.97	1.69 - 2.00	1.23 - 1.50	3.00 - 5.45
140	0.98 - 1.14	1.97 - 2.37	1.44 - 1.75	3.50 - 6.36

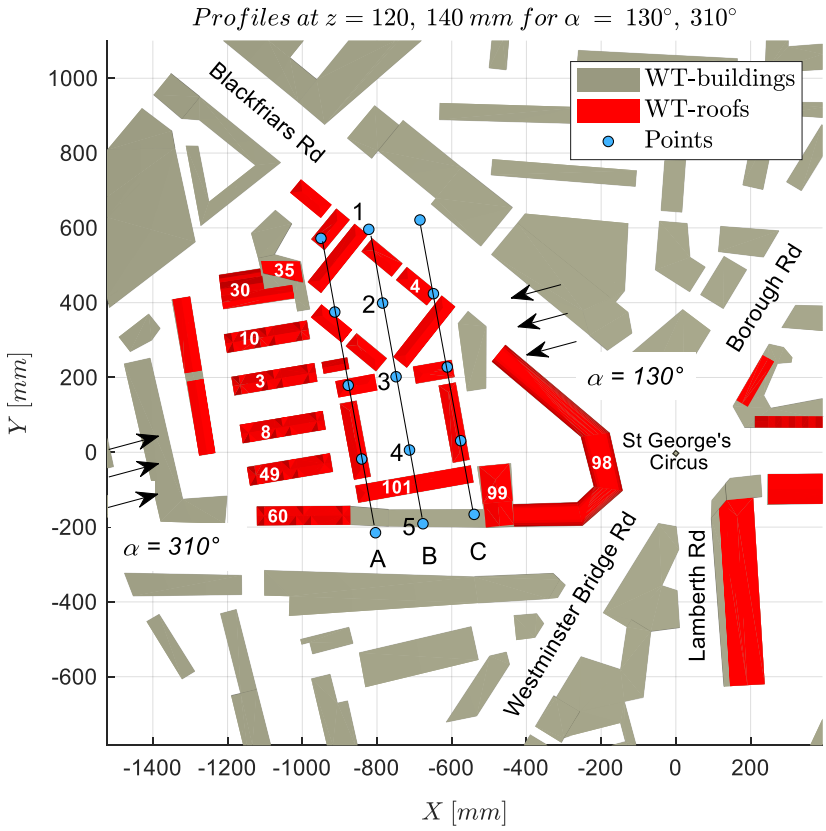

Figure 4.16 - Three span-wise profiles (A,B,C) on the wind tunnel model: measurement points (blue circles with black number) at MAGIC site for the meteorological wind directions (black arrows on the left side) equal to 130°, 310°. The most important buildings are numbered in white. Red geometries represent the roofs above buildings.

Results for wind direction equal to 310° do not show significant differences between the three configurations maybe for the not favourable height chosen for the measurements. For this reason they are not reported here. On the other hand with the 130° wind direction some differences can be seen for both the first and the second order statistics, especially for points 3, 4, and 5 with peak values at point 4. These points outcomes exhibits lower stream-wise Figure 4.17 and higher vertical velocities (Figure 4.18) in case of *All Roofs* configuration respect to the others and a similar trend was registered also for the variance factors (e.g. Figure 4.19). As a matter of fact, from point 3 to point 5 differences through the configurations have not got a linear trend and point 4 appears particularly influenced by the roof presence with discrepancies evaluated in a range of $0.2 - 0.3$ for streamwise component and around $0.05 - 0.08$ for the vertical component. Regarding the turbulent quantities, differences are around $20 - 40$ %. By increasing the measurement height from $z = 120\,mm$ (left panel of Figure 4.17-Figure 4.19) to $z = 140\,mm$ (right panel of Figure 4.17-Figure 4.19), the differences increase and from profile C to profile A, going downstream, the first one (and closest to buildings 98 and 99), is the most affected by discrepancies. Even though quite obvious, it is important to underline that the 5 Roofs configuration is here correctly showing the same results as the *No Roofs* case. In fact, the 5 buildings with gable-dormer roofs for the particular wind direction considered, are downstream the measuring region.

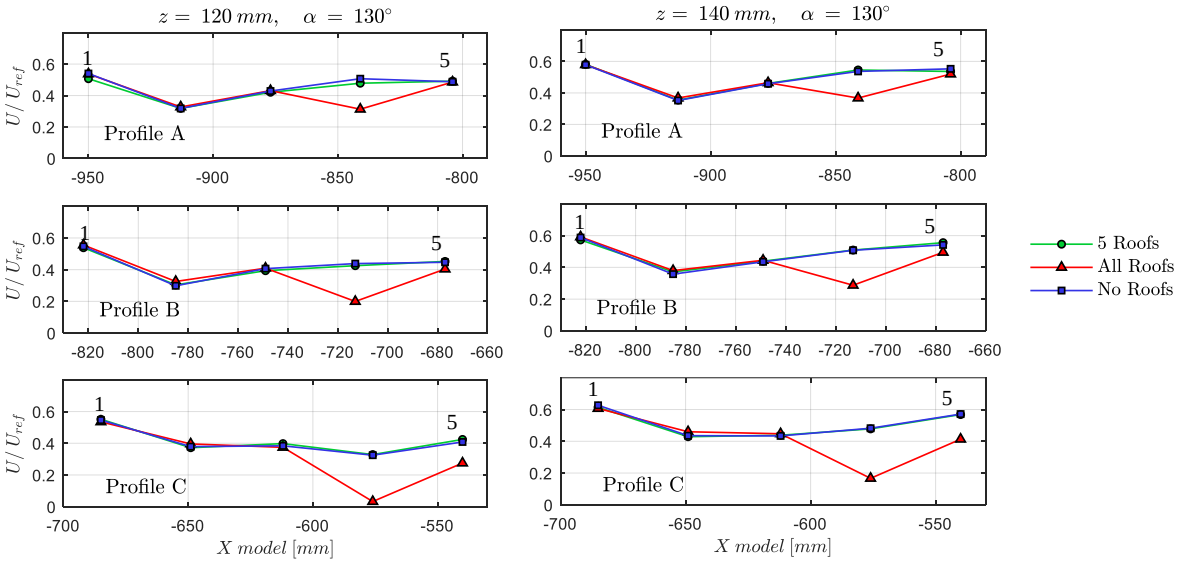

Figure 4.17 - Mean stream-wise velocity for lateral profiles A, B, C at z = 120 mm (left panel), z = 140 mm (right panel) and the wind direction equal to α = 130°. Quantities are made non dimensional by the free stream velocity U_{ref}

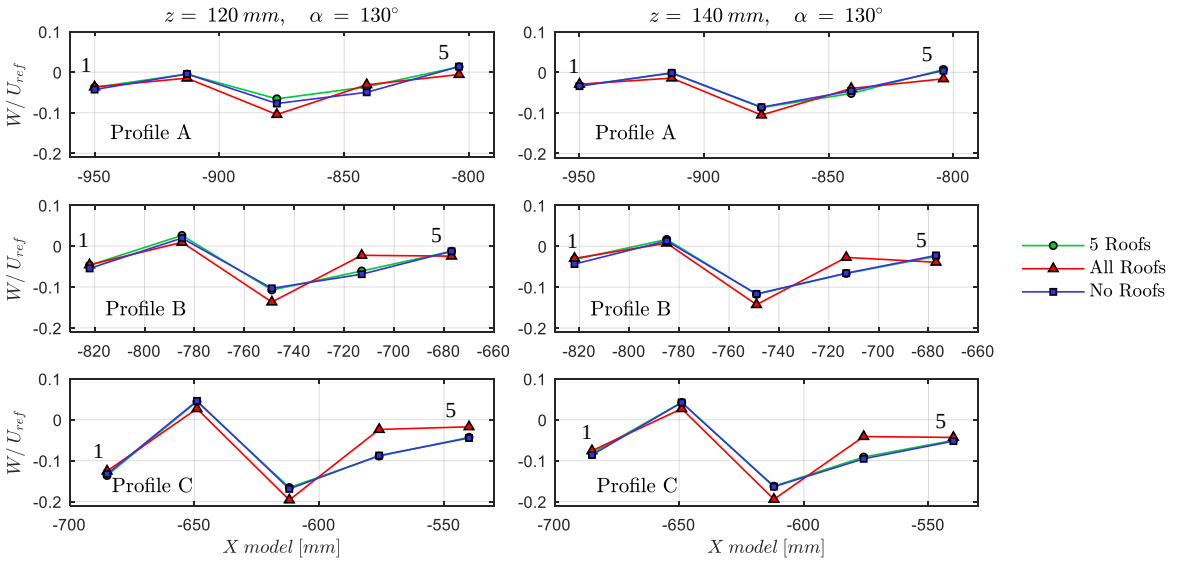

***Figure 4.18* - Mean vertical velocity for lateral profiles A, B, C at z = 120 mm (left panel), z = 140 mm (right panel) and the wind direction equal to α = 130°. Quantities are made non dimensional by the free stream velocity U_{ref}.**

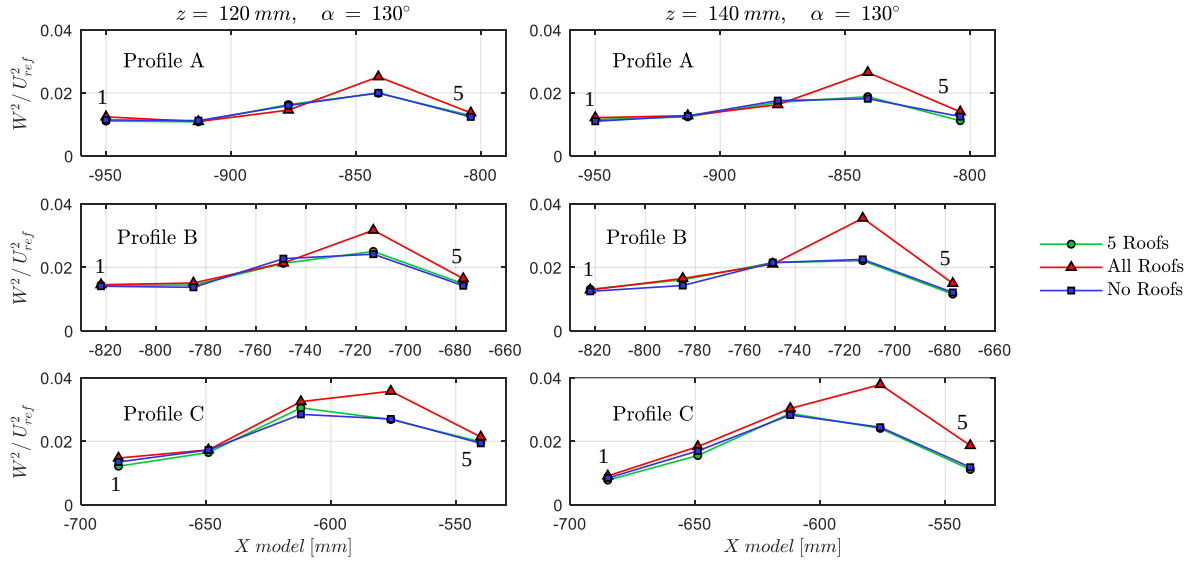

Figure 4.19 - Variance of the mean vertical velocity for lateral profiles A, B, C at z = 120 mm (left panel), z = 140 mm (right panel) and the wind direction equal to α = 130°. Quantities are made non dimensional by the free stream velocity U_{ref}

4.5.1.3 Conclusions on the preliminary analyses

The preliminary analysis of wind direction and roof variability within the MAGIC model in London South Bank, has been presented. Differences within the configurations were identified for both the channelling and recirculation flow respectively with the parallel and perpendicular approaching wind flow on the analysed building walls. The introduction in the model of just five roofs was found to strongly influence the flow locally, while to usage of a major number of roofs in a district was found useful in order to better estimate the mean and turbulent flow components. Indeed roofs effects are overlapped and they have a strong impact at the intersections. The most interesting results were found for the wind direction perpendicularly approaching the street canyon and the building main facades in general and for the courtyard of building 98, tallest than the others around. Very gentle sloped roofs and very short buildings wide spaced, were not found of interest maybe also for the limitations of instrumentation in the same specific area of the model. Indeed the minimum height achievable to the probe in z direction was $z = 30\,mm$ (that means $z/H = 0.5$ in case of buildings 101, 103, etc. which formed the squared courtyards), the minimum distance from walls and from the roofs was 15 mm, which do not allowed to properly investigate flow close to the buildings. Results from lateral profiles shown that, at higher levels, turbulent quantities increase at certain distance and height from the upstream buildings.

Accordingly to these aspect some assumptions were taken for the following work: the 5 Roofs configuration will not be further investigated; the wind angle around $\alpha = 220°$ will be used in order to focus on the street canyon, the courtyard of building 98 and on a main road in the district representing a channelling flow (Blackfriars Rd); higher spatial resolution will be employed as well as measurement points closer to the building walls; the maximum height position will be around $z/H = 2$. As final note, even though no general conclusion can be stated at this stage of the work, measurements have given an insight in the complexity of the flow in a real urban area.

4.5.2 North-west district investigation

The measurements were carried out with the wind direction set equal to $\alpha = 220°$, which represents the meteorological direction with the most frequent and intense wind speeds in London. This was actually chosen in order to be perpendicular to the relatively simple array of 5 buildings (Nos. 60, 49, 8, 10, 3) and 4 canyon with similar dimensions. This configuration is particularly interesting as it is similar to the street canyon configuration usually analysed in the literature with both 2D and 3D models. Although gabled-dormer roofs with different slope are not yet studied, we can assimilate their behaviour with the gabled roof analysis just for comparisons with the literature cases. The goal of this section is to understand the differences in the flow, both below and above roof level, around buildings with and without shaped roofs. Measurements were performed as vertical profiles with 16 points from $z = 30\ mm$ at model scale, equivalent to 6 m at full scale, equally spaced with $z = 10\ mm$ until $z = 160\ mm$ (or 32 m at full scale). Locations of the measurement points are reported in Figure 8 and Table 3 together with details of the closest building (height, roof type, slope) and some further comments. Results are split into three main groups: points 1-10 are in the courtyard of building 98; points 11-16 and 21 are in Blackfriars Rd; points 17-22 and 23 are downstream of Waterloo Rd, in the street canyons between buildings array 60, 49, 8, 3 and 10. The total number of investigated points was 23.

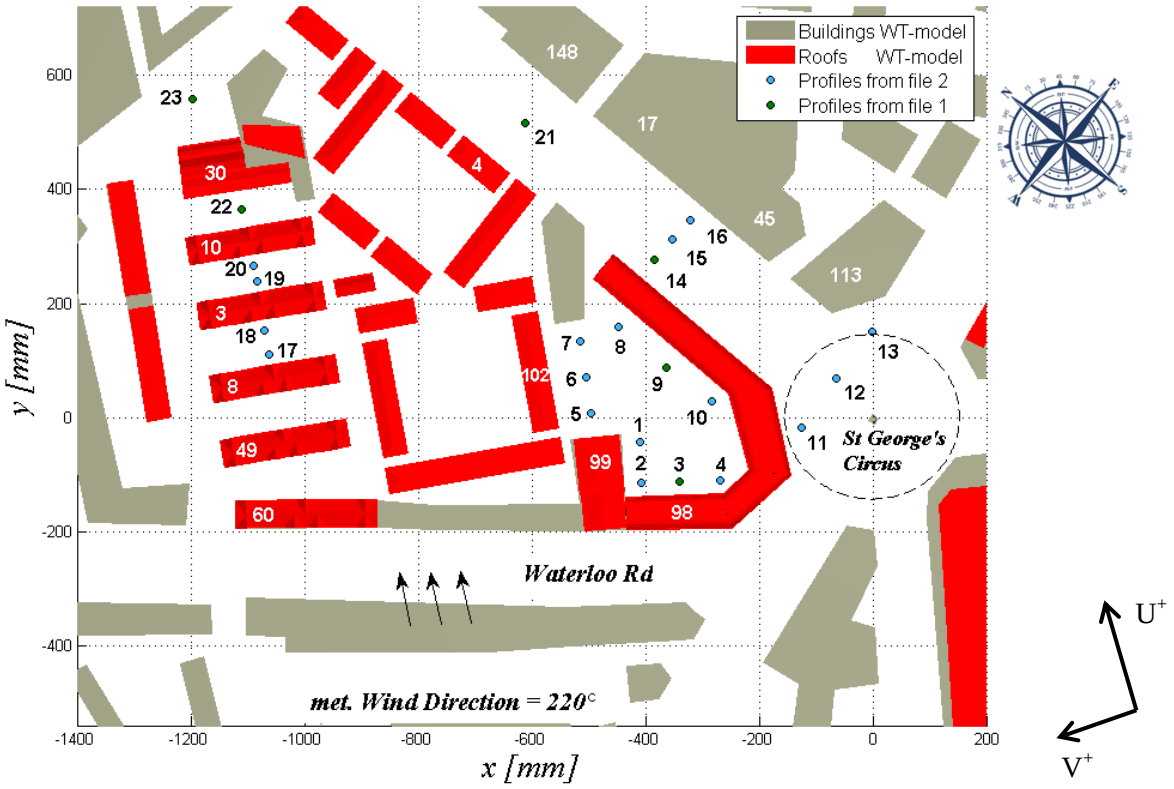

Figure 4.20 - Wind tunnel model: measurement points in the north-west part of the MAGIC site, through Waterloo Rd, Blackfriars Rd and St. George's Circus. Meteorological wind direction is 220°.

Table 4.5 - Characteristics of measurement points for the analysis in the north-west part of the MAGIC site.

Point n	Building n	Building + Roof Height	Roof type	Roof Slope α	Comment
1	99	65.8 + 20.0	Hip + gable	28	Courtyard
2	98	123.2 + 20.0	Vaulted	-	Courtyard
3	98	123.2 + 20.0	Vaulted	-	Building Corner, courtyard
4	98	123.2 + 20.0	Vaulted	-	Courtyard
5	102	59.0 + 12.1	Hip	28	Courtyard
	99	65.8 + 20.0	Hip + gable	26	
6	102	59.0 + 12.1	Hip	28	Courtyard
	99	65.8 + 20.0	Hip + gable	26	
7	102	59.0 + 12.1	Hip	28	Courtyard
	99	65.8 + 20.0	Hip + gable	26	
8	98	123.2 + 20.0	Vaulted	-	Courtyard
9	98	123.2 + 20.0	Vaulted	-	Courtyard
10	98	123.2 + 20.0	Vaulted	-	Courtyard
11	98	123.2 + 20.0	Vaulted	-	St George's Circus
12	-	-	-	-	Central in St George's Circus
13	113	120	Flat	0	St George's Circus
14	98	123.2 + 20.0	Vaulted	-	Blackfriars Rd
15	-	-	-	-	Central point in Blackfriars Rd
16	45	405.0	Flat	0	Blackfriars Rd
17	8-3	80.0 + 17.5	Gable dormers	35-41	3rd street canyon
18	8-3	80.0 + 17.5	Gable dormers	35-41	3rd street canyon
19	3-10	80.0 + 17.5	Gable dormers	35-41	4th street canyon
20	3-10	80.0 + 17.5	Gable dormers	35-41	4th street canyon
21	98	123.2 + 20.0	Vaulted	-	Central point in Blackfriars Rd
22	10-30	80.0 + 17.5	Gable dormers	35-41	5th street canyon
23	30	22.0 + 9.9-18	Gable	30-45	Upstream various building

4.5.2.1 Courtyard: point 1-10

Ten measurements points were investigated by vertical profiles, in the courtyard composed by building 98, 99 and 104, with different characteristics. Building 98 is sited in the corner through St. George's Circus, Waterloo Rd and Blackfriars Rd; it is 123.2 mm height (equal to 24.64 m at the real scale) without roof and 143.2 mm with the vaulted roof perpendicularly invested by the wind. Building 99 is 65.8 + 20 mm height (respectively with and without roofs, that means 13.16 + 4 m at the real scale); above this a mixed roof (gable + hip with the mean slope equal to 27°) is mounted and it is invested by the flow in the parallel way respect to facades. Building 104 is 64.7 mm height (in model scale, corresponding to 12.94 m at real scale), with a flat roof. To better understand differences within the two configurations (with and without roofs) profiles were split up into three groups.

Starting with point 1, results show that the stream-wise velocity (u) is the main influenced component by the roof variation: vortex that is visible in case without roofs, seems disappearing in presence of roofs, but it could be suppose that vortex centre is shifted in a different position (both for y and z coordinates) at least for the effect of the increasing total height of the building. The velocity components v appears higher, considering the absolute value, for both the lower and the higher levels, while vertical velocities (w) are not influenced at all. Looking at points 2-4, can be notice that the point in the middle of building wall width, considering the longitudinal direction, is the main affected by the presence of roofs with respect to the others closed to the corners. Results for the central point

(point 3) are reported in Figure 4.21-Figure 4.22 respectively for the first and the second order statistics.

Analysing velocities, shapes of profiles suggested that, in case with roof the vortex is shifted up. This is evident for all the three velocity components. However also quantitative differences are presents: the stream-wise velocity under the eaves level is lower in case with roof with a maximum around 30% lower in the layer between the eaves and the top of the roof. In the same layer the vertical component w shows higher values enabling higher vertical flux exchanges at roof level.

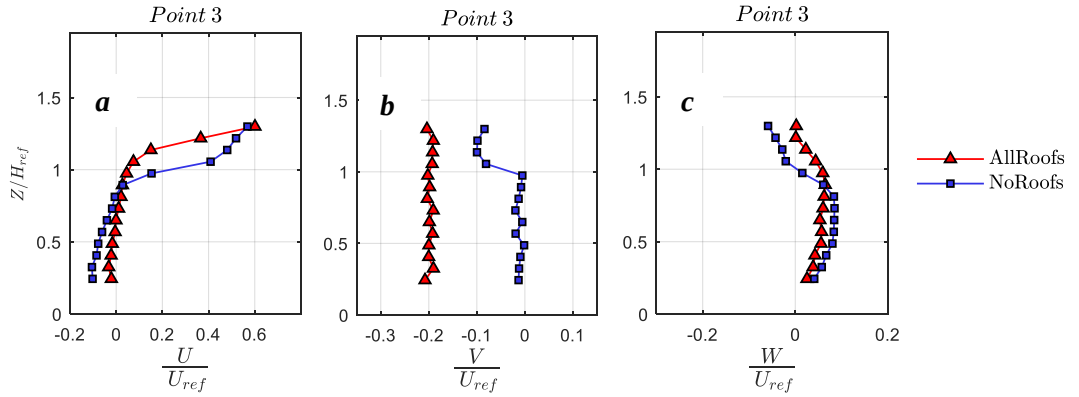

Figure 4.21 - First order statistics of the mean stream-wise (a), span-wise (b), vertical (c) components of the velocity, for point 3. Quantities were made non dimensional by the free stream velocity U_{ref}, measured at z = 1 m. Building 98 height is H_{ref} = 123.2 mm (without roof) and 143.2 mm with roof.

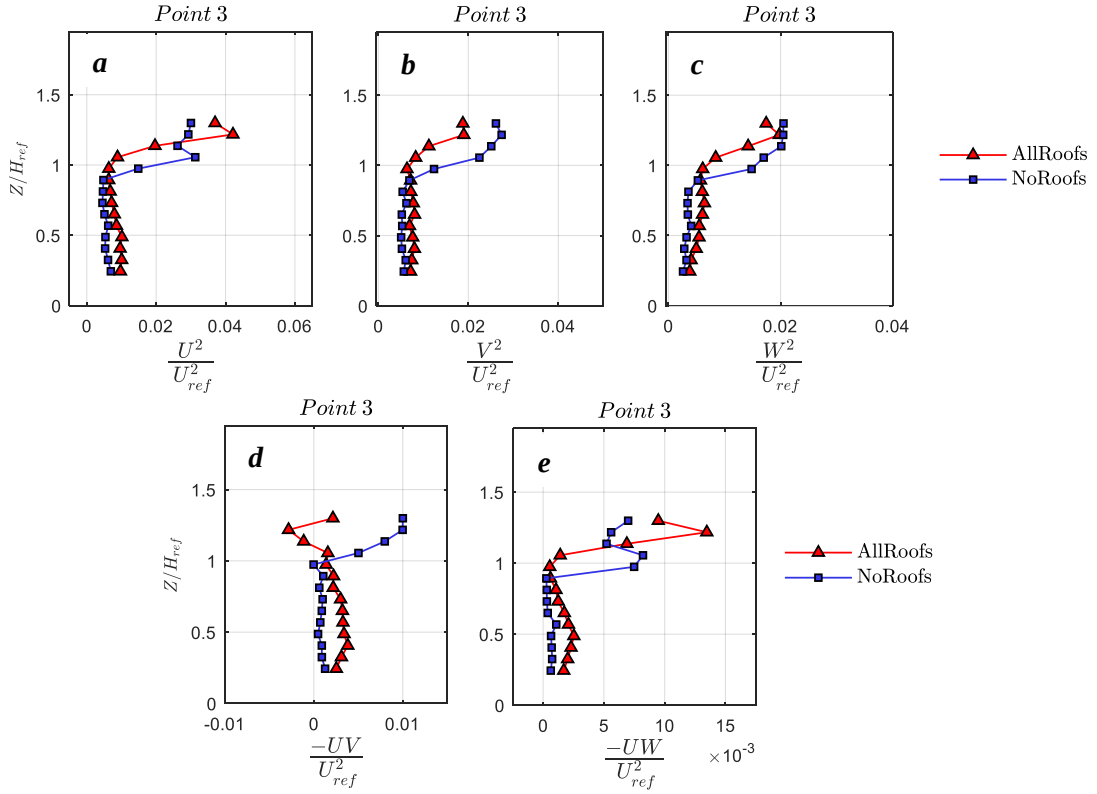

Figure 4.22 - Second order statistics of the mean stream-wise (a), span-wise (b), vertical (c) components of the velocity, for point 3. Quantities were made non dimensional by the free stream velocity U_{ref}, measured at z = 1 m. Building 98 height is H_{ref} = 123.2 mm (without roof), and 143.2 mm with roof.

The really interesting results is the span-wise direction that completely change in values for all the entire profile, with differences between 10% and 20%. The profile in Figure 4.21 b show that, in presence of roofs, the flow moves with higher velocities to the centre of the model, effect that takes away heading towards the point 4. This should be done by the presence of a gable roof 28° sloped, above the building 99, on the opposite corner respect point 4.

Turbulent quantities show a similar behaviour with a shifted up shape profile for every parameters. While at lower levels, until the eaves height, higher turbulence are widely registered, even if differences are limited, between eaves and the top of the roof values are generally lower in case with roof, but faster increase becoming higher above the roof for the variance of U, W, and the mean turbulent momentum flux (Figure 4.22 a, c, e).

Points 5, 6, 7 are positioned downstream to the hip roof of the building 99 and are spaced around 50 mm one from the other. The mean stream-wise velocity is higher for all the three profiles in presence of roofs, but the trend do not change. Looking at vertical velocities the same behaviour could be notice, with estimable differences around 12% at lower levels, near the ground, for the closest point to the building 99. For both u and w velocities, going downstream from the closest point to building 99, differences gradually disappear. Focusing on mean span-wise velocity (v), at lower levels flow substantially differs for all the three points and, going downstream from the point 5 to point 7 (Figure 4.23), differences grow up by involving also the higher flow.

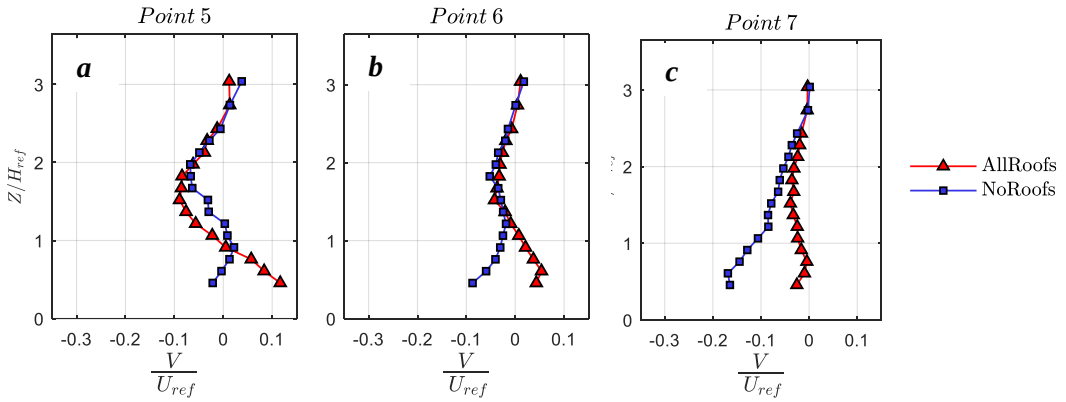

Figure 4.23 - Span-wise velocity component for points 5 (a), 6 (b), 7 (c). Quantities were made non dimensional by the free stream velocity U_{ref}, measured at z = 1 m. Building 99 height is H_{ref} = 65.8 mm (without roof) and 85.82 mm with roof.

It is important to underline that the lower span-wise flow is also affected by a change of direction in points 5 and 6, particularly evident for point 6, where the blue line (configuration without roofs) reveals the v component is headed to the centre of the model and the red line in the opposite way, changing mark just under the eaves level. For point 7 the direction remain the same for both the curves. It is reasonable to explain this behaviour with the presence of a hip roof above the building 102, whose facades are parallel to the wind direction. It could be suppose that the presence of roofs completely change the flow in the perpendicular direction respect to facades of the roof 102, going downstream to the building 99. About turbulent quantities, there are no relevant variation in values and trend between two configurations.

Points 8, 9, 10 are located in the courtyard along the wall of the building 98 which is parallel to the Blackfriars Rd. Point 10 is positioned in a corner between two facades, while points 9 and 8 are respectively downstream at 100 mm and 200 mm along the wall (in the model scale, corresponding to 20 m at full scale); they are positioned around 20 mm far from the wall (corresponding to 4 m at full scale).

Central point along the building facade (9 in Figure 4.20) appears the most influenced by the presence of roofs and it is well visible looking at full results in Figure 4.24-Figure 4.25. Despite for point 8 differences are not meaningless, only point 9 results were here reported. Velocity components (Figure 4.24) show higher vertical and stream-wise velocities in case without roofs for all the building height. As already stated, the recirculation vortex closed to the wall, changes shape and appears extended upward with a slower trend. However main differences are within span-wise velocities, for which fluxes come in the opposite way in the two configurations.

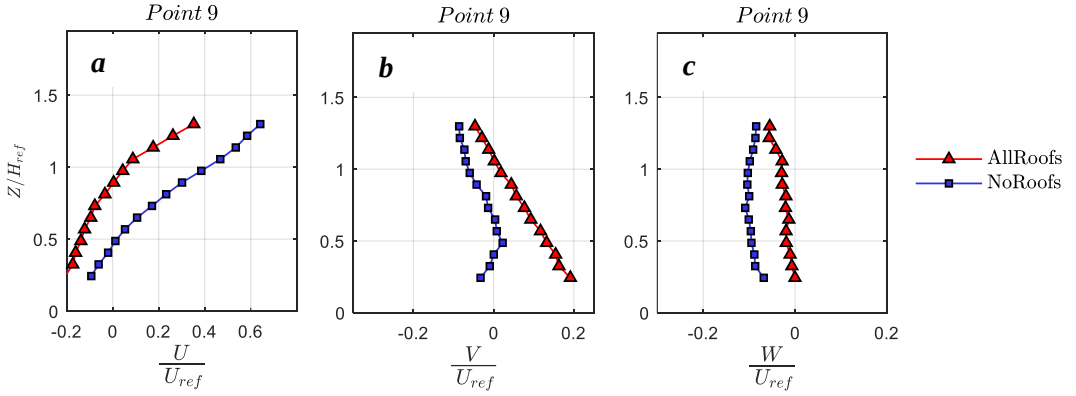

Figure 4.24 - Stream-wise (a), span-wise (b) and vertical (c) velocity components for points 9. Quantities were made non dimensional by the free stream velocity U_{ref}, measured at z = 1 m. . Building 98 height is H_{ref} = 123.2 mm (without roof), and 143.2 mm with roof.

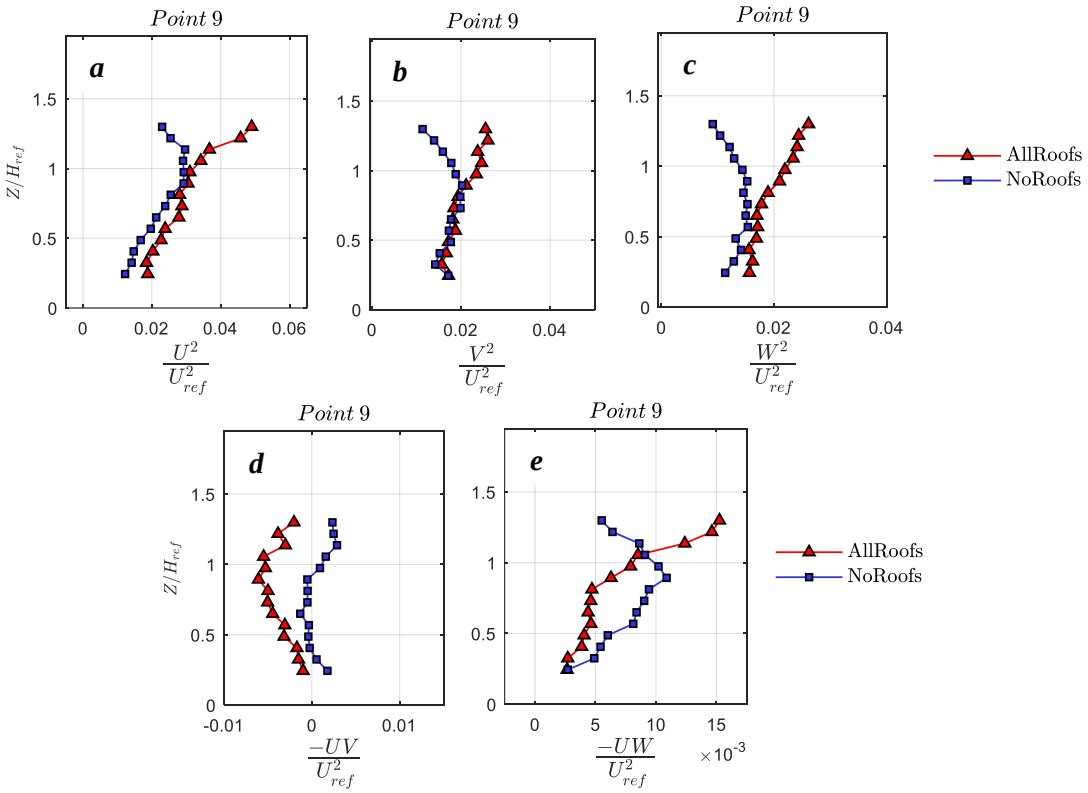

Figure 4.25 - Variance factor of the stream-wise (a), span-wise (b) and vertical (c) velocity components, lateral (d) and vertical (e) shear stress for points 9. Quantities were made non dimensional by the square of the free stream velocity U_{ref}, measured at z = 1 m. . Building98 height is H_{ref} = 123.2 mm (without roof), and 143.2 mm with roof.

Second order statistics (Figure 4.25) for the same point, show values too different in the region above the roofs and various behaviour under these. In particular variance factors (Figure 4.25 a, b, c), converge at heights around the eaves level and diverge at higher level. The lateral fluxes (Figure 4.25) display negative values for all the building height in presence of roofs, while in case without roofs the majority of z positions have positive or quasi zero values. The maximum difference is in the layer between the eaves level and the top. Regarding the turbulent momentum flux (Figure 4.25 e) the maximum discrepancy inside the courtyard appears for z level around the 75% of the building height and above for the highest point measured in these profiles.

4.5.2.2 Blackfriars Rd: points 11-16

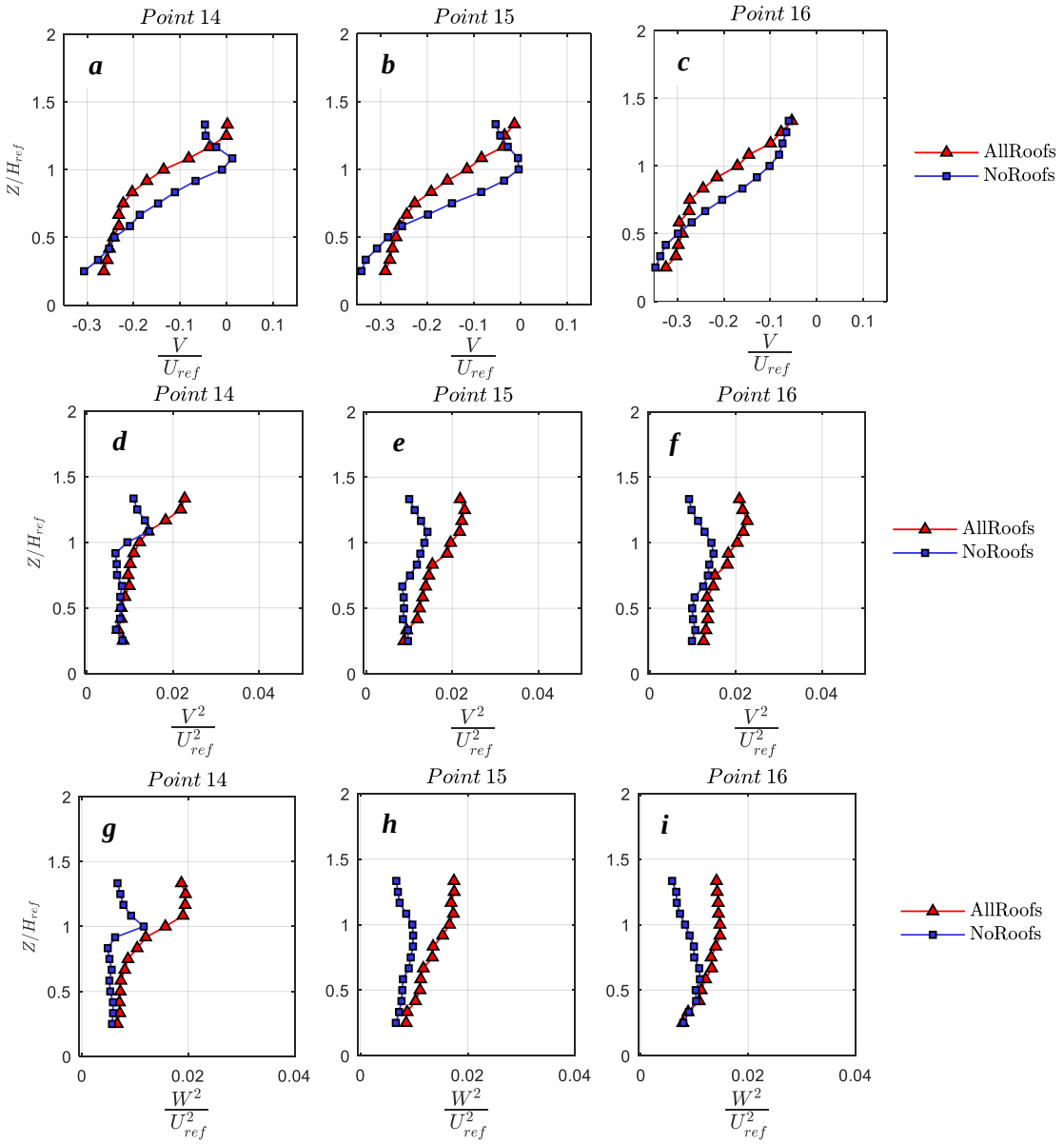

Figure 4.26 - First and second order statistics for points 14, 15, 16. Span-wise velocity component (a, b, c), variance of the span-wise velocity component (d, e, f) and variance of the vertical velocity component (g, h, i). Quantities were made non dimensional by the free stream velocity U_{ref}, measured at z = 1 m. The most frequent building height in Blackfriars Rd is H_{ref} = 120 mm (without roof).

The two series of points in Blackfriars Rd where chosen to be equidistant respectively at 0.25, 0.50 and 0.75 respect to the street width. Points 11, 12, 13 were positioned at the intersection between Blackfriars Rd and St. George's Circus and points 14, 15, 16 at around $400\,mm$ downstream (~2 street widths, see **Figure 4.20**). St George's Circus is a relatively well ventilated junction and the flow is channelled towards Blackfriars Rd. The more typical height of buildings in this area is $120\,mm$ ($24\,m$ full-scale); only Building 45 is higher with $h = 405\,mm$ ($81\,m$). Differences between the two configurations are minimal and apparent only at point 11 which is sited upstream and close to building 98. The lack of variation between two cases, underlines the fact that flow is very ventilated and channelled. However it is important to remember that upstream of this section, there are not too many buildings with shaped roofs and even those are not of a height likely to influence conditions at St. George's Circus. Anyway, the possibility of larger effects at other wind direction cannot be excluded. Results for points 11, 12, 13 are reported in Figures 7 and 8 of the attachments.

Despite the fact that the flow is completely channelled, the second series of points (14, 15, 16) shows roof shapes having some influence, even though the basic flow is a helical vortex in both cases. Variations are evident in the span-wise velocity components (Figure 4.26 a, b, c) and the variance of the span-wise and vertical velocity components (respectively in Figure 4.26 d, e, f and g, h, i). Once again, in the flow configuration with roofs, the flow is shifted upwards and the span-wise component appears to be influenced more than the vertical component, especially in the first order statistics. The regions near roof level are where the most obvious differences in the turbulence stresses are seen, with levels somewhat higher in the shaped roof cases. However, is beyond doubt the fact that the vaulted roof above Building 98 makes the flow behaviour different and generally somewhat more ventilated throughout the canyon depth.

4.5.2.3 Street canyon: points 17-20

The profiles for points 17, 18, 19, 20 are placed in the third and forth canyons of the array composed by the buildings 60, 49, 8, 3, 10 (see Figure 22, from Waterloo Rd downstream). Except for the building 60, which is a little bit longer than the others and have a different incident wind angle, blocks are characterised by the same incident angle respect to the wind direction (with the longest walls perpendicular to wind), and by the same sizes. The eaves height is h = 80 mm, the width in stream-wise direction is 50 mm and 150 mm in the span-wise direction, thus the aspect ratios of the buildings are $AR_{B(x)} = 0.625$ and $AR_{B(y)} = 1.875$ (in, where $AR_B = B/H$ and H is the reference height at eaves level, B is the building width in stream-wise, x, and span-wise, y, direction respectively). The aspect ratio of the street canyon is $AR_C = 0.8$ (where $AR_C = W/H$ and W is the canyon width), so the flow can be consider in the skimming flow regime (Oke 1988). For this array of buildings realistic shapes of roofs were chosen, thus they were built like gabled with 35° sloped with dormers positioned in a different way on the two facades, with 41° sloped. This similarity with the modelled case widely discuss in literature works is the reason why we got attention on their, with the specific objective to understand if results obtained for simplified geometries are assumable as good with respect to more complicated urban geometries like the MAGIC model. Measurements points were chosen to be in the mean section along the canyon.

Two main conclusions should be done by considering the first order statistic: firstly comparing the two canyons, flow seems do not be largely affected in trends as we can see, for example, in the u velocity component (Figure 4.27a-c, b-d). This is quite interesting considering the usual suggestions about the number of canyons that should be consider both in computational and in experimental analyses, in order to have a completely developed flow and to well represent the street canyon flow behaviour. However information in this work, are no sufficient to state something different from literature works that suggest at least 8 identical canyon as necessary to ensured that the roughness layer generated by

the building series reached its equilibrium (Brown et al., 2000; Llaguno-Munitxa et al., 2017). Secondly, the main differences between the two configurations (with and without roofs) is that the vortexes appear higher in case with roofs, coherently with literature works (e.g. Garau et al. 2018). Indeed the red profiles shown lower values for the u component of the velocity from the eaves level, to the top. The span-wise component (v) show very low value in both the two configuration, with negligible differences, while the mean fluctuation seems more influent. These results underline that this case cannot be consider in the same way of the idealised 2D or 3D street canyon usually analysed in literature works, even if the general behaviour in the middle section is too similar.

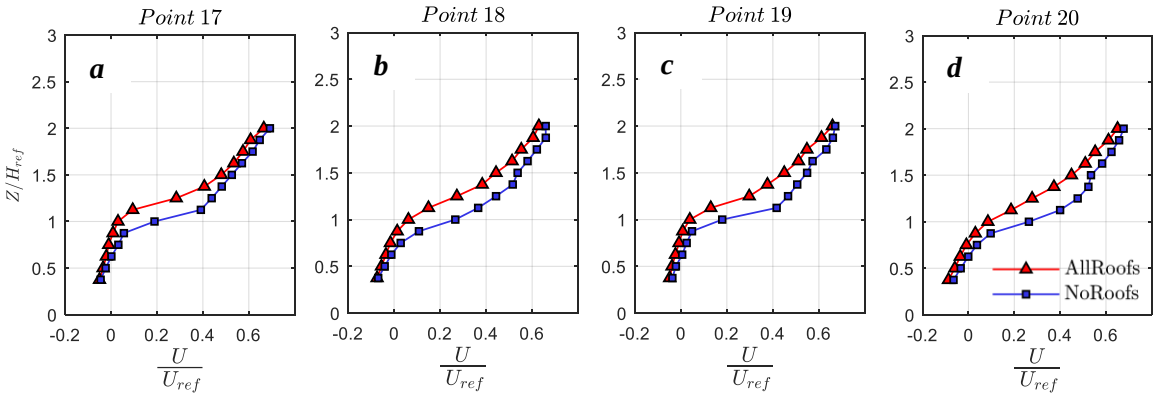

Figure 4.27 - Stream-wise velocity component for points 17, 18, 19, 20, made non-dimensional by the free stream velocity U_{ref} at z = 1 m. Points 17 (a), 19 (c) are in the leeward position, points 18 (b), 20 (d) are in the windward position. H_{ref} = 80 mm (without roofs) and 97.5 mm with roof.

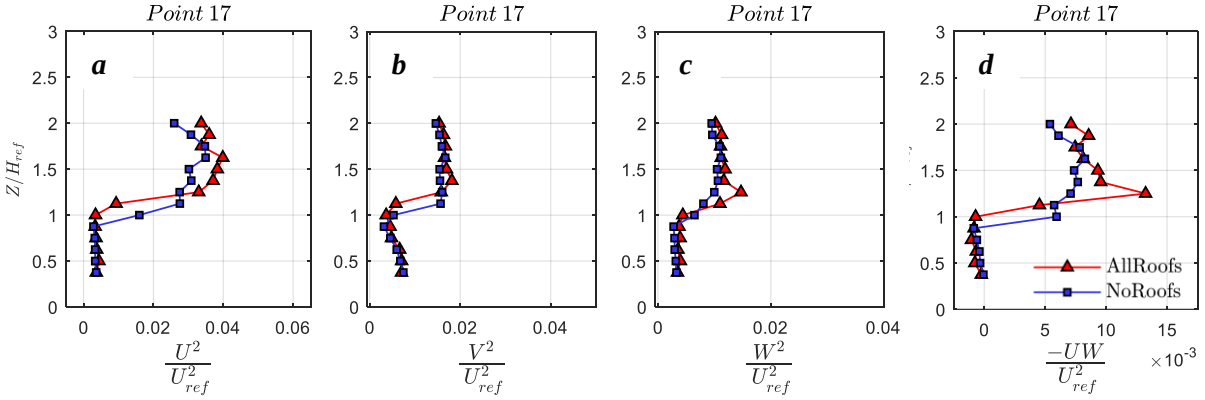

Figure 4.28 - Variance of the stream-wise (a), span-wise (b), vertical (c) components of the velocity, and momentum flux (d) made non dimensional by the square of the free stream velocity U_{ref} at z = 1 m. H_{ref} = 80 mm (without roofs) and 97.5 mm with roof.

The vertical velocity component (w) shows little differences for all the points, with higher values in configuration with roofs, around $z = 0.75H$ (where $H = 80\ mm$) in the downwind points (18-20) and around $z = 0.25H$ in the upwind points (17-19). Although differences are small they can bring important differences in air exchange. Indeed it is well known that vertical velocities drive the exchange flux from the canyon to the overlaying air along the vertical direction and it is the main influence component in the mean section of the canyon that we are analysing. The second order statistics shown higher values in the layer around the roof level, where, in presence of roofs, profiles are characterised by a quick increase of values and higher pick. This behaviour is reported below (Figure 4.28) where, as example, the point 17 was chosen.

4.5.2.4 Conclusions on the North-west district investigation

In order to summarise results previously described, profiles of differences occurring between the configurations with and without roofs, were evaluated for every parameters. Velocities were made non dimensional by the free stream velocity U_{ref} and the z values employing the mean eaves level of nearest buildings. Data were split in the three groups from the simplest (street canyon on the left hand of the graphs) to the more complicated case (courtyard of building 98 on the right hand of the graphs), as it is possible to see in Figure 4.29 where, as an example, only the velocities component are here reported. The street canyon cases, where flow perpendicularly approach building walls and canyons, show a very delineated trend for which significant no zero values are clearly disposed around the roof level for the stream-wise (u) velocity component and around the eaves level for the vertical velocity component (w). The span-wise (v) profile behaviour states that the presence of roof do not affects at all the third component of the flow in the central sections of the canyon.

Blackfriars case, where flow is quite parallel to the street and buildings are tall (H mean is equal to $120\,mm$), show more dispersed values around the zero, for all the z positions. However differences are quite regular for all the levels below the $z/H = 0.8$ of eaves level. Above this limit, for the v component of the velocity, differences increase a little bit until the $z/H = 1.2$ of eaves level. Indeed this layer corresponds to the vaulted roof level for building 98, that affects the flow more in span-wise than in vertical direction. As regards the stream-wise component, higher value were founded just above the eaves level.

The most complicated case, as already discuss in the previous paragraphs, is the courtyard of building 98: for all the three components (Figure 4.29 a, b, c right panels), differences are quite dispersed around the blue line that represent the mean difference values. At first sight is well visible that flow is strongly three dimensional: the stream-wise components is main affected at the roof level and above, where is characterised by a general decrease. However at lower levels, differences are not negligible because evaluated around the ± 0.2 of the U_{ref}. Also the other two components show a strongly irregular behaviour, especially for the span-wise component, for which differences increase from the eaves level to the bottom, twisting the scenario that could be analysed considering only the configuration with flat roof buildings.

Moreover, to enhance these results for every parameter, the maximum and medium values of the standard deviation (σ) for differences was evaluated (Table 4.6). If each of the three case is singularly analysed, the maximum standard deviation value as well as the difference between the maximum and the mean values, can be found in a different velocity component. For the *Street Canyon* case, they are higher for the vertical velocity component and for the stream-wise and span-wise variance as regards the second order statistics; in case of *Blackfriars Rd* higher values are for the stream-wise velocity component and for the variances of vertical and span-wise directions; in case of the *Courtyard* the span-wise velocity component have the maximum value for the standard deviation and for the variance of the same component, even if results are too similar with respect to the stream-wise velocity.

On the other hand, considering each parameter singularly, the higher variability and dispersion of data was measured at *Blackfriars Rd* in case of stream-wise velocity, at the *Courtyard* for v and at the *Street Canyon* for w, while for every second order statistics parameter, highest values are achieved for the *Courtyard* case which registered also the highest values for the mean standard deviation for every parameters.

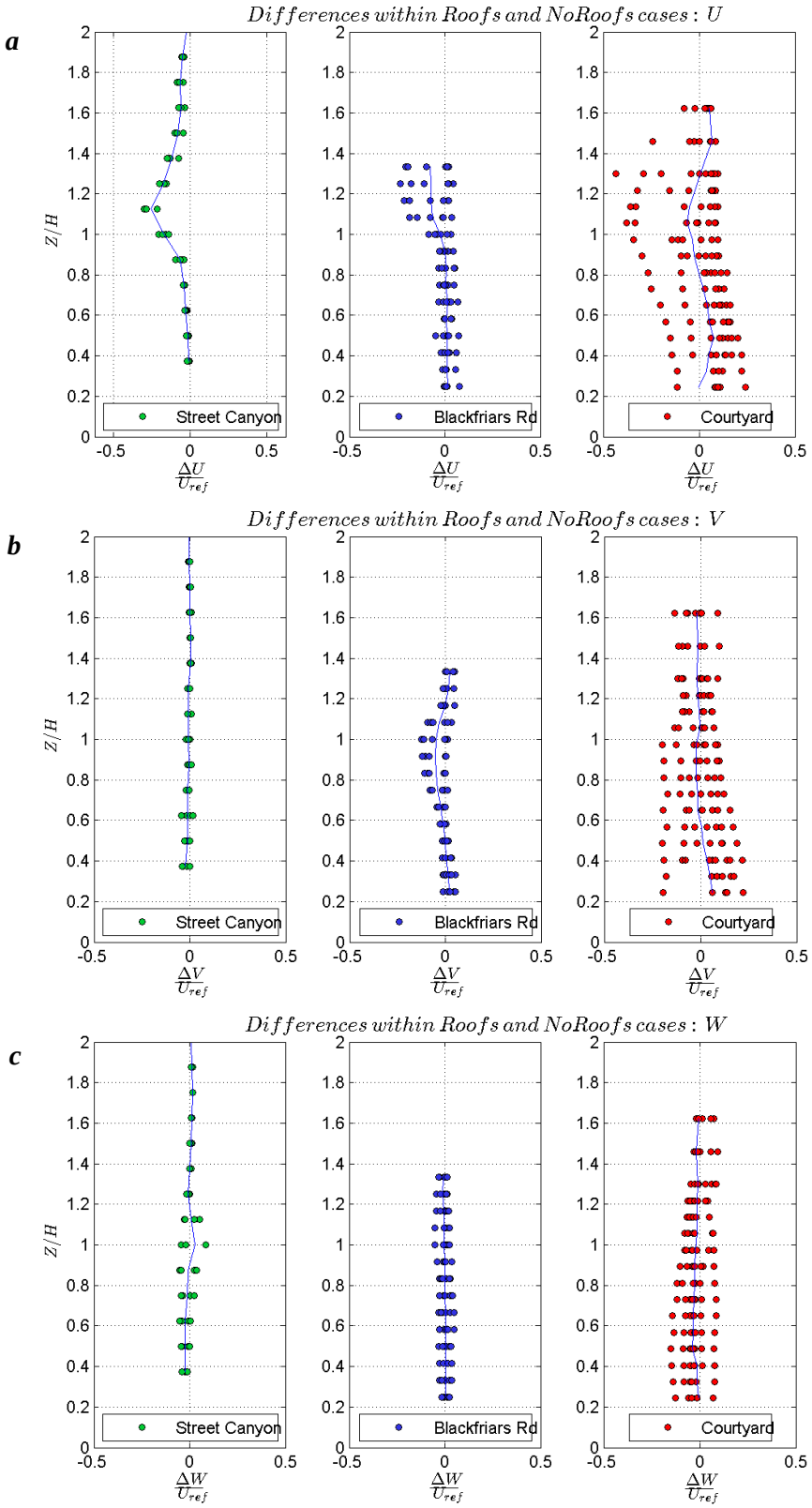

Figure 4.29 - Value of U (a), V (b) and W (c) differences between the two configurations (with and without roofs). Values are reported for the three different locations: Street Canyon (green), Blackfriars Rd (blue) and Courtyard of building 98 (red). Velocities are made non dimensional by the free stream velocity U_{ref}, measured at z = 1m.

Table 4.6 - Mean and maximum standard deviation of differences evaluated for every parameter (first and second order statistics) and for the three analysed cases. Orange numbers are the differences between the maximum and the mean standard deviation.

Case	σ	U	V	W	U^2	V^2	W^2	UW	UV
Street Canyon	max	0.044	0.026	0.067	0.004	0.004	0.003	0.002	0.001
	mean	0.018	0.009	0.020	0.002	0.002	0.001	0.001	0.001
		0.026	*0.017*	*0.047*	*0.002*	*0.002*	*0.002*	*0.001*	*0*
Blackfriars Rd	max	0.117	0.061	0.031	0.004	0.006	0.006	0.003	0.003
	mean	0.051	0.032	0.024	0.002	0.003	0.003	0.001	0.001
		0.066	*0.029*	*0.007*	*0.002*	*0.003*	*0.003*	*0.002*	*0.002*
Courtyard	max	0.073	0.114	0.052	0.006	0.007	0.005	0.003	0.004
	mean	0.035	0.079	0.034	0.003	0.004	0.002	0.002	0.003
		0.038	*0.035*	*0.018*	*0.003*	*0.003*	*0.003*	*0.001*	*0.001*

Concluding this section, it can be stated that variations of roof shapes strongly affected the flow not only at higher levels, but also near the bottom. Very complex 3D flow behaviour can be observed were building facades are not perfectly parallel or perpendicular respect to the flow. However also in the simplest configuration like the street canyon array, differences are not negligible for all the three velocities components even if little discrepancies from the perfect perpendicular wind direction usually employed in modelled cases (especially in CFD) are here guesses.

This observations suggest that for realistic analysis of urban canopy air quality, especially for evaluation at lower levels, consider the shape of roofs is necessary. This priority is more relevant where buildings are not modelled with simplest geometries and the urban canopy is not regular. The consequences of this results on the concentration dispersion will be treated in next paragraphs.

4.5.3 Skimming flow regime investigation

The goal of this section is to analyse the effects of differences occurring between configurations with and without roofs, already discuss in Sections 4.5.2.3 and 4.5.2.4, with respect to the pollutant dispersion into the street canyon. The 5 buildings array characteristics (see Figure 4.30) were already discussed, however is here important to underline that the aspect ratio of this series of canyons is equal to $AR_c = 0.8$, so the flow can be consider in the skimming flow regime (Oke 1988).

Meteorological wind direction was chosen equal to 220° in order to be perpendicular to the consider street canyons, but it also represent the most frequent and intense wind registered for London (see Section 4.4.1) .

Both pointwise and linear sources, with a constant flow rate equal to $Q = 0.036\,[l/m]$, were employed and tested for the experiments, locating their upstream to the street canyon, in the larger and high-traffic street of the area (Waterloo Rd). However only results about the linear source were here reported. Indeed the pointwaise source was found not representative for the urban pollutant release.

The source is given in Figure 4.31 with a yellow line, togheter with the measuring point positions, whose main characteristics are also provided in Table 4.7. Profiles were divided into two groups: points 1-3 were analysed by means 3 vertical profiles, positioned in the medium section respect to the longitudinal building walls, from $z_{min} = 11\,mm$ to $z_{max} = 115\,mm$ (at the model scale), with a higher z resolution near the ground and the eaves and roof levels for a total number of 12 positions; points 4-8 were analysed by means 5 vertical profiles, positioned $50\,mm$ far in y from the other group, from $z_{min} = 70\,mm$ to $z_{max} = 100\,mm$ (at the model scale), with higher resolution near eaves and roof levels for a total number of 6 z positions equispaced with $\Delta z = 5\,mm$. For both the two groups, the closest profiles to the walls are $x = 15\,mm$ far and for first group points are equidistant with $\Delta x = 17\,mm$ while for the second group points are spaced with $\Delta x = 8.5\,mm$. At the real scale this means that the first point near the ground is at $z = 2.2\,m$, just above the pedestrian level, and the closest profiles to the walls are $x = 3\,m$ spaced.

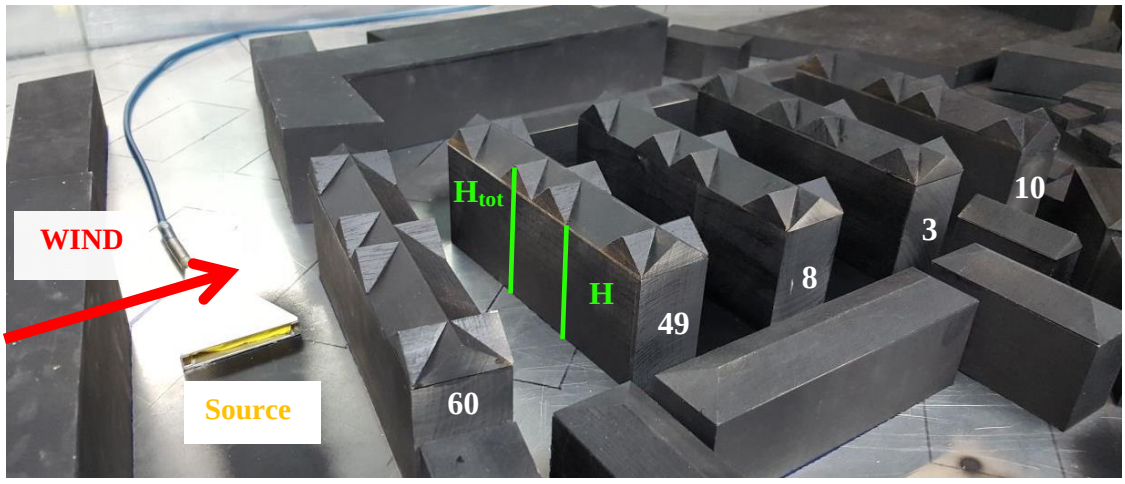

Figure 4.30 - Wind tunnel model: characteristics of configurations for experiments in the skimming flow regime with the array of 5 identical buildings 60, 49, 8, 3, 10. H = 80 mm is the height at eaves level; H_{tot} = 97.5 mm is the top level of the roofs. Meteorological wind direction 220° is perpendicular to the building array.

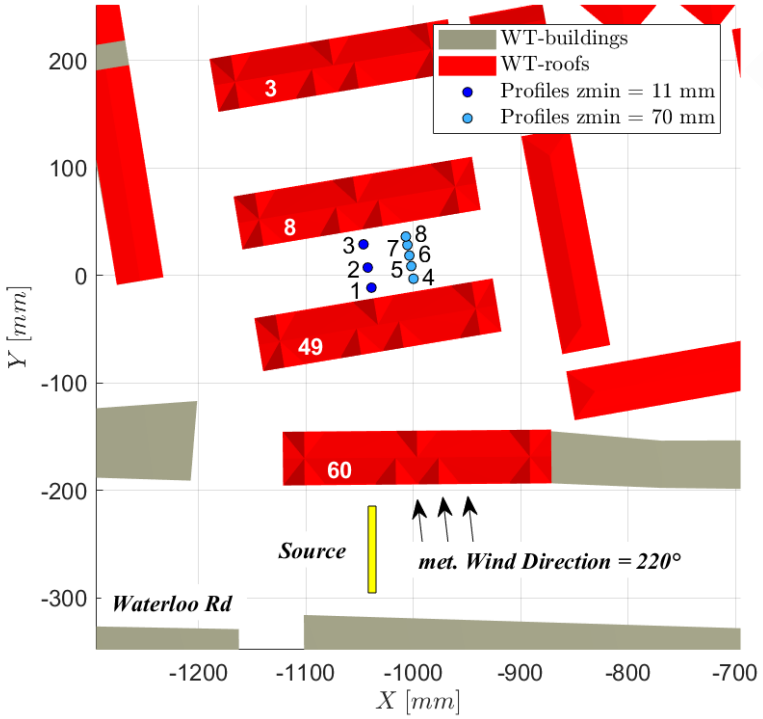

Figure 4.31 - Wind tunnel model: measurement points in the second street canyon respect to the array of buildings 60, 49, 8, 3, 10. Points are divided in two blocks: points 1-3 and points 4-8. The other characteristics of the model are: the meteorological wind direction equal to 220° (black arrows), the source point (yellow star); grey blocks are buildings without roofs; red blocks are building with roof. Buildings numbers are writen in white.

Table 4.7 - Characteristics of measurement points for the skimming flow investigation case.

Point n	Building n	Building + Roof Height	Roof type	Roof Slope α	Comment
1 2 3	49-8	80 +17.5	Gabled + dormers	32 + 40	Upstream: 12 mm far from the wall Centred: 32 mm far from the wall Downstream: 12 mm far from the wall
4 5 6 7 8	49-8	80 +17.5	Gabled + dormers	32 + 40	Upstream: 12 mm far from the wall Upstream: 22 mm far from the wall Centred: 32 mm far from the wall Downstream: 22 mm far from the wall Downstream: 12 mm far from the wall

The main difference between the two series of points was the shape of roofs above the leeward and windward walls: in the medium section the presence of one dormer on the leeward wall and two dormers on the windward wall, allow us to consider the wall facades heigth equal to the total height of the building (H_{tot}), while for the section with the 5 helved profiles the roof is gabled and the walls height corresponds to the eaves level.

4.5.3.1 First and second order statistics

By using a total number of 5 profiles equally spaced (points 1-3 and the border conditions with zero values on the walls) and the linear interpolation, evaluation of first and second order statistics fields was possible for both the configurations in the central section. The mean stream-wise velocity fields are reported in Figure 4.32 (a, b) respectively for cases without and with roofs. The increase of height in *AllRoofs* configuration is well underlined by the shape of vortex that appears extended in height. This behaviour is similar to previous work reported in literature for $AR_C = 1$ and the shape of the vortex in the *NoRoofs* configuration well agree with experiments done for example by Kovar et al., (2002) where the $AR_C = 0.7$ was considered.

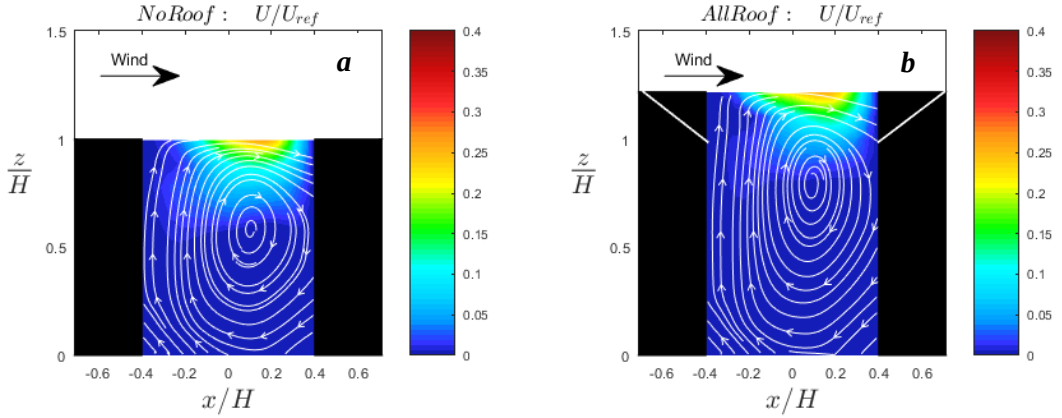

Figure 4.32 - Streamlines of the mean velocity and mean stream-wise velocity field, made non-dimensional by the free-stream velocity (U_{ref} at z = 1 m), for the configuration without roofs (a) and with roofs (b).

Also the vertical components of the velocity reported in Figure 4.33 (a, b), and the turbulent momentum flux (Figure 4.34 a, b) showed a good similarity both in shapes and magnitude with respect to previous experimental and numerical work (Figure 3.4-Figure 3.14). Positive vertical velocities near the leeward wall are extended in height and appears a little bit more intense just like the negative ones, for case with roofs. This behaviour is better visible in the quantitative comparison made with vertical profiles not reported here.

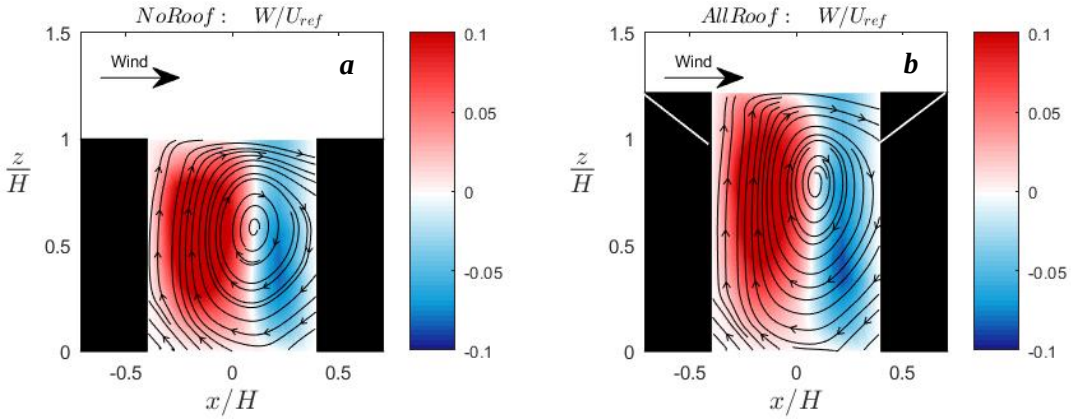

Figure 4.33 - Streamlines of the mean velocity and mean vertical velocity field, made non-dimensional by the free-stream velocity (U_{ref} at z = 1 m), for the configuration without roofs (a) and with roofs (b).

Mean turbulent transport fluxes show the typical shape like a tongue with higher values at lower level into the canyon near the windward wall, more extended in case of *AllRoofs* configuration and lower values on the top at the total height level with quite more intense values in case with roofs.

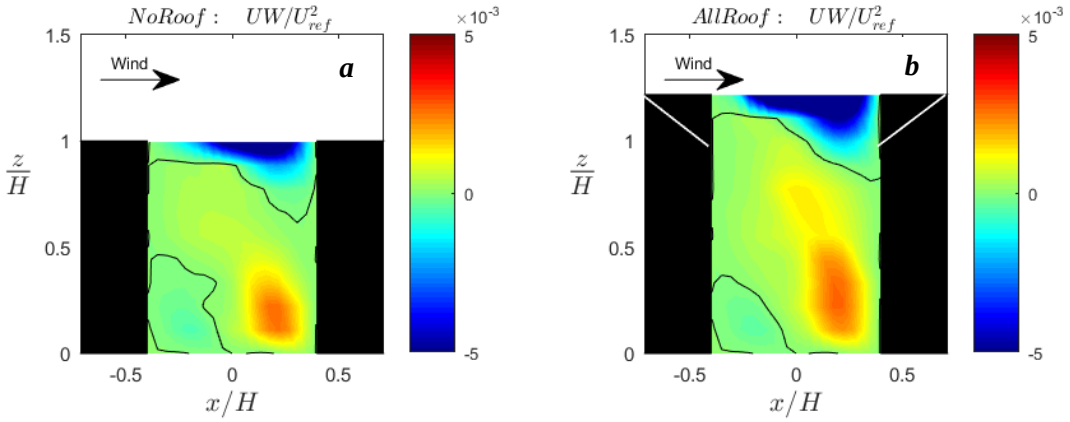

Figure 4.34 - Turbulent momentum flux field, made non-dimensional by the free-stream velocity (U_{ref}^2 at z = 1 m), for the configuration without roofs (a) and with roofs (b). Black contour lines marks the transition from the negative to the positive values.

Looking at the field maps is not possible to recognise so many differences, however huge discrepancies occurred in concentration behaviour. In order to show their, the three full profiles at the central section were chosen.

Profiles of non-dimensional mean concentration (Figure 4.35 a, b) reveal that in case without roofs (a) values are quite doubled for the points 2, 3 and also in point 1 are higher respect to the *AllRoofs* configuration. The three profiles are completely overlapped from around $z/H = 0.9$ to the bottom in case without roofs, while at the eaves level they start to diverge. In case with roofs trends are different for all the heights. Otherwise, just looking above the top level of buildings, it is important to underline that the amount of pollutant coming into the canyon is lower in case with roofs. These results enforced the thesis already discussed in Section 3.4.3.3 and suggested that in the skimming flow regime, where the ventilation process becomes poor and poor with the AR_C decreasing, roofs above buildings seems to have a prevention function with respect to the contamination of air into the canyon.

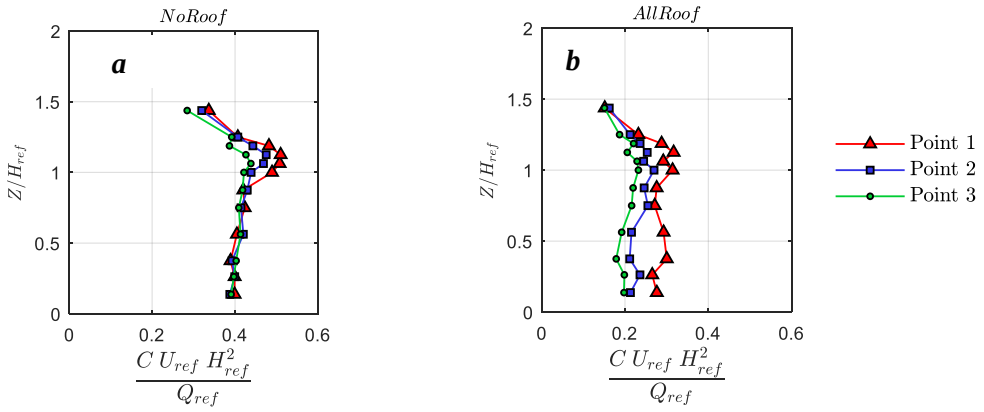

Figure 4.35 - Vertical profiles of mean concentration made non dimensional by the square of the reference height (H_{ref} = 80 mm at the eaves level), the free stream velocity (U_{ref} at z = 1 m) and the flow rate velocity (Q_{ref} = 0.036 l/m). Panel a show the configuration without roofs, panel b the configuration with roofs, for point 1 (near the leeward building), red triangle; point 2 (central point in the street canyon), blue square; point 3 (near the windward building), green circles.

4.5.3.2 Dispersion mechanism of air pollutants

The transport mechanism could be explained analysing the vertical momentum flux by employing the quadrant analysis. As reported by Wallace, (2016), the Reynolds shear stress in a turbulent boundary layer flow is related with the joint probability distribution function (JPDF) by the relation:

$$uw = \int_{-\infty}^{\infty} uwP(u,w)dudw \qquad 4.3$$

where $P(u,w)$ is the JPDF. The scheme used for the momentum transport mechanism, depending on the signs of the two quantities, is provided in Figure 4.36. In analogous way the vertical component of the turbulent pollutant flux could be divided into four contributes, but their definition differs respect to the turbulent momentum flux and the literature nomenclature is various (Raupach, 1981; Kikumoto, and Ooka 2012; Nosek et al., 2017). The scheme employed in this work is reported in Figure 4.37, where the table (Katul et al., 1997; Katsouvas et al., 2007; Cheng and Liu, 2011) indicates the more common nomenclature and the graph shows a briefly definition of events. Anyway it is important to clarify that 'clean air' and 'polluted air' are relative concepts, respectively meaning lower and higher instantaneous concentrations compared to the mean value.

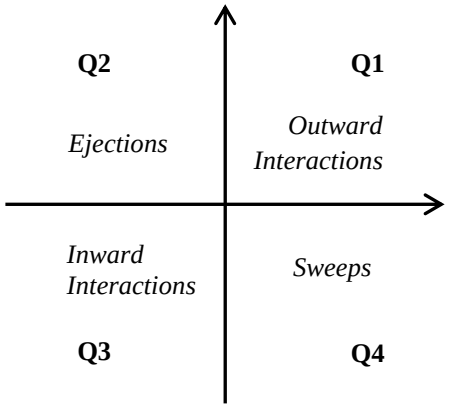

Quadrants	Directions
Q1 = Outward interactions	u' > 0, w' > 0
Q2 = Ejections	u' < 0, w' > 0
Q3 = Inward interactions	u' < 0, w' < 0
Q4 = Sweeps	u' > 0, w' < 0

Figure 4.36 - Quadrant analysis scheme for the vertical momentum flux ($u'w'$)

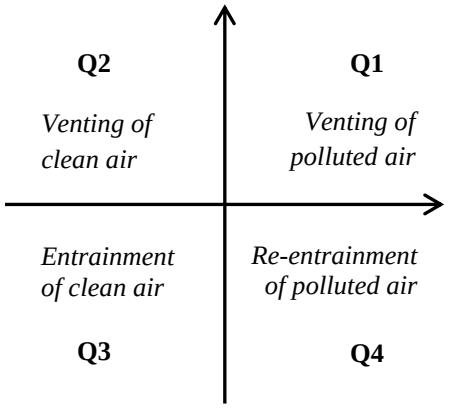

Quadrants	Directions
Q1 = Ejections	c' > 0, w' > 0
Q2 = Outward interactions	c' < 0, w' > 0
Q3 = Sweeps	c' < 0, w' < 0
Q4 = Inward Interactions	c' > 0, w' < 0

Figure 4.37 - Quadrant analysis scheme for the vertical pollutant flux (c'w')

Considering the eaves level $H = 80\ mm\ (z/H = 1)$ for the central street canyon profile, Figure 4.38 show the JPDF for the *NoRoofs* (a) and the *AllRoofs* cases (b). Results for flat roof buildings were compared to similar literature works (Cheng and Liu, 2011; Kikumoto and Ooka, 2012) where the 2D street canyon model with flat roof and $AR_C = 1$ was employed. Comparisons were made in terms of JPDF and occurrence frequencies, finding the same trend and very close values. Differences between the two configurations are well visible: locations of the peck for case a, representing the highest probability events, are in Q2 - Q4, and the maximum probability values is through the ejection events; on the other hand, case b show a flat behaviour, with no predominant mechanism of ventilation (even if the highest values seems in Q1) and the central point with the highest probability of occurrence closest to the axes origin. This means that while the momentum transport at the eaves level is dominated by ejections and sweeps events for the flat roof buildings, big differences are not visible in presence of roofs and this should be explained by the very closed position respect to the stagnation point represented by the centre of the vortex, already shown in Figure 4.32-Figure 4.33 b. Indeed, if we consider the total height of the no flat roof buildings H_{tot} instead of H, the JPDF in Figure 4.38 b, would be evaluated at the level $z/H_{tot} = 0.82$. This statement was enforced by the evaluation of the JPDF for *NoRoof*s case at the similar level, $z/H \cong 0.80$ that exhibit the same trend.

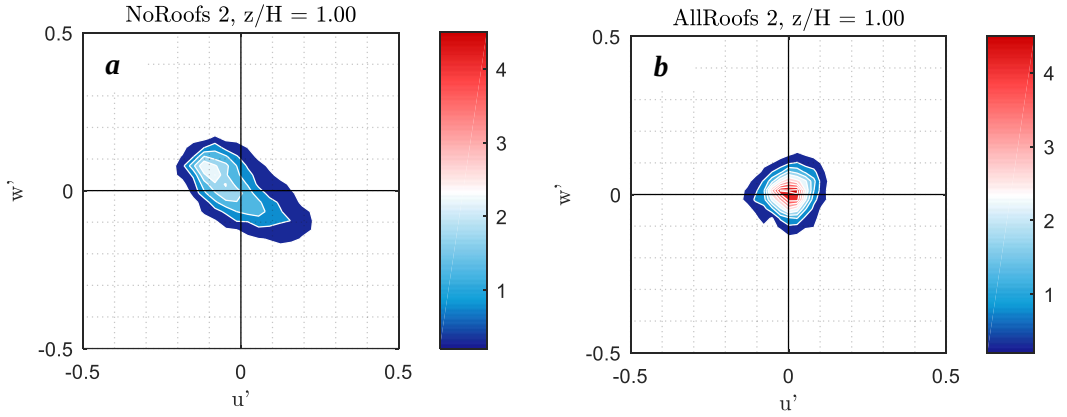

Figure 4.38 - Joint probability density function (JPDF) of stream-wise and vertical velocities fluctuations for case without roofs (a) and with roofs (b), for the central point of the street canyon (point 2, Figure 4.31) at the eaves level z/H = 1.

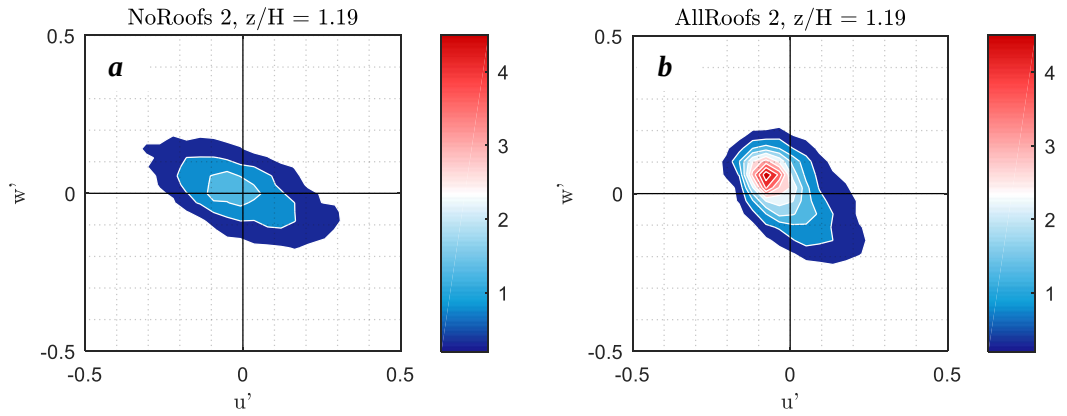

Figure 4.39 - Joint probability density function (JPDF) of stream-wise and vertical velocities fluctuations for case without roofs (a) and with roofs (b), for the central point of the street canyon (point 2, Figure 4.31) at the top height of gable roof buildings equal to z/H = 1.19

Looking at the building top level along the same central profile, the *NoRoofs* case show the highest events in the Q2-Q4 direction and the highest probability in Q2, very closed to the centre of axes but with very low probability in all the area. However the case with roofs reveals a very similar shape respect to the point at $z/H = 1$ in case without roofs (Figure 4.39 a), with the most intense events in Q2-Q4 and the most probable in the same position. Variations are visible for the probability values, that in case with roofs are doubled, and in shape because the curve appears more extended along the direction Q3-Q1. All this considerations suggested that the total height of buildings should be considered as the proper surface of exchange between the canyon and the overlaying flow. However is important to remember that this particular section is effected by the presence of dormers on the roofs, then more analysis should be done in order to generalise conclusions.

The quadrant analysis of vertical pollutant flux was realised in a similar way. However, to synthetize their and to look both the two quantities together, occurrence frequency histograms for the vertical momentum and the vertical pollutant fluxes were realised like in Kikumoto and Ooka, (2012). Quadrant 2 and 4 are here indicated with negative ordinate axes, in accordance with the phenomenon, then percentage values are reported above the bars.

In case without roofs at the eaves level (H) Figure 4.40 shows that momentum flux ejections (Q2) occurs most frequently ($\cong$ 53%), followed by sweep ($\cong$ 35%), while outward and inward interacions are rare with the 6% for each one. This values are consistent with other authors results (e.g. Cheng and Liu, 2011; Kikumoto and Ooka, 2012).

On the other hand vertical pollutant fluxes appears higher for the sweep (Q3 $\cong$ 35%) events so sweeps are the most effective mechanism of transport for that contaminants move into the canyon, in this particular configuration with the upstream pollutant source. Outward interactions (Q2 $\cong$ 29%) drive the air with less pollutants out of the canyon.

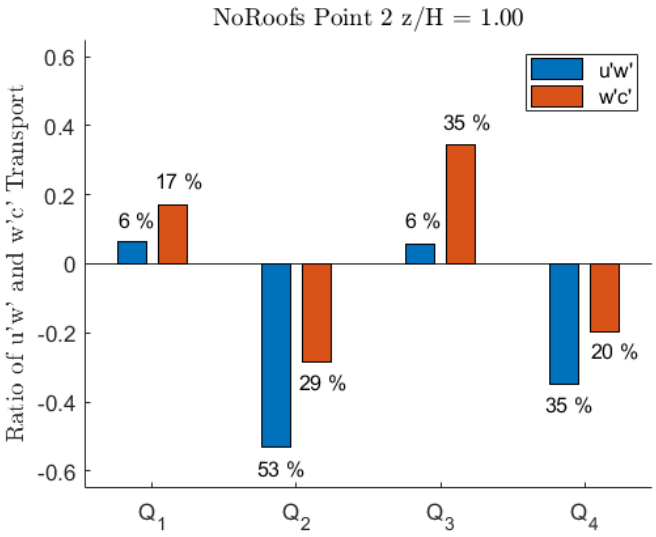

Figure 4.40 - Occurrence frequency for quadrant analysis of the vertical momentum flux (u'w') and the vertical transport flux (w'c') for the central point of the street canyon (point 2, Figure 4.31) at the eaves level z/H = 1

The gable roof configuration was analysed at the top level (H_{tot}) and momentum flux results were founded too closed respect to the *NoRoofs* case, as show in Figure 4.41. Ejections (Q2) occurs most frequently ($\cong$ 56%) followed by sweep ($\cong$ 30%), while outward and inward interactions are smaller, equal to the 8% and 6% respectively. Otherwise in the transport flux, even if sweeps are once again the most effective events with an occurrence of 36% (Q3), ejections appeared more influent respect to

outwards interactions and consequently the more polluted air should be taken from the canyon to the free stream flow.

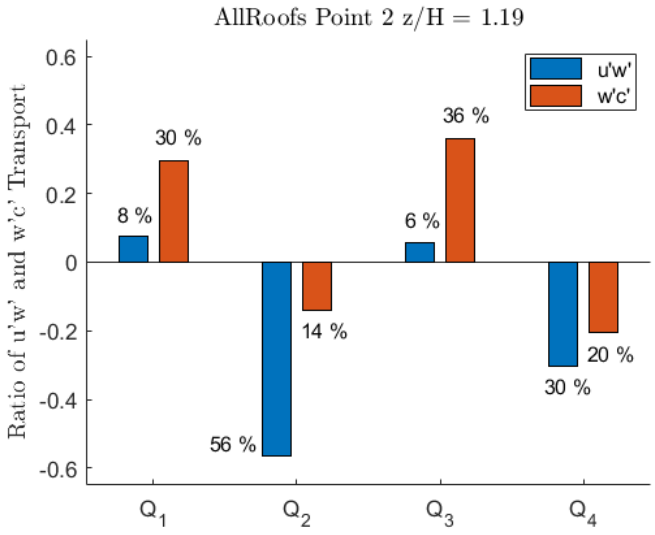

Figure 4.41 - Occurrence frequency for quadrant analysis of the vertical momentum flux (u'w') and the vertical transport flux (w'c') for the central point of the street canyon (point 2, Figure 4.31) at the top level z/H = 1.19

4.5.3.3 Conclusions on the skimming flow regime

The skimming flow regime case of the street canyon was in this section analysed making use of the 5 buildings array with two configurations: with and without roofs. Two sections were used in order to investigate the flux in the central section of the street canyon and near this were the roof was not influenced by the presence of dormers. However analyses were here presented only for the central section, investigated with three entire profiles from the bottom to the doubled height of buildings. Even if the first and second order statistics for the velocity fields appear not so different between the two configurations, the concentration quantities reveal a huge discrepancy, showing halved value in case with roofs. This was found a consequence of the strong dispersion action due by the higher turbulence in case with roofs, above their.

In addition to this, the quadrant analysis for the vertical momentum flux and for the vertical transport flux were analysed. Comparison revealed a quite different behaviour into the canyon, with more probable values for ejections respect to sweeps an configurations with roofs, and more intense outward and inward interactions inside the canyon. Finally the presence of roofs should be consider a good way to prevent the entrance of pollutant air into the canyon.

Results referred to this particular configurations with gable-dormers roofs and with the aspect ratio of the canyon (AR_C) equal to 0.8 and the aspect ratio of the buildings (AR_B) equal to 0.625.

4.5.4 Wake interference regime

Measurements were performed as 20 vertical profiles with 10 points each from $z_{min} = 11\ mm$ to the $z_{max} = 90\ mm$ (model scale and $z_{min} = 2.2\ m$, $z_{max} = 18\ m$ at real scale). Vertical points are not equally spaced, but were chosen with higher resolution near the ground, around the eaves and roof level ($z = 16, 20, 30, 40, 45, 55, 60, 70, 90$ mm). Profiles were divided into four sections ideally joining the two buildings facades Figure 4.43. However, only sections A, B and D were usable and were reported. The wind direction was chosen perpendicular with respect to London Rd, that is the main road going from St. George's Circus.

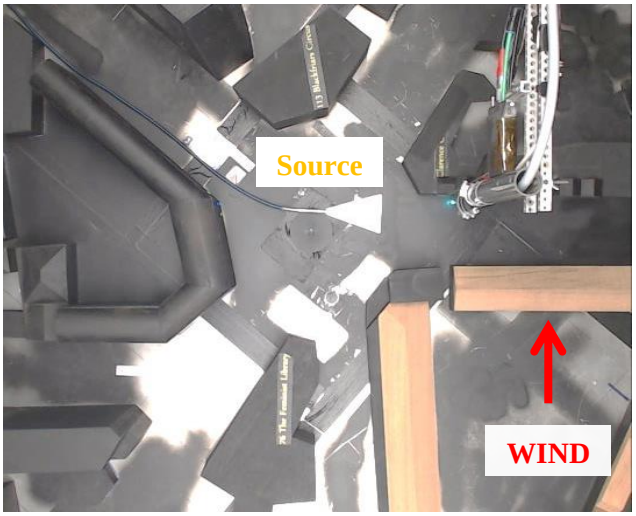

Figure 4.42 - Wind tunnel model: characteristics of configurations for experiments in the wake interference regime. H = 46 mm is the mean height at eaves level of the buildings around London Rd. Meteorological wind direction 230° is perpendicular to London Rd.

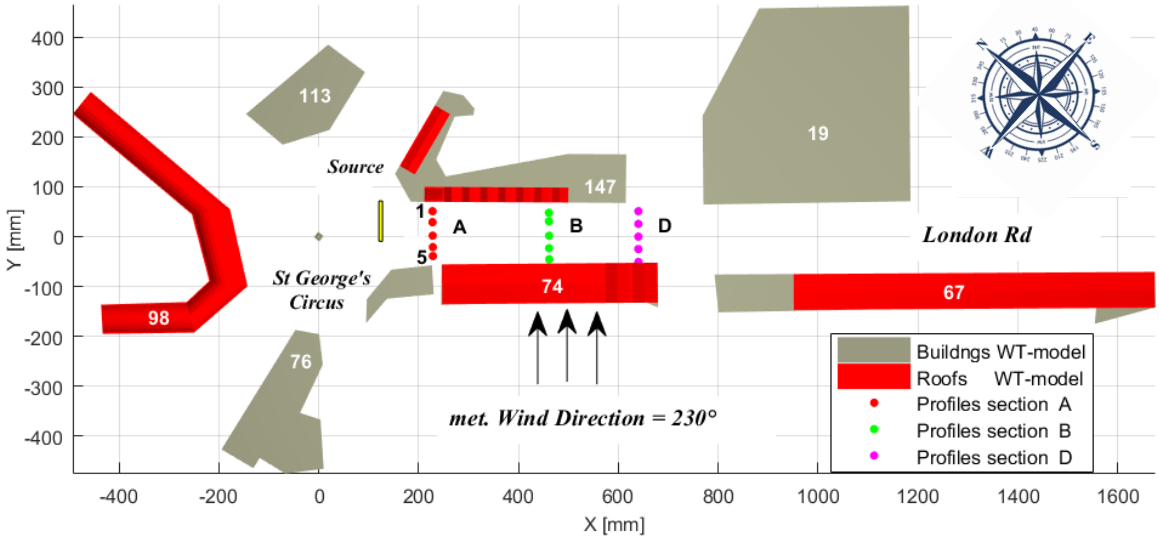

Figure 4.43 - Wind tunnel model: measurement points along London Rd at the MAGIC site. Points are divided into section A (red circles), B (green circles), C (pink circles), D (black circles) where each one is compounded of 5 points (1 - 5 respectively from the downstream position to the upstream one). Meteorological wind direction is equal to 230° (reported with black arrows), perpendicular to London Rd. The mean source point is positioned in St George's circus, corresponding to London Rd position (yellow line). Grey blocks are buildings without roofs. Red blocks are building with roofs. Buildings numbers are written in white

Table 4.8 - Characteristics of measurement points for the skimming flow investigation case.

Point n	Building n	Building + Roof Height	Roof type	Roof Slope α	Comment
1A	147	45.0+10	Gabled	29°	Roof parallel to wind
5A	14, 74	51.5, 46.6+23		0°, 30°	Roof perpendicular to wind
1B	147	45.0+10	Gabled	29°	Roof parallel to wind
5B	74	46.6+23		30°	Roof perpendicular to wind
1D	147	45.0+10	Gabled	29°	Roof parallel to wind
4D	74	46.6+23		30°	Roof parallel to wind

A linear source with flow rate identical to the skimming flow regime case (Section 4.5.3), equal to $Q = 0.036\, l/m$, was located at St. George's Circus, as visible in Figure 4.42. The main road (London Rd) width varied a little bit on the way, but the mean value of the aspect ratio, was estimated as $AR_c = 2.7$, considering the mean height of the buildings equal to $H = 46\, mm$. At the same time, the aspect ratio of buildings was estimated between $AR_B = 1.6$ and $AR_B = 1.9$. The meteorological wind direction was chosen equal to 230° in order to be perpendicular to London Rd, similar to the most frequent and intense wind registered for London (see Section 4.4.1).

4.5.4.1 First and second order statistics

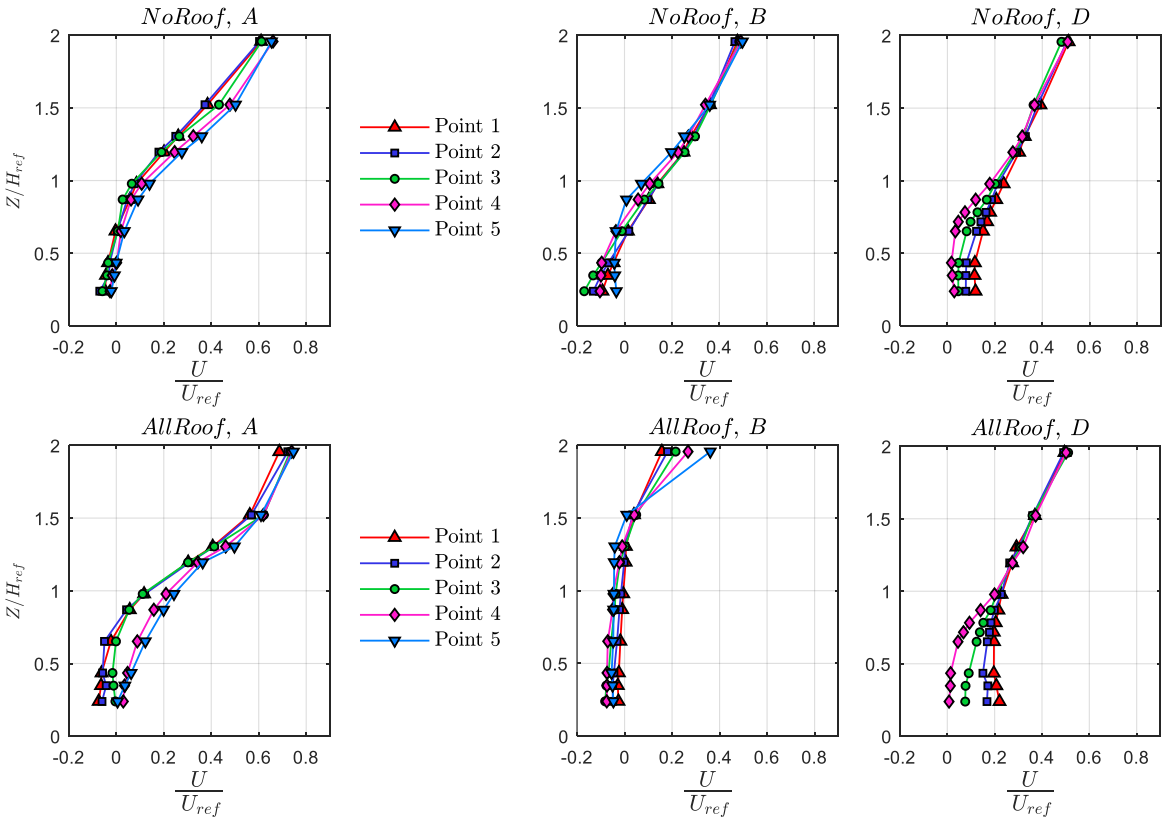

Figure 4.44 - Vertical profiles of mean stream-wise velocity component made non dimensional by the free stream velocity (U_{ref} at z = 1m). a-c: configuration without roofs; d-f: configuration with roofs, respectively for sections A,B,C

Vertical profiles of stream-wise velocities are reported in Figure 4.44 (a-c for the *NoRoofs* case and d-f for the *AllRoofs* case) for the three sections along London Rd. In section A, differences are visible

in all the profiles for the entre height. In the case without roofs curves tend to overlap especially into the canyon, while in the case with roofs a larger difference is visible in the highest part of the canyon ($0.5 < z/H < 1.2$) between the two mid-parts of the section. Anyway, velocities above the roofs seem faster in the case with roofs and results converged at $z/H > 2$, which corresponds to the maximum z level in present graphs. This aspect is better visible in section B (Figure 4.44 e) positioned at the centre of the upwind building 74 and at the end of gable roofs above the building 147, for which the total height becomes $z/H = 1.2$. However, understanding the reason why at such a high level, z/H =1.5, all curves converged, and then in the case with roofs, from points 1 to 5 of the section (see Figure 4.43), velocity increased is not clear enough. Thus results reported here appear not sufficient to fully understand the flow behaviour in this area and further measuring campaigns or numerical simulations will be useful. However, the main objective of this work is to verify if there are differences in flow behaviour between the two configurations. Regarding section D, velocity appears higher at lower levels especially for point 1, that is close to the Clarence Centre.

The vertical velocities component shows huge differences in sections A and B for the entire profiles, not only in trends, but also in intensity. In fact, while in the roofless case the 5 points for section A show positive vertical velocities with increasing values going upwind along the section, and in section B they assumed the canonical behaviour with positive values in the first mid part of the section and negative in the second one, with the highest values at mid-depth canyon (around $z/H = 0.5$), in *AllRoofs* configuration, the trends are opposite. In section A, near Clarence Centre vertical velocities are negative, quite high with respect the *NoRoofs* configuration and positive from the central point of the street, while the highest values are at the eaves level for all the 5 measuring points. In section B, all values are positive, with the highest values registered around the roof level. In the third section differences are lower and trends similar.

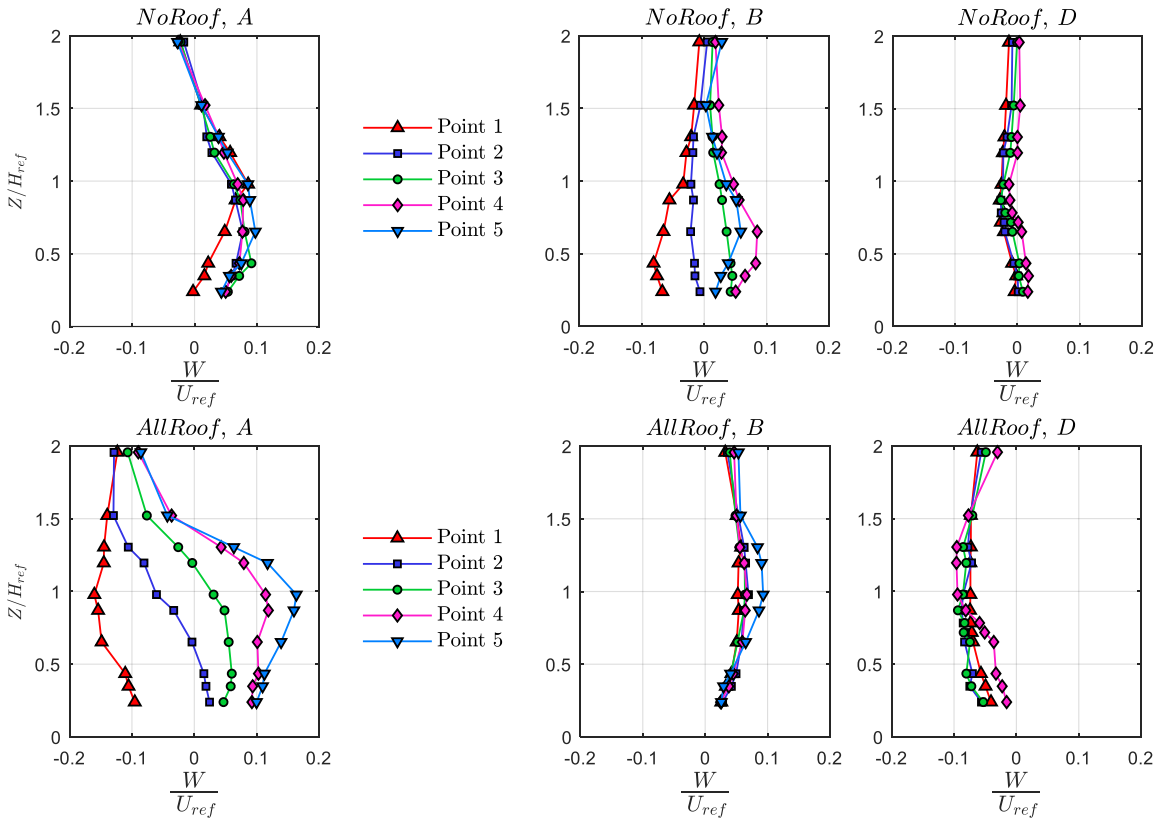

Figure 4.45 - Vertical profiles of mean vertical velocity component made non dimensional by the free stream velocity (U_{ref} at z = 1 m). a-c: configuration without roofs; d-f: configuration with roofs, respectively for sections A, B, C.

Analysing first order statistics, the complexity of flow behaviour is well visible and measuring the span-wise velocity component would be useful. An element that plays a part on this might be the intersection between buildings 74 and 14, but the influence of roofs upstream might also be relevant and both should be investigated.

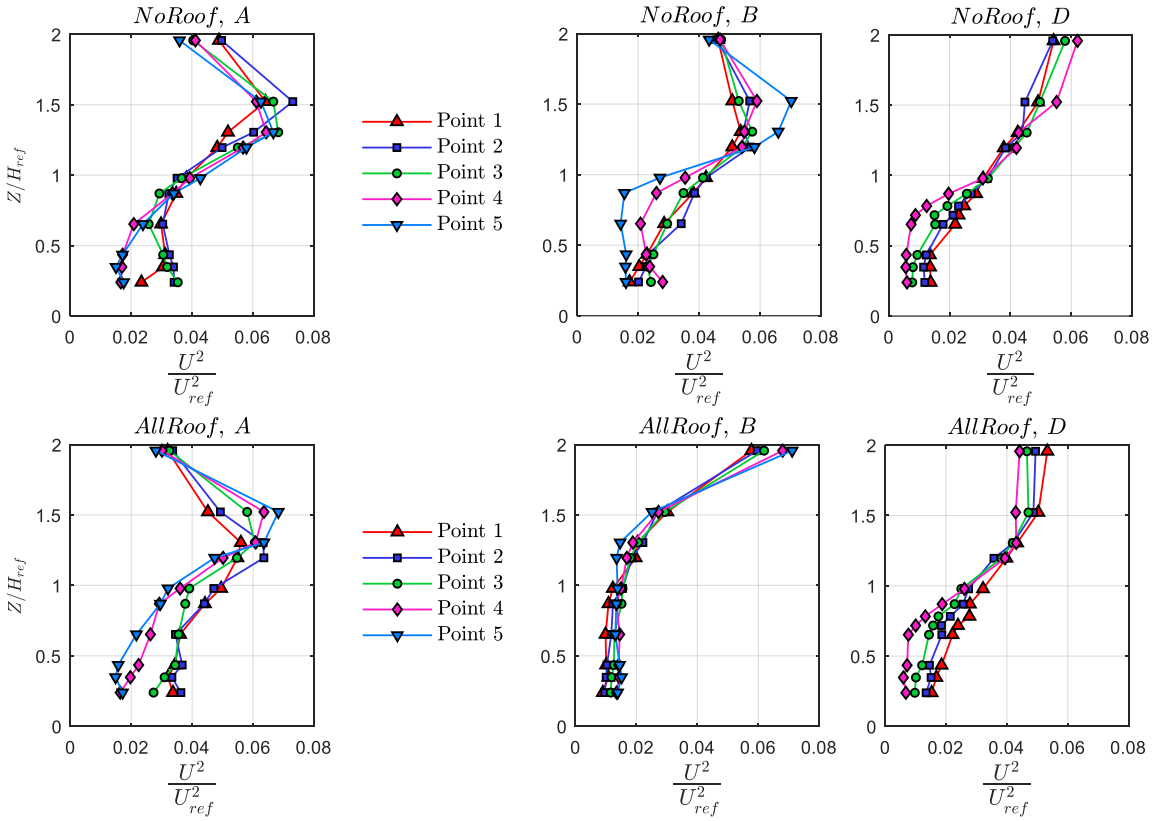

Figure 4.46 - Vertical profiles of mean variance of the stream-wise velocity made non dimensional by the free stream velocity (U_{ref} at z = 1 m). a-c: configuration without roofs; d-f: configuration with roofs, respectively for sections A, B, C.

Looking at second order statistics, the variance of stream-wise velocities (Figure 4.46) comparing the two configurations, shows similar behaviour in section A, with highest values at lower levels for profiles 1-3 and the maximum achieved at $z/H = 1.5$. Section B presents a completely different behaviour between the configurations: in the roofless case up to the eaves level the 5 profiles have various trends. Among them, the profile closest to building 74 presents the lowest value at lower levels, while above the roofs it reaches the highest value. Differently, in the roofs configuration all the 5 profiles have the same behaviour, with a fast increase of turbulence above the roofs, at higher levels. Variance of vertical velocities (Figure 4.47) appears similar to the previous results, with no relevant differences between the two configurations at section D and with a completely different trend in section B, where the highest turbulence is visible at higher levels. Into the canyon, the homogeneity among profiles is higher in the presence of roofs. At section A, for the *NoRoof* case, turbulence decreases from point 1 to point 5 for the entire profile, while the roof results are quite non homogeneous. Above roofs the highest value is achieved for $z/H = 1.25$ even if in a different position along the section. As expected, the two configurations presented huge differences also in the dispersion behaviour.

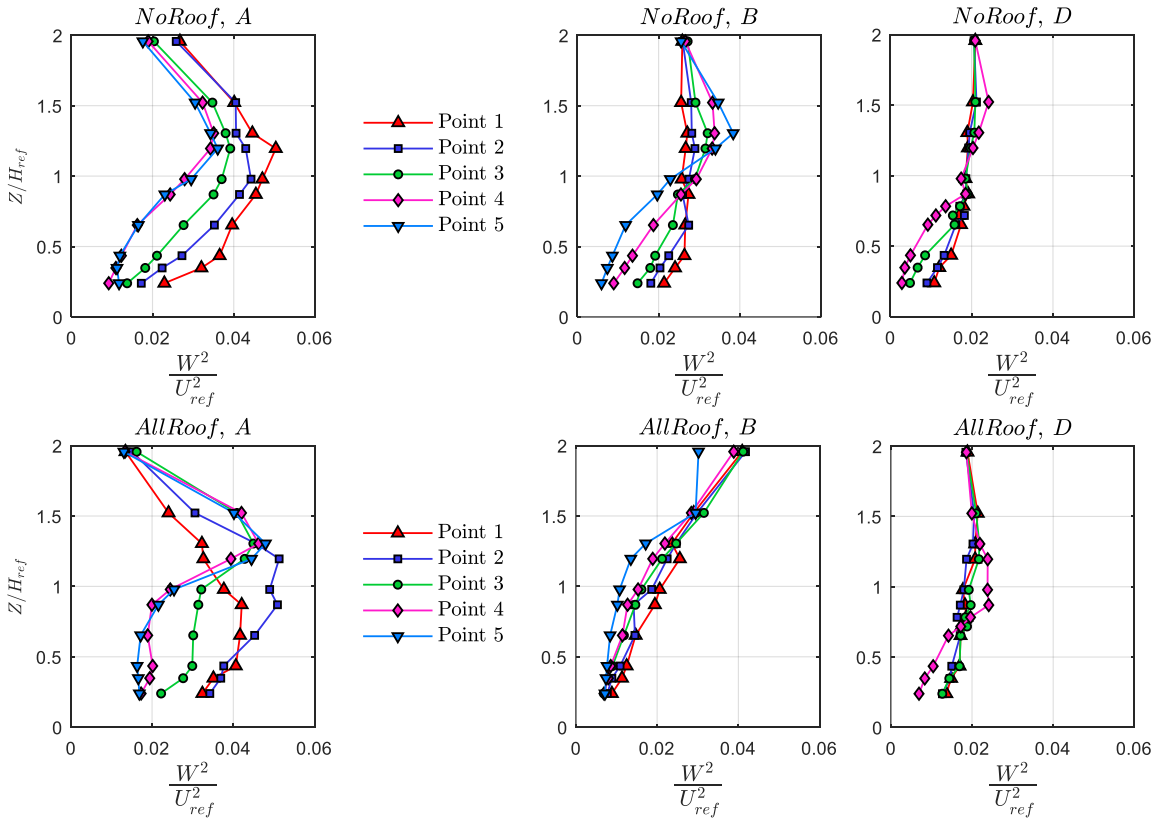

Figure 4.47 - Vertical profiles of mean variance of the vertical velocity made non dimensional by the free stream velocity (U_{ref} at z = 1m). a-c: configuration without roofs; d-f: configuration with roofs, respectively for sections A,B,C

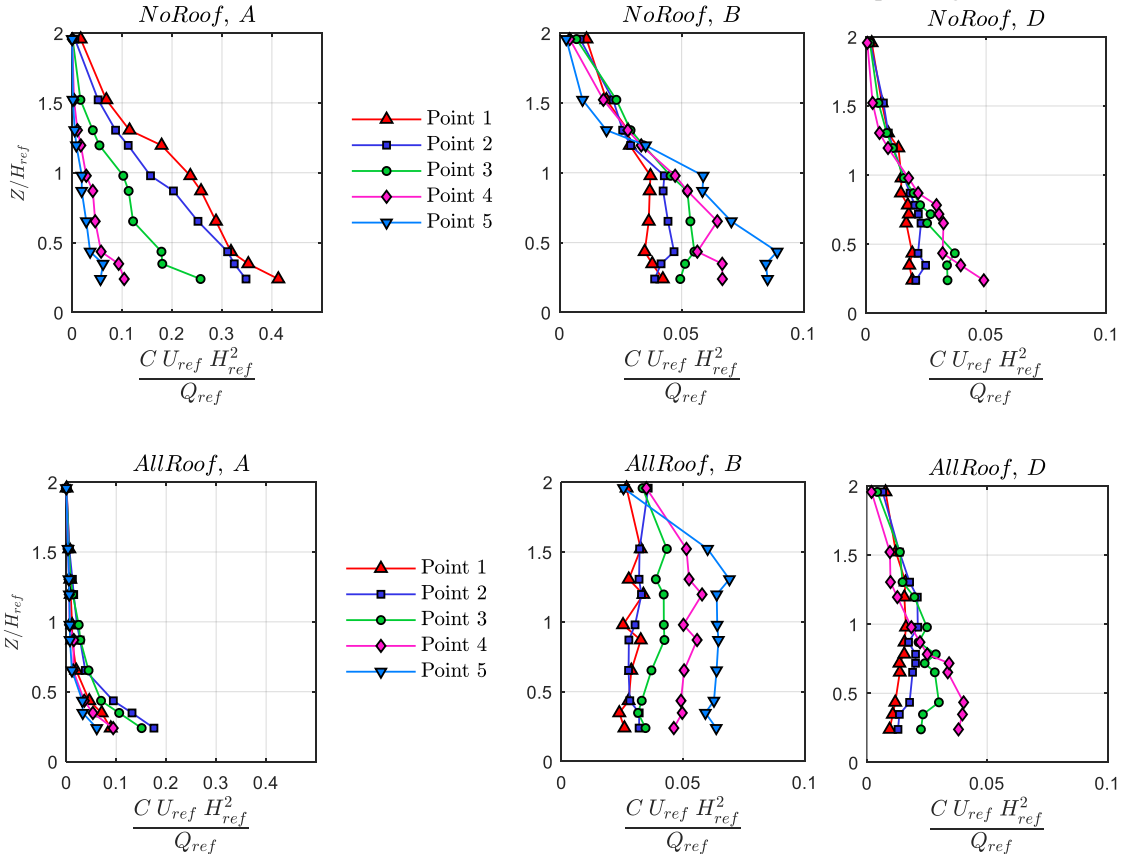

Figure 4.48 - Vertical profiles of mean concentration made non dimensional by the square of the reference height (H_{ref} = 80 mm at the eaves level), the free stream velocity (U_{ref} at z = 1 m) and the flow rate velocity (Q_{ref} = 0.036 l/m). a-c: configuration without roofs; d-f: configuration with roofs, respectively for sections A, B, C.

As visible in Figure 4.48, section D shows the same concentration level for both configurations in all the 4 measured profiles, increasing from point 1 to point 4.This means that pollutants tend to accumulate near the wall of building 74 and are taken downstream towards an intersection. Section A, which is closest to the source, registered huge differences with quite doubled values in the case without roofs; while this puts in evidence an increase of concentration from point 5 to point 1, with the highest values at the Clarence Centre wall, in the roofless case concentrations seem higher in the middle of the section. As regards section B, for both configurations values increase from Clarence Centre to building 74. However, in the case with roofs, at lower levels concentrations are lower especially for points 3-5, but the same concentration level is maintained until the roof level, after which a slow decrease of concentration is shown.

4.5.4.2 Conclusions on the wake interference regime

A series of preliminary analyses were made in London Rd in order to understand the influence of roofs on flow and pollutant dispersion. Measurements were made by means of 14 vertical profiles divided into three sections from St George's Circus to the end of building 74 (Figure 4.43). First and second order statistics results, together with the concentration profiles are here reported. Outcomes have shown the complexity of fluxes in this area and huge differences when the roofs are employed. In the roofless case pollutants seem to be transported along London Rd, from one hand of the canyon (Clarence Centre in Figure 4.48 section A) to the other (building 74 in Figure 4.48 section B). Concentrations slowly decrease along the way thanks to higher stream-wise and vertical turbulence levels into the canyon and they are quite completely removed going downstream towards the intersections present after building 74. In case with roofs concentration levels are very low at the beginning of the road, in agreement with the strongest vertical velocities and variances. Pollutants seem to be transported along the way and accumulate in the central section before being dispersed at higher levels.

The present results are strongly dependent on the source point, thus conclusions cannot be generalised. Furthermore, measurement points are not sufficient to completely understand fluid dynamics in this area, so that measuring the third velocity components as well appears to be necessary.

However, outcomes are sufficient to clarify that not considering roofs in a model could induce huge errors with respect to the actual wind and pollutant behaviour.

4.6 Conclusions

In the present work the effects of roofs on flow and pollutant dispersion was investigated for the field study site on the South Bank of the Thames River in London UK. This was part of the Managing Air for Green Inner Cities (MAGIC) project being carried out by the university of Cambridge, Imperial College London, London South Bank University and the University of Surrey. The experiments were carried out in the EnFlo meteorological wind tunnel at the University of Surrey (Mechanical Engineering Sciences Department). The aim of the work was to understand if in a real urban pattern (buildings with different height and width; streets with various canyon depth and aspect ratio; non uniform intersections; etc.), differences between flat roofs and shaped roofs models exist in terms of ventilation and pollutant removal, not only in the flow above buildings, but also at pedestrian level.

In order to do this, a preparatory work was done by analysing the real roof shapes of the area and then, the previous wind tunnel model with flat roofs was modified. Subsequently, both configurations, with and without roofs, were employed for analyses by dividing them into four big measurement campaigns: preliminary analysis; North-West district investigation on three different areas; skimming

flow regime with the pollutant source in Waterloo Rd; wake interference regime with the pollutant source in St George's Circus.

The most interesting results were found for the wind direction around α=220°-230° which perpendicularly approach London Rd, Clarence Centre, Waterloo Rd and the main facade of building 98, for which flow dynamics into the courtyard is very complex and interesting.

By splitting data into three groups, from the simplest (street canyon in the skimming flow regime) to the most complicated case (courtyard of building 98 on the right hand of the graphs), and by analysing all the three velocity components, huge differences were found especially in the courtyard case, where discrepancies are great and dispersed around the mean trend (Figure 4.29). The flow appears strongly three dimensional: the stream-wise components is mainly affected up to the roof level. At the same time, at lower levels, differences are not irrelevant. The other two components show a strongly irregular behaviour as well, especially in the case of span-wise velocities, for which differences increased from the eaves level to the bottom, twisting the scenario, that could be analysed considering only the configuration with flat roof buildings. In the simplest configuration too, e.g. the street canyon array, relevant differences were found for all the three velocities components. It is worth mentioning that the wind direction we considered was not perfect perpendicular with respect to the building walls and, as such, it did not exactly match the usual modelling conditions (especially in CFD).

The concentration quantities in the skimming flow case revealed huge discrepancies, showing halved values in the case with roofs at the mid-section of the street canyon (Figure 4.35). This was a consequence of the strong dispersion action due to the higher turbulence above roofs.

In addition to this, the quadrant analysis for the vertical momentum flux and for the vertical transport flux presented probability values higher for ejections than for sweeps in the roofs configurations (Figure 4.41), and more intense outward and inward interactions inside the canyon, underlying the benefits of employing roofs, which increase the ventilation mechanism. In the wake interference regime too, outcomes have shown the complexity of fluxes and considerable differences when the roofs are employed. However, this series of data was found insufficient to fully understand the flow behaviour.

In conclusion, all the observations suggested that taking roofs into consideration is necessary for realistic analysis on the urban canopy air quality. This priority is more relevant where buildings are not modelled with simplest geometries, the urban canopy is not regular and building facades are not perfectly parallel or perpendicular with respect to the approaching flow. In these cases very complex 3D flow structures can be observed and deep analyses are required.

The results on pollutant dispersion are strongly dependent on the source point, thus conclusions cannot be generalised. Furthermore, differences suggested that variations of roof shapes strongly affected the flow not only at higher levels, but also near the bottom; their presence should be considered a good way to prevent the entrance of pollutant air, at least in some particular buildings packages.

Finally, outcomes are sufficient to clarify that not considering roofs in a model could induce huge errors with respect to the actual wind and pollutant behaviour.

4.7 References

Abohela, I., Hamza, N., Dudek, S., 2013. Effect of roof shape, wind direction, building height and urban configuration on the energy yield and positioning of roof mounted wind turbines. Renewable Energy 50, 1106–1118. https://doi.org/10.1016/j.renene.2012.08.068

Ahmad, K., Khare, M., Chaudhry, K.K., 2005. Wind tunnel simulation studies on dispersion at urban street canyons and intersections—a review. Journal of Wind Engineering and Industrial Aerodynamics 93, 697–717. https://doi.org/10.1016/j.jweia.2005.04.002

Badas, M.G., Ferrari, S., Garau, M., Querzoli, G., 2017. On the effect of gable roof on natural ventilation in two-dimensional urban canyons. Journal of Wind Engineering and Industrial Aerodynamics 162, 24–34. https://doi.org/10.1016/j.jweia.2017.01.006

Brown, M.J., Lawson, R.E., Decroix, D.S., Lee, R.L., 2000. Mean Flow and Turbulence Measurements Around a 2-D Array of Buildings in a Wind Tunnel. https://nepis.epa.gov/Exe/ZyPURL.cgi?Dockey=P100G6C6.txt

Carpentieri, M., Hayden, P., Robins, A.G., 2012. Wind tunnel measurements of pollutant turbulent fluxes in urban intersections. Atmospheric Environment 46, 669–674. https://doi.org/10.1016/j.atmosenv.2011.09.083

Carpentieri, M., Robins, A.G., 2015. Influence of urban morphology on air flow over building arrays. Journal of Wind Engineering and Industrial Aerodynamics 145, 61–74. https://doi.org/10.1016/j.jweia.2015.06.001

Cheng, W.K., Summers, T., Collings, N., 1998. The fast-response flame ionization detector. Progress in Energy and Combustion Science 24, 89–124. https://doi.org/10.1016/S0360-1285(97)00025-7

Cheng, W.C., Liu, C.-H., 2011. Large-Eddy Simulation of Flow and Pollutant Transports in and Above Two-Dimensional Idealized Street Canyons. Boundary-Layer Meteorol 139, 411–437. https://doi.org/10.1007/s10546-010-9584-y

Facilities | University of Surrey. https://www.surrey.ac.uk/aerodynamics-environmental-flow-group/environmental-flow-research-centre/facilities

Garau, M., Badas, M.G., Ferrari, S., Seoni, A., Querzoli, G., 2018. Turbulence and Air Exchange in a Two-Dimensional Urban Street Canyon Between Gable Roof Buildings. Boundary-Layer Meteorol 167, 123–143. https://doi.org/10.1007/s10546-017-0324-4

Garau, M., Badas, M.G., Ferrari, S., Seoni, A., Querzoli, G., 2019. Air Exchange in urban canyons with variable building width: a numerical LES approach. Special Issue: HARMO18, Int. J. Environ. Pollut. http://www.inderscience.com/info/ingeneral/forthcoming.php?jcode=ijep

Ho, Y.-K., Liu, C.-H., Wong, M.S., 2015. Preliminary study of the parameterisation of street-level ventilation in idealised two-dimensional simulations. Building and Environment 89, 345–355. https://doi.org/10.1016/j.buildenv.2015.02.042

Huang, Y., Hu, X., Zeng, N., 2009. Impact of wedge-shaped roofs on airflow and pollutant dispersion inside urban street canyons. Building and Environment 44, 2335–2347. https://doi.org/10.1016/j.buildenv.2009.03.024

Irwin, H.P.A.H., 1981. The design of spires for wind simulation. Journal of Wind Engineering and Industrial Aerodynamics 7, 361–366. https://doi.org/10.1016/0167-6105(81)90058-1

Katsouvas, G.D., Helmis, C.G., Wang, Q., 2007. Quadrant analysis of the scalar and momentum fluxes in the stable marine atmospheric surface layer. Boundary-Layer Meteorol 124, 335–360. https://doi.org/10.1007/s10546-007-9169-6

Katul, G., Kuhn, G., Schieldge, J., Hsieh, C.-I., 1997. The ejection-sweep-character of scalar fluxes in the unstable surface layer. Boundary-Layer Meteorology 83, 1–26. https://doi.org/10.1023/A:1000293516830

Kikumoto, H., Ooka, R., 2012. A numerical study of air pollutant dispersion with bimolecular chemical reactions in an urban street canyon using large-eddy simulation. Atmospheric Environment 54, 456–464. https://doi.org/10.1016/j.atmosenv.2012.02.039

Kovar P. A., Louka, P., Sini, J.-F., Savory, E., Czech, M., Abdelqari, A., Mestayer, P.G., Toy, N., 2002. Influence of Geometry on the Mean Flow within Urban Street Canyons – A Comparison of Wind Tunnel Experiments and Numerical Simulations. Water, Air, & Soil Pollution: Focus 2, 365–380. https://doi.org/10.1023/A:1021308022939

Ledo, L., Kosasih, P.B., Cooper, P., 2011. Roof mounting site analysis for micro-wind turbines. Renewable Energy 36, 1379–1391. https://doi.org/10.1016/j.renene.2010.10.030

Llaguno-Munitxa, M., Bou-Zeid, E., Hultmark, M., 2017. The influence of building geometry on street canyon air flow: Validation of large eddy simulations against wind tunnel experiments. Journal of Wind Engineering and Industrial Aerodynamics 165, 115–130. https://doi.org/10.1016/j.jweia.2017.03.007

MAGIC-air.uk. MAGIC-air.uk. Magic Air. http://magic-air.uk/home.html

Marucci, D., Carpentieri, M., Hayden, P., 2018. On the simulation of thick non-neutral boundary layers for urban studies in a wind tunnel. International Journal of Heat and Fluid Flow 72, 37–51. https://doi.org/10.1016/j.ijheatfluidflow.2018.05.012

Natalini, M.B., Morel, C., Natalini, B., 2013. Mean loads on vaulted canopy roofs. Journal of Wind Engineering and Industrial Aerodynamics 119, 102–113. https://doi.org/10.1016/j.jweia.2013.05.001

Nosek, Š., Kukačka, L., Kellnerová, R., Jurčáková, K., Jaňour, Z., 2016. Ventilation Processes in a Three-Dimensional Street Canyon. Boundary-Layer Meteorol 159, 259–284. https://doi.org/10.1007/s10546-016-0132-2

Nosek, Š., Kukačka, L., Jurčáková, K., Kellnerová, R., Jaňour, Z., 2017. Impact of roof height non-uniformity on pollutant transport between a street canyon and intersections. Environmental Pollution 227, 125–138. https://doi.org/10.1016/j.envpol.2017.03.073

Oke, T.R., 1988. Street design and urban canopy layer climate. Energy and Buildings 11, 103–113. https://doi.org/10.1016/0378-7788(88)90026-6

OS Map, The National Grid. https://www.ordnancesurvey.co.uk/resources/maps-and-geographic-resources/the-national-grid.html

Os-mastermap-topography-layer-user-guide.pdf

QGIS, https://www.qgis.org/it/site/

Rafailidis, S., 1997. Influence of Building Areal Density and Roof Shape on the Wind Characteristics Above a Town. Boundary-Layer Meteorology 85, 255–271. https://doi.org/10.1023/A:1000426316328

Raupach, M.R., 1981. Conditional statistics of Reynolds stress in rough-wall and smooth-wall turbulent boundary layers. Journal of Fluid Mechanics 108, 363. https://doi.org/10.1017/S0022112081002164

Ricci, A., Kalkman, I., Blocken, B., Burlando, M., Freda, A., Repetto, M.P., 2017. Local-scale forcing effects on wind flows in an urban environment: Impact of geometrical simplifications. Journal of Wind Engineering and Industrial Aerodynamics 170, 238–255. https://doi.org/10.1016/j.jweia.2017.08.001

Snyder, W.H., 1981. Guideline for fluid modelling of atmospheric diffusion. https://nepis.epa.gov/Exe/ZyPURL.cgi?Dockey=2000MVTD.txt

Snyder, W.H., Castro, I.P., 2002. The critical Reynolds number for rough-wall boundary layers. Journal of Wind Engineering and Industrial Aerodynamics 90, 41–54. https://doi.org/10.1016/S0167-6105(01)00114-3

Soulhac, L., Garbero, V., Salizzoni, P., Mejean, P., Perkins, R.J., 2009. Flow and dispersion in street intersections. Atmospheric Environment 43, 2981–2996. https://doi.org/10.1016/j.atmosenv.2009.02.061

Tominaga, Y., Akabayashi, S., Kitahara, T., Arinami, Y., 2015. Air flow around isolated gable-roof buildings with different roof pitches: Wind tunnel experiments and CFD simulations. Building and Environment 84, 204–213. https://doi.org/10.1016/j.buildenv.2014.11.012

Tropea, C., Yarin, A. L., Foss, J.F. (Eds.), 2007. Springer Handbook of Experimental Fluid Mechanics, Springer Handbooks. Springer-Verlag, Berlin Heidelberg. ISBN 978-3-540-25141-5

Van Hooff, T., Blocken, B., 2010. Coupled urban wind flow and indoor natural ventilation modelling on a high-resolution grid: A case study for the Amsterdam ArenA stadium. Environmental Modelling & Software 25, 51–65. https://doi.org/10.1016/j.envsoft.2009.07.008

Wallace, J.M., 2016. Quadrant Analysis in Turbulence Research: History and Evolution. Annual Review of Fluid Mechanics 48, 131–158. https://doi.org/10.1146/annurev-fluid-122414-034550

Xie, X., Huang, Z., Wang, J., 2005. Impact of building configuration on air quality in street canyon. Atmospheric Environment 39, 4519–4530. https://doi.org/10.1016/j.atmosenv.2005.03.043

Xu, Y.L., Reardon, G.F., 1998. Variations of wind pressure on hip roofs with roof pitch. Journal of Wind Engineering and Industrial Aerodynamics 73, 267–284. https://doi.org/10.1016/S0167-6105(97)00291-2

Yassin, M.F., 2011. Impact of height and shape of building roof on air quality in urban street canyons. Atmospheric Environment 45, 5220–5229. https://doi.org/10.1016/j.atmosenv.2011.05.060

Zhang, Z., 2010. LDA Application Methods: Laser Doppler Anemometry for Fluid Dynamics, Experimental Fluid Mechanics. Springer-Verlag, Berlin Heidelberg. ISBN 978-3-642-13514-9

Chapter 5

Conclusions

5.1 Summary of results

Air Quality is a key social and environmental issue. It is a multidisciplinary topic that involves a wider group of disciplines from the mathematical or chemical science to the legal and social studies, for which research is a fundamental tool to understand the problem in depth, and to plan solutions and preventive measures. Cities represent a critic and fragile environment, where the majority of pollutants are emitted and whose residents are heavily exposed to them. As a consequence, finding healthier ways to live cities is pressing due to the continuous urbanisation process. In this scenario, knowledge on ventilation plays a central role in order to understand and control many urban environment phenomena, such as the dispersion and the pedestrian wind comfort (i.e. Moonen et al., 2012). Despite the many research works which have largely investigated this issue, a lot of aspects still have to be deepened, because of the complexity of cities. Different approaches exist to investigate urban flow, from the most idealised ones, as the analysis of 2D urban canyons, to the most complex, as the simulations of real geometries. The first ones are preferred in order to understand basic phenomena, while the second ones are employed where a higher level of detail is needed in order to evaluate a specific case.

Two main techniques are usually applied: the experimental simulations in laboratory models, such as those reproduced in a water channel or in a wind tunnel, and the numerical simulations performed by means of computational fluid dynamic (CFD); each one presents positive aspects as well as limitations and it implies specific errors in results (Section 5.2). In addition to this, in-situ campaigns are also employed in order to validate the other ones or to apply more realistic initial conditions.

This thesis investigated the influence of two specific geometrical parameters, the building aspect ratio (i.e. the building width to height ratio) and the gable roof slope instead of the flat roof commonly employed, on the wind flow and the air exchange process. This was made at first considering series of urban basic units with variable widths, namely street canyons, and then by modelling a district of London in which the quasi-real 1:200 scaled geometries were employed. The main outcomes of each chapter are reported as follows:

Chapter 2 - Influence of building aspect ratio

A virtually infinite series of two-dimensional street canyons with two different canyon aspect ratios (AR_C = 0.5, 1.0) was numerically simulated considering the building aspect ratio variations (AR_B = 0.1, 0.2, 0.3, 0.4, 0.5, 1.0, 1.5 and 2.0), in order to study wind flow and ventilation mechanism

in the typical narrow canyon configurations of Mediterranean cities, such as Cagliari (Badas et al., 2019; Salvadori et al., 2018). Depending on the aspect ratio width, the flow shows a completely different behaviour inside the canyon: instead of a single main vortex, two counter-rotating vortexes are shown in the narrower canyon (Figure 2.6). This involves relevant differences in vertical velocities, thus in ventilation intensity, especially at pedestrian level, with possible consequences on the air quality if pollutants are emitted or come inside the canyon. Indeed, the residence time (Figure 2.14), clearly shows the poor capability of pollutant removal in case of $AR_C = 0.5$.

By varying the building aspect ratio, a relevant improvement of this behaviour was found. The analysis of the exchange rates between the canyon and the overlaying boundary layer, indicated that the flow rate increases for narrow buildings, irrespective of the canyon shape, and the minimum is observable for $AR_B = 1.5$. However, the mean trends are characterised by a different slope, while the increase of ventilation at roof level (or the decreasing of the residence time) is faster for the $AR_C = 0.5$ series. As a consequence the AR_B variation is more efficient in the latter.

Concluding, results suggested that the building aspect ratio is a crucial parameter when predicting pollutant removal in urban boundary layer modelling.

Chapter 3 - Influence of roof shape

The effect of a typical building covering with gabled roofs was investigated by means of several arrays of two-dimensional prismatic obstacles. Two series with gable roof slope $\alpha = 0°$ and $\alpha = 45°$, were experimentally performed by varying the canyon aspect ratio from 1.0 to 6.0, so exploring the entire range of flow regimes (Oke, 1988). In addition to this, two series of similar configurations were numerically carried out, by fixing the canyon width as 1.0 and 2.0, and by changing the roof slope from 0° to 45° (0°, 10°, 20°, 30°, 45°).

Experimental outcomes reveal a delay in the transition from one flow regime to another when the gable roof is employed, since the vortex shape appears to be affected by the overall height of the building (Figure 3.4). This behaviour is particularly evident in the narrowest canyon configuration, and it decreases with the canyon width. Nevertheless, numerical results highlighted that the 45° gable roof behaviour is quite far from the others and it has to be considered as a particular case.

Anyway, the presence of sloped roofs perturbs a larger portion of flow above the canopy, as can be observed both in the streamlines (Figure 3.4-Figure 3.14) and in the vertical mean velocity profiles (Figure 3.9 a-Figure 3.18). As regards turbulence levels, pitched roofs generate a thicker and more intense turbulent layer, just above the building. This was pointed out in the horizontally averaged mean profiles of the momentum fluxes (Figure 3.9b - Figure 3.20) and of the velocity variances (Figure 3.10- Figure 3.19) in which the maximum is quite quadrupled above the roof level, going from 0° to 45° (Figure 3.19a).

The exchange flow rate analysis shows that the overall rate increases from the bottom to the roof level in a faster and more evident way for the narrowest canyons. Indeed, a little gable roof slope variability (Figure 3.22a), produces a considerable increase in ventilation. The increasing slopes gives rise to different trends in the upper part of the canyon. The maximum was reached for 30° at $z/H \approx 0.7$, with a 40% gain with respect to flat roof. The 45° roof case assumes a quite linear trend, with increasing values from the ground to the half part of pitches for both quantities.

45° gabled roofs display lower residence times compared to the flat-roof counterpart, which exhibits a very weak dependence on the aspect ratio. A residence time increment of about 30% (Figure 3.13) was registered when the aspect ratio decreased from 6.0 to 2.0 and a further 70% is visible when AR_C becomes unitary. Nevertheless, this behaviour might not guarantee a good ventilation at the pedestrian levels, as shown by the flux exchange index (Figure 3.22).

These results are particularly meaningful and investigations should be extended to narrowest street canyons, which are normally affected by a very poor ventilation, and to additional roof shapes or more detailed urban configurations.

Chapter 4 - 3D simulations: influence of roof shapes at a field study site in London

The effects of roofs on flow and pollutant dispersion was investigated at the field study site on the South Bank of the Thames River in London UK. The experiments were carried out in the EnFlo meteorological wind tunnel at the University of Surrey with the aim to understand if the increasing level of detail(obtained by adding roofs to the model), could affect flow fields in a relevant way. A preparatory work was made by analysing the real roof shapes of the district and then by choosing the roofs and their level of detail, so that they could match the existing wind tunnel model. Subsequently, both configurations, with and without roofs, were employed for analyses by dividing them into four big measurement campaigns: preliminary analysis; North-West district investigation on three different areas; skimming flow regime with the pollutant source in Waterloo Rd; wake interference regime with the pollutant source in St George's Circus. The most intense and frequent wind in London (α = 220°-230°), which perpendicularly approached the main reference buildings and streets of the model(London Rd, Waterloo Rd, Clarence Centre and the main facade of building McLaren House), revealed the most interesting results.

By splitting data into three groups, from the simplest (street canyon in the skimming flow regime) to the most complex case (courtyard of the McLaren House), and by analysing all the three velocity components, huge differences were found between the with roof and no roof configurations, especially in the courtyard case (Figure 4.29, Table 4.6). In the latter the flow showed a strongly three-dimensional behaviour: the stream-wise component was mainly affected at roof level; the other two components appeared strongly irregular, with increasing differences from the eaves level to the bottom. This fact twisted the scenario which usually results from the analysis of the configuration with flat roof buildings only.

Even simplest configuration (street canyon array) displayed significant differences for all the three velocity components. Despite a little discrepancy from the perfectly perpendicular wind direction usually employed in modelled cases, such as the one discussed in Chapters 2 and 3, the MAGIC model results (Section 4.5.3) appeared quite similar to the previous ones.

In the skimming flow case the concentration measurements outcomes revealed huge modifications, showing halved values in the case with roofs at the mid-section of the street canyon and this is related to the higher turbulence. In addition to this, the quadrant analysis for both the vertical momentum flux and the vertical transport flux presented higher probability values for ejections than for sweeps in the configurations with roofs, and more intense outward and inward interactions inside the canyon. All of the above highlighted the benefits of employing roofs, as they increase the ventilation mechanism. In the wake interference regime too, outcomes demonstrated huge differences when roofs are employed. However, this series of data was found insufficient to fully understand the flow dynamics in London Rd. Pollutant dispersion is strongly dependent on the source point, so these outcomes cannot be generalised; however, the measurements here performed appear sufficient to clarify that not considering roofs in a model could lead to huge estimation errors.

Overall, our work demonstrated the necessity to employ roofs in models for a more efficient analysis on the urban air quality. The use of roofs should be considered a good way to mitigate pollutant concentration within urban canyons.

In the case of old cities, some generalisations could be pointed out by classifying and studying the traditional shape patterns, and they could be brought to the attention of urban planners and designers.

5.2 Implications for urban planning and further works

This study represents a first step toward suggesting that more attention in urban planning and in building design, could positively affect comfort and healthy air into urban canopy. Indeed we demonstrated the importance of roofs in ventilation , together with the complexity of flow dynamics in employing more realistic urban morphologies.

For some specific cases such as the street canyon for various regimes, an analysis on models with high level of simplifications may be extensively applied in order to create tables of roof shapes air ventilation efficiency, with respect to the building geometric parameters and the wind direction. These tables could be employed by designers as guidelines, not only for new construction, but also for refurbishments or building extensions.

If urban shapes are more complex and interactions among buildings very influent, tabulated values are not eligible and specific experiments or numerical evaluations will be needed.

In the case of old cities, some generalisations could be pointed out by classifying and studying the traditional shape patterns, and they could be brought to the attention of urban planners and designers.

The development of guidelines for ‘wide-ranging construction’ would be an added value to urban projects. In addition to this, tabulated values could be employed for a multi-criteria analysis to estimate the breathability performance certificate of a building, similar to the already existing energy performance certificate.

Paying attention to these aspects would be relevant, not only for existing cities (new construction, rehabilitation projects of derelict areas, vertical extension of existing housing), but also for developing countries. In fact the urbanisation process in those countries has recently begun and it is increasing at a fast pace, without a proper control on ventilation and a proper evaluation of air quality problems that may take place in the future.

5.3 Limitations of the work

5.3.1 2D street canyon configuration

The street canyon configuration is a particular condition, ideally referred to a street with buildings lined up along the two sides, and very extended in this direction (Nicholson, 1975). The original definition refers to a quite narrow street, but a broader definition is usually employed, in order to include also larger streets, called avenue canyons, and streets were buildings are not perfectly continuous on the sides (Vardoulakis et al., 2003). Obviously, it is not possible to represent an urban canopy with only this idealised configuration, but it can be considered as a fundamental unit which, in some cases (like in Section 4.5.3), well corresponds to realistic conditions, at least in the mid-section of the street. Indeed, the real wind circulation through buildings is tri-dimensional and, if sections closer to the lateral limits of the canyon are considered, the scenario completely changes. Therefore, studying the 2D street canyon configuration was an important and useful simplification for a parametric representation of basic flow processes (Fernando et al., 2010), but outcomes have to be considered as affected by these limitations. The validity of the results to describe flow at real urban pattern is reduced in case of wider street canyons.

5.3.2 CFD technique limitations

The Large Eddy Simulation (LES) numerical technique was carried out in this work. The common numerical approaches are the Reynolds-averaged Navier-Stokes (RANS), unsteady Reynolds averaged Navier-Stokes (URANS) and the LES, since the Direct Numerical Simulation is too much expansive

for urban physics simulation. Each one differs on the way turbulence is modelled, thus results are mainly limited due to this issue. The other simplification employed concerns the specific boundary conditions (described in Section 2.3.1) and the number of simulated canyons, since some authors prefer to set up five street canyons with cyclic conditions, in order to better estimate the pollutant transport.
Statistical samples were sufficient to provide good estimates in the target region, i.e. near the canyon where flow structures are not very persistent. The data obtained are sufficient to give proper measurements of mean quantities also in the upper part of the domain; however, longer simulations should be performed in order to obtain more robust statistics at high levels, where flow structures are larger and more persistent.

5.3.3 Experimental techniques limitations

In the performed wind tunnel experiments, the most relevant simplifications involved the model is the assumption of neutral stratification (see Section 5.3.4) and the measurement techniques. Geometrical simplifications were adopted for buildings, avoiding less important details and differences in material. Very small roughness elements were placed upstream the model, not fully representative of the remaining part of the city. This might cause an overstatement of the difference occurring between flat roof and no-flat roof model, but this issue was not further investigated.
Some practical problems occurred during the LDA measurements. In fact, the probe dimensions limited the measuring range close to the roof or the walls (also considering the model scale of 1:200). Moreover, some issues with back reflections of the laser from the surfaces with a consequent loss of some results. Another reason of concern may come from the blockage of the LDA (with the mirror) and FID probes. However, the technique is very established and previously employed in other works (e.g. Carpentieri et al., 2012), moreover it is not supposed to be too influent in differences occurring through different configurations (for which the same probe is used).

5.3.4 Other simplifying assumptions

Neutral stratification was employed in this work, hence ignoring wall heating effects any stratification in the approaching flow. However, the anthropogenic heat on local temperatures (Ohashi et al., 2007) was found to improve model results. For both velocity field and dispersion, thermal conditions are very relevant (Marucci and Carpentieri, 2018) and should be considered, especially in cities under predominant sunny conditions. However, neutral conditions were preferred to simplify the scope of the research.

Another important assumption made is represented by the choice of a single source to study dispersion in Sections 4.5.3-4.5.4. The source is respectively located upstream the street canyon array and sideways with respect the considered street. These two points (one for each case) were chosen as representative of the largest traffic-emission points in the areas, but, of course, they only approximate the realistic traffic source. However, this allowed establishing a clear relationship between source and receptor. Furthermore, a compromise has to be done also regarding the choice of the source emission velocity. In fact, larger velocities would not be representative of traffic emission sources, while lower quantities would be difficultly measured by the probe.

5.4 References

Badas, M.G., Salvadori, L., Garau, M., Querzoli, G., Ferrari, 2019. Urban areas parameterisation for CFD simulation and cities air quality analysis. International Journal of Environment and Pollution. http://www.inderscience.com/info/ingeneral/forthcoming.php?jcode=ijep

Carpentieri, M., Hayden, P., Robins, A.G., 2012. Wind tunnel measurements of pollutant turbulent fluxes in urban intersections. Atmospheric Environment 46, 669–674. https://doi.org/10.1016/j.atmosenv.2011.09.083

Fernando, H.J.S., Zajic, D., Di Sabatino, S., Dimitrova, R., Hedquist, B., Dallman, A., 2010. Flow, turbulence, and pollutant dispersion in urban atmospheres. Physics of Fluids 22, 051301. https://doi.org/10.1063/1.3407662

Marucci, D., Carpentieri, M., 2018. Wind tunnel study on the effect of atmospheric stratification on flow and dispersion in an array of buildings. Proc. 10th International Conference on Urban Climate. New York, U.S.A., 6-10 Aug.

Moonen, P., Defraeye, T., Dorer, V., Blocken, B., Carmeliet, J., 2012. Urban Physics: Effect of the micro-climate on comfort, health and energy demand. Frontiers of Architectural Research 1, 197–228. https://doi.org/10.1016/j.foar.2012.05.002

Nicholson, S.E., 1975. A pollution model for street-level air. Atmospheric Environment (1967) 9, 19–31. https://doi.org/10.1016/0004-6981(75)90051-7

Ohashi, Y., Genchi, Y., Kondo, H., Kikegawa, Y., Yoshikado, H., Hirano, Y., 2007. Influence of Air-Conditioning Waste Heat on Air Temperature in Tokyo during Summer: Numerical Experiments Using an Urban Canopy Model Coupled with a Building Energy Model. J. Appl. Meteor. Climatol. 46, 66–81. https://doi.org/10.1175/JAM2441.1

Oke, T.R., 1988. Street design and urban canopy layer climate. Energy and Buildings 11, 103–113. https://doi.org/10.1016/0378-7788(88)90026-6

Salvadori, L., Badas, M.G., Querzoli, G., 2018. Caratterizzazione morfometrica della zona urbana di Cagliari. Presented at the XXXVI Convegno Nazionale di Idraulica e Costruzioni Idrauliche, Ancona.

Vardoulakis, S., Fisher, B.E.A., Pericleous, K., Gonzalez-Flesca, N., 2003. Modelling air quality in street canyons: a review. Atmospheric Environment 37, 155–182. https://doi.org/10.1016/S1352-2310(02)00857-9